

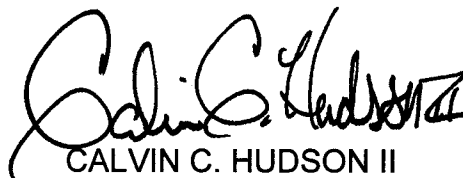
17 FEB 2016

CESWF-EC-G

MEMORANDUM FOR RECORD

SUBJECT: Study - Dam Safety Implications of Drilling, Hydrofracturing and Extraction at Joe Pool Dam, Grand Prairie, Texas

1. In order to evaluate the impact of activities associated with the development of the gas-rich Barnett Shale formation which underlies the Joe Pool Lake project, the U.S. Army Corps of Engineers (USACE) contracted the services of an expert in the fields of petroleum engineering, geomechanics, and hydraulic fracturing. Using both published data and site specific information obtained from drilling companies that were willing to share information with USACE, our expert assessed the possible impacts that drilling, hydraulic fracturing, injection, and extraction could have on the structural integrity of the project. The expert also evaluated the adequacy of the 3,000-foot exclusion zone which was implemented more than 20 years ago in order to safeguard the project and authorized project purposes from minerals related activities.
2. The completed study was used to inform a risk assessment of the project. The risk assessment identified potential failure modes associated with minerals extraction processes, and evaluated the consequences of those failure modes on project performance, and ultimately, public safety.
3. Both the study and risk assessment were subjected to an Independent External Peer Review (IEPR), the agency's highest level of review. The IEPR team members were selected independently of USACE, and included experts in the field of structural geology, geotechnical engineering, drilling and hydraulic fracturing, seismic engineering, and dam safety. They were tasked with reviewing the study and risk assessment for technical adequacy, and making any other recommendations they considered necessary for safeguarding the project.
4. From this process, it was concluded that the 3,000-foot exclusion zone at the project does not meet agency tolerable risk guidelines and, as a result, puts the project and public at risk. As a result, USACE has adopted a 4,000-foot exclusion zone at Joe Pool Dam within which no drilling will be allowed, regardless of depth. Additionally, in order to protect the project from induced seismicity, USACE will work to limit injection wells within five miles of the Joe Pool project. These recommendations are more conservative than the subject study recommends; however, they are considered necessary to ensure that public safety is not reduced as a result of minerals related activities at Joe Pool.



CALVIN C. HUDSON II  
Colonel, EN  
Commanding

**REPORT OF**

Engineering Services  
for  
Dam Safety Implications of  
Drilling, Hydrofracturing and Extraction

Joe Pool Dam, Grand Prairie, Texas

Contract No.: W91237-10-D-0006

Task Order No. 0010

Final Submittal



**DLZ National, Inc.**  
6121 Huntley Road  
Columbus, Ohio 43229-1003

DLZ National Job No.:  
1021-3005.10

February 2015

Prepared for:



U.S. Army Corps of Engineers  
Huntington District



**REPORT OF**

**ENGINEERING SERVICES**

**FOR**

**DAM SAFETY IMPLICATIONS OF**  
**DRILLING, HYDROFRACTURING, INJECTION AND EXTRACTION**

**JOE POOL DAM, GRAND PRAIRIE, TEXAS**

**Contract No.: W91237-10-D-0006**  
**Task Order No. 0010**

**February 2015**

**Prepared by:**

**DLZ National, Inc.**  
**6121 Huntley Road**  
**Columbus, Ohio 43229-1003**

**DLZ National, Inc. Project No.**  
**1021-3005.10**

## **Table of Contents:**

Section 1: Executive Summary and Conclusions

Section 2: Main Report

Appendix A: The Barnett Shale: Geologic Setting, Oil and Gas Development Practices, and Environmental Considerations (May 2012)

Appendix B: Review of Earthquakes Triggered by Human Activities, Focusing on Texas and the Barnett Shale

Appendix C: Texas Tectonic Map

Appendix D: Texas Oil and Gas Map

Appendix E: References Cited

## Section 1: Executive Summary and Conclusions

## **Executive Summary and Conclusions**

### *Nature of the study*

This study was conducted by myself, Dr. Jon E. Olson, P.E., with the help of two subcontractors, Dr. Cliff Frohlich, P.G., and Ms. Kim Gordon, P.E., of Platt Sparks and Associates of Austin, TX. While I am an Associate Professor in the Cockrell School of Engineering at The University of Texas at Austin, and Dr. Frohlich is an Associate Director and Senior Research Scientist in the Jackson School of Geosciences at The University of Texas at Austin, this work was performed as an independent consulting project and as such the results are not endorsed by The University of Texas at Austin in any way.

The conclusions and recommendations in this report reflect a good faith effort to apply the current, commonly accepted standards, practice and knowledge from geomechanics, geophysics, geology and petroleum engineering in order to assess the impact of natural gas production and related activities in the Barnett shale on the area surrounding Joe Pool Dam and Lake. There are limitations to any study like this with regard to

- access to pertinent data, such as detailed subsurface geology and rock property information, drilled well information, and production and injection data,
- uncertainty in the understanding of geologic processes and the interplay between human activity and natural systems, and
- project scope, in particular regarding the choice in this project to rely on published, available data and analytical models (as opposed to collecting new site specific data and using sophisticated numerical models).

The report points out where there are limitations, and based on professional engineering and geoscience judgment, recommends whether further work is justified.

In addition to published resources, the study team of Dr. Jon E. Olson and USACE employee Ms. Anita Branch were given limited access to data from companies operating in the vicinity of Joe Pool Dam, which included supervised viewing of 3d seismic data, well files, and well logs. This site specific data is protected by a

confidentiality agreement and is not available for review or presentation, but my interpretations and analysis based on the data are presented.

### *Study Summary and Conclusions*

The overall assessment of drilling, hydraulic fracturing, gas extraction and related activities in the vicinity of Joe Pool Dam is that there are some potential consequences that could impact the performance of the dam. There are four sources of uncertainty as to the seriousness of the impact of examined activities on dam performance:

1. Lack of site specific data or the wide ranges of published values for mechanical and flow properties in the subsurface in the Joe Pool region.
2. The need for follow-up numerical modeling to evaluate estimated impacts where analytical models could not evaluate all aspects of the problem (such as evaluating the importance of local mechanical anisotropy and heterogeneity in geomechanical processes).
3. The need for the estimated impacts (such as subsidence estimates) to be evaluated by dam experts to determine if they would adversely affect dam performance.
4. The lack of extensive earthquake data prior to the past 10 years, and uncertainty as to the genetic relationship between oil and gas operations and earthquake triggering.

Given the constraints described above, the results and conclusions of this study are summarized below, emphasizing the most significant aspects of the findings.

#### **1. Review of Existing Data.**

Based on documentation of the dam site preparation, small-scale pre-existing faults were described as having 15 ft or less of offset. There was no active seepage along the faults noticed during construction, and other studies in the region suggest that the faults in the Cretaceous rocks that underlie the dam are not prone to fluid flow. Geomechanically, the anticipated stress perturbations coming from drilling, hydraulic fracturing, gas extraction and related activities are not anticipated to be significant enough to reactivate any of these faults. However, these surface faults could extend 1500 ft or more into the subsurface, and pose a potential risk factor if an underground blowout were to occur in the vicinity of the dam.

## 2. Overview of Geologic Setting.

The Joe Pool area in SW Dallas County overlies some of the deepest productive Barnett shale in the Fort Worth Basin. There were some seismically discernible faults in the Paleozoic section above the Barnett shale, trending roughly NNE-SSW, but they did not appear to extend past the Paleozoic-Cretaceous unconformity. General geologic information for the area, taken from surface geology maps and cross-sections, supports the premise that there is no extensive faulting that connects the deeper Paleozoic (including the Barnett) and the overlying Cretaceous rocks, which are the formations that act as the region's aquifers (primarily the Trinity and Woodbine formations). Groundwater modeling published by the Texas Water Development Board also supports the idea that there is poor hydrogeologic communication between the Cretaceous and the underlying Paleozoic.

## 3. Estimation of Engineering Properties.

Overall, the geologic section in the Joe Pool region is consolidated and competent. The only site specific information available was the mechanical properties log for a well close to Joe Pool Dam. Mechanical property estimates from this log vary considerably depending on assumptions related to the dynamic to static correction. The log measures dynamic properties at small strain magnitude but high strain rate. Important physical processes such as hydraulic fracture propagation and reservoir compaction represent larger magnitude strain imparted at much lower strain rate, which are termed static properties. Two approaches were used to correct dynamic log results to static values needed for geomechanical analysis – the Biot-Gassman correction equations and a published correction factor based on core measurements from many unconventional gas reservoirs. Using the Biot-Gassman approach resulted in less value correction from the dynamic values, meaning higher stiffnesses in general. The Paleozoic section from 2000 ft to the top of the Barnett (slightly below 8000 ft) ranges in Young's modulus from  $E_{Gassman}$  of  $3 \times 10^6$  to  $6 \times 10^6$  psi. Using the lab based correction factor, the estimated values are approximately half as large,  $E_{low} = E_{Gassman}/2$ . In the Barnett Shale, the estimated values were from  $E_{low} = 2.5 \times 10^6$  psi to  $E_{Gassman} = 5.5 \times 10^6$

psi. Beneath the Barnett Shale, the estimated values for the Ellenburger were from  $E_{low} = 4.5 \times 10^6$  psi to  $E_{Gassman} = 10.5 \times 10^6$  psi.

Published reports indicate variation between the dynamic and static Poisson's ratio, but experimental reports showed scatter where the static values were both higher and lower than the dynamic ones. Based on a published study focused on unconventional gas reservoirs, it was assumed that  $\nu_{stat} = 0.945 \nu_{dyn}$ . Using this relation,  $\nu_{stat} = 0.3$  from 2,000 ft to the top of the Barnett. In the Barnett Shale the Poisson's ratio drops to  $\nu_{stat} = 0.15$ .

Biot's poroelastic constant in the Barnett Shale, important for stress estimation and reservoir compaction determination, varied from  $\alpha_{Gassman} = 0.4$  to  $0.6$  to  $\alpha_{low} = 0.7$  to  $0.8$ , depending on the static Young's modulus value used. (The subscripts Gassman and low refer to the method for estimating Young's modulus. The low Young's modulus case actually gives the highest poroelastic constant.)

#### **4. Changes in Stress State.**

Reported fracture gradients in the area are from 0.7 to 0.85 psi/ft, consistent with calculations using critically stressed crust theory given the local estimated pore pressures of 0.48-0.55 psi/ft. Hydraulic fracture containment within the reservoir or treatment zone depends on variation of the horizontal stress with depth. Using the above stress values within the Barnett Shale as calibration, a vertical profile of horizontal stress was computed using the mechanical property log, and the lower fracture stress barrier was estimated to have an  $S_{hmin}$  4000 to 6000 psi higher than the Barnett, while the upper fracture stress barrier was estimated to have an  $S_{hmin}$  800 to 1000 psi higher than the Barnett.

Changes in stress state at the earth's surface caused by either hydraulic fracturing or gas extraction are estimated to be unobservable. Stress changes within the reservoir are expected to be 0.6 to 0.8 times the magnitude of the pore pressure change. Stress change within the reservoir due to hydraulic fracturing is expected to

reach only to a distance of 1 to 2 times the hydraulic fracture height, which would be hundreds of feet laterally and less vertically.

## **5. Impacts of Hydrofracturing.**

Fracture treatment size, based on local wells, consists of 5 to 7 fracture stages composed of 6 perforation clusters spaced evenly over 400 ft along a horizontal well 3500 ft long. Approximately 15,000 bbls of fluid and 400,000 lbs of proppant are pumped for each stage. Created hydraulic fracture length per stage is estimated to be 35,000 linear ft. Published microseismic monitoring data and numerical simulations suggest the fracture geometry is complex, possibly consisting of a dendritic or orthogonal vertical fracture arrangement propagating out from the wellbore.

Based on estimated stress profiles and microseismic monitoring from other Barnett shale regions, it is unlikely that Barnett shale fracture treatments propagate significant distances out of zone. There is no geomechanically plausible mechanism for aquifer contamination directly from the Barnett shale via hydraulic fracturing, but if fracturing fluid were to propagate up a poorly cemented annulus between the casing and the drilled hole, there is a chance for loss of fluid control below the setting depth of the surface casing (see Section 8 for further discussion).

Using an idealized two-dimensional model for estimating the effective modulus of a fractured elastic medium, the computed 35,000 linear ft of vertical fractures evenly distributed throughout the estimated reservoir volume contact by one fracture stage could reduce the horizontal component of Young's modulus by 90%. This assumes extensional deformation and no proppant within the fractures. Further study to determine a better estimate of the effect of the fracturing on effective elastic properties of the Barnett is justified given this apparently significant effect. Three-dimensional elastic modeling could be done to improve on this assessment as well.



## 6. Subsidence.

The subsidence results are strongly influenced by two factors – the elastic properties of the reservoir rock (i.e., the Barnett), and the extent of depletion in the subsurface around Joe Pool Dam. In order to aid in evaluating the potential impact of gas production on surface subsidence (there is no estimated subsidence impact from hydraulic fracturing operations), several scenarios were evaluated. Three different mechanical property estimations were employed – 1) a best case (i.e., least predicted deformation) based on the Biot-Gassman Young's modulus for the Barnett of  $E_{best}=5.5 \times 10^6$  psi, 2) a conservative case with  $E_{con}=2.5 \times 10^6$  psi based on the lower bound of laboratory measured dynamic to static corrections for unconventional gas reservoirs, and 3) a worst case of  $E_{worst}=1.0 \times 10^6$  psi, intended to bound the realm of possible outcomes, where the effective Young's modulus governing reservoir compaction might be reduced by inelastic effects such as creep or modulus softening induced by fracturing. Poisson's ratio was varied from 0.2 to 0.15 to 0.1 for the best to conservative to worst case scenarios, respectively.

Using an elastic reservoir compaction and subsidence approach based on Geerstma (1973), it is clear that a single isolated well cluster estimated to have a depletion radius of 2500 ft would have no impact on surface elevations. Subsidence is dependent on the ratio of the depth of the depleted zone to its radius, and for a single isolated well cluster, this ratio is high and subsidence is predicted to be a very small fraction of the reservoir compaction (20% or less). However, current development in the area includes closely spaced wells and large blocks of contiguous depleted reservoir volume. Using a semi-analytical model based on published work from the petroleum industry, several different well development scenarios are evaluated to determine the effect of exclusion zones of various radii around Joe Pool Dam on surface subsidence mitigation.

Using the three mechanical property scenarios, the maximum possible subsidence was computed to be 1.8 inches, 6.5 inches and 21 inches for the best, conservative and worst case scenarios, respectively. When taking into account the location of the dam within the subsidence bowl for the estimated configuration of wells, the subsidence from

one end of the dam to the other varied from the best case estimate of less than one inch to the worst case of 8 inches.

Exclusion zones were drawn as stand-off distances measured perpendicular to the dam all along its length. Partly because of the 8600 ft depth of the Barnett Shale and the great lateral extent of the development area, simulated subsidence bowls showed that a considerable fraction of the maximum displacement reaches out 10,000 to 20,000 ft from the edge of the subsurface Barnett reservoir. Consequently, a 5,000 ft standoff distance (which is slightly larger than the current policy of the US Army Corps for Joe Pool) had little impact on reducing subsidence seen at the dam. Increasing the standoff to 10,000 ft reduced estimated subsidence by about half. A 20,000 ft standoff cut the subsidence seen at the dam by a factor of 3 compared to the full depletion case.

Other development geometry scenarios included looking at the impact of gas development moving eastward past the dam to the location of N. Hwy 67, which looks to be the furthest extent of the Barnett in the subsurface. Currently there is little development to the ESE of Joe Pool Lake. The modeling showed that given each exclusion zone case (5,000 ft, 10,000 ft, and 20,000 ft stand-off), the progression of development eastward past the lake didn't appreciably change the predicted subsidence.

This report does not assess what level of subsidence around Joe Pool Dam is acceptable. Also, since there is no differential leveling data that I was able to find for the region, it is hard to evaluate which subsidence modeling scenario is most likely. It is recommended that leveling data be collected along a line that extends from within the heavily developed Barnett area to well outside of it (at least several miles beyond the extent of drilling) in the Joe Pool region. Prudence would suggest that planning should account for the possibility of at least the conservative case coming true.

There are several reasons why the actual subsidence result could be less severe than the best case scenario. There are other reasons why the actual result could be worse

than the worst case scenario. The primary uncertainty lies with the mechanical properties of the Barnett itself. Most published studies would estimate the static Young's modulus for the Barnett shale to be  $4 \times 10^6$  psi or higher. However, the dynamic result from the well log near Joe Pool falls at the lower end of the published static range. It is possible that in this region, the Barnett is less stiff than in other regions further to the north and west. Also, the modeling and properties used were elastic, but it is well known that actual subsidence is not simply elastic but also has inelastic components such as creep that increase the subsidence. Consequently, the elastic calculations for compaction and subsidence should be considered minimum estimates for the presumed mechanical properties. To better evaluate the potential for inelastic enhancement of compaction and subsidence, long term creep testing is needed for the Barnett. All I found in the literature was one short term study. Finally, one factor of uncertainty currently under more scrutiny in the industry that could reduce the estimate of compaction and subsidence is the nature of depletion in a gas shale like the Barnett. The pore structure of these rocks is poorly understood, as is the interconnection between pores and the matrix flow mechanics. In the calculations here, it was assumed that the entire 350 ft of the Barnett was depleted, and the depletion occurred throughout the 2500 ft radius of each reservoir disc that represented a well cluster. If the depletion is more incomplete or doesn't affect the entire thickness of the Barnett, then the compaction and subsidence would be reduced. Since *in situ* measurements of pore pressure in tight rocks like the Barnett Shale are so difficult to make, improving on estimates of how depletion proceeds will probably require laboratory testing combined with simulation.

## **7. Hydrofracturing Pressures.**

Hydraulic fracturing surface wellhead pressures can be in the thousands of psi's, but proper planning should make such pressures safe. Wellheads and tubulars can be found to match most any requirement. Downhole, observed net pressures (fracturing fluid pressure above the minimum horizontal stress) for the Barnett Shale are on the order of 500 to 1000 psi. None of these pressures are out of the ordinary for sandstone or shale hydraulic fracturing operations. It is not apparent that setting limits on

pressures or rates to be allowed for hydraulic fracturing would be productive, although best practice on the part of the operator is required to assure that tubulars, wellheads, casing and cement are designed to withstand and endure repeated cycles of the kind of pressurization that happens during multi-stage hydraulic fracturing.

## **8. Fracture Zone.**

Theoretical and empirical data indicate that the hydraulic fracture treatments in the Barnett shale are largely contained within the formation. There are instances of some height growth, but there is no documented case of a fracture treatment propagating from Barnett depth toward the surface to contaminate an aquifer. For a deep reservoir like the Barnett, there is as much as 6,000 ft of rock between the gas producing zone and the closest near surface aquifer. It is considered unlikely that the hydraulic fracture treatment could connect directly between the Barnett Shale and overlying, naturally fractured rocks that reach to the surface. However, there is a possibility of underground blowout conditions contacting near-surface faults in the vicinity of Joe Pool Dam. This scenario is based on the fact that current well designs leave an uncemented annulus around the production casing at depths below the surface casing (~2200 ft) to about 6500 ft. If fluids escape the completion zone in the Barnett through the wellbore due to bad production casing cement, this annulus could be exposed to high pressure. Similar effects could occur during drilling after setting the surface casing. Under this scenario, if wells are located too close to Joe Pool Dam, there is a possibility of high pressure gas or fluid reaching the surface under the embankment or outlet works. It is recommended that a standoff of at least 3000 ft be maintained around the dam and related structures to protect against this scenario. This exclusion distance applies to all wells, whether they are intended for production or injection. A larger exclusion distance is recommended for injection wells related to induced seismicity.

## **9. Induced Seismicity.**

There is no documented case of induced seismicity beyond microseismic events to have occurred in the Barnett shale due to hydraulic fracturing. Microseismic is on the order of magnitude M1.0 or less, but mostly M0.0 or less. A magnitude M0.0 is

comparable to a fault patch that is 12 meters on a side slipping by 1.2 mm. Such an event poses no risk to any surface structures. In order for an earthquake to be felt by humans, it needs to be magnitude M2.0 or M3.0, which represents 1,000 to 30,000 times more energy than a magnitude M0.0 micro-seismic event, respectively.

There is no documented case of gas extraction related earthquakes in the Barnett shale. The reservoir compaction and stress change that comes with reservoir pressure depletion can induce earthquakes in some formations, but that has not been observed in the Barnett to date. However, injection induced earthquakes have occurred in the Barnett shale area, associated with wells that inject produced water from Barnett wells into the underlying Ellenburger formation. There are numerous injection wells in the Fort Worth Basin and only a few of them have been suspected of causing problems, but the fact that the earthquakes do occur suggests that more care should be taken in choosing injection well sites (avoid proximity to major pre-existing faults). Also, more scrutiny should take place in the permitting process with regard to allowable injection rates and pressures, and pre-injection testing of wells for evaluating fracturing pressures, pore pressure, and the proximity of flow boundaries, which could be faults.

Frohlich states that triggered earthquakes (caused by injection or extraction) should not exceed the magnitude of local natural earthquakes. To date, the largest earthquake in the Fort Worth Basin area has been on the order of M3.5. However, the largest induced earthquake in Texas was M4.6, and the largest recorded (natural) earthquake was M5.8. Without further statistical support, it seems reasonable to estimate that a M4.5 to M5.0 is possible in the Fort Worth Basin vicinity, although unlikely.

## **10. Risk Reduction.**

As mentioned already, an exclusion zone of 3,000 ft is recommended with regard to blowouts. The risk of hydraulic fractures propagating from the depths of the Barnett shale to the depth of an aquifer is minimal. As such, restricting operations with regard to rate or pressures doesn't seem warranted. Also, microseismic data collected for thousands of hydraulic fracture treatments does not show a strong correlation between

the magnitude of the microseismic event and the rate or volume pumped. Green fluids should be encouraged, particularly in order to prevent hazards from surface spills and need for disposal when the fluids are produced back from the formation. A 3,000 ft exclusion zone seems reasonable for protecting the dam from surface events such as spills and explosions, although if surface spills are considered, surface locations for wells should have a considerable stand-off from the lakeshore as well to protect the water.

With regard to induced seismicity and ground acceleration, a 16,400 ft stand-off between Joe Pool Dam and any injection well is recommended, assuming a worst case earthquake of M5.0 induced by wastewater injection.

#### **11. Best Practices: Drilling, Hydrofracturing and Extraction & Well Construction**

Best practices continually evolve as service companies and operators strive to optimize performance and cost. To highlight the topics dealt with in detail in the report, best practice involves:

- multi-well pads to minimize the land footprint of operations,
- procedures that provide for protection against and mitigation of surface spills of solid concentrates and liquids,
- good cementing practice with regard to cement mixture and pumping procedures, designing for good placement and durability for multiple cycles of high pressure during fracture treatments as well as long term loading conditions during production,
- recycling of produced water where applicable and the use of green fluids, and
- attention to fugitive gas and emissions from flaring to minimize air pollution.

#### **12. Other Potential Impacts.**

In the SOW this topic was intended to discuss injection wells, but that topic is covered mainly in the section on induced seismicity. One other topic of interest, however, is the idea that there may be productive zones above the Barnett that could be developed for gas. In looking at the logs from local wells, there were a couple of electrically resistive

sands above the Barnett that could have producible hydrocarbons. If these zones were depleted, that could add to the surface subsidence calculated for the Barnett.

### **13. Evaluation of Baldwin Hills Failure and Comparison to Joe Pool.**

The Baldwin Hills Case is a famous example from 1963 where a dam failed in the Los Angeles area. The dam was built in an active strike-slip fault zone, but it appears that oil production immediately adjacent to the dam and reservoir accelerated the problem. This example is not similar to the Barnett case for several reasons. Firstly, the geologic setting is very different – the Baldwin Hills Reservoir is in an active tectonic setting, the main producing zone is very shallow (~1200 ft), and the oil reservoir rock is highly porous and compressible, uncemented sand. In contrast, the Barnett is in a quiet tectonic setting, fairly deep (8600 ft), and represents a low porosity, low compressibility siliceous shale. In the Baldwin Hills example, it was determined that faults extended from within the oil reservoir all the way to the surface underneath the dam. Water injection was used to waterflood the reservoir at Baldwin Hills, and the pressures were very high, making the rock more susceptible to shear failure. The injection in the Barnett play is not into the Barnett, but into the Ellenburger. Currently, there is no close injection well to Joe Pool Dam with the nearest being approximately 9 miles away.

### **14. Recommendations (for further work).**

The potential areas for additional research and engineering that could improve the assessment of dam safety implications of drilling, hydrofracturing and extraction include:

- better static and long-term creep behavior testing of the Barnett,
- a leveling survey to establish whether any subsidence can be detected in and around Joe Pool Dam and Lake,
- better characterization for the main injection target, the Ellenburger formation,
- numerical modeling that accounts for heterogeneity and anisotropy of the subsurface geology, and
- earthquake monitoring in the vicinity of injection wells.

## Section 2: Main Report



# **Dam Safety Implications of Drilling, Hydrofracturing and Extraction**

**Joe Pool Dam, Grand Prairie, Texas**

**Contract No. W91237-10-D-0006**

**Task Order 0010**

**Prepared by**

**Jon E. Olson, JEO Associates**



Appended Topical Studies:

The Barnett Shale:

Geologic Setting, Oil and Gas Development Practices, and Environmental  
Considerations

by Kimberly Gordon, Platt, Sparks and Associates, Austin, TX

Review of Earthquakes Triggered by Human Activities, Focusing on Texas and the  
Barnett Shale

by Cliff Frohlich, The University of Texas at Austin

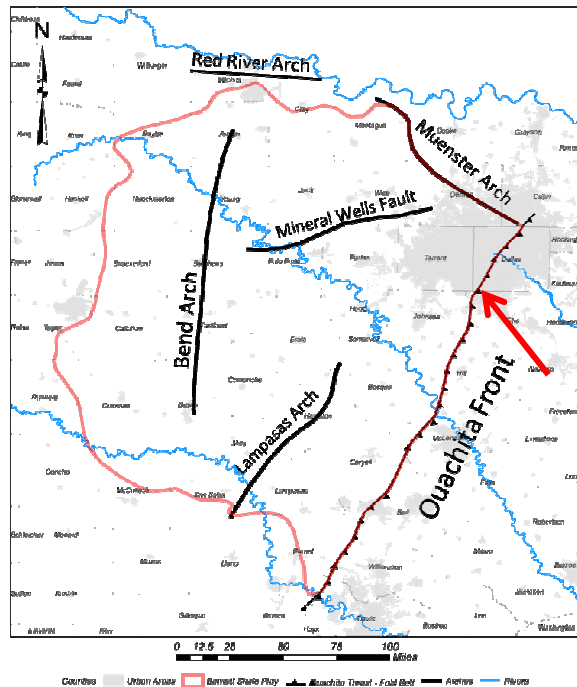
**1. Review of Existing Data.** The Joe Pool Dam embankment is described as founded on clay overburden which overlies the Eagle Ford Formation (USACE, 1991). Outlet Works are built upon the Britton Member of the Eagle Ford Formation. As described in the Final Foundation Report (Marr, 1983), the Britton is the lowermost member of the Eagle Ford and is approximately 160 ft thick. The Eagle Ford itself is approximately 225 ft thick at Joe Pool Dam. The Britton is divided into three units: the Lower Britton, Units I and II, and the Upper Britton. The outlet works foundations lie on the Lower Britton, Unit II and the Upper Britton. The geology of these units is described as

Lower Britton, Unit II - moderately hard to hard, thick bedded, occasionally jointed, tannish-gray very calcareous clay shale.

Upper Britton – soft to moderately hard, slightly calcareous, highly jointed and fractured bentonitic clay shale.

Bedding dips are described as varying from 50 to 200 ft per mile (about 0.5 to 2.0 degrees from horizontal). Seven minor normal faults were observed to cross the outlet

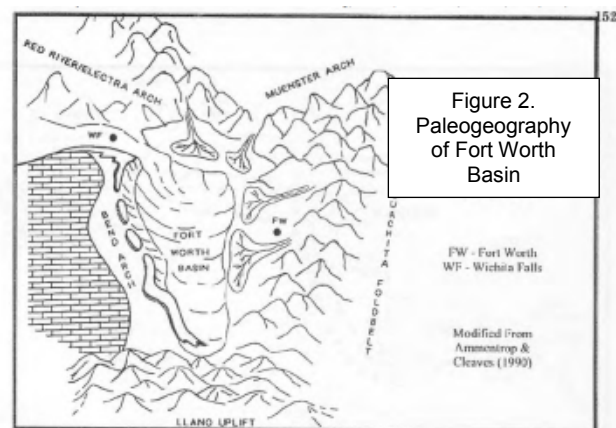
Figure 1. Regional setting of Barnett shale in the Fort Worth Basin. Red arrow points to approximate location of Joe Pool Dam and Lake, on the easternmost edge of the Barnett play where it is cut off by the Paleozoic Ouachita Thrust Front. From Pollastro et al. (2007)



works foundation with displacements of less than 15 feet, with changes in dip sometimes observed where minor faults crossed the outlet works. Fault planes were described as tight brecciated zones less than 6 inches thick. Published data on faults in various geology settings suggests there is a relationship between fault slip and fault size (length and height). Kim and Sanderson (2005) published observational data on faults indicating fault slip to be on the order of  $1/100^{\text{th}}$  of fault size (with a fair degree of scatter), which is consistent with theoretical estimates of Pollard and Segall (1987). Given the measured 15 ft offset on some faults in the outlet works foundation, it is possible that these faults have heights on

the order of 1500 ft. There were no reports of significant groundwater flowing into the excavations, particularly not from the faults.

**2. Overview of Geologic Setting.** The Barnett Shale play of the Fort Worth Basin is located in North-Central Texas, including the area under and around Joe Pool Lake and Dam (Figure 1 – Joe Pool area indicated with arrow). The Fort Worth Basin is a foreland basin related to the Paleozoic Ouachita Orogeny, collecting sediments that were shed to the north and west ahead of the collisional uplift caused by South America and Africa converging with North



America. The basic paleogeography during mid to late Paleozoic time (Fig. 2), the time when the Barnett Shale and younger Paleozoic rocks were deposited, has the basin bounded on the north by the Red River and Muenster arches, on the west by the Bend Arch, on the south by the Llano Uplift, and on the east by the Ouachita fold and thrust belt (Thomas, 2003). The general depositional systems are depicted in Figure 3, with a major unconformity on top of the Ordovician Ellenburger forming the floor of the basin. The deepest part of the Fort Worth Basin is shown to be truncated on the east by the Ouachita fold and thrust belt. The Viola is the first unit deposited on top of the Ellenburger, and it pinches out to the west. On top of the Viola is the Barnett, which to the west is deposited directly on top of the Ellenburger. On top of that is the Marble Falls and other carbonate shelf deposits. There is a thin veneer of the Smithwick pro-delta basinal rocks followed by a huge thickness of fan delta and slope sediments of the Atoka.

In Dallas County, Figure 3 indicates the youngest preserved Paleozoic rocks are of the Strawn fluvial-deltaic system and that they are truncated by the Cretaceous unconformity. The upper Pennsylvanian Canyon and Cisco as well as any Permian rocks only occur in the subsurface further to the west.

The Hosston member of the Cretaceous Travis Peak Formation was deposited on the unconformity surface, and in SW Dallas County, the depth to the unconformity is estimated to be 2150-2200 ft (Harden and Associates, 2004). Cretaceous rocks persist to the surface (as described in the USACE embankment and outlet works reports), and the bedrock beneath Joe Pool Lake and Dam is the Eagle Ford Formation (see present day geologic map, Fig. 4). To the east of Joe Pool and stratigraphically higher is the Austin Chalk, and to the west and stratigraphically lower is the Woodbine Formation. In much of the Joe Pool area, lying unconformably on top of the Eagle Ford, are Quaternary deposits related to a major ancestral NW-SE drainage coincident with the present-day Trinity River. Details of the Cretaceous stratigraphy, with formation names and approximate thicknesses, can be found in Table 1.



is consistent with the surface geology in the Joe Pool region (Fig. 4). There is a normal fault trend ~45 miles to the east of Joe Pool (in Kaufman County, NE of Corsicana) which is likely an expression of the Balcones Fault trend that runs from East Texas to San Antonio (see Texas Tectonic map in Appendix C), but there are no major surface structures closer than that, except one lone normal fault mapped to the southeast, just north of Waxahachie. Consequently, it appears there is no surface expression of the Ouachita thrust system in the Cretaceous cover above the Paleozoic-Cretaceous unconformity, which would project to surface in the outcrop belt of the Austin Chalk (symbol Kau on map) in Figure 4. Smaller scale fractures, as evidenced by the foundation reports for Joe Pool, are most likely present throughout the region in brittle units such as carbonates, sandstones, and siliceous shale such as the Barnett. However, these fractures are likely strata-bounded, stopping at thicker, more ductile shales widely present in the stratigraphic section above the Barnett. Examples of natural fracture height containment are documented in the Austin Chalk (Corbett et al., 1987 and Friedman et al., 1994). With regard to mechanical and hydrologic communication between the Paleozoic (where the Barnett shale gas development is occurring) and the overlying Cretaceous (where the major aquifers lie), there are no obvious large scale short-cuts or connections indicated by hydrologic studies (discussed later). This is consistent with the informal viewing of 3d seismic offered to the study team by local companies, where there was evidence of a few faults in the Paleozoic within and above the Barnett in the Joe Pool area, but no evidence that such faults crossed the Paleozoic-Cretaceous unconformity. (Site specific information provided for use in this study is protected by a confidentiality agreement. This information is only referenced and not available for review or presentation).

The study was given access to logs from two wells from local companies for investigation. Formation tops were not picked on the logs, but general geology can be inferred from the gamma ray, porosity and resistivity logs. The shallowest 2000 ft were not logged in either well because they were behind the surface casing before the open hole logging run was made. The first thing evident about the logs is that the section is predominantly high gamma ray, indicating a predominance of shale or other fine grain

rock. The mineralogic log track confirms this correlation of high gamma ray with high clay content for the entire log except the Barnett, where the gamma ray is the highest of any zone in the well, but the clay content actually drops in favor of increased silica content. There are thin zones in both logs where the gamma ray indicates less clay or fines, looking like interbedded sands, several of which have high resistivity, suggesting they might be hydrocarbon-bearing. Below the Barnett there is an increase in clay for about 100 ft (the Viola formation), and then the mineralogy becomes 90% carbonate, indicating the Ellenburger. This predominance of clay in the section between the Barnett and the basal Cretaceous unconformity suggests a low likelihood for significant matrix or fracture flow to move vertically through the section.

With regard to petroleum geology, the Barnett is not the only formation in the region that produces hydrocarbons in the Fort Worth Basin (see Table A2, Appendix A). Beneath the Barnett, the Ellenburger and Chappell Limestone are producers. Above the Barnett, there is production from the Bend Group and the Strawn. However, in the immediate vicinity of Joe Pool, the Barnett is the only active play. The Oil and Gas Map of Texas (BEG, 2005 – reproduced in Appendix D) shows that prior to 2005, there was no oil and gas development in Dallas County. It has just been in more recent years (since 2007) that Barnett development has encroached farther to the southeast.

A more detailed description of the geology of the region is presented in Appendix A, including related maps and cross-sections and individual formation descriptions.

Table 1. From Harden & Associates, 2004. Geologic data from Klemt et al. (1975) and Nordstrom (1987).

System	Series	Groups	Formation				Approximate Maximum Thickness	
			North		South		North	South
Tertiary	Undifferentiated							
Cretaceous	Gulfian	Navarro	Undifferentiated		Undifferentiated		800	550
		Taylor					1500	1,100
		Austin					700	600
		Eagle Ford					650	300
		Woodbine					700	200
	Comanchean	Washita	Grayson Marl		Buda, Del Rio		1,000	150
			Mainstreet, Pawpaw, Weno, Denton		Georgetown			150
			Fort Worth, Duck Creek					
			Kiamichi		Kiamichi			50
		Fredericksburg	Goodland		Edwards		250	175
					Comanche Peak			150
					Walnut Clay			200
		Trinity	Antlers	Paluxy	Paluxy		400	200
				Glen Rose	Glen Rose		1,500	1,500
				Twin Mountains	Travis Peak	Hensell	1,000	1,800
						Pearsall/ Cow Creek/ Hammett		
					Hosston/Sligo			
Paleozoic	Undifferentiated							

### 3. Estimation of Engineering Properties.

The main source for mechanical property data for this study was log data from a nearby well. (Site specific information provided for use in this study is protected by a confidentiality agreement. This information is only referenced and not available for review or presentation.) This section describes how mechanical properties are derived from logs and compares Joe Pool area results to those in the literature.

Acoustic logs typically do not record seismic velocities but instead are presented as slowness (the inverse of velocity). Thus, as slowness goes down, velocity goes up. The slowness for the compressional wave generally decreases with depth from almost 100 microseconds/ft at 2200 ft to 50 microseconds/ft at almost 9000 ft in the Ordovician Ellenburger (these slowness values correspond to velocities of 10,000 ft/s to 20,000 ft/s, respectively). The shear wave slowness values are about twice the compressional wave values, ranging from over 200 microseconds/ft at around 2500 ft to 95 microseconds/ft at the bottom of the well in the Ellenburger (these correspond to velocities of 5,000 ft/s to 10,500 ft/s, respectively). Log value accuracy can be affected by the condition of the wellbore. There are some zones of hole enlargement in the well, but the slowness data in those sections do not depart from the range of values seen in other depths where the hole that is in better condition.

The elastic properties of subsurface formations can be calculated from the shear and compressional wave slowness and rock bulk density. Poisson's ratio,  $\nu$  (dimensionless), and shear modulus,  $G$  (psi), are calculated directly from the log data as

$$\nu = \frac{0.5R^2 - 1}{R^2 - 1} \quad (1)$$

and

$$G = 1.34 \times 10^{10} \frac{\rho_{bulk}}{\Delta t_s^2} \quad (2)$$



where  $R=\Delta t_s/\Delta t_p$ ,  $\Delta t_s$  is shear wave slowness and  $\Delta t_p$  is compressional wave slowness, both in  $\mu\text{sec}/\text{ft}$ , and  $\rho_{\text{bulk}}$  is the bulk density in  $\text{g}/\text{cc}$ . Young's modulus can be calculated as

$$E = 2G(1 + \nu) \quad (3)$$

Two other elastic parameters of importance are the bulk modulus (which is the inverse of compressibility)

$$K = \frac{E}{3(1-2\nu)} \quad (4)$$

and Biot's poroelastic constant,

$$\alpha_p = 1 - K/K_g \quad , \quad (5)$$

where  $K$  is the bulk modulus of the entire rock and  $K_g$  is the bulk modulus of the individual grains (i.e., bulk modulus of the primary mineral, such as quartz or calcite).

It is widely observed that rocks are not perfectly elastic, one aspect of which is strain-rate dependent stiffness (which can be described using viscoelastic constitutive models). The importance of this strain-rate dependency for log interpretation is that mechanical properties inferred from log velocities measured at high frequency (on the order of 20 to 40 kHz) are typically stiffer (higher Young's and shear modulus) than static values (measured at very slow strain rates). Considering that hydraulic fracturing acts on a scale of hours and reservoir depletion acts on a scale of years, corrections must be made to the microsecond scale measurements from the log in order to utilize log-based properties for production-scale processes. One explanation for this strain-rate dependent behavior is the fact that at high, log frequency strain rates, the rock is essentially undrained, so fluids that are compressed by the acoustic wave cannot move and therefore add stiffness to the rock. Slower rate deformation allows enough time for fluid to drain out of the strained region without increasing fluid pressure and rock

stiffness. One method of correction for this behavior is the Biot-Gassman equation (Guegen and Bouteica, 2004, pg. 14),

$$K = K_u - \alpha_p^2 \left[ \frac{\phi}{K_f} + \frac{\phi - \alpha_p}{K_g} \right]^{-1}. \quad (6)$$

where  $K$  is the static value of bulk modulus,  $K_u$  is the log measurement,  $K_f$  is the bulk modulus of the pore fluid, and  $\phi$  is porosity. Assuming gas-free water as the pore fluid gives the strongest correction ( $K_f=400,000$  psi was assumed here based on Earlougher, 1977). For the local log, the ratio of drained to undrained bulk modulus ranges from 0.85 to 0.95 throughout most of the depth range. In a gas producing zone,  $K/K_u$  would be expected to approach 1 as the gas has a very high compressibility which makes for a small  $K_f$ .

Another way to correct for dynamic (or undrained) behavior is empirically with laboratory experimental data from core samples. The advantage of this method is that it can correct for drained vs. undrained behavior as well as any other strain-rate dependent mechanism that might be operating in the rock. Baree et al. (2009) evaluated the static to dynamic ratio on tight-gas sand and shale gas samples (Fig. 5). I added the dashed

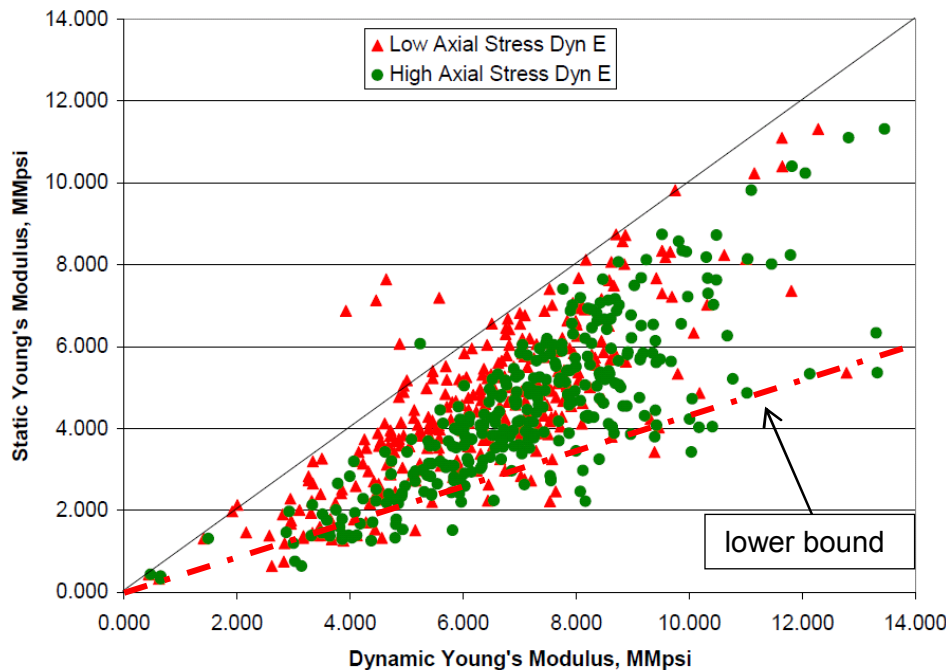


Figure 5. Dynamic vs. static Young's modulus data for shale gas and tight gas samples. Lower bound has been added for this report to bound mechanical properties for the Barnett Shale. Modified from Baree et al. (2009).

line as a boundary that encompassed at least 90% of their data to be used as a lower limit (worst case scenario) on the static to dynamic ratio, which is  $E_{stat}/E_{dyn}=0.43$ . Baree et al. (2009) also examined Poisson's Ratio and proposed best fit predictive models with a very narrow range of behavior,  $0.93 < v_{stat}/v_{dyn} < 0.96$ . However, the data they used shows a considerable scatter (Figure 6), with no apparent trend of the dynamic Poisson's ratio being higher or lower than the static value, although at higher dynamic Poisson's ratio the static value was more likely to be lower.

Sone and Zoback (2011) evaluated non-elastic behavior in gas shales, finding the Haynesville most susceptible to creep in a 3 hour test, while the Barnett, Fort St. John

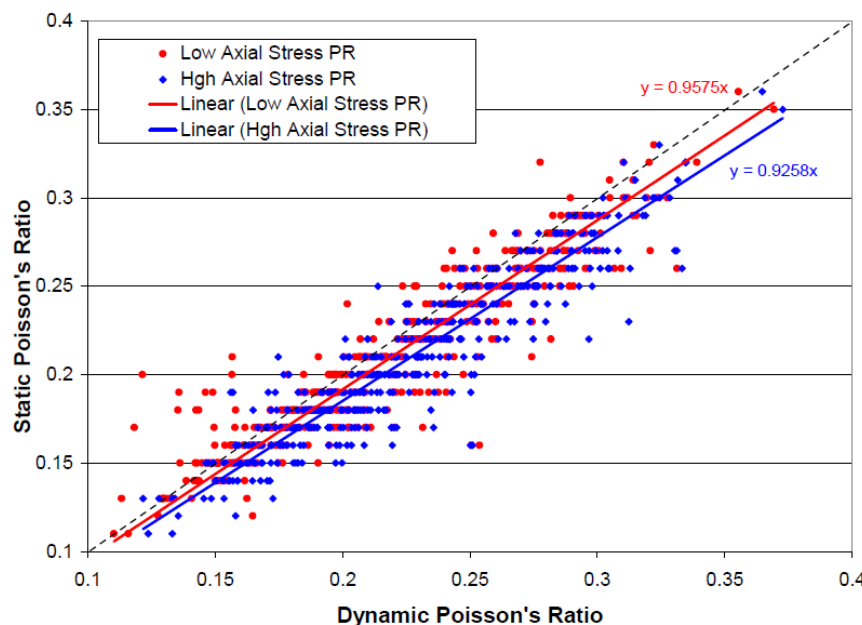


Figure 6. Static versus dynamic Poisson's ratio measurements for shale gas and tight gas sandstone samples, from Baree et al. (2009).

and Eagle Ford were all less susceptible. The magnitude of the 3 hour creep strain in an  $E = 4.3 \times 10^6$  psi Barnett sample at 5800 psi differential stress was on the order of  $\epsilon=1 \times 10^{-4}$ . At this stress state for this Young's modulus, the elastic axial strain would be on the order of  $1 \times 10^{-3}$ , making the creep strain

approximately 10% of the elastic strain. Presumably at long time periods that fraction would increase, but there was no long term data in the paper. The comparable Haynesville percentage of creep to elastic strain was more than 3 times higher than the Barnett.

Consequently, two values were computed from logs for Young's modulus,  $E_{Gassman}$  for the Biot-Gassmann correction of equation (6), and  $E_{low}$  for the lower limit, lab-data based correction of  $E_{low} = 0.43 * E_{dyn}$ . When calculating  $E_{Gassman}$ , the dynamic Poisson's ratio was used to avoid double correction, since the corrected bulk modulus embodies both Young's modulus and Poisson's ratio. For Poisson's ratio processing, the average correction factor was used from Baree et al. (2009) of  $\nu_{stat} = 0.945 * \nu_{dyn}$ .

The corrected Poisson's ratio stays very close to  $\nu_{stat} = 0.3$  from 2000 ft to the top of Barnett section, where it drops to about  $\nu_{stat} = 0.15$ . A possible reason for this reduction comes from Baree et al. (2009) who suggest that such a fall in Poisson's ratio, measured using acoustic velocities, can be a function of gas saturation in the pore space. Young's modulus increases with depth in general, but there is a big jump at the Ellenburger / Barnett contact. Values are very different, however, depending on the dynamic to static correction method employed. The Biot-Gassman correction scenario results in higher moduli values, the shallow depths in the log have  $E_{Gassman}$  averaging about  $3 \times 10^6$  psi down to 3500 ft, where the value jumps to  $4 \times 10^6$  psi. The modulus slowly increases to about  $6 \times 10^6$  psi down to 7800 ft, where it drops back to  $5 \times 10^6$  psi above and through the Barnett (from 8500 to 8850 ft). There is a big jump to over  $10 \times 10^6$  psi for the Ellenburger below the Barnett. Using the lower limit scenario described above,  $E_{low}$  varies from averaging about  $1.3 \times 10^6$  psi in the shallow section of the log to  $2 \times 10^6$  psi by 6000 ft and about  $2.5 \times 10^6$  psi in the Barnett shale. The jump to the Ellenburger is only to  $4.5 \times 10^6$  psi.

Data for the Barnett shale from the literature has a wider variation than the local log data examined (static values of  $E_{low} = 2.5 \times 10^6$  psi to  $E_{Gassman} = 5 \times 10^6$  psi). Sone and Zoback (2011) report static Young's modulus for Barnett Shale from  $4 \times 10^6$  to  $13 \times 10^6$  psi, while Tutuncu and Mese (2011) report a range of  $5 \times 10^6$  to  $9 \times 10^6$  psi. Akrad et al. (2011) found a range of  $E$  from  $6 \times 10^6$  to  $11 \times 10^6$  psi, but this was using a micro-indenter, so such measurements would not be considered as reliable as a triaxial test on a core plug. One interesting result of the Akrad et al. (2011) study, however, was

that they observed from 30 to 40% reduction in Young's modulus for Barnett samples exposed to fracturing fluids for extended time at temperature.

The rock bulk modulus,  $K_r$ , was computed from the lower limit and Biot-Gassman correction scenarios for use in equation (5) to arrive at two values of Biot's poroelastic constant,  $\alpha_{low}$  and  $\alpha_{Gassman}$ . The  $\alpha_{low}$  case (using the lower limit estimate of Young's modulus) has the higher poroelastic constant value, around 0.8 throughout the log as it reduces the rock bulk modulus. This poroelastic response will be important for both *in situ* stress calculations for hydraulic fracturing analysis and reservoir compaction and surface subsidence calculations. The lower limit Young's modulus case should show the greatest possible surface deformations as a result of gas production or water injection. In the Biot-Gassmann correction case, the calculated poroelastic constant is lower overall and more variable. At the top and the bottom of the log,  $\alpha_{Gassman} = 0.5$ . In the intervening strata we have  $\alpha_{Gassman} < 0.5$ , with values as low as  $\alpha_{Gassman} = 0.2$  around 7500 ft. Within the Barnett, for the  $E_{Gassman}$  case, Biot's constant is  $\alpha_{Gassman} = 0.4$  to  $0.6$ . For the  $E_{low}$  case,  $\alpha_{Biot} = 0.7$  to  $0.8$ .

#### 4. Changes in Stress State.

With regard to stress state, the best starting point is the concept of critically stressed faults (Zoback and Healy, 1984; Zoback, 2007), where it is assumed that the frictional strength of pre-existing faults in the earth's crust limits the amount of differential stress ( $S_1-S_3$ ) that can be sustained. As differential stress in the crust increases, the shear stress,  $\tau_{applied}$ , increases as (for two dimensional plane strain)

$$\tau_{applied} = \frac{S_1-S_3}{2} \sin 2\beta, \quad (7)$$

where  $\beta$  is the angle between the fault normal and the  $S_1$  direction. The frictional resistance of the fault is proportional to the normal stress acting across the fault times the friction coefficient as given by

$$\tau_{fric} = \mu(S_n - P_p) = \mu \left\{ \frac{S_1 + S_3}{2} + \frac{S_1 - S_3}{2} \cos 2\beta - P_p \right\}, \quad (8)$$

where  $\mu$  is the friction coefficient of the fault,  $S_n$  is the normal stress acting on the fault, and  $P_p$  is the pore pressure. If  $\tau_{applied}$  exceeds  $\tau_{fric}$ , the fault should slip, relieving the differential stress, and thus defining a limit to stress magnitude in the earth's crust. The critically stressed crust theory goes further to assume that there are numerous faults in the crust of many different orientations, such that there exists an optimally oriented fault at

$$\beta = \text{atan} \left( \frac{1}{-\mu} \right), \quad (9)$$

defined from linearized Mohr-Coulomb theory as that angle at which the Mohr circle just becomes tangent to the failure envelope. Making this assumption allows the equations for shear failure of faults to be rewritten with respect to fault stability, which limits the differential stress, as (Zoback, 2007)

$$(S_1 - P_p) \leq \left( \sqrt{1 + \mu^2} + \mu \right)^2 (S_3 - P_p) \quad (10)$$

Additionally, Byerlee (1978) showed that for most rock types, the friction coefficient can be assumed to have a limited range of  $0.6 \leq \mu \leq 1.0$ . For a normal faulting stress regime like that believed to be prevalent in the present day Fort Worth Basin, equation (10) can be used to constrain the magnitude of the minimum horizontal stress,  $S_{hmin}$ . Given the Andersonian faulting theory premise for normal faulting that  $S_1 = S_v$  and  $S_3 = S_{hmin}$ , the critically stressed crust theory's lower limit on  $S_{hmin}$  is given by

$$S_{hmin} \geq \frac{(S_v - P_p)}{(\sqrt{1 + \mu^2} + \mu)^2} + P_p, \quad (11)$$

where  $S_v$  is the vertical stress, equal to the integration of the specific weight ( $\rho_b g$ ) of the overburden to a given depth as

$$S_v = \int_0^z (\rho_b g) dz, \quad (12)$$

where  $\rho_b$  is the bulk density of the overburden,  $z$  is depth from the earth's surface, and  $g$  is the acceleration of gravity. In typical sedimentary basins, the specific weight (i.e., vertical stress gradient) is approximately 1 to 1.1 psi/ft, corresponding to an average density of about  $\rho_b = 2310$  to  $2540 \text{ kg/m}^3$  (the Joe Pool area logs indicate an average density at the high end of this range). Following Zoback (2007) and assuming a friction coefficient of  $\mu = 0.6$ , the limit on the horizontal stress gradient (i.e., the “frac” gradient) can be written as

$$dS_{hmin}/dz \geq 0.32 \left( dS_v/dz - dP_p/dz \right) + dP_p/dz \quad (13)$$

Bowker (2007) estimates Barnett Shale pore pressure to be on the order of  $dP_p/dz = 0.49 - 0.52$  psi/ft. Local company data reports drilling with mud densities of 9.3 to 10.5 ppg (pounds per gallon), which if balanced drilling is assumed (mud pressure equals formation pore pressure), corresponds to pore pressures of  $dP_p/dz = 0.48$  to  $0.55$  psi/ft. So expanding the Bowker (2007) range to  $dP_p/dz = 0.48$  to  $0.55$  psi/ft and using  $dS_v/dz = 1.1$  psi/ft (based on local density log data), the minimum frac gradient for the Barnett should be on the order of  $dS_{hmin}/dz = 0.68$  to  $0.73$  psi/ft. These values are on the high side of the range reported by Montgomery et al. (2005) for the Barnett Shale of  $dS_{hmin}/dz = 0.5$  to  $0.7$  psi/ft, but are lower than what is reported in local well files for 12 different treatment stages from two wells, where fracture gradient is reported to range from  $0.7$  psi/ft to  $0.85$  psi/ft. Based on local well file notes, these frac gradients are based on ISIP's (instantaneous shut-in pressures), and as such should then be considered high side estimates of the actual  $S_{hmin}$  gradients in the area. Favoring local data and discounting the highest values because they probably came from ISIP

measurements and not fracture closure, a frac gradient in the neighborhood of 0.7 to 0.8 psi/ft seems to be a reasonable estimate. These stress and pressure estimates should be expected to be inexact in shale gas, however, because of the extremely low permeability of formations like the Barnett. Pore pressure estimates are difficult to make as they require extended shut-in periods (months or more), and most operators cannot afford the economic loss that would engender. Fracture closure pressure can also require extended shut-in periods in tight rocks, and when fracturing multiple stages in a long horizontal well, time is a premium, not to mention the difficulties in interpretation that often accompany complex near-wellbore geometries that are common in horizontal well fracturing. Table 2 summarizes the pore pressure and stress data discussed.

<b>Table 2. Pore pressure and stress gradient estimation</b>		
<b>Pore Pressure Gradient</b>	<b>Frac Gradient</b>	<b>Source of Information</b>
0.49-0.52 psi/ft	<i>0.68-0.71 psi/ft (calculated from equation 13)</i>	Bowker (2007)
0.48 psi/ft	<i>0.68 psi/ft (calculated from equation 13)</i>	Mud weight of 9.3 ppg from company A
	0.5-0.7 psi/ft	Montgomery et al. (2005)
0.55 psi/ft (10.5 ppg mud weight)	0.7-0.85 psi/ft	From well files for company B

The discussion above assumes a homogenous gradient of stress across the thickness of the crust, not accounting for how mechanical property variation from layer to layer can influence stress magnitudes. An estimate of stress variation with depth can also be derived from elastic equations and the mechanical property data. This technique has been developed over many decades and has been applied to many different basins with success (Anderson et al., 1973; Prats, 1981; Narr and Currie, 1982; Warpinski, 1989). Blanton and Olson (1999) showed that log-derived stress values for sands and shales could be reasonably calculated with limited calibration information in South Texas tight gas sandstones and in siliceous mudrocks in San Joaquin Basin in California. This approach is applied here to estimate  $S_{hmin}$  variation with depth and to estimate the



magnitude of  $S_{Hmax}$ . The equations for  $S_{hmin}$  and  $S_{Hmax}$  assuming an extensional tectonic strain are (after Blanton and Olson, 1999)

$$S_{hmin} = \frac{\nu}{1-\nu} S_v + \alpha_p \frac{1-2\nu}{1-\nu} P_p + \frac{E \varepsilon_{tect}}{1-\nu^2} + \frac{E \alpha_T \Delta T}{1-\nu} \quad (14)$$

$$S_{Hmax} = \frac{\nu}{1-\nu} S_v + \alpha_p \frac{1-2\nu}{1-\nu} P_p + \frac{\nu E \varepsilon_{tect}}{1-\nu^2} + \frac{E \alpha_T \Delta T}{1-\nu}, \quad (15)$$

where  $\alpha_T$  is the linear thermal expansion coefficient (for most rocks,  $\alpha_T=5 \times 10^{-6}/^\circ\text{F}$ ),  $\Delta T$  is geothermal gradient times depth, and  $\varepsilon_{tect}$  is the tectonic strain, which is the calibration factor for both equations. Calibration can be achieved with a single  $S_{hmin}$  measurement at a depth where the rest of the information is known (requiring pore pressure, geothermal gradient and a mechanical properties log). In this study, the limiting critically stressed crust value for  $S_{hmin}$  was used as the matching value for the Barnett Shale.

The stress state computed from logs was calibrated to a 0.7 psi/ft fracture gradient in the Barnett Shale. The Barnett shows up as a local minimum in  $S_{hmin}$ , which is a good result for hydraulic fracture containment. There is a huge stress barrier predicted moving into the Ellenburger (stress difference of 4000 to 6000 psi), a result of the significant increase in Young's modulus. There is also a stress barrier above the Barnett, which for the low modulus case is on the order of 800 psi and using the Biot-Gassmann case the barrier stress difference is almost 1100 psi. In addition to the stress barrier immediately above the Barnett, there are some high modulus zones another 500 ft shallower that have very high predicted stresses that could also serve as barriers to upward fracture growth.

Finally, as mentioned earlier, the log-based stress prediction method can be used for  $S_{Hmax}$  as well as  $S_{hmin}$ . The low modulus case predicts a very small difference between  $S_{hmin}$  and  $S_{Hmax}$  of about 150 psi. The higher modulus case predicts a stress difference

on the order of 1000 psi. There is no good constraint on which scenario is the more reasonable case – there are no evaluations of  $S_{Hmax}$  magnitude in the Joe Pool area, but based on reports in the literature concerning hydraulic fracture complexity in the Barnett, it seems the low modulus case with the lowest differential stress is most consistent with observations. Most important for the purpose of protecting groundwater resources and the Joe Pool Dam and Lake is the fact that both Young's modulus scenarios have multiple apparent stress barriers to upward height growth above the Barnett.

One last consideration in the stress state is how things will change with depletion. We have assumed a beginning pore pressure of 0.5 psi/ft. If that is depleted to 0.1 psi/ft within the Barnett, the horizontal stress will decrease as

$$dS_h/dP_p = \alpha_p \frac{1-2\nu}{1-\nu} \quad (16)$$

Given a Poisson's ratio of about 0.2 and a Biot's alpha of 0.8 for the low modulus case, for every psi of pore pressure drop there should be a 0.6 psi drop in  $S_{hmin}$ . For the 0.4 psi/ft pore pressure depletion suggested, there would be a 3500 psi pore pressure drop and  $S_{hmin}$  would reduce by about 2100 psi. Consequently, refracturing in depleted zones should be even more secure with regard to height growth than initial fracture treatments. The Barnett stress could drop by as much as 2000 psi due to depletion, while the barrier zones would not be depleted, so the stress difference barrier could increase by the 2000 psi.

Changes in stress can permanently result from gas production or ephemerally result from the hydraulic fracture treatment. Segall and Fitzgerald (1998) describe the magnitude of stress change outside of a compacting reservoir. They derive an expression that states the stress change due to pore pressure change,  $\Delta S_h/\Delta P_p$ , is given by

$$\frac{\Delta S_h}{\Delta P_p} = \alpha_p \left( \frac{\pi}{4} \right) \frac{(1-2\nu)}{(1-\nu)} \frac{H}{2R} \quad (17)$$

where  $H$  is the thickness of the reservoir and  $R$  is the radius (the reservoir is assumed to take an ellipsoidal shape). Using the Joe Pool mechanical properties and a reservoir radius of 2,500 ft (the single well cluster case), the proportionality factor on the right hand side of equation (17) is only 0.025, suggesting that only 4% of the reservoir pressure changes translates into effective stress change in the overburden above the reservoir. Higher stress changes are induced at the edge of the reservoir, but Segall and Fitzgerald (1998) state that those will die off quickly away from the reservoir. They do suggest, however, that if faults are near slipping already, those near the reservoir could be induced to slip due to even minor stress perturbations. Zoback (2007) reiterates this point, hypothesizing that it is true that most of the earth's crust is critically stressed and close to the failure envelope, so that minor perturbations can cause slip. However, it is also clear that these stress perturbations, which are small near the reservoir, die off quickly and do not create measureable stress change at the surface.

Stress change due to the hydraulic fracture can be described with analytical equations from fracture mechanics. For example, the change in the stress component perpendicular to the fracture plane,  $\Delta S_n$ , due to pressurization is given by (Pollard and Segall, 1987)

$$\Delta S_n = P_{net} \left( 1 - \frac{|x^3|}{(x^2 + H_f^2/4)^{3/2}} \right) \quad (18)$$

Plotting this function (Figure 7) versus normalized horizontal distance from the fracture,  $x/H$ , shows that the stress perturbation around the hydraulic fracture dies off by 70% at one fracture height away, and 90% by a distance of twice the fracture height. Consequently, no substantial stress perturbation is expected at the earth's surface due to the hydraulic fracture. The distance to which stress acts is discussed in Fisher and

Warpinski (2012) with regard to microseismic activity. They find that typical microseismic signals are largely contained within the Barnett Shale near the hydraulic fractures. The excursions of 1000 ft or more have a different seismic character and are attributed to fluid penetration into pre-existing faults.

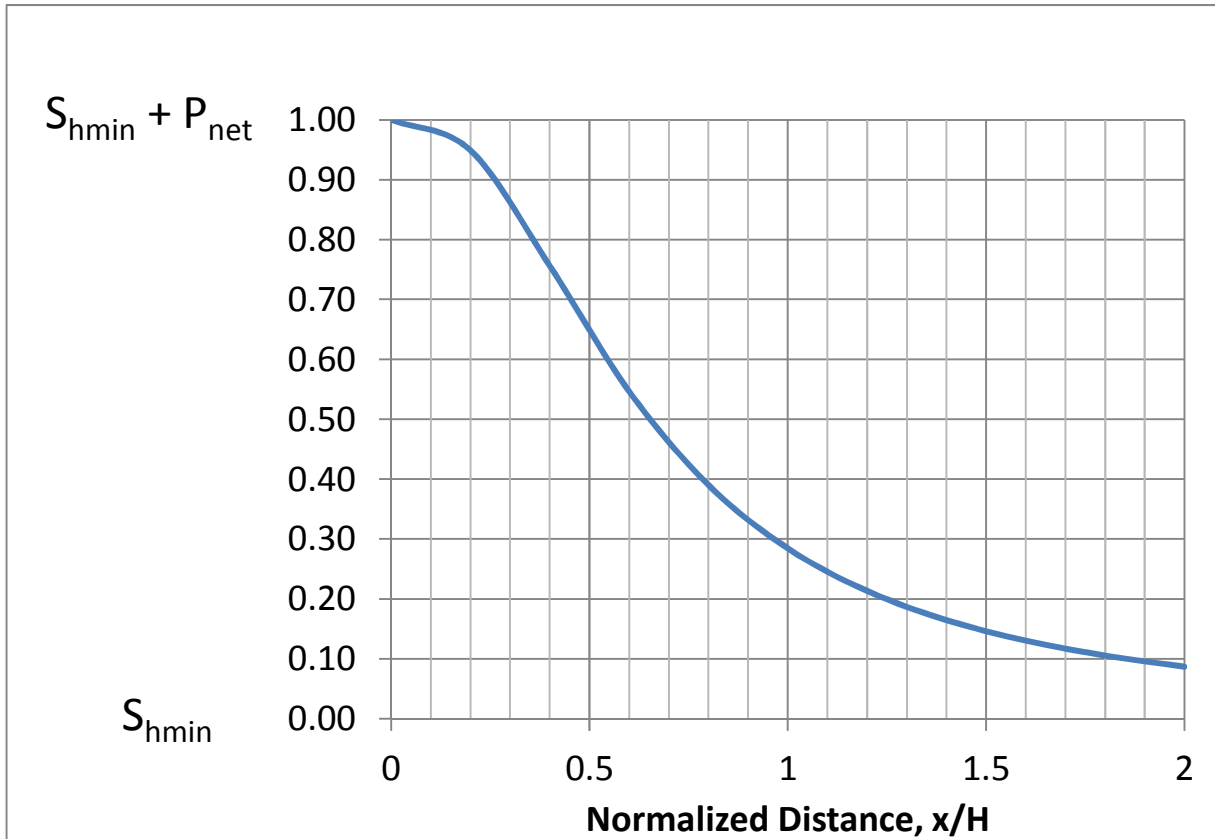


Figure 7. Stress component acting perpendicular to a hydraulic fracture of height  $H=H_f$ . The stress at the fracture face is  $S_{xx}=S_{hmin} + P_{net}$ , but at two fracture heights away ( $x/H=2$ ), the stress perturbation has diminished by 90%.

## 5. Impacts of Hydrofracturing.

Looking at local company practice for fracturing in the Joe Pool area, one well had 7 fracture stages over 3500 ft of lateral. The stages consisted of 6 perforation clusters spread over 400 ft with approximately a 300 ft spacing between stages. Each stage pumped on the order of 15,000 bbls of fluid and 400,000 lbs of sand at an average rate of 70 bbls/min. To get an idea of the extent of the fracture length, two-dimensional analytical models can be used, although standard industry practice is to use pseudo-3d numerical models when precise fracture dimensions are desired. The two dimensional

model equations are published in Valko and Economides (1995) for the Geerstma-deKlerk (GdK) and Perkins-Kern (PK) models (an equivalent source is Geerstma, 1989). For simplicity and since the Barnett shale has such a low permeability, the no leak-off versions of the models are used here. The equations are reproduced in Table 3.

<b>Table 3. Plane strain, two dimensional hydraulic fracture equations with no leak-off (after Valko and Economides, 1995)</b>	
<b>Model-parameter</b>	<b>Equations, <math>E'=E/(1-\nu^2)</math></b>
PK-length	$x_f = 0.524 \left( \frac{q^3 E'}{\mu h_f^4} \right)^{1/5} t^{4/5}$
PK-net pressure	$P_{net} = 1.52 \left( \frac{\mu q^2 E'^4}{h_f^6} \right)^{1/5} t^{1/5}$
PK-average width	$w_{avg} = 3.04 \frac{\pi}{4} \left( \frac{\mu q^2}{E' h_f} \right)^{1/5} t^{1/5}$
GdK-length	$x_f = 0.538 \left( \frac{q^3 E'}{\mu h_f^4} \right)^{1/6} t^{2/3}$
GdK-net pressure	$P_{net} = 1.09 \left( \frac{\mu E'^4}{h_f^6} \right)^{1/3} t^{1/3}$
GdK-average width	$w_{avg} = 2.36 \frac{\pi}{4} \left( \frac{\mu q^3}{E' h_f^3} \right)^{1/6} t^{1/3}$

Using the equations in Table 3, the fracture dimensions for the local well can be estimated. Table 4 gives the input based on local practice, and Table 5 gives the fracture dimensions and net pressure. The results demonstrate the differences between the PK and GdK geometry assumptions (see Figure 8 for geometry idealizations). The PK model, because its compliance with regard to fracture opening is proportional to the fracture height (which in this case is the shortest dimension) has a smaller width and greater net pressure (harder to pump viscous fluid down the narrower slot). Unlike the PK model (Figure 8), the GdK model has no variation in width over the height of the fracture, a geometry that might result if there were freely slipping horizontal

bedding planes at the top and bottom of the fracture. Because of this geometry simplification (to make this model 2d instead of 3d), the fracture opening compliance is related to fracture length. Since length is expected to be the greatest dimension for a height contained fracture case like the Barnett, the GdK model is more compliant and predicts greater fracture opening and a corresponding lower net pressure.

Both of the net pressures computed (using the PK and GdK models), however, are lower than the 500 psi or more observed in the field. This is a commonly observed limitation of 2d models when comparing them to field data, but the PK and GdK equations do honor material balance (the fracture volume is equal to the volume injected, as efficiency is 100% with no leak-off) and have results that vary with the appropriate field conditions, so these calculations are good estimates for gross fracture dimensions, assuming the fractures are actually planar and symmetric bi-wing fractures, an assumption that is not widely held with respect to shale gas fracturing in the Barnett.

**Table 4. Input parameters for fracture dimension estimation**

Parameter	Value	Units	Converted Value	Units for use in Table 5 equations
$q^{**}$	11.7	bbls/min	65.45	ft <sup>3</sup> /min
$E'$	$4.17 \times 10^6$	psi	$6.00 \times 10^8$	lb/ft <sup>2</sup>
$h$	350	ft	350	ft
viscosity	10	cp	$3.48 \times 10^{-6}$	lb-min/ft <sup>2</sup>
time	215	min	215	min
**Rate of 70 bbls/min was assumed to be divided evenly over the 6 perforation clusters.				

**Table 5. Fracture dimensions for typical fracture**

	PK	GdK
$P_{net}$	124 psi	13 psi
$x_f$	3068 ft	2024 ft
$w_{avg}$	0.16 inches	0.24 inches

Fracture dimensions and stimulated reservoir volume are more generally viewed to be a result of a complex hydraulic fracture geometry resulting from hydraulic fractures interacting with and intersecting natural fractures. The extent of hydraulic fracture

penetration into the reservoir is instead estimated empirically with microseismic data (Fisher et al., 2005), which reflects the adjustment of pre-existing natural fractures due to the stress perturbation and fluid leak-off around the propagating fracture. The empirical micro-seismic interpretation and the numerical modeling depiction of hydraulic fractures interacting with natural fractures shown in Figure 9 suggest that the hydraulic fracture network will occupy a certain volume within the reservoir and the spacing between the fractures will depend on the amount of total length created. Figure 9b can be imagined to be the fracture length created from one treatment stage, as local practice spaces 7 perforation clusters over 400 ft, which is similar to the dimensions used for the simulation. Additional discussion of Barnett Shale completions is in Appendix A.

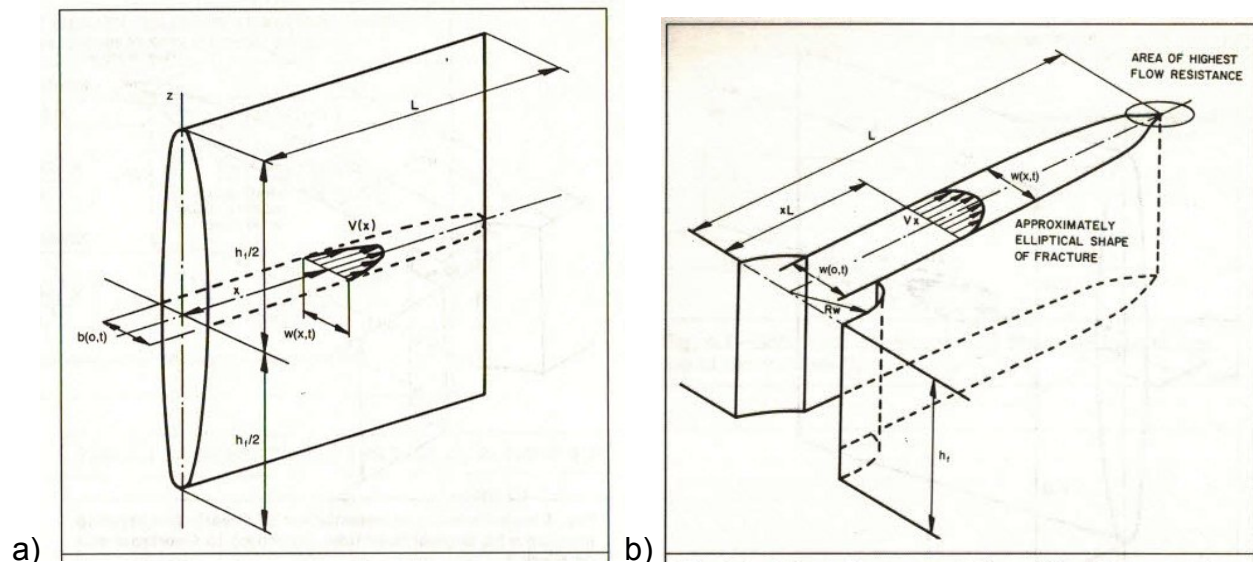


Figure 8. Two dimensional, plane strain hydraulic fracture model geometry idealizations. a) Perkins-Kern (PK). b) Geertsma-deKlerk (GdK). From Geerstma (1989).

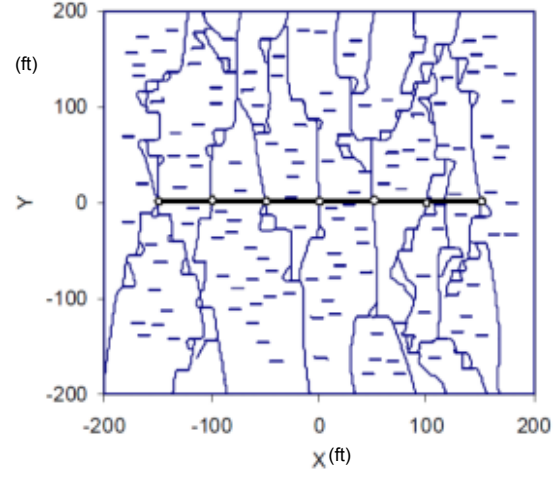
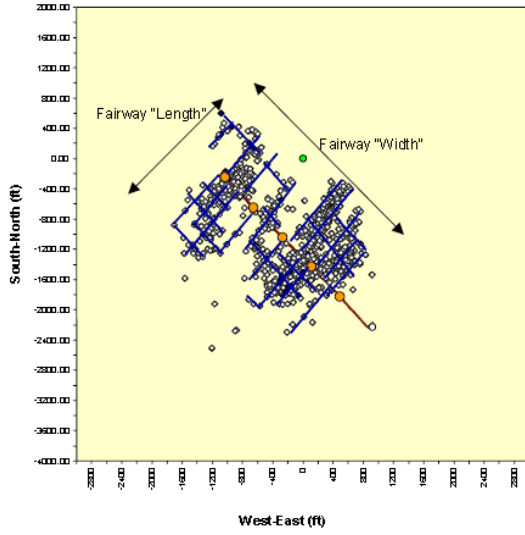


Figure 9. a) Microseismic estimation of hydraulic fracture extent around a horizontal wellbore in the Barnett Shale (Fisher et al., 2005). b) Numerical model of fracture propagation from a horizontal well stage with 7 perforation clusters (after Olson, 2008).

One point of trying to estimate fracture network geometry, beyond optimizing gas production, is to estimate whether the fracture network is sufficiently intense to alter the mechanical properties of the rock. Laboratory testing has shown that the presence of fractures in rock samples can reduce the wave propagation velocities and correspondingly the effective elastic properties (Pyrak-Nolte, 1996). Using a simple two dimensional effective Young's modulus model from Walsh (1965) as applied by Segall and Pollard (1983) for fracture patterns in rock, the ratio of effective to intrinsic modulus is given by

$$\frac{E_{eff}}{E} = \frac{1}{1 + 2\pi(1 - \nu^2)\rho} \quad (19)$$

where the fracture density  $\rho$  is defined as

$$\rho = 1/A \sum_{n=1}^N c_n^2 \quad (20)$$



The challenge is to compute a reasonable fracture dimension. The best approach using a two dimensional case is to look at the horizontal Young's modulus. A total fracture length for a given stage,  $L_{stage}$ , can be estimated using the average wing length between the GdK and PK models of 2500 ft. This computes to

$$L_{stage} = 7 * 2 * x_f = 14 * 2500 \text{ ft} = 35,000 \text{ ft}.$$

Assuming the fractures are not bi-wing planar fractures, but are arranged in a regular grid within the drainage area, the fracture spacing can be estimated. The width of a stage is 400 ft plus a 300 ft spacer, so we will use  $w_{stage}=700$  ft. In addition, to accommodate some fracture penetration in the traditional sense away from the wellbore, roughly as shown in Figure 9a, the drainage length perpendicular to the wellbore will be assumed to be 1400 ft. With these assumptions, the approximate spacing between fractures in each direction is 50 ft (twelve 700 ft fractures spaced along  $w_{stage}$  and twenty-four 700 ft fractures spaced along  $L_{stage}$ ). Since we are doing the horizontal effective modulus in a cross-section, however, the half-dimension,  $c_n$ , for equation 23 is the half-height, which would be  $H_f/2=175$  ft (Figure 10). The fracture density,  $\rho$ , is evaluated as

$$\rho = \frac{1}{700 \text{ ft} \cdot 350 \text{ ft}} 12 \cdot (175 \text{ ft})^2 = 1.5$$

and the effective modulus ratio is

$$\frac{E_{eff}}{E} = \frac{1}{1 + 2\pi(1 - .2^2) \cdot 1.5} = 0.10$$

Given the estimated density of the hydraulic fracturing, then, the horizontal Young's modulus could be reduced 90% with regard to extension. With regard to contraction, the result would depend on what is filling the fractures. Presumably the proppant would have a lower Young's modulus than the Barnett shale around it, as the proppant is simply randomly pack sand grains, and there may be some unpropped regions of the

fracture that stay open because of fracture roughness related asperities. Consequently, the closing stiffness would be greater, but I was unable to find an appropriate analytical relationship to assess by how much. A conservative approach might be to assume halfway between 0.10 and 1.0, or about 0.55. With regard to reservoir compaction, which will be discussed later, the horizontal Young's modulus is less important than the vertical Young's modulus, but it will contribute to the ability of the reservoir to contract laterally as depletion occurs, and it will affect the elastic anisotropy in the shale, which is already thought to be considerable (Baree et al., 2009).

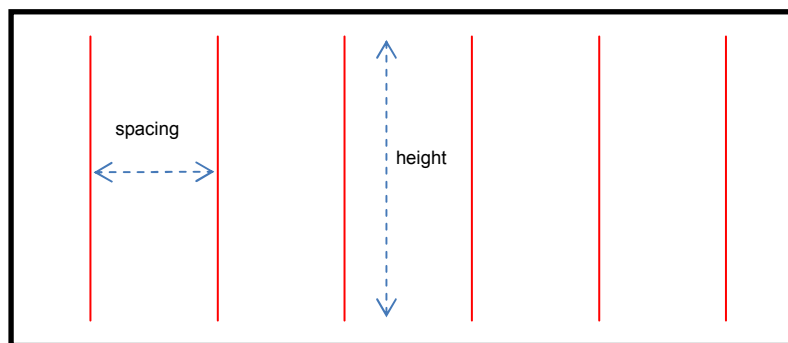


Figure 10. Vertical cross section for visualizing the horizontal effective Young's modulus calculation. Body is two dimensional, plane strain, and infinite, but fracture array has regular spacing and limited height.

## 6. Subsidence.

Normally, surface subsidence is only of concern for very shallow reservoirs or highly compressible formations. Ground subsidence of 5 ft or more has been experienced over depleting shallow oil reservoirs in California (Inglewood Field, Thumbs, Lost Hills, Belridge). Significant deformation has also been observed on the Gulf coast in Texas due to oil and gas depletion and aquifer pumping. In the Fort Worth Basin, subsidence seems a remote possibility considering the depth and siliceous nature of the Barnett Shale, and the competent nature of formations throughout the geologic column, with stiff limestones below the Barnett and in much of the Cretaceous section. However, even small vertical movements can be a potential concern for large surface structures like a dam and its impounded lake, where surface tilt and elevation change could adversely affect their performance.

This study uses published analytical equations to make scoping calculations of the magnitude of potential elastic surface deformations in the Joe Pool area. If the magnitude of the signal calculated in this manner is significant, a more rigorous numerical study would most likely be justified, where earth heterogeneity could be accommodated and non-elastic mechanisms included.

Elastic reservoir compaction,  $\Delta h$ , can be written as (Geertsma, 1973)

$$\Delta h = hc_m \Delta P \quad (21)$$

where  $h$  is the thickness of the depleting reservoir,  $\Delta P$  is the amount of pressure depletion, and  $c_m$  is the uniaxial compaction coefficient, defined as

$$c_m = \alpha_P \frac{(1+\nu)}{(1-\nu)} \frac{c_b}{3} \quad (22)$$

where  $c_b$  is the reservoir rock's bulk compressibility, which is the inverse of bulk modulus,  $K_b$  (see equation 4). Geertsma (1973) presents an analytical solution for a horizontal, circular disk shaped reservoir in a homogeneous elastic halfspace which is convenient for our scoping study. Maximum subsidence for a reservoir with a given ratio of depth to radius, or  $\eta=Z/R$ , is given by

$$u_z^{max} = 2(1-\nu)\Delta h \left(1 - \frac{\eta}{\sqrt{1+\eta^2}}\right) \quad (23)$$

Du and Olson (2001) illustrate that as the depth to radius ratio,  $\eta$ , increases, the amount of reservoir compaction that is expressed as subsidence diminishes (Figure 11). Also, the gradient of displacement moving from the middle of the subsidence bowl to the outer edge becomes gentler for deeper reservoirs. The other thing that should be noted is that the maximum displacement gradients (tilts) come at the edge of the reservoir.

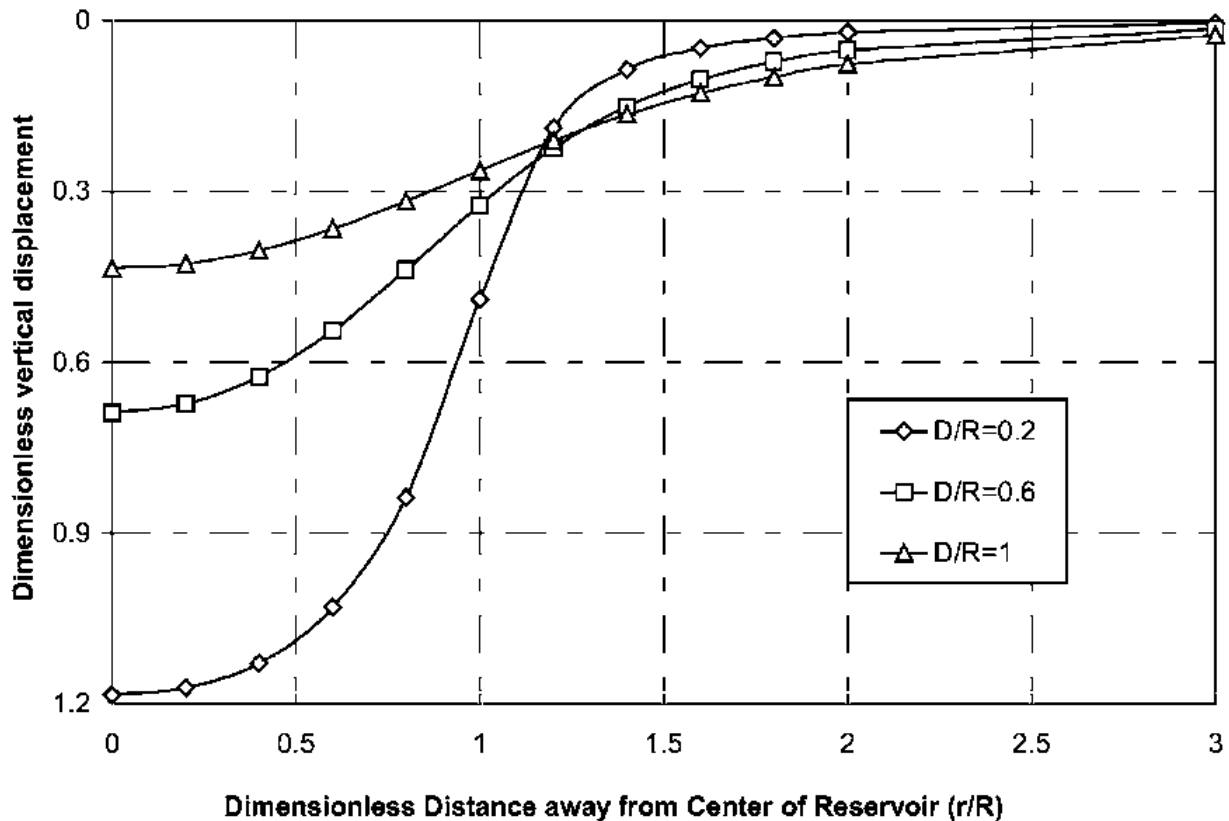


Figure 11. Impact of depth to reservoir radius ratio,  $Z/R$ , on subsidence bowl shape. From Du and Olson (2011).

Chan and Zoback (2006) employed Geerstma's method to model land subsidence on the Louisiana coast. A big difference between that case and the Barnett shale is the compressibility of the geologic column, including the reservoir. In the Louisiana case, the reservoir is unconsolidated sand, and the overburden is young, poorly consolidated sand and shale with common listric normal faulting, a trait of recent, unconsolidated sediment. In that situation, an elastic model is expected to underpredict subsidence because of likely inelastic (viscoelastic and plastic) deformation that occurs as the reservoir compacts. Chan and Zoback (2006) found that the computed 8 cm of subsidence using the Geerstma approach underpredicted the observed subsidence over the reservoir of approximately 15 cm. They subsequently applied an elastic-viscoplastic model (based on work in Hagin and Zoback, 2004) and found that it slightly overpredicted the subsidence, but the two models bracketed observations. The main contribution of faulting was concluded to be in the shape of the subsidence pattern. The

Geerstma approach resulted in a generally symmetric subsidence bowl given the symmetric shape of the reservoirs, but the leveling data showed a strong deepening toward the east signal that was attributed to slip on a nearby fault, although the goodness of fit between the observations and model predictions was pretty low.

Using equation (21) and (22), elastic reservoir compaction in the Barnett Shale can be approximated. A problem with estimating subsidence in this situation is uncertainty about mechanical properties. No laboratory samples were collected or tested for this study. Mechanical property estimation, as described earlier, relied on one dipole log from the Joe Pool area and data from the literature. As described above, log analysis of Joe Pool area wells resulted in Young's modulus values of  $2.5 \times 10^6$  to  $5 \times 10^6$  psi depending on the dynamic to static correction method chosen, and these values are at the lower end of the published static modulus range in the literature of  $4 \times 10^6$  to  $13 \times 10^6$  psi. Since the Joe Pool area has only been recently developed (starting in 2007), much of the property data in the literature appears to be from other parts of the Barnett Shale play, such as in the core area of the Newark East field, so one explanation could be that the Barnett in the Joe Pool area is substantially different than what is found elsewhere in the Fort Worth Basin. Verification of such a hypothesis would require acquiring and testing core – a priority for future study. In the meantime, however, three scenarios have been chosen to try to bracket possible deformations over a 30 year lifespan of Barnett shale gas production in the Joe Pool area. The high end Young's modulus is chosen to be the value from the log using the Biot-Gassman correction, a value of  $E_{best} = 5 \times 10^6$  psi for the best case scenario (i.e., least deformation). The limiting static corrected value based on Baree et al. (2009) of  $E_{con} = 2.5 \times 10^6$  psi will be used for the conservative scenario, and the worst case scenario will use  $E_{worst} = 1 \times 10^6$  psi. This additional reduction in modulus is intended to allow for possible reduction in long-term Young's modulus due to water weakening and creep (Akrad et al., 2011; Sone and Zoback, 2011). Poisson's ratio is presumed to be 0.15 for the conservative case scenario, as this was the value from the log and is the most likely value as it is the only measurement. For the best and worst case scenario Poisson's ratio is varied  $\pm 0.05$ , using 0.2 for the best case and 0.1 for the worst case. The dependence of compaction

and subsidence on Poisson's ratio is primarily through the compressibility as shown in equation (4), and higher Poisson's ratio increases bulk modulus which in turn results in lower compressibility.

This worst case scenario value of Young's modulus is pretty low as compared to the general static (but short term) values discussed in the literature, but as has been discussed, elastic compaction/subsidence models are already expected to underestimate subsidence and compaction because of excluding heterogeneity and inelastic deformation. Even though the worst case is unlikely, it is valuable to evaluate as a bounding case, for if the worst case scenario is still within the safety limits for the performance of Joe Pool Lake and dam, then there should be no concern nor need for better data collection. If the worst case (or any) scenario generates results of concern, more study would be warranted, particularly with regard to the time-dependent behavior of the Barnett shale under increased effective stress caused by gas production.

In addition to using three scenarios for mechanical properties, two approaches were used to calculate surface deformation for the Joe Pool area. Firstly, the simple analytic equations (21) to (23) were utilized to estimate bounding values of maximum subsidence. Secondly, the more expansive equations of Geerstma (1973) were used to populate the subsurface with multiple disc-shaped reservoirs roughly corresponding with expected development well density, and the spatial variation of surface subsidence was computed numerically using a spreadsheet and discretized integral tables.

Firstly, Table 6 gives the common data for all scenarios used to compute reservoir compaction (eqn. 21) and maximum subsidence (eqn. 23).  $K_{grain}$  is used to calculate Biot's poroelastic constant (eqn. 5). Reservoir thickness is assumed to be 350 ft based on local resistivity logs, and the same logs were used to determine depth to the center of the reservoir as 8600 ft. The 3440 psi pressure drawdown, assumed to be the 30 year abandonment pressure, is estimated as 0.4 psi/ft reduction in pore pressure gradient by depletion. Lewis and Hughes (2008) show long term bottomhole flowing pressures data as low as 100 psi for Barnett wells, theoretically implying that long term reservoir pressure could reach that low. If initial reservoir pressures are on the order of

0.55 psi/ft as suggested by local drilling practice, a depletion of 0.4 psi/ft would still leave on the order of 1300 psi in the reservoir, suggesting the chosen depletion amount is not unreasonable.

Table 6. Common Input Data		
Parameter	Value	Comments
$K_{\text{grain}}$	$5.4 \times 10^6$ psi	Assuming quartz grain material
Reservoir thickness, H	350 ft	based on local logs
Depth to center of reservoir, Z	8600 ft	based on local logs
Pressure depletion in 30 years	3440 psi	

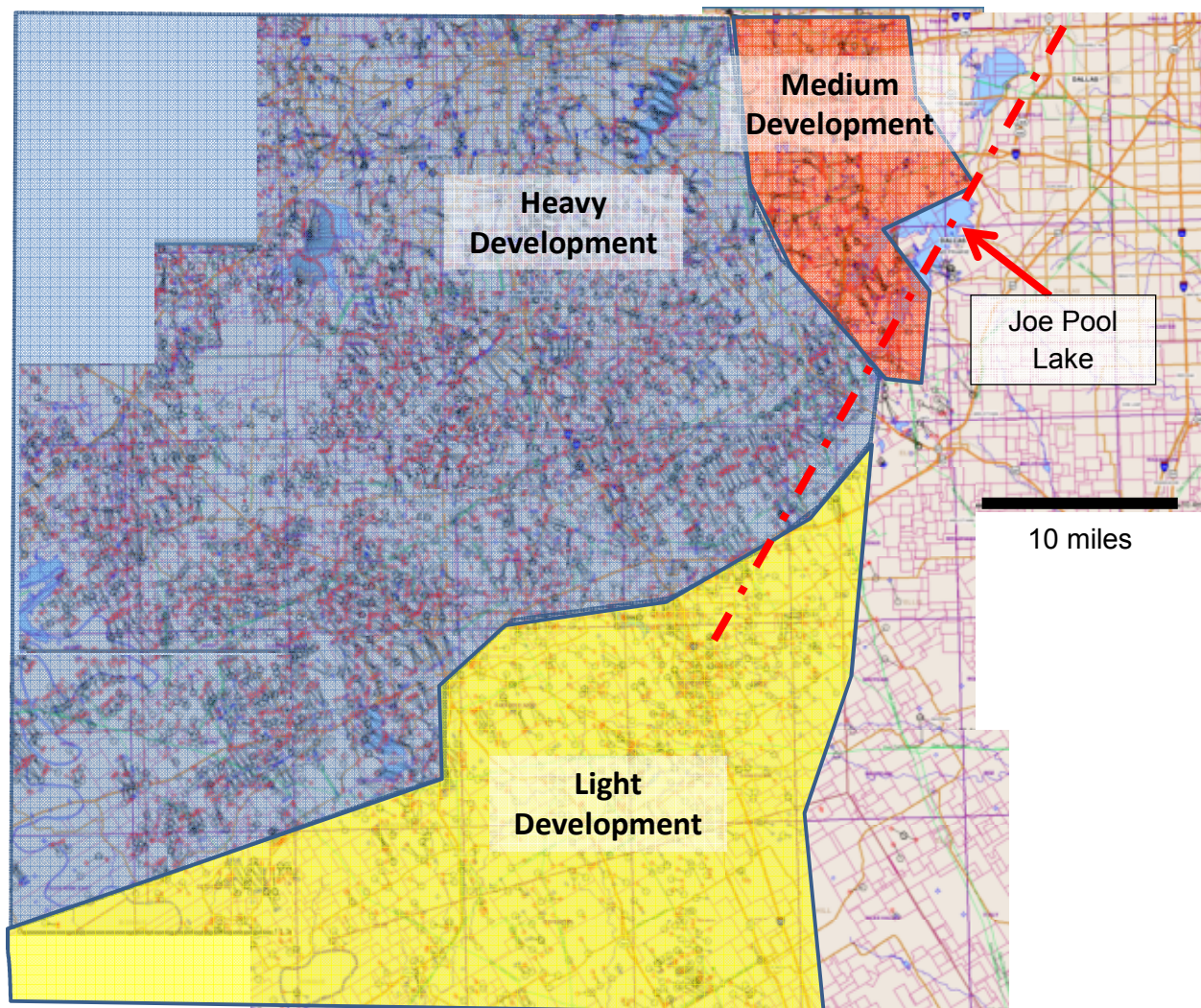


Figure 12. Location map for Joe Pool Lake, well surface locations (black pentagons) and bottomhole locations (red circles with outward spokes). Straight lines connecting surface and bottomhole locations are not well trajectories – they are just straight lines for reference. From <http://www.rrc.state.tx.us/data/online/gis/index.php>.



With the common data given in Table 3, the conservative case scenario in Table 4 depicts the rest of the parameters used to calculate compaction and subsidence for a single well pad in isolation (estimated to have a depletion radius of 2500 ft) and for the larger reservoir in the Joe Pool area (a reservoir radius of 15 miles is assumed - see Fig. 12). Looking at Fort Worth Basin-wide development, however, a radius of more like 50 miles could be argued based on well intensity according to Texas Railroad Commission records, queried on July 1, 2012 at (<http://www.rrc.state.tx.us/data/online/gis/index.php#>). Nonetheless, at a depth to radius ratio,  $\eta = Z/R = 0.1$ , the  $\eta$  factor in equation (21) is already 0.9 (the maximum is 1), so increasing the reservoir depletion radius beyond 15 miles will have little impact on results.

In the conservative scenario,  $E_{con} = 2.5 \times 10^6$  psi and Poisson's ratio is  $\nu_{con} = 0.15$ , which dictate the other mechanical properties in Table 4, including  $\alpha_p = 0.824$  and  $c_b = 1.05 \times 10^{-6}$ /psi (about 1 microsip, *a.k.a* msip). With these values, and *for one pad in isolation*, the reservoir compaction is expected to be 4.3 inches over the total vertical thickness of 350 ft, giving a vertical strain in the reservoir of only 0.1%. This 4.3 inches of compaction results in only 0.29 inches of subsidence for a single well pad. However, if we look instead at the additive effect of many such wells densely spaced under Joe Pool Lake and to the west, the same compaction of 4.3 inches (note the compaction value doesn't depend on the reservoir radius) causes 6.5 inches of subsidence at the surface. This number is actually greater than the compaction, a phenomenon that is predicted for very low ratios of depth to radius, as is the case here ( $\eta = 0.11$ ). This implies that not only does the reservoir compact, but the bottom of the reservoir is actually pushed down into the substrate due to the deformation. Given the fact that the Ellenburger is nearly twice the Young's modulus of the Barnett and maybe 3 times the stiffness of the overburden, this extra subsidence effect might be suppressed in a simulation including a layered elastic modulus heterogeneity. The expectation then would be that the maximum subsidence for this case of small depth to radius,  $\eta$ , would be unlikely to exceed the compaction amount.



<b>Table 7. Conservative Case Scenario</b>		
E (Young's modulus)	$2.50 \times 10^6$ psi	based on local logs for overburden
$\nu$ (Poisson's Ratio)	0.15	based on local logs for overburden
$K_{rock}$ (bulk modulus)	$1.19 \times 10^6$ psi	based on local logs for overburden
$\alpha_p$ (Biot's poroelastic constant)	0.780	based on local logs for overburden
$c_b$ (bulk compressibility)	$0.84 \times 10^{-6}$ /psi	
$c_m$ (uniaxial compaction coefficient)	$0.29 \times 10^{-6}$ /psi	eqn. (22)
<b>A) Single pad</b>		
Reservoir radius, R, for one pad	2500 ft	estimated from wellbore trajectories, lateral length, and frac job microseismic
$\eta=Z/R$	3.44	Geertsma (1973)
$\Delta h$ (reservoir compaction)	<b>4.27 inches</b>	eqn. (21)
Maximum subsidence (centered over reservoir)	<b>0.29 inches</b>	eqn. (23)
<b>B) Multiple Wells over Region</b>		
Reservoir radius, R	79,200 ft (15 miles)	based on development around Joe Pool
$\eta=Z/R$	0.109	
$\Delta h$	<b>4.27 inches</b>	eqn. (21)
Maximum subsidence	<b>6.47 inches</b>	eqn. (23)

The best case scenario constitutes applying the stiffest possible parameters for the mechanical properties to diminish subsidence and compaction. With  $E_{best} = 5 \times 10^6$  psi and  $\nu_{best} = 0.20$ , the poroelastic constant is very low,  $\alpha_p = 0.486$ , as is the compressibility at  $c_b = 0.36 \times 10^{-6}$  /psi. Now the predicted reservoir compaction is only 1.26 inches, and the surface expression for a single well pad shrinks to 0.08 inches. The more realistic geometry for subsidence, taking into account the greater reservoir extent, still only reaches a maximum subsidence of 1.80 inches.

<b>Table 8. Best Case Scenario</b>		
E (Young's modulus)	$5.00 \times 10^6$ psi	based on local logs for reservoir
$\nu$ (Poisson's Ratio)	0.2	based on local logs for overburden
$K_{rock}$ (bulk modulus)	$2.78 \times 10^6$ psi	based on local logs
$\alpha_p$ (Biot's poroelastic constant)	0.486	based on local logs
$c_b$ (bulk compressibility)	$0.36 \times 10^{-6}$ /psi	
$c_m$ (uniaxial compaction coefficient)	$0.09 \times 10^{-6}$ /psi	eqn. (22)
<b>A) Single pad</b>		
Reservoir radius, R, for one pad	2500 ft	estimated from wellbore trajectories, lateral length, and frac job microseismic
$\eta=Z/R$	3.44	Geertsma (1973)
$\Delta h$ (reservoir compaction)	<b>1.26 inches</b>	eqn. (21)
Maximum subsidence (centered over reservoir)	<b>0.08 inches</b>	eqn. (23)
<b>B) Multiple Wells over Region</b>		
Reservoir radius, R	79,200 ft (15 miles)	based on development around Joe Pool area
$\eta=Z/R$	0.109	
$\Delta h$	<b>1.26 inches</b>	eqn. (21)
Maximum subsidence	<b>1.80 inches</b>	eqn. (23)

Finally, the worst case scenario reduces the conservative Young's modulus by  $\frac{1}{2}$  to  $E_{worst} = 1 \times 10^6$  psi. A lower bound value of  $\nu_{worst} = 0.10$  is included as well, giving a compressibility of  $c_b = 2.40 \times 10^{-6}$  /psi (2.4 msip), a number high enough to account for any possible non-elastic response. Additionally, Biot's poroelastic constant is calculated to the highest scenario value of  $\alpha_p = 0.923$ . With these limiting values, reservoir compaction is 13.03 inches, three times the conservative case estimate. The maximum surface subsidence for an isolated pad is only 0.93 inches, however, indicating the importance of the ratio  $\eta$ . However, assuming field-wide depletion, subsidence escalates to almost 21 inches. Figure 13 depicts subsidence for the whole reservoir depletion case versus mechanical properties, highlighting the strong but non-linear dependence of subsidence results on Young's modulus.

Table 9. Worst Case Scenario		
E (Young's modulus)	$1.00 \times 10^6$ psi	lowering elastic constant to account for possible non-elastic effects
$\nu$ (Poisson's Ratio)	0.1	
$K_{\text{rock}}$ (bulk modulus)	$4.16 \times 10^5$ psi	based on local logs
$\alpha_p$ (Biot's poroelastic constant)	0.923	based on local logs
$c_b$ (bulk compressibility)	$2.40 \times 10^{-6}$ /psi	
$c_m$ (uniaxial compaction coefficient)	$9.02 \times 10^{-8}$ /psi	eqn. (22)
A) Single pad		
Reservoir radius, R, for one pad	2500 ft	estimated from wellbore trajectories, lateral length, and frac job microseismic
$\eta = Z/R$	3.44	Geertsma (1973)
$\Delta h$ (reservoir compaction)	<b>13.04 inches</b>	eqn. (21)
Maximum subsidence (centered over reservoir)	<b>0.93 inches</b>	eqn. (23)
B) Multiple Wells over Region		
Reservoir radius, R	79,200 ft (15 miles)	based on development around Joe Pool area
$\eta = Z/R$	0.109	
$\Delta h$	<b>13.04 inches</b>	eqn. (21)
Maximum subsidence	<b>20.93 inches</b>	eqn. (23)

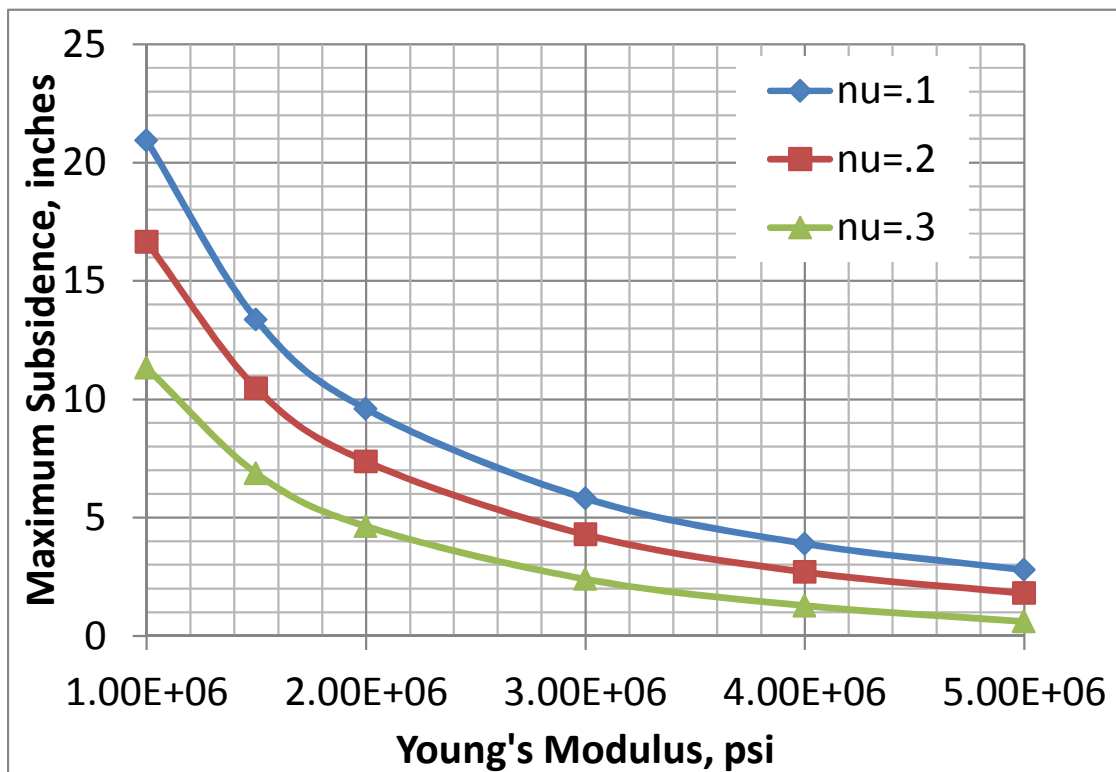


Figure 13. Dependence of subsidence on elastic properties for the whole reservoir depletion case (R=15 miles).

In addition to the single value of maximum subsidence, the distribution of that vertical displacement is important, as is the distribution of the reservoirs that are causing the subsidence. The impact can be very different if the subsidence is concentrated over a few hundred lateral feet at the surface or spread over miles. It is also important whether wells are beneath Joe Pool or far away, and it is important whether each depleted region butts up against the neighboring depleted zone or if they are widely space. To answer these questions, and to put these number in perspective considering the size of Joe Pool Dam and Lake, numerical computations were performed to include the spatial variation of wells around Joe Pool and to compute the spatial variation of subsidence.

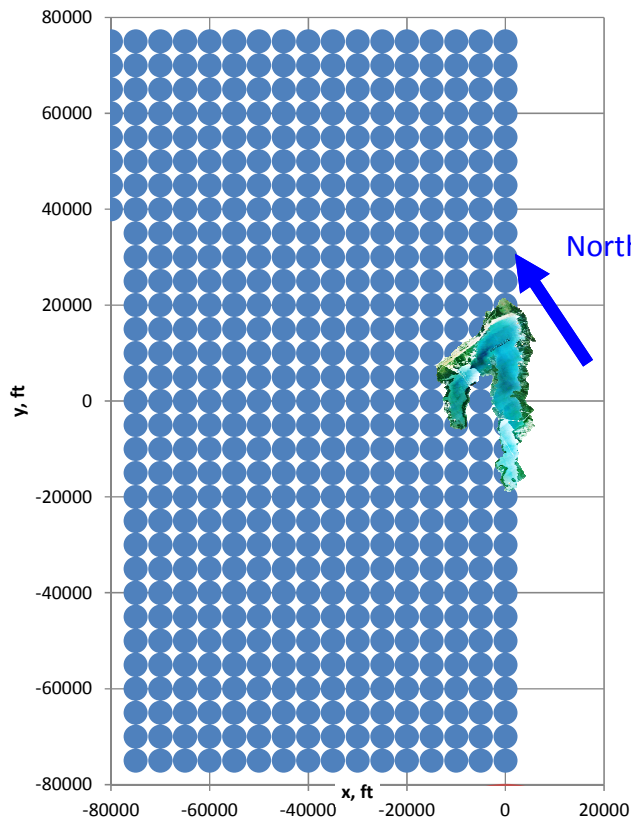


Figure 14. Disc-shaped reservoir locations for the case of full Barnett Shale development up to and under the eastern leg of Joe Pool Lake. Reservoir discs have a 5000 ft diameter, a 350 ft thickness and an 8600 ft depth. Image of Joe Pool is included to scale, and blue arrow indicates north.

In addition to using the best, conservative and worst case scenario properties, two new field development geometries are introduced. The first case, which is the worst case geometry scenario, but probably the most likely, is for every possible well location for Barnett development within 30 miles of Joe Pool Lake to be drilled and depleted. The second scenario is to make an assessment of development intensity based on current

well locations, and using that estimation the ultimate subsidence effects are computed assuming no more drilling.

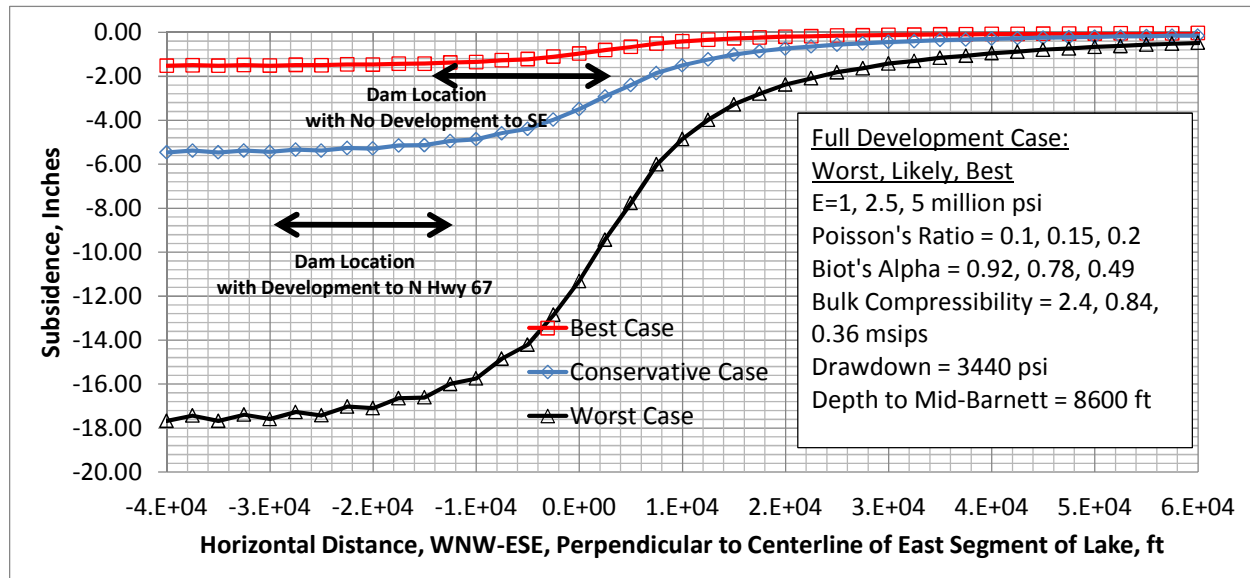
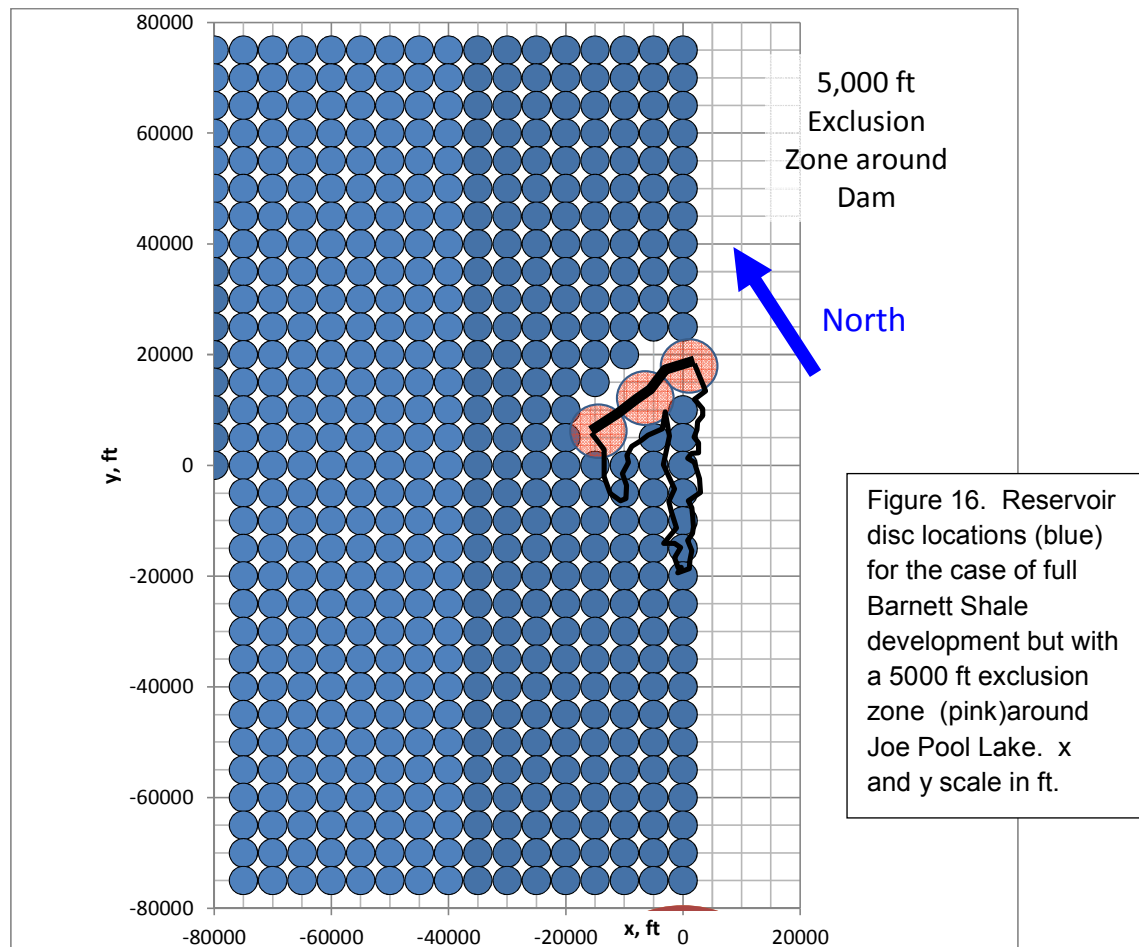


Figure 15. Subsidence along the x-direction at the coordinate of y=0 in Figure 14 (y runs NNE-SSW).

Starting with the more likely full development case, we have two variations. In the first, well pad locations are limited to the present-day boundary of no development to the east of the eastern leg of Joe Pool Lake (see red dashed line in Fig. 12). The other variation is to have development continue another 15,000 ft ESE to the location of N. Hwy 67. From Figure 1, it is clear that the Fort Worth Basin is truncated to the southeast by the Ouachita front, and its mapped location is close to the trace of the highway. Figure 14 shows the location of a regular grid of 2500 ft radius, disc-shaped reservoirs (representing typical well clusters) with Joe Pool added to scale. Figure 15 shows the subsidence in the Joe Pool area for the development geometry described using the conservative, best and worst mechanical property scenarios. The easternmost well clusters have their centers at x=0 and a corresponding reservoir edge at x=2500 ft, but it is evident that the subsidence bowl reaches much further to the ESE. The location of each end of Joe Pool Dam is indicated for the variation where development doesn't move eastward past the dam and for the case when wells run up to N. Hwy 67. (Instead of moving the well locations to recompute the problem for the

figure, the dam was instead moved 15,000 ft to the WNW to reflect its position further into the subsidence bowl.)

The steepest slope on the margin of the subsidence bowl runs from approximately  $x=0$  to 10,000 ft, rising in the worst case at approximately 0.08 inches per 100 linear ft (or roughly 8 inches from one end of Joe Pool Dam to the other, noting that the dam is askew to the computation trace along the x-axis). In the conservative case, this is reduced by two thirds, and for the best case scenario, the maximum slope is on the order of 0.001 ft per 100 ft.



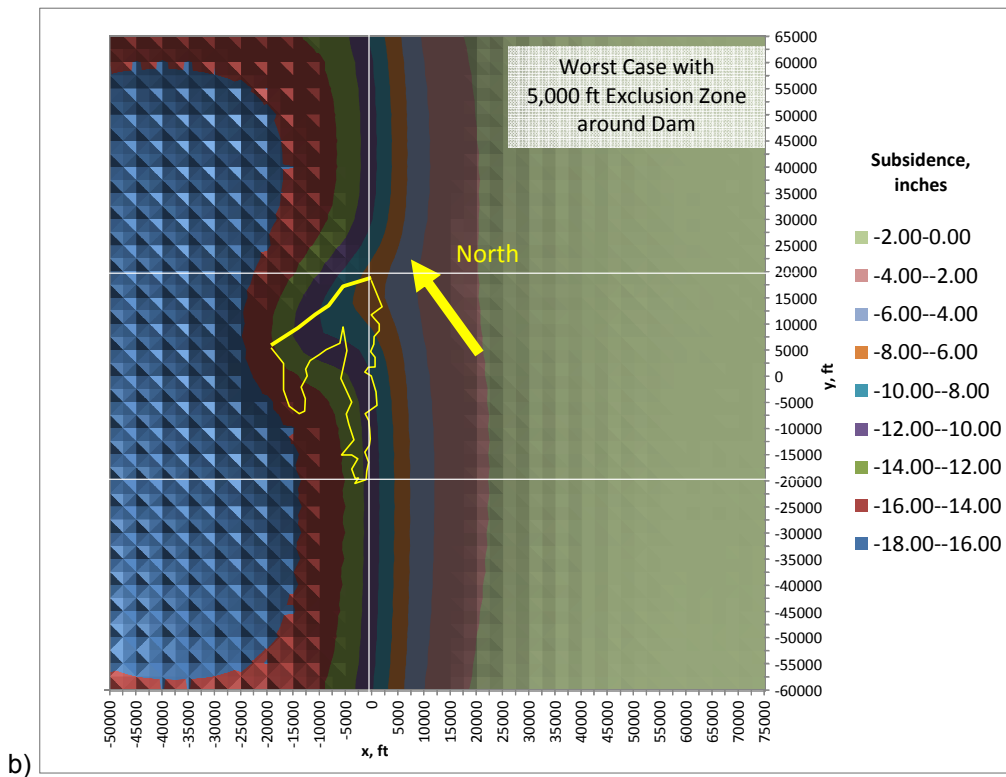
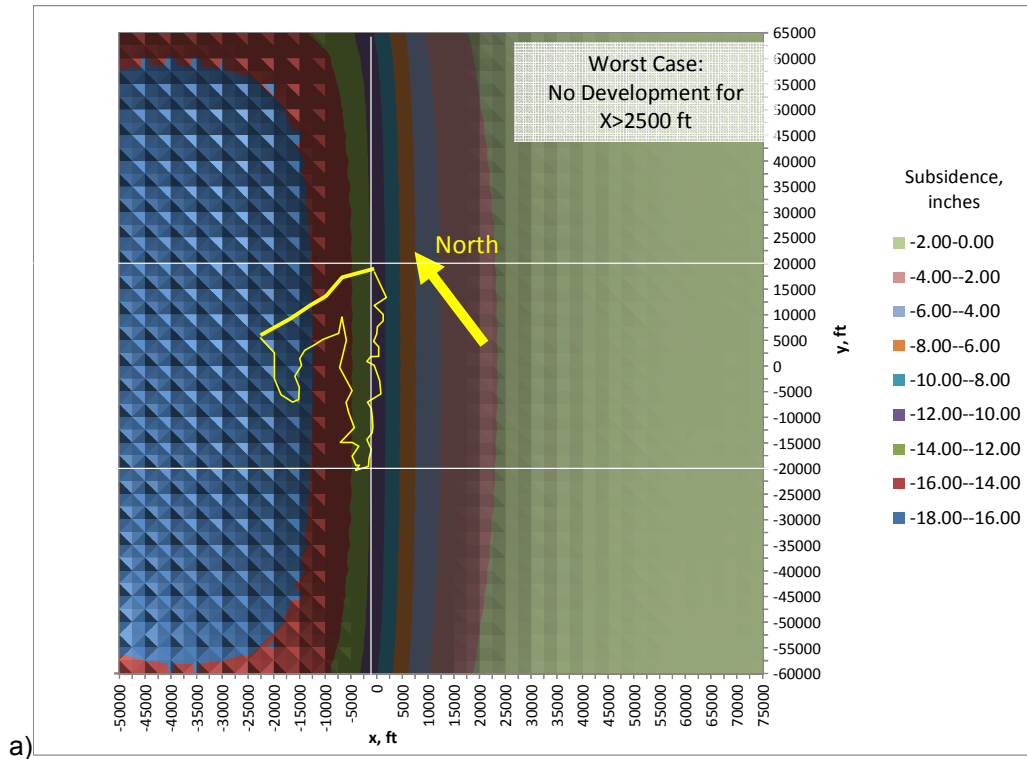


Figure 17. Subsidence bowl for Joe Pool area a) without and b) with the 5000 ft radius exclusion zone using Worst Case mechanical properties (see Table 9). Subsidence scale is in inches, x and y are in ft., and both plots have the same scale. Thin yellow line outlines Joe Pool Dam and lake.

Assuming the subsidence from the conservative or worst cases might be too much to maintain dam performance, additional calculations were made with exclusion zones of varying magnitude placed around the dam to see if they could mitigate the subsidence at the dam. The subsidence evaluations are for full depletion as before, and assuming intense development everywhere around the dam except within the exclusion zone. Figure 16 shows the trace of the dam and lake, with light red circles indicating a 5000 ft radius exclusion zone. Starting with the worst case mechanical properties, the spatial distribution of subsidence is shown with no exclusion zone (Fig. 17a) for reference. In the case with a 5000 ft radius exclusion zone (Fig. 17b), there is a clear excursion in the subsidence around the dam caused by the exclusion zone, but the subsidence magnitude experienced by the dam is still pretty large, from 14 inches at the west end to 7 inches on the east end.

Increasing the exclusion zone to 10,000 ft (Fig. 18a) reduces the subsidence range on the dam to 10 inches at the eastern end and 5 inches at the east (Fig. 18b). Doubling the exclusion zone again to 20,000 ft (Fig. 19a) cuts the subsidence down to a range of 5 to 3 inches (Fig. 19b). These calculations show that there is a mitigation solution for dam subsidence that can work, but there are already numerous wells within these exclusion areas.



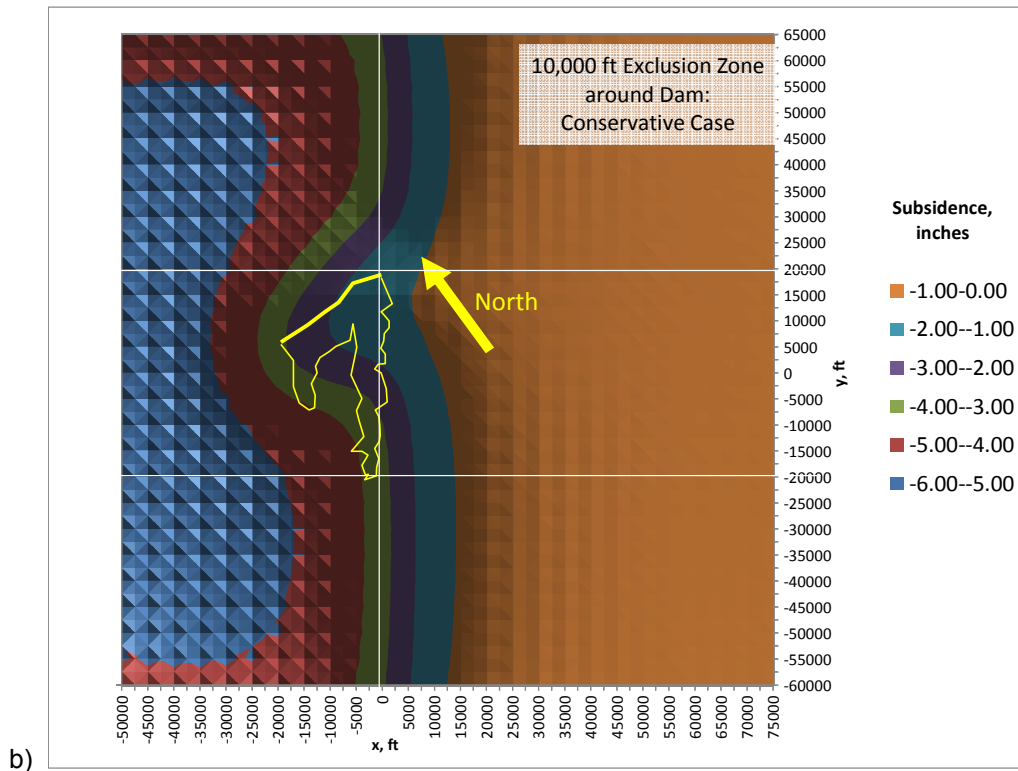
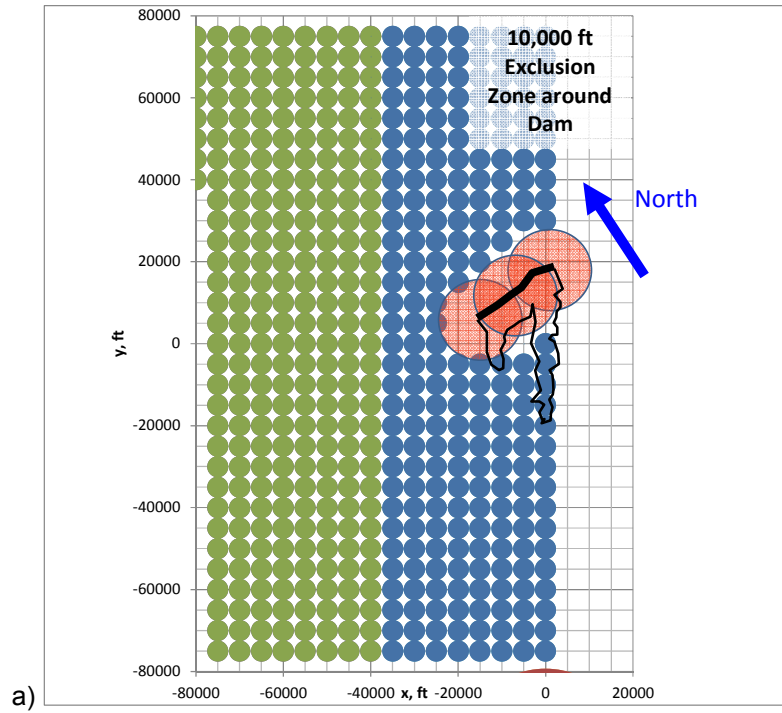


Figure 18. a) Reservoir disc geometry with a 10,000 ft exclusion zone around Joe Pool Dam. b) Subsidence for the Worst Case mechanical properties. Subsidence scale is in inches, x and y are in ft.

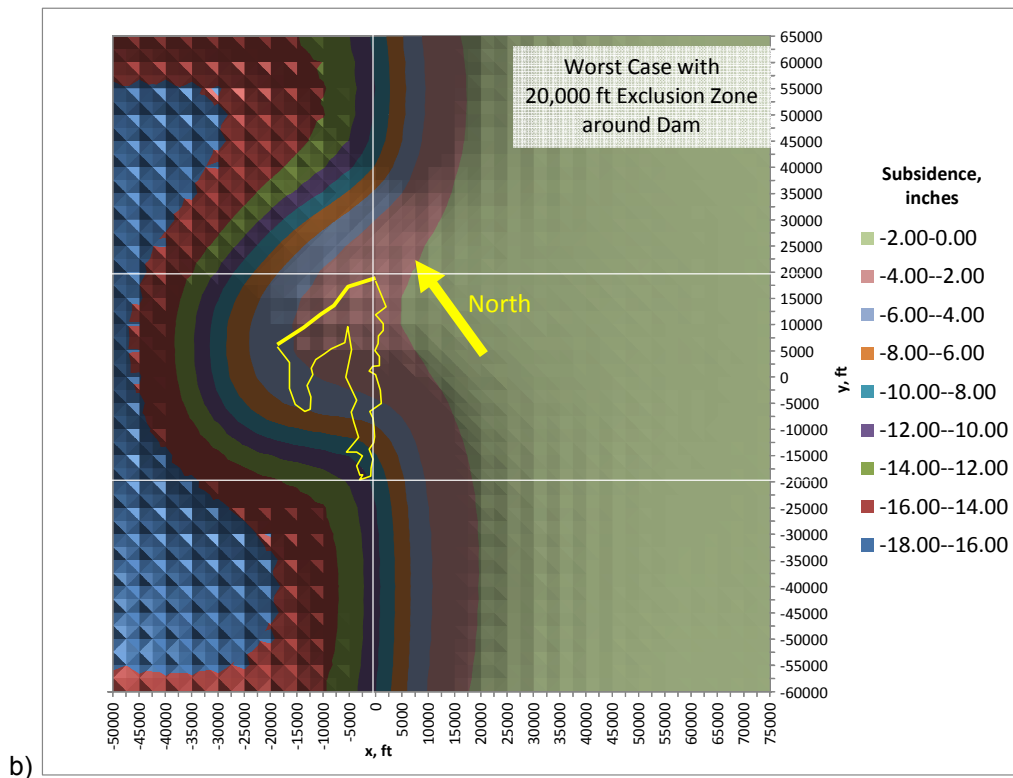
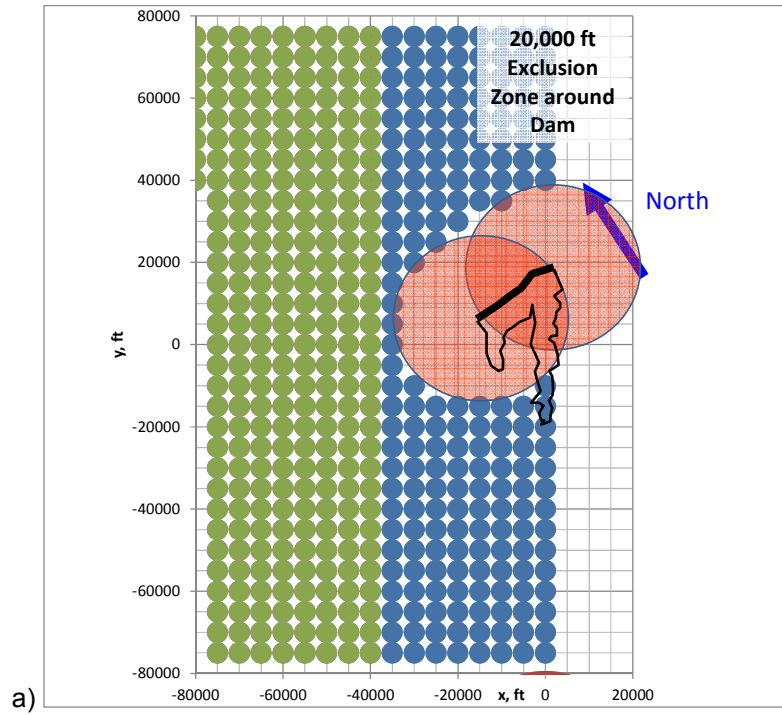
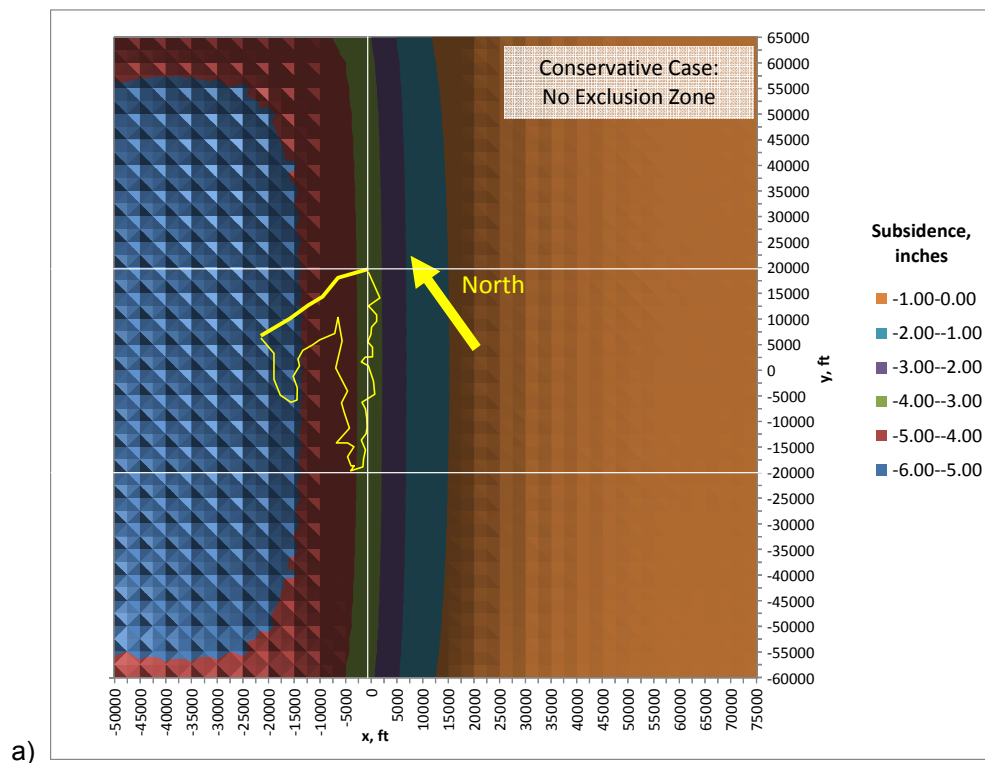
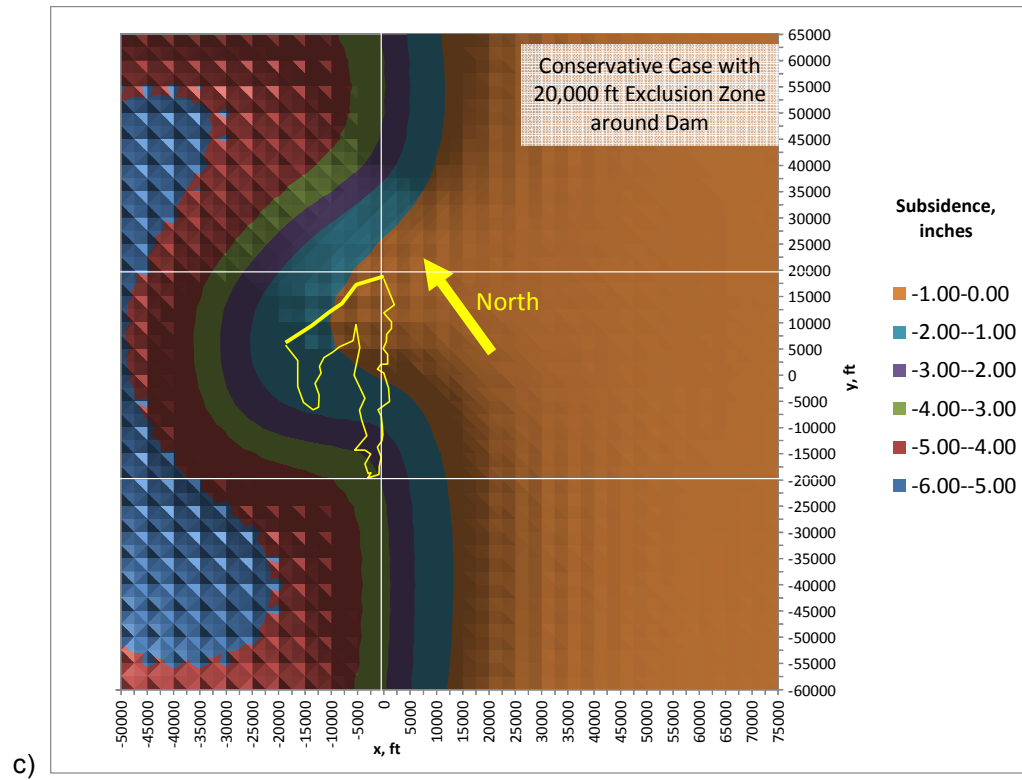
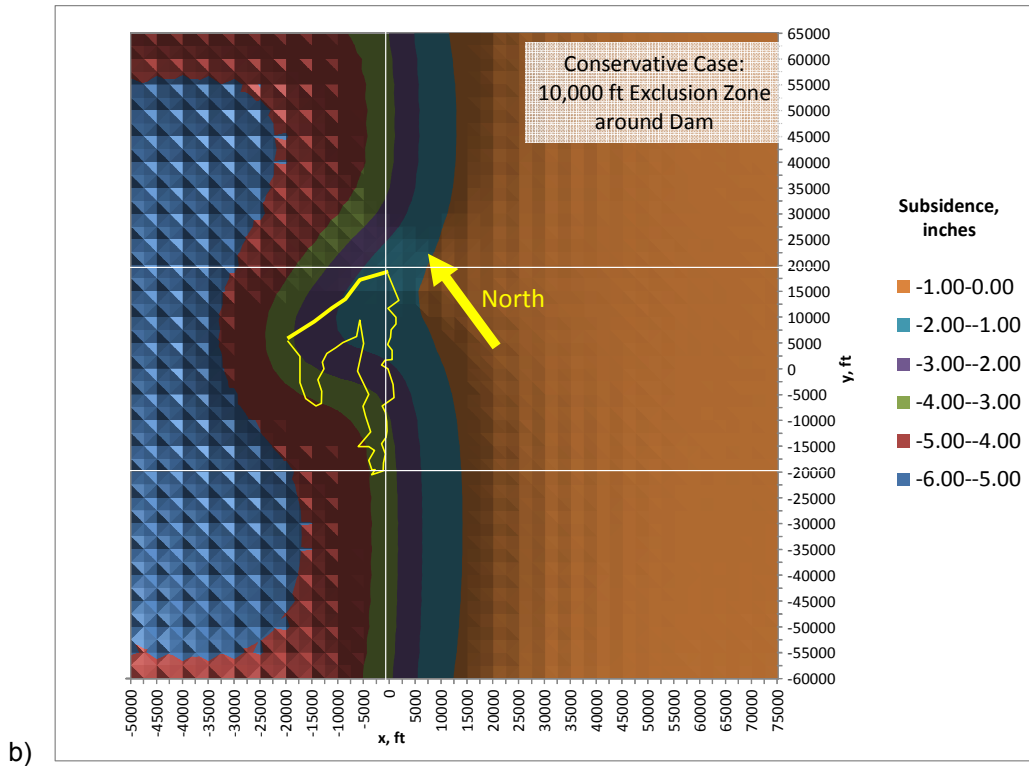


Figure 19. a) Reservoir disc geometry with a 20,000 ft exclusion zone around Joe Pool Dam. b) Subsidence for the Worst Case mechanical properties. Subsidence scale is in inches, x and y are in ft.

The conservative case is probably a more realistic mechanical property scenario, so it is worth examining the various radii of exclusion zones for this case as well (no mitigation is needed for the best case scenario). In Figure 20a, with full development, the dam experiences 3 to 6 inches of subsidence from one end to the other. With a 10,000 ft exclusion zone, the dam sees from 2 to 4 inches of subsidence (Figure 20b). Increasing the exclusion zone to 20,000 ft from the dam (Figure 20c) reduces the maximum subsidence at the dam to less than 2 inches.

Figure 20. Subsidence with the Conservative Case mechanical properties. a) Full Development to the eastern leg of the lake. b) 10,000 ft exclusion zone. c) 20,000 ft exclusion zone. Subsidence is in inches, x and y dimensions are in ft.





All of the above calculations assume the region between Joe Pool and N. Hwy 67 will not be developed. If development were to proceed to the highway, then Joe Pool

would be completely surrounded by production, which could adversely affect the subsidence at the dam. The conservative case scenario was examined by adding wells another 15,000 ft to the ESE (in the direction of x) for the 10,000 ft (Figure 21) and 20,000 ft (Figure 22) exclusion zones. Comparing the results to the previous cases where development doesn't surround the dam, the range of subsidence values for the dam are the same, albeit with a slightly different distribution. It is apparent that as long as the same exclusion zone radius is enforced, the encroachment of development to completely surround Joe Pool does not worsen the expected subsidence magnitude.

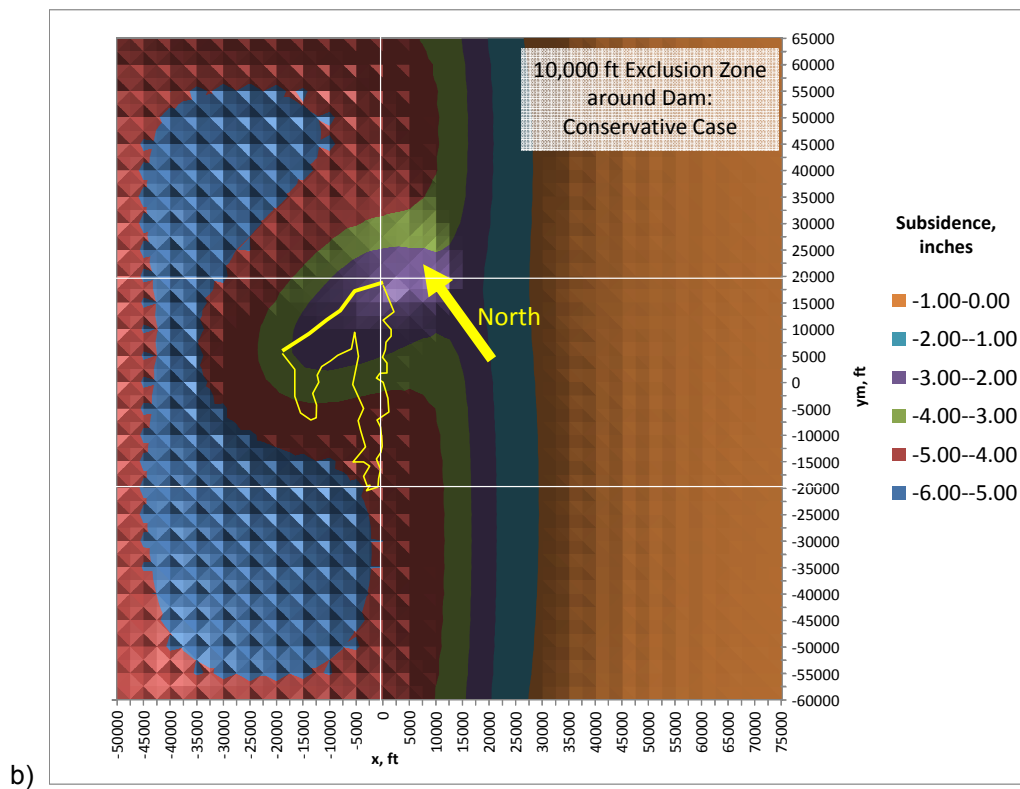
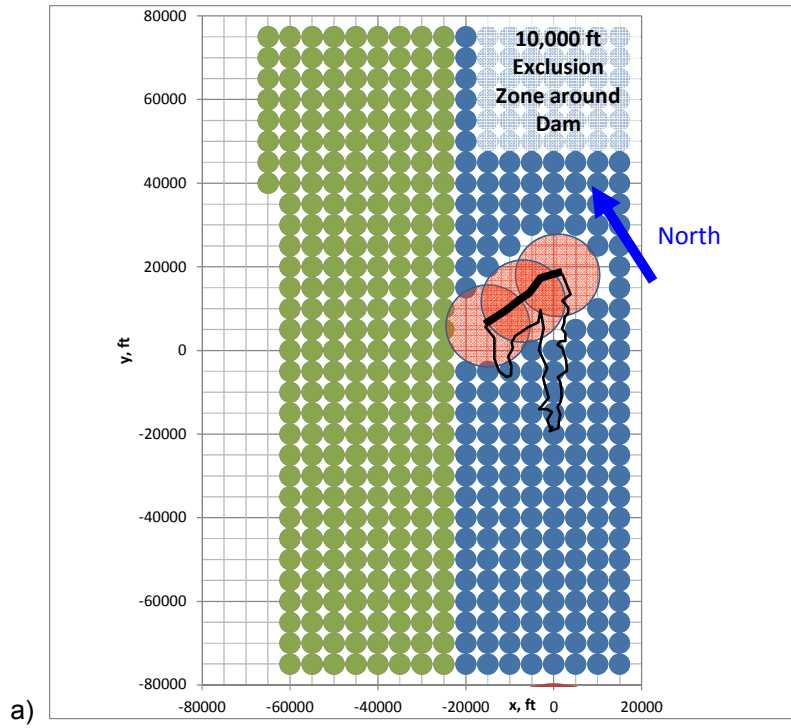


Figure 21. Conservative case mechanical properties, showing a) well locations and b) subsidence for the 10,000 ft exclusion zone when well development reaches N. Hwy 67. Subsidence is in inches, x and y dimensions are in ft.

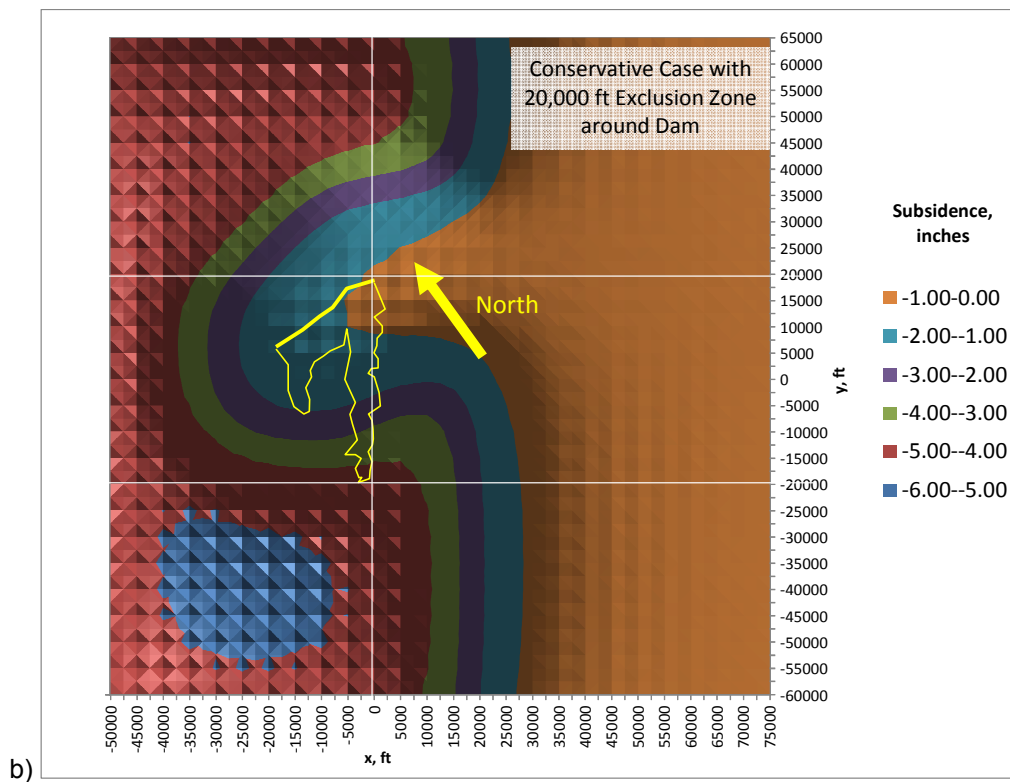
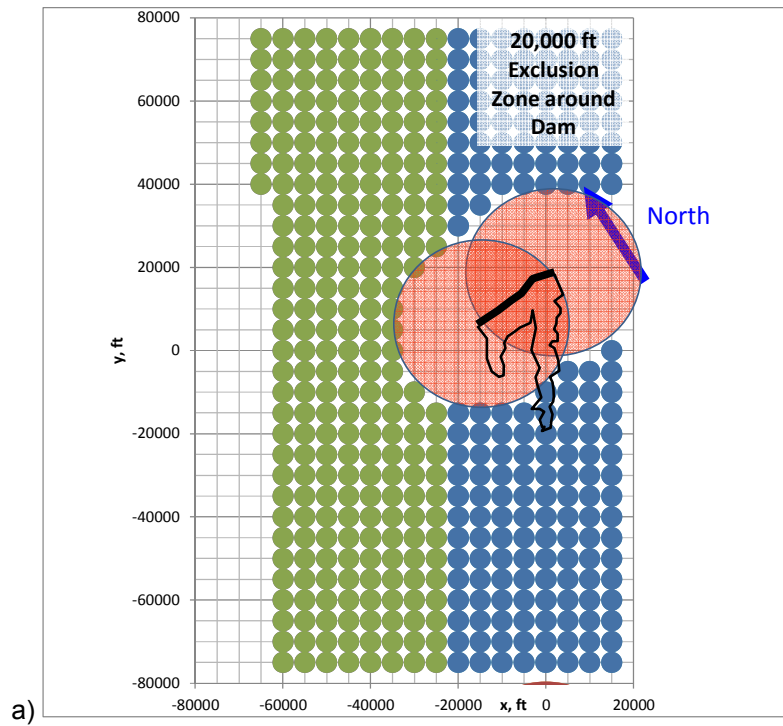
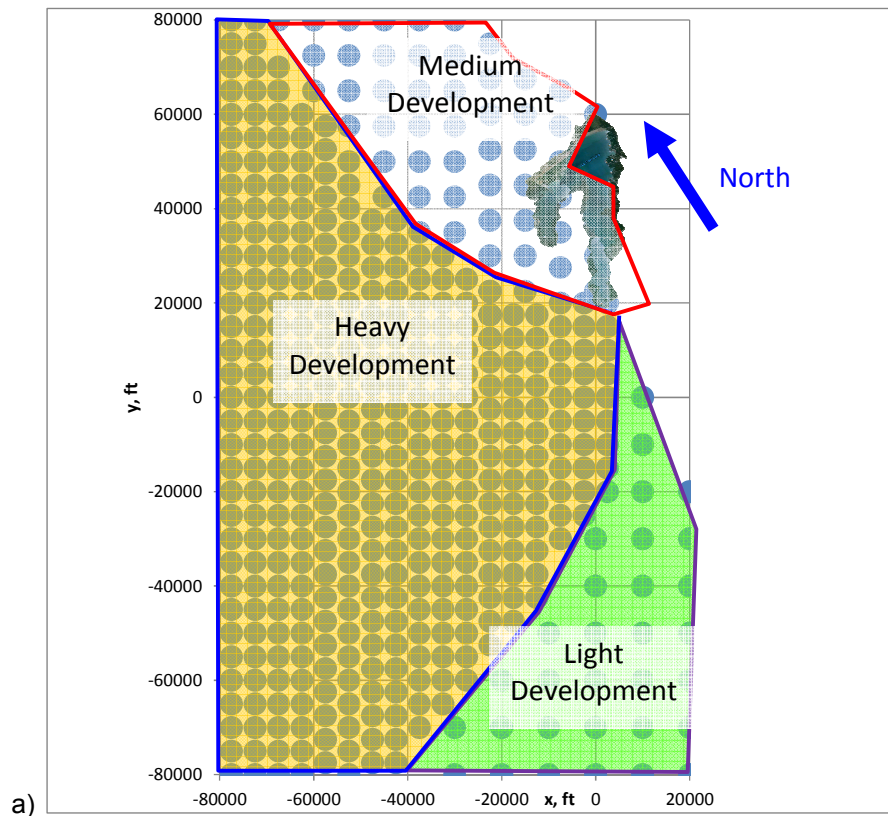


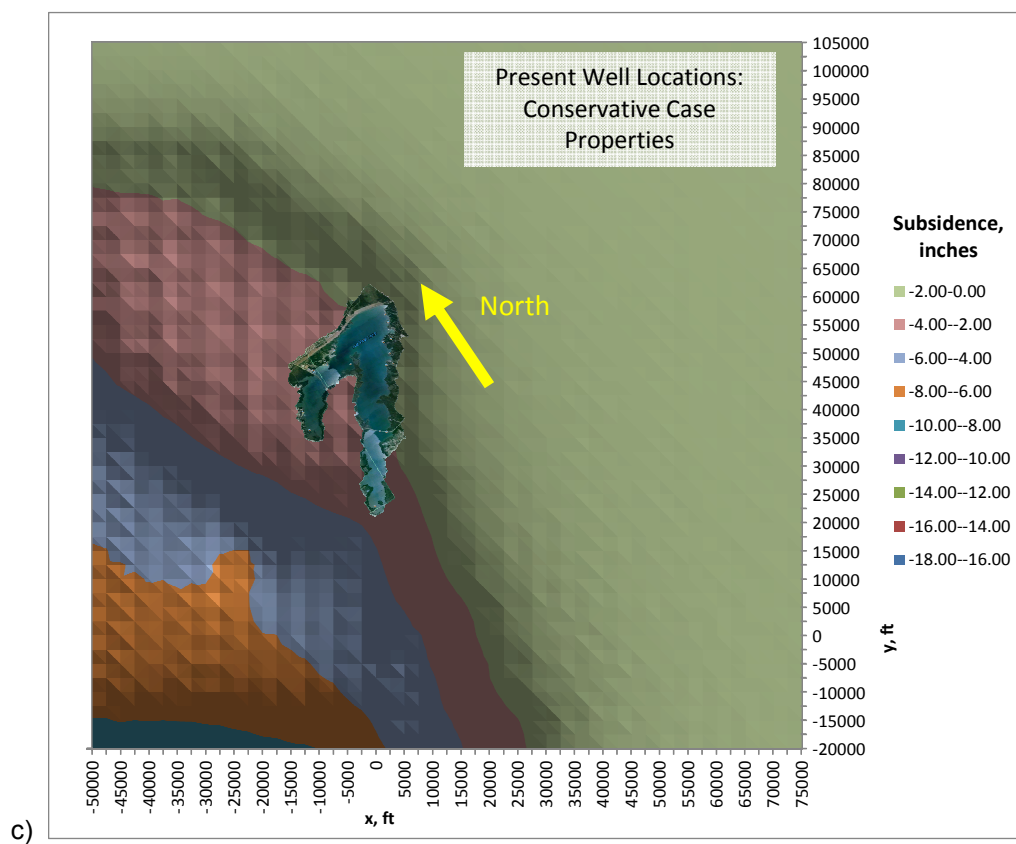
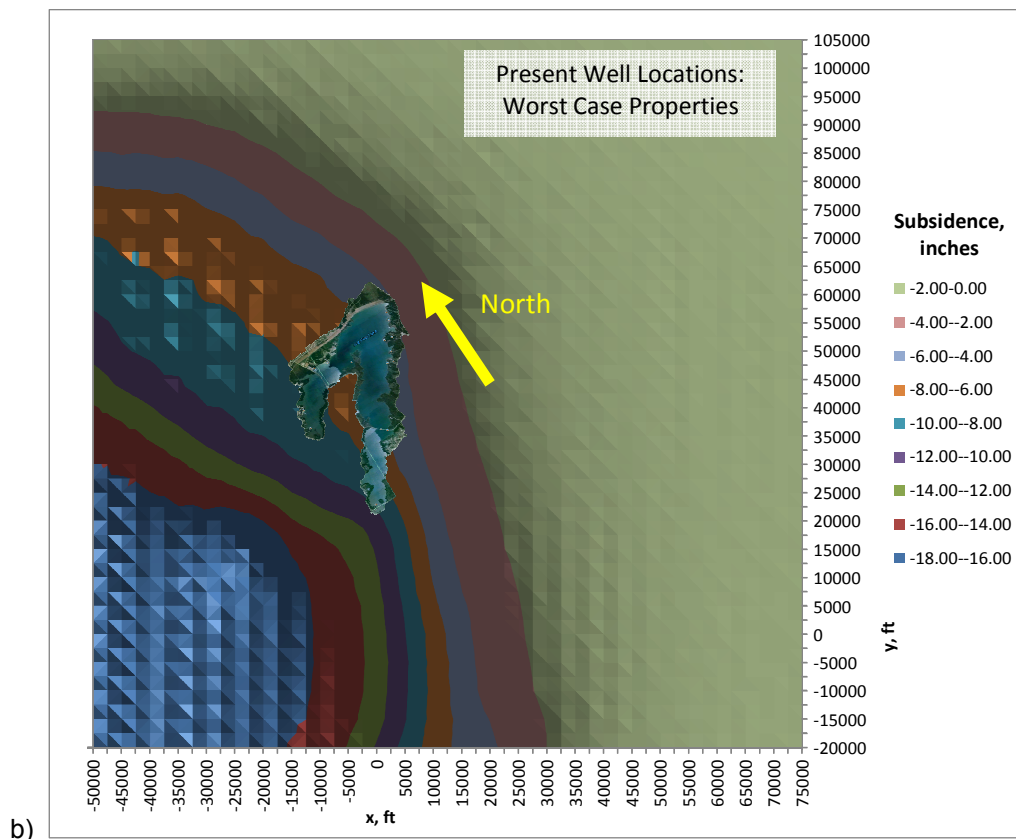
Figure 22. Conservative case mechanical properties, showing a) well locations and b) subsidence for the 20,000 ft exclusion zone when well development reaches N. Hwy 67. Subsidence is in inches, x and y dimensions are in ft.

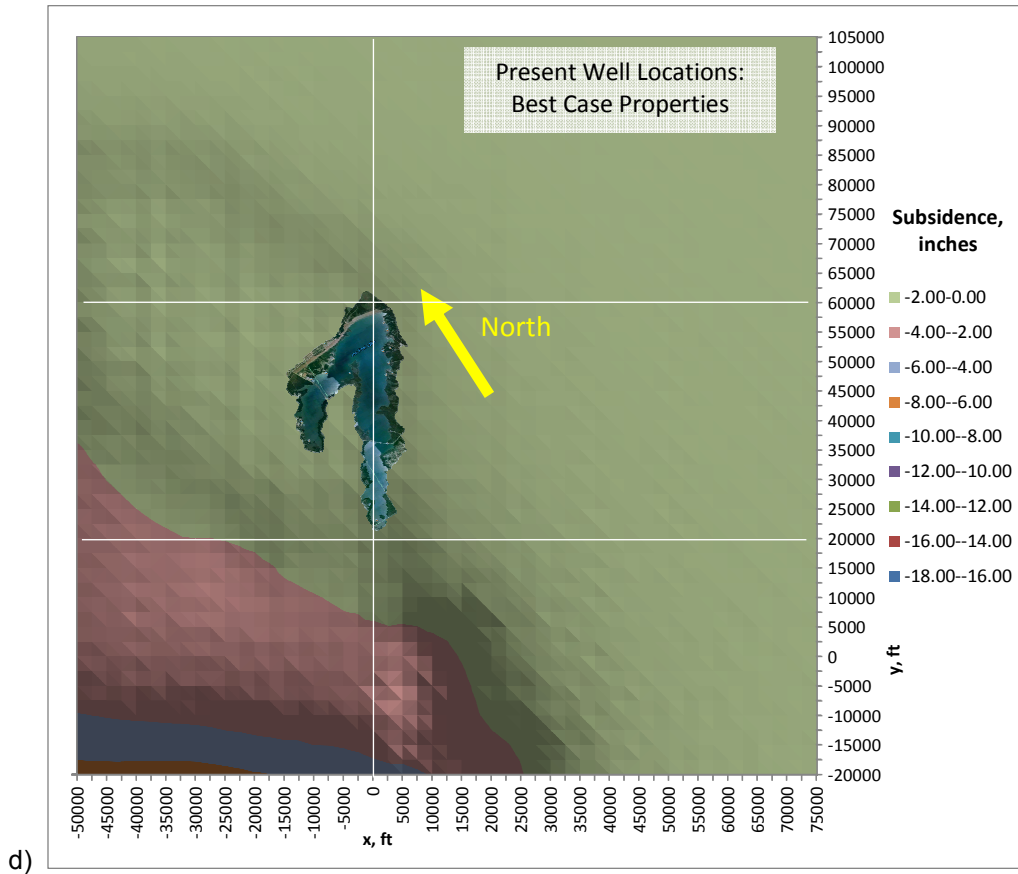
The last set of subsidence calculations is to look at the present day arrangement of development and how that could affect surface elevations after full depletion. (Since subsidence is a linear function of drawdown pressure, earlier time subsidence values can be proportioned from the full depletion estimates. For instance, the subsidence at an earlier time with only 25% of the drawdown would have only 25% of the subsidence, assuming all wells are tracking at the same pressure through time.) Using the Texas Railroad Commission well locations illustrated in Figure 12, a model was built with varying spacing between well clusters (still using a 2,500 ft radius) to approximate development intensity for the model (Figure 23). Joe Pool Dam and Lake are currently outside of the area of heavy development, but there are wells to within 3,000 ft (or a few closer) currently.

Figure 23. Subsidence using well locations approximating current development (a), and subsidence for the three mechanical property scenarios: b) Worst Case, c) Conservative Case, and d) Best Case. Subsidence is in inches with the same color scale for b, c and d; x and y dimensions are in ft.









In the Worst Case, subsidence at the dam is 4 to 8 inches (Fig. 23b). It is important to remember that although this is approximated to be present day well locations, the subsidence results from full 30 year depletion. In the Conservative Case, subsidence is from 2 to 4 inches (Fig. 23c), and in the Best Case, subsidence is less than 2 inches (Fig. 23d). The significant observation with this case is that it is not just the location of the dam relative to the edge of production which is important (such as with enforcing an exclusion zone), but the density of well development as well. Although most shale resource plays ultimately strive for the depletion of 100% of the reservoir volume, another way to mitigate surface subsidence, if it is deemed to be a problem, is to enforce a minimum distance between well clusters so as to diffuse the deformation with undepleted, uncompacted pillars between zones of depletion, much like leaving behind pillars in mining operations to prevent roof collapse.

## 7. Hydrofracturing Pressures.

The surface pressure behavior of a fracturing treatment depends significantly on the type of fluid being pumped. In the Barnett, most of the treatments are high rate slickwater jobs (low viscosity fluid, mostly water with friction reducer and a small amount of gel). Lohoefer et al. (2006) published rate and surface pressure for a 7 stage treatment in a 3300 ft horizontal well, pumping 1.3 million lbs proppant with 100,000 bbls fluid (Figure 24). The surface pressure ranged from 4000 to 8000 psi for injection rates that reached 140 bbls/min. A big component of the surface pressure is the friction pressure of the fluid going down the pipe to the completion interval, so fracturing behavior can be masked.

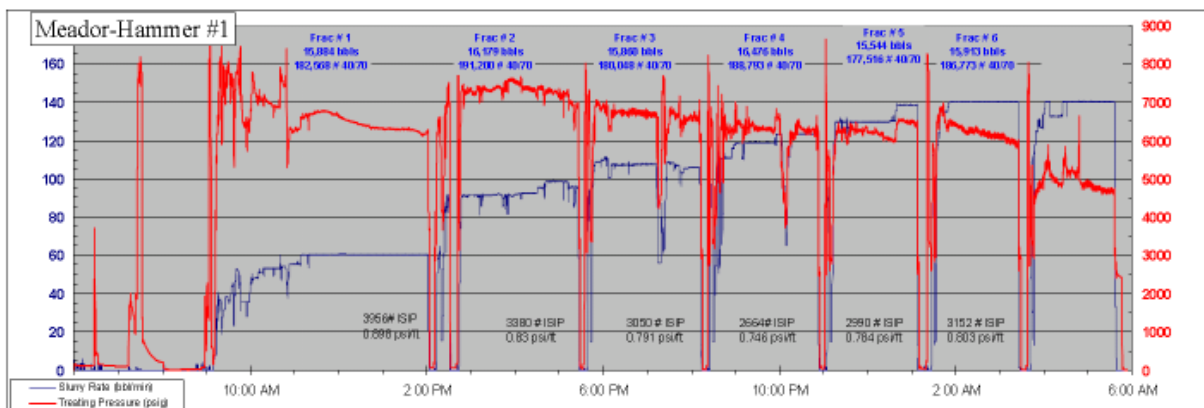


Figure 24. Surface treating pressure and rate data for multiple hydraulic fracture treatments in a Barnett shale well. From Lohoefer et al. (2006).

Interpreting downhole fracture propagation requires bottomhole treating pressure, BHTP. It is preferable to have downhole measurements for BHTP, but it can also be estimated from surface pressure, taking into account fluid density and friction pressure in the pipe. Fisher et al. (2005) present a plot of the net pressure during a 60 bbl/min treatment (Figure 25). Net pressure runs around 500 psi for the first half of the treatment, and then begins to climb, which is an indication of height growth restriction for the fracture (it is getting longer but not wider, so it takes more pressure to keep pumping down a longer fracture at the same rate). When sand is ramped up from just a trace amount to 1 lb/gal at 200 minutes into the job, the pressure very quickly rises, suggesting some sort of bridging of the proppant in the fracture, indicating a screenout, or insufficient fracture width for the proppant to move. The rate was shut down and the

treatment ended. Although screenouts are neither desired nor typical, net pressures on the order of 100's to 1,000 psi are not uncommon.

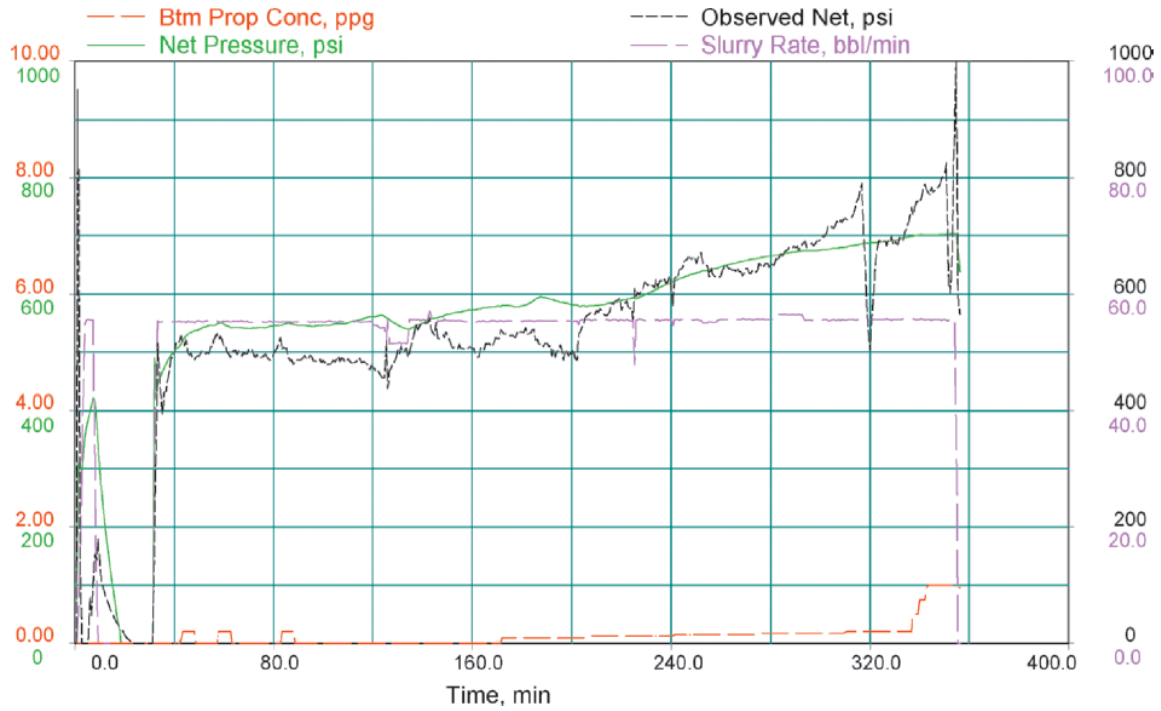


Figure 25. Net pressure and rate for a Barnett Shale fracture treatment. From Fisher et al. (2005).

## 8. Fracture Zone.

In addition to creating width for the entry of proppant to the fracture, the importance of hydraulic fracturing pressure is the propensity of the fracture to grow in height. As shown in the above example, fracture containment within zone often corresponds to a slow increase in pressure with time, while abrupt increase in pressure indicates screenout (Nolte and Smith, 1981). Steady decrease in pressure with time is typically interpreted to be rapid height growth, comparable to the rate of length increase. Such a fracture would be considered uncontained. Natural barriers to height growth include the variation in stress from

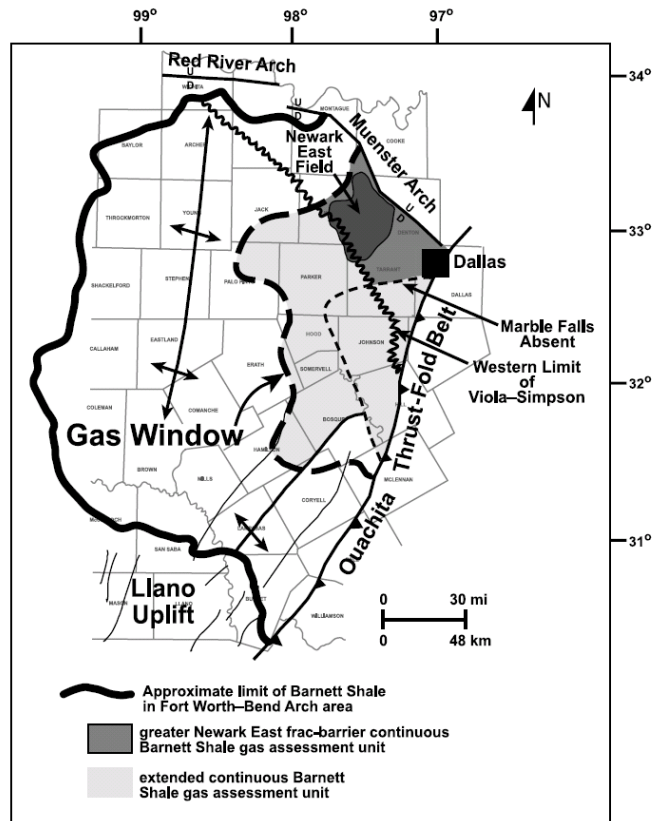
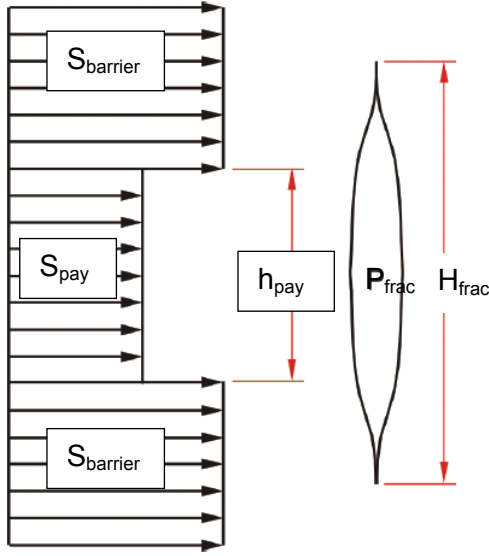


Figure 26. Fort Worth basin petroleum geology features. From Montgomery et al. (2005).

layer to layer in a heterogeneous geologic media. In this regard the Barnett shale has two major height growth barriers that have been identified in practice (Montgomery et al 2005). Beneath the Barnett is the Viola-Simpson shale, which typically has a higher  $S_{hmin}$  than the Barnett and prevents downward growth of the hydraulic fracture into the Ellenburger limestone. Above the Barnett is the Marble Falls limestone, which is a barrier to upward growth. In the Joe Pool area, the Viola is present but the Marble Falls is not (Fig. 26). However, local logs indicate that even though the Marble Falls is not present in this region, there appear to be higher stress zones immediately above the Barnett with  $S_{hmin}$  stress differences of 1000 psi. There are also some isolated thin zones about 600 ft above the Barnett that indicate similar high stress difference barriers.



The principle behind height growth barriers and

Figure 27. Hydraulic fracture and surrounding layers showing how varying stress can contain fracture height.

stress is illustrated in Figure 27. The hydraulic fracture is an opening mode fracture, and as such the pressure inside the fracture,  $P_{frac}$ , needs to exceed the normal

stress acting perpendicular to the fracture, typically  $S_{hmin}$ . When the net pressure,  $P_{net} = (P_{frac} - S_{hmin})$  is greater than 0, the fracture will open, and this opening generates stress

concentration at the fracture tips. The stress concentration is quantified from fracture mechanics using the stress intensity factor,  $K_I$ , and propagation is achieved when  $K_I > K_{Ic}$ , where  $K_{Ic}$  is the fracture toughness. Looking at the height growth problem, the stress intensity factor at the top tip of the fracture is of interest, and can be computed as (Warpinski, 2012)

$$K_I^{top} = \frac{1}{\sqrt{\pi H_f/2}} \int_{-H_f/2}^{H_f/2} P_{net}(z) \sqrt{\frac{H_f/2+z}{H_f/2-z}} dz \quad (24)$$

where  $H_f$  is the total height of the fracture,  $z$  is vertical location (positive is up), and  $P_{net}(z)$  is the variation of  $P_{frac} - S_{hmin}(z)$  along the height of the fracture. The increase in  $S_{hmin}$  outside of the pay zone will hinder the propagation of the fracture out of zone. The higher the net pressure of the fracture, the taller the fracture can be, and for an equilibrium calculation with symmetric stress barriers above and below of magnitude  $S_{barrier}$ , the ratio of fracture height,  $H_{frac}$ , to pay zone height,  $h_{pay}$ , can be determined by solving the equation (after Warpinski, 1989)

$$S_{barrier} - P_{frac} = \frac{2}{\pi} (S_{barrier} - S_{pay}) \sin^{-1} \left( \frac{h_{pay}}{H_{frac}} \right) - \frac{K_{Ic}}{\sqrt{\pi H_f/2}} \quad (25)$$

This equation implies unlimited height growth if  $S_{barrier} < S_{hmin}$ , but this is not the case in the Barnett Shale, and if such a case were to occur, other factors would limit height growth. These other factors (Fisher and Warpinski, 2012) include the potential for interbedded sedimentary rocks to have weak horizontal interfaces, especially in shales, which can be opened by an approaching hydraulic fracture and divert fluid horizontally and stop propagation. Additional stress barrier zones above the immediate fracture treatment depth, which probably exist in the Joe Pool area as suggested by local logs, can also stop the height growth of a propagating fracture. Permeable layers can also act as thief zones for the fracturing fluid, enhancing leak-off which will eventually rob the fracture of its mechanism to transmit pressure to the fracture tip to cause propagation. Local logs indicate several permeable zones above the Barnett that could act as such permeability barriers to fracture height growth. Finally, the basic material balance of injection is probably the most concrete restriction on fracture height growth. A hydraulic fracture represents a volume (height times length times width), and that volume cannot exceed the amount of fluid injected minus the fluid that has leaked off into the formation. Consequently, the injected volume limits the height growth of the fracture. While injecting, the efficiency of a fracture treatment is computed as the ratio of the fracture volume created to the fluid volume injected,  $e = V_{frac}/V_{inj}$ . In gas shales efficiency while pumping is fairly high ( $e > 90\%$ ) because of the extremely low permeability of the formation, but when the pumps shut down, all of the fluid eventually leaks off or is produced to the surface through the wellbore, so ultimately  $e$  reaches zero (neglecting preserved opening made possible by the proppant, but at that point the fracture is no longer propagating). For fracture treatments that stay within zone, fracture width is estimated to be very small (less than 0.5 inches), and fractures are interpreted to reach lengths on the order of 1000's of feet and height of 100's of feet for a typical Barnett fracture treatment. If the fracture were to break through the overlying stress barrier and propagate toward the surface, its extent would be limited by the volume injected, and one might conclude that the magnitude of the height may reach 1000's of feet and the length be only 100's of feet, given the interpretation for fracture widths for fractures that stay in zone. However, Fisher and Warpinski (2012) point out that as a fracture moves up toward the surface, the overall tendency is for  $S_{hmin}$  to reduce proportionally to the

reductions in pore pressure and vertical stress that would be expected at shallower depths, according to equation (13). Given the local fracture gradient,  $dS_{hmin}/dz$ , as presented in Table 2,  $S_{hmin}$  should reduce on the order of 0.75 psi/ft as the fracture grows upward. However, the density of the fracturing fluid dictates the change in  $P_{frac}$  as the fracture moves upward, and this gradient would be on the order of 0.44 psi/ft. Consequently, the net pressure of the fracture will increase dramatically with upward growth, causing a significant ballooning in fracture width. The dependence of maximum fracture width on net pressure can be seen from the standard fracture mechanics equation for fracture width given a uniformly loaded crack,

$$w_f^{max} = P_{net} \frac{2(1-\nu^2)}{E} H_f. \quad (26)$$

Thus, given the numbers above, the net pressure would grow on the order of 0.3 psi/ft. If the fracture started out with a net pressure on the order of 500 psi, that net pressure could double (with the associated doubling of fracture width) in 2000 ft. As illustrated in Figure 28 from Fisher and Warpinski (2012), the injected volume would be exhausted before the fracture could reach the earth's surface.



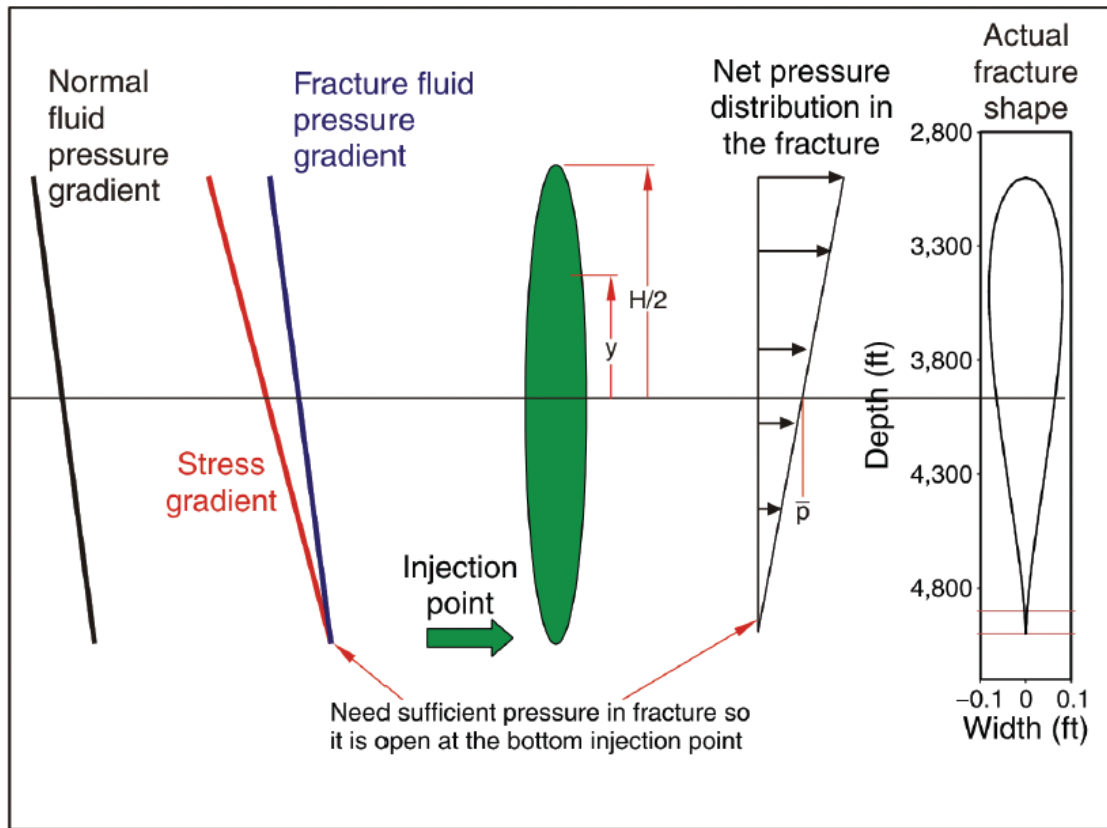


Figure 28. Diagram showing how upward fracture height growth results in ballooning of fracture opening because earth stress reduces faster than fluid pressure. The increased net pressure with upward growth increases fracture width and volume. From Fisher and Warpinski (2012).

Perhaps more important than the theoretical predictions of how fractures grow are the actual empirical observations. Microseismic monitoring has been used extensively in shale gas development, and Fisher and Warpinski (2012) show the accumulated data for thousands of Barnett shale treatments. The micro-seismic events (typically Richter magnitude -2 to 0), track slight movements on natural fractures and bedding planes responding to stress perturbations around the hydraulic fracture or fluid from fracture leak-off. The blue lines in Figure 29 represent the vertical extent from the surface of groundwater zones, the other lines, color-coded by county, represent the extent of height growth of the hydraulic fracture as measured by microseismic. As discussed by Fisher and Warpinski, the greatest spikes in the data represent minor slip on faults during the fracture treatments, and as such show that not only does the hydraulic fracture treatment not reach the surface, but fault slip during the fracture job extends at

most 1000 to 2000 ft. Additionally, although 1000 ft sounds like a significant fault reactivation, all of these events recorded during the fracture treatments are microseismic events, not reaching the realm of even felt earthquakes, much less surface damaging events.

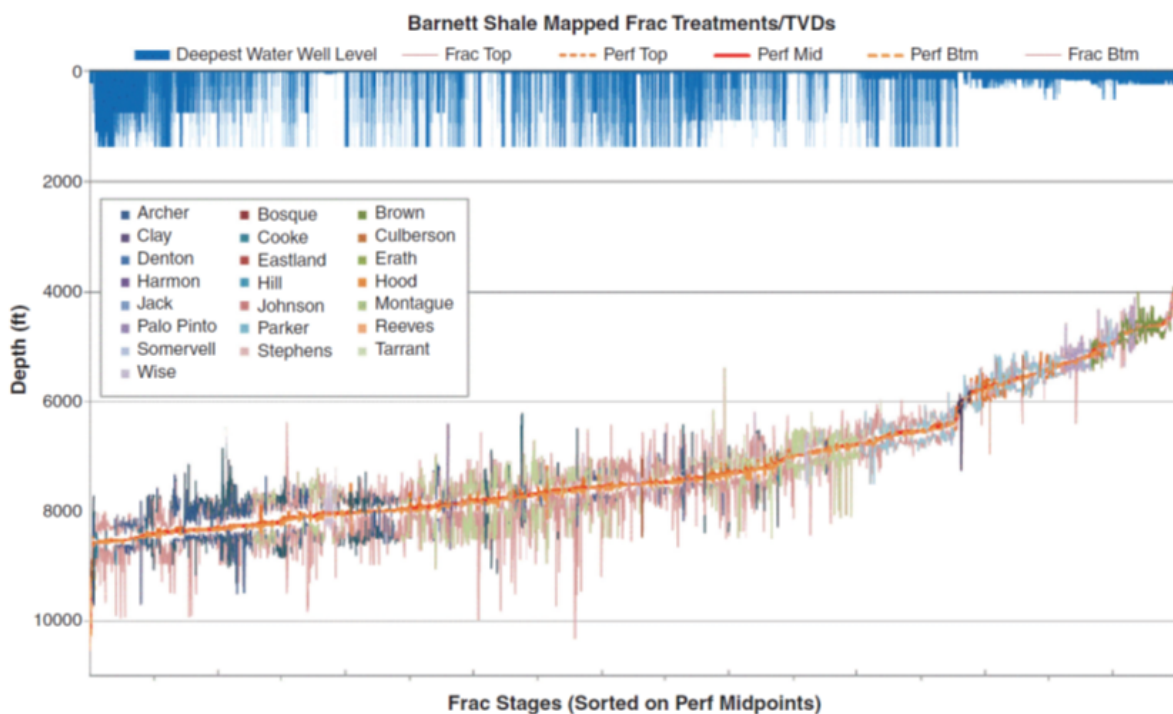


Fig. 2—Barnett shale measured fracture heights sorted by depth and compared to aquifers.

Figure 29. Diagram from Fisher and Warpinski (2012) showing vertical extent of microseismic events during Barnett Shale fracture treatments and vertical extent of Fort Worth Basin aquifers.

One other piece of data that speaks to the idea of hydraulic fractures propagating to the surface comes from tiltmeter data (Fisher and Warpinski, 2012). It is widely observed that in the near surface (depths less than 1000 or 2000 ft), the least principal stress,  $S_3$ , is the vertical stress (i.e., the horizontal stresses are more compressive than the vertical stress). Since hydraulic fractures propagate in a direction that minimizes the energy expended, they tend to align perpendicular to  $S_3$  and thus tend to dip horizontally in the near surface. This phenomenon is confirmed by tiltmeter data for shallow hydraulic fracturing treatments, where the amount of horizontal opening detected by the tiltmeters increases significantly at depths shallower than 2500 ft (Fig. 30 – data from all types of reservoirs at various depths from Fisher and Warpinski, 2012). This implies an

additional barrier to fracture height growth, which would be the tendency for the fracture to roll over horizontally as it reached shallow depths.

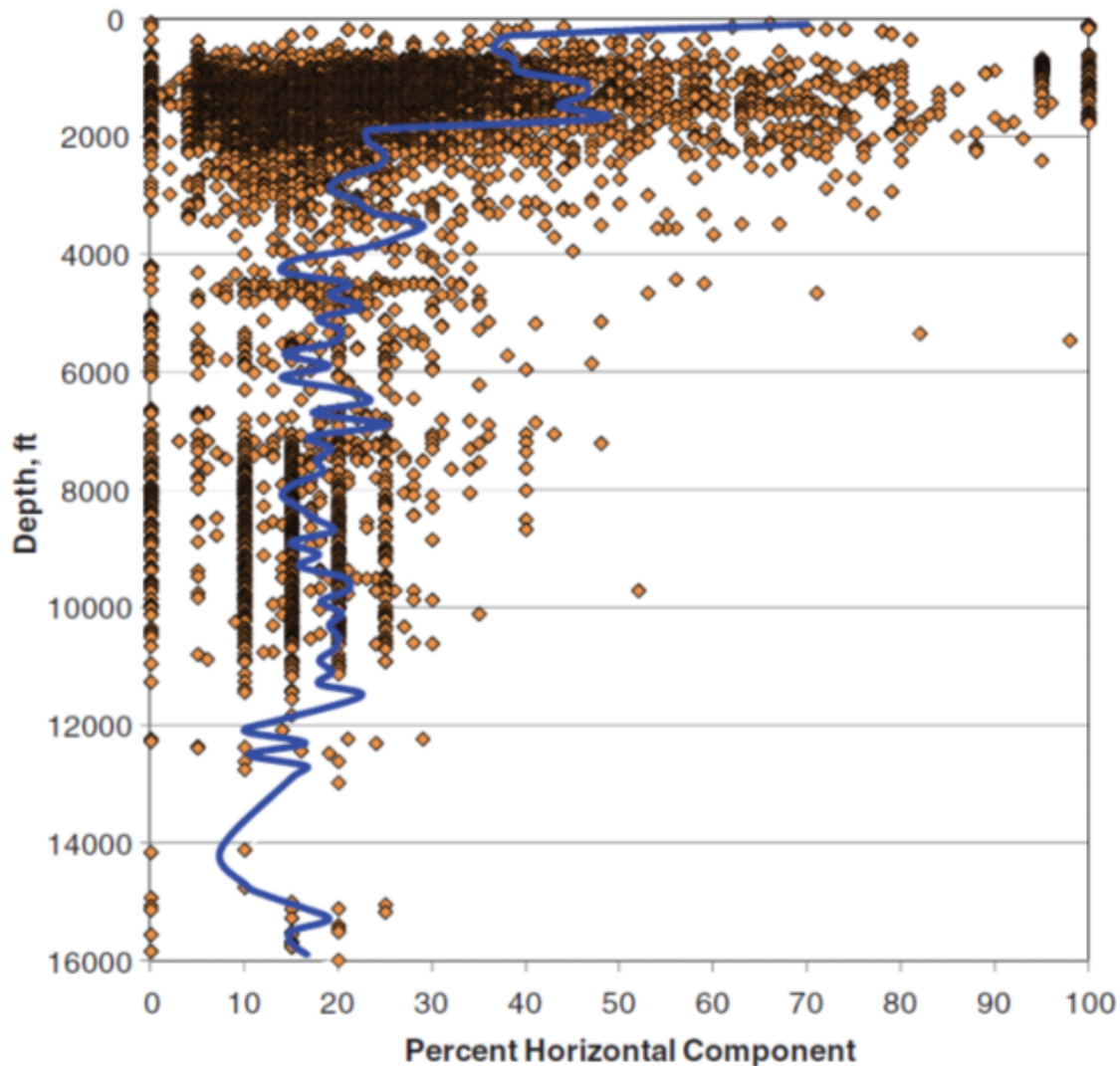


Figure 30. Tiltmeter data from hydraulic fracture treatments at varying depths showing an increase in horizontal component of fracture creation increasing at shallower depths, suggesting fractures are no longer vertical at shallow depths. From Fisher and Warpinski (2012).

Allowing that a hydraulic fracture treatment is unlikely to propagate to the surface, there is another fracture related risk associated with the wellbore. A typical completion sets surface casing at a depth of 2000 ft. Well control issues at these depths are unlikely as the gas-bearing zones are typically deeper. However, based on the review of local operators' files, the next casing set point after the surface casing is typically the total

depth of the well. There are gas zones between 2000 ft and the Barnett, such that there is potential for a well control problem during drilling prior to the installation of production casing. After installation of production casing, there is another opportunity for loss of well control during hydraulic fracturing. These events are unlikely but not impossible. Groat (2012) reports 12 recorded blowouts for the Barnett Shale, 2 of which were determined by the Railroad Commission to have blown out “underground”, meaning the fluid left the wellbore before reaching the surface. Given the approximately 15,000 wells drilled through 2012 in the Barnett, 12 blowouts represents a frequency of approximately 1 in 1000 wells. This is consistent with statistics published in Considine (2012), reporting 4 of 3533 wells in the Marcellus having blowout or venting violations – again a frequency of approximately 1 in 1000.

Given the recognition that blowouts can and do occur in shale gas wells, the next step is to assess how such an event might impact Joe Pool Dam. One risk of blowout is fire and explosion, and the current USACE exclusion zone of 3000 ft around the Joe Pool Dam structures is based on this hazard. Another risk worth examining, related to natural fractures, is the possibility of gas or other high pressure fluid escaping the wellbore underground and traveling up a permeable fault to the surface near the dam or beneath the dam. Based on the offset observed on faults intersecting the surface during excavation work for Joe Pool Dam (see Section 1), it is possible that surface faults could extend to depths of 1500 ft or more. The clay-rich nature of the rock in this section and the hydrologic observations in the region (see Section 13; Harden and Associates, 2004) suggest that flow along such faults is unlikely, but under blowout conditions, where such faults would be exposed to high pressure gas, leakage up the fault cannot be ruled out. Given the possibility of fault leakage during an underground blowout, the following paragraphs discuss what well offset distance from the dam might be needed for risk reduction.

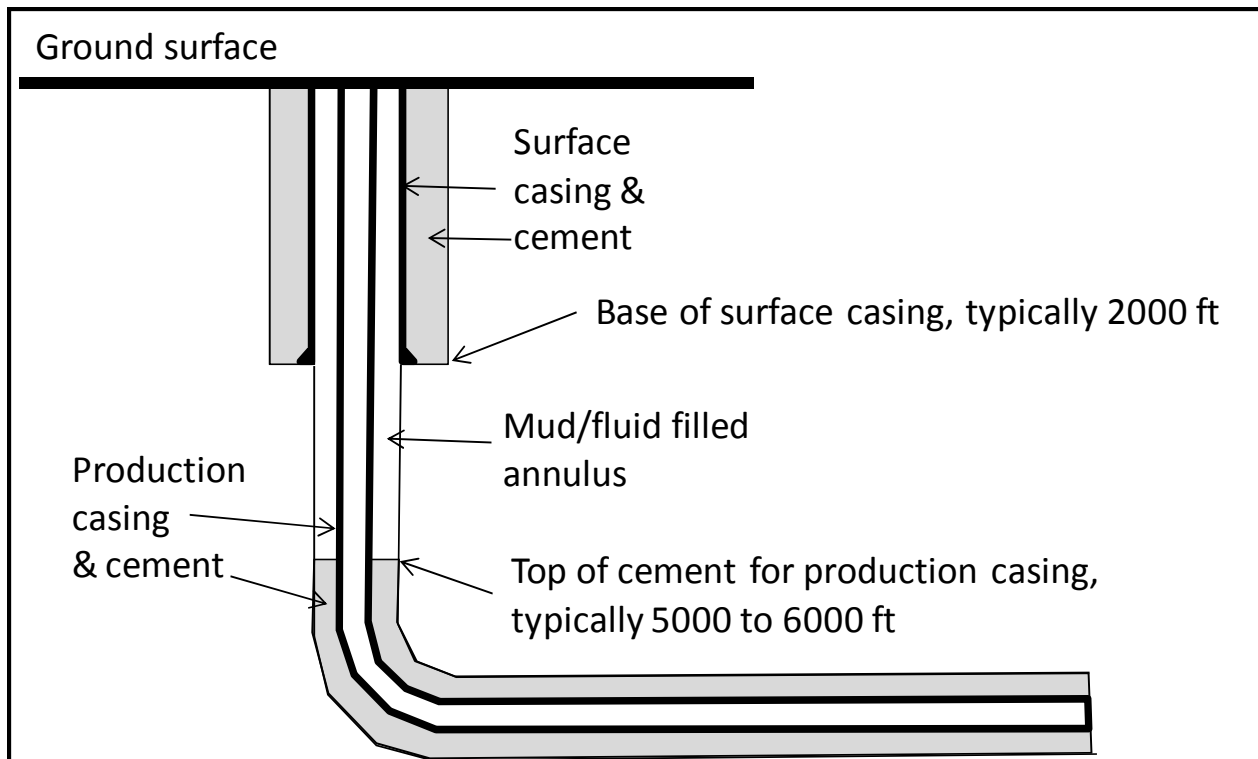


Figure 31. Cross-section diagram showing approximate depths for casing and cement in a typical Barnett Shale well in the vicinity of Joe Pool Dam (drawing not to scale).

Figure 31 illustrates the typical casing and cement construction of Barnett Shale wells in the Joe Pool area. Surface casing is typically run to 2000 ft and cemented back to surface. This surface casing depth is dictated by the location of the deepest groundwater aquifer to be protected, which in this area is likely in the Cretaceous Trinity Formation. The production casing is run from surface to the bottom of the horizontal leg, but is only cemented to approximately 2000 ft above the reservoir (i.e., top of cement would be at 5000 to 6000 ft). This leaves an annulus between the production casing and unprotected rock formations over the depth interval bounded by the base of the surface casing (~2200 ft) and the top of cement from the production casing (~6000 ft). This annulus is typically filled with drilling mud or completion fluid. If this annulus gets pressurized, either due to production casing cement failure during the fracture treatment or during gas production, there is a possibility of an underground blowout. While drilling, prior to running the production casing, the formations below the base of the surface casing are also at risk of underground blowout. The risk is greatest just below the base of the surface casing because the formation is unprotected (not behind

casing) and this is where the earth stress is the least. Loss of well control could bring high gas pressure to this near surface location, and this gas could leave the wellbore through a near-surface fault or newly created fracture and travel to the earth's surface (Figure 32).

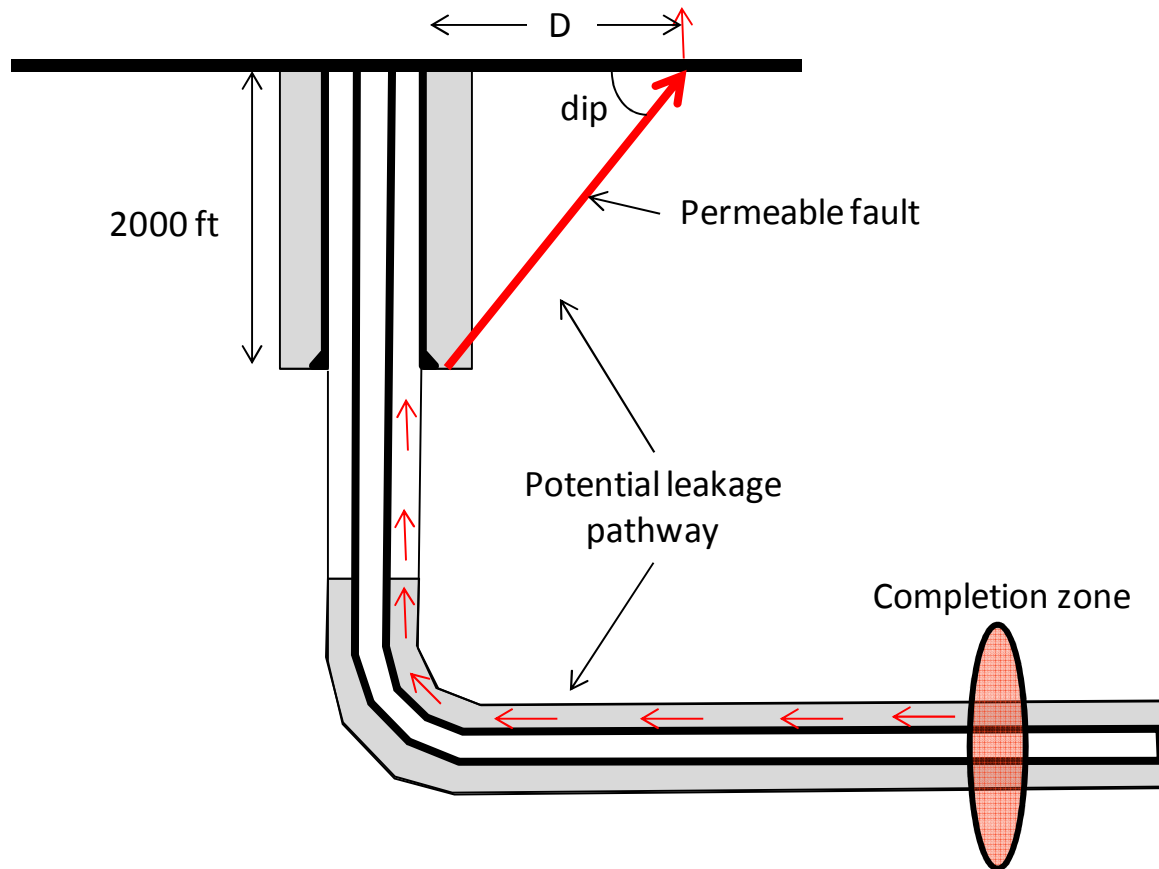


Figure 32. Possible scenario for gas to travel through the cement sheath of the production casing (either due to channels created during emplacement, or due to failure during fracturing or production). The red arrows indicate gas traveling from the reservoir through the cement to the uncemented portion of the production casing annulus. Assuming the surface casing integrity holds, the most likely underground leakage would be at the base of the surface casing, which could connect to permeable faults extending to the surface (drawing not to scale).

If we assume that the most likely depth for gas to escape the wellbore is at the base of the surface casing (as argued above), then the lateral offset distance to which escaping gas could reach is given by  $D$  (Fig. 32), which can be computed as

$$D = (\text{vertical depth to fault intersection}) / \tan (\text{dip}) \quad (27)$$

The Cretaceous rocks in the Fort Worth area have predominantly normal faults, and normal faults typically dip 50°-70° from horizontal. Assuming fault intersection at the base of the surface casing at 2200 ft and a 50° fault dip, the offset distance, D, to avoid gas escaping underneath the dam would be 1850 ft. Factors that could increase this distance are: lower angle faults; gas escape from the wellbore along a horizontal, high permeability zone prior to traveling up a fault; wellbore/fault intersection at a depth greater than the bottom of the surface casing; and along strike transport of gas once it enters a fault. Given these additional factors, a conservative approach would be to increase the offset distance to protect from underground blowout. Increasing the offset to 3000 ft. would be in agreement with the current minimum standoff distance mandated for the project by SWDP 1110-2-1156 and minerals leasing stipulations administered by the Bureau of Land Management for government lands.

## **9. Induced Seismicity.**

Induced seismicity has become a major public concern. A recent article by Zoback and Gorelick (2012) questioned the feasibility of widespread CO<sub>2</sub> injection into the subsurface (required for climate change mitigation from the burning of fossil fuels) because the earth's crust is widely populated with critically stressed faults. In this report we will address 3 issues: 1) earthquakes caused by hydraulic fracturing, 2) earthquakes caused by shale gas production, and 3) earthquakes caused by waste water injection related to shale gas operations. In Appendix B is a report on induced seismicity that was written for this project by Dr. Cliff Frohlich. This should be considered an authoritative assessment of induced seismicity for the Barnett Shale from a recognized expert in the field. This section will review some of the main points of Frohlich's report and relate the topic of induced seismicity to the rest of the report, but the reader should consider the Appendix an equally important source.

Before proceeding it is worth defining the different methods for quantifying the magnitude of an earthquake. The scalar seismic moment,  $M_0$ , is calculated based on the static energy release of a slip event as (Pollard and Segall, 1987)

$$M_o = GAd \quad (28)$$

where  $G$  is the shear modulus of the rock ( $G = E/2/(1+\nu)$ ),  $A$  is the area of the patch that slipped, and  $d$  is the magnitude of the slip. Thus,  $M_o$  has units of (force) x (length) or energy. For elastic deformation, Pollard and Segall (1987) estimate that reasonable stress drops on earthquakes indicate that fault slip is on the order of  $d = 0.01L$ , where  $L$  is the length of the fault segment that is slipping. Wells and Coppersmith (1994) show earthquake data suggesting a smaller ratio on the order of  $d = 0.0001L$ , which implies larger faults would be required to achieve a given earthquake magnitude.

The seismic moment is related to the moment magnitude scale,  $M_w$ , equivalent to the more commonly referenced Richter earthquake magnitude scale (Hanks and Kanamori, 1979; Warpinski et al., 2012) as

$$M_w = 2/3 (\log M_o - 16.1) \quad (29)$$

where  $M_o$  is in N-m (Newton-meters). To put microseismic slip events in perspective, the relation between magnitude, fault size and slip is presented in Table 10. From the table, a magnitude M0 microseismic event, which is on the large end of the reported range of microseisms in the Barnett, represents 1.2 mm of slip on a fault of 12 m on a side. The felt earthquakes in nearby Cleburne, TX, with a magnitude of about M3.0, are estimated to be about 4.0 cm of slip on a fault that is 387 m on a side.



**Table 10 – Earthquake magnitude related to fault dimensions and slip (assuming a “square” fault,  $L = H$ ,  $d = 0.0001L$ , and the conservative case mechanical properties,  $E = 2 \times 10^6$  psi = 13.8 GPa,  $\nu = 0.15$  and  $G = 6.0$  GPa).**

slip, $d$ (m)	Area, $L^2$ (m <sup>2</sup> )	Length, $\sqrt{A}$ (m)	Scalar Seismic Moment, $M_o$ (N-m)	Moment Magnitude Scale, $M_w$
0.0004	15	4	3.49E+07	M-1.0
0.0012	150	12	1.10E+09	M0.0
0.0039	1,500	39	3.49E+10	M1.0
0.0122	15,000	122	1.10E+12	M2.0
0.0387	150,000	387	3.49E+13	M3.0
0.1225	1,500,000	1,225	1.10E+15	M4.0
0.3873	15,000,000	3,873	3.49E+16	M5.0
1.2247	150,000,000	12,247	1.10E+18	M6.0

Tens of thousands of fracture treatments have been pumped every year over the last decade. Many of those treatments, particularly in shale gas plays, have been monitored with downhole microseismic equipment. The events recorded are typically so small that not only can they not be felt by humans at the surface, they cannot be detected with surface seismic monitoring equipment. A dataset of thousands of monitored fracture treatments (Warpinski et al., 2012) shows all events to be less than M1.0 and as small as M-3.0 (Figure 33).

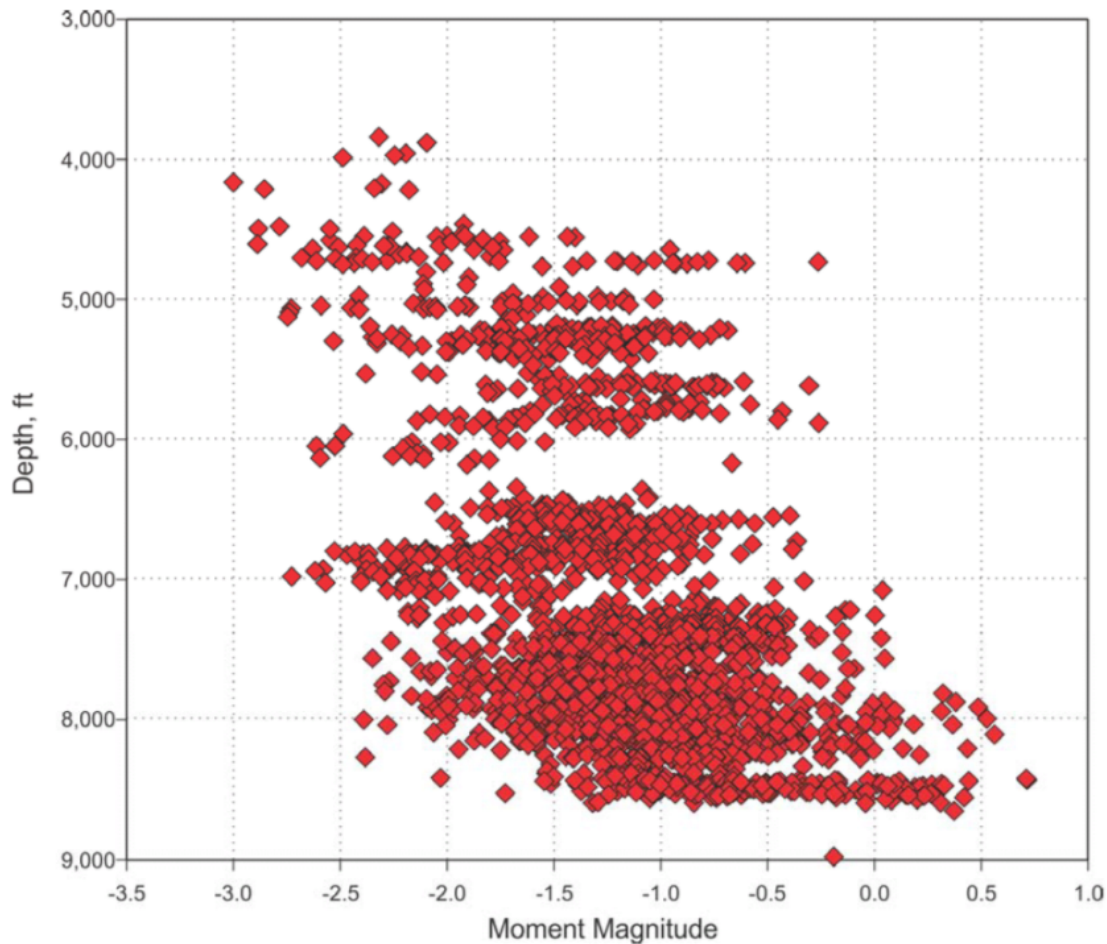


Figure 33. Plot of microseismic event magnitude versus depth for hydraulic fracture treatments.

However, there are a few cases that suggest felt earthquakes associated with hydraulic fracturing. Quoting from Appendix B, there are three events of note listed below.

*Orcutt, California:* Kanamori and Hauksson (1992) describe a M3.5 earthquake that occurred on 31 January 1991, a few hours after a hydrofracturing operation finished. Hydrofracturing at a pressure of 80 bars (~1160 psi) was being done at depths of 100-300 meters (~330 to 1000 ft); because liners in several wells were deformed at these depths they concluded that the earthquake was caused by failure of sediments at shallow depth. This is remarkably shallow for an earthquake—much shallower than the depths of most earthquakes of tectonic origin—and Kanamori and Hauksson's (1992) paper focuses more attention on the peculiar seismograms generated by the earthquake than on its relationship to hydrofracturing.

*Garvin, Oklahoma:* Holland (2011) describes a series of small earthquakes (largest M2.8) that occurred 17-23 January 2011 near Garvin, OK, with epicenters 1-4 km from an ongoing hydrofracturing operation. The earthquakes began about 7 hours after hydrofracturing commenced, and mostly stopped occurring within 24 hours

after hydrofracturing ceased. The U.S. Geological Survey's National Earthquake Information Center (NEIC) reports earthquakes with M4.2 and 4.5 occurring in 1994 and 1997 at distances of 30 km and 90 km.

*Fylde Coast (Blackpool), United Kingdom:* News reports and de Pater and Baisch (2011) describe two small earthquakes (M1.5 and M2.3) occurring in April and May, 2011, occurring within 2 km of an experimental hydrofracture operation on the Fylde Coast near Blackpool, United Kingdom. Injection operations began in March, 2011; following the May 2011 earthquake, the operator terminated the project, allegedly "Britain's only shale gas project". The NEIC reports several previous M3-M4 earthquakes within 100 km of this location; M5.4 and M5.0 earthquakes at distances of 130-160 km occurred in 1984 and 2002.

There are no documented cases of felt earthquakes in Texas as a result of hydraulic fracturing. This is a notable statement considering Texas is the number 1 state in the United States with regard to oil and natural gas production. This implies, as Frohlich concludes in his report, that oil and gas operations trigger earthquakes that are no bigger than historic earthquakes in a region, and that triggered felt earthquakes require very favorable stress conditions and fault geometry.

There have been no historic earthquakes associated with fluid extraction (i.e., gas production) in the Barnett shale, but there are several instances in other places in Texas where events up to M4.8 have been observed (see Appendix B for details). Fluid injection is a more common cause of induced earthquakes, and there are examples from the Barnett Shale region in particular where fluid injection is proposed to be the cause of felt earthquakes. Since 2008, earthquakes of up to M3.0 have been attributed to water injection wells near the DFW airport and in Cleburne.

The induced earthquake risk from injection wells comes from reduced friction coefficient and reduced effective stress across the fault planes when exposed to increased pore pressure and rock-water interaction. This risk is referenced in the recent paper by Zoback and Gorelick (2012), and it is the mechanism of the well-known case of injection-induced earthquakes in Colorado at the Rocky Mountain Arsenal in the 1960's (Healy et al., 1968). After the Rocky Mountain Arsenal incident, the US Geological Survey collaborated with Chevron to directly test the hypothesis that injection can

trigger earthquakes by intentionally changing the pore pressure in the vicinity of a fault in the Rangely Field in NW Colorado. They were able to show that there was a critical pore pressure below which seismicity was suppressed and above which it was enhanced, surprisingly consistent with a simple Mohr-Coulomb type shear failure criterion (Raleigh et al., 1976).

## **10. Risk Reduction.**

One possible aspect of risk reduction is to limit the range of operating conditions for hydraulic fracture treatments. Another is to impose a stand-off between well operations and Joe Pool Dam. In this section, I discuss risk associated with induced earthquakes caused by hydraulic fracture treatments, gas production and water injection for disposal. I also review risk factors identified by industry experts as published by King (2012).

As already mentioned, Warpinski et al. (2012) shows known Barnett Shale microseismic events caused by hydraulic fracturing are all less than M1.0. Secondly, Warpinski's dataset shows that the main correlation between magnitude and operational parameters is that magnitudes increase slightly with depth. There is no strong correlation between microseismic event size and hydraulic fracture treatment size (Figure 34) nor with injection rate (Figure 35).

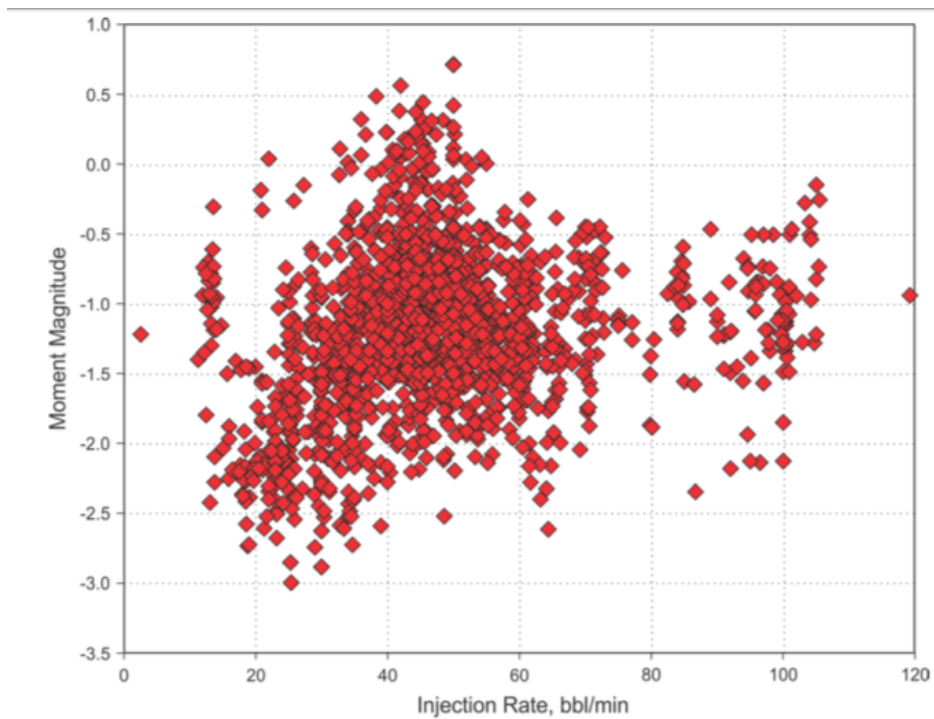


Figure 34. Microseismic moment magnitude for hydraulic fracture treatments in the Barnett Shale plotted versus injection rate (from Warpinski et al., 2012).

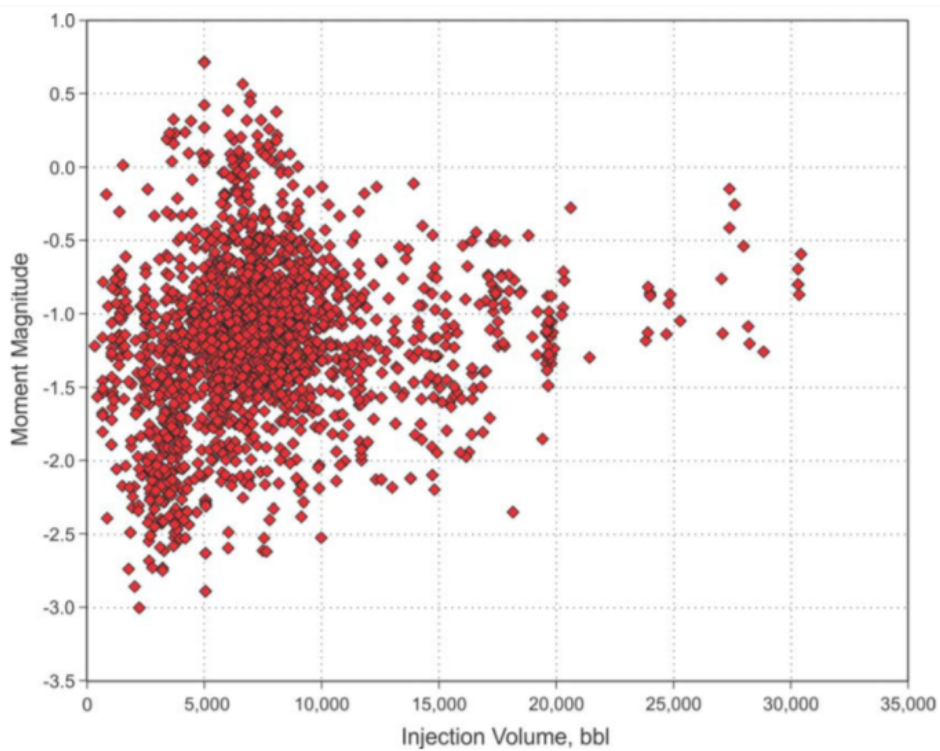


Figure 35. Microseismic moment magnitude for hydraulic fracture treatments in the Barnett Shale plotted versus injection volume (from Warpinski et al., 2012).

Water injection wells, as mentioned earlier, are the primary risk for induced seismicity. In researching the literature and web for this report, it seemed apparent that data on the Ellenburger's injectivity and stress are sparse. In one Texas Railroad Commission report (OIL AND GAS DOCKET NO. 09-0249380, <http://www.rrc.state.tx.us/meetings/ogpfd/09-49380-r9p.pdf>), a recent injection well permit file had the following data:

- maximum injection 20,000 bbls/day, expected average of 7,000 bbls/day
- maximum surface pressure of 2,000 psi enforced by automatic switch, daily pressure recording required
- injected fluid assumed to be 9.6 ppg density
- step rate done in the Terry SWD No. 1, 58 miles away, but considered representative of Ellenburger throughout the Fort Worth Basin
- step rate test run from 4 to 9 bpm and showed no evidence of fracturing
- "the examiners do not recommend that a step rate test be required for the proposed well prior to commencing disposal"
- injection zone is the lower part of the Ellenburger, expected at 7,000 – 8,000 ft, and the thickness in a nearby well suggests a total Ellenburger of 2,500 ft

There are several issues of possible concern from this report. First of all, considering the potential risk for induced seismicity and injection out of zone, all injection wells should perform a step rate test after being drilled to confirm the fracture gradient and safe injection rates. A step rate test from an equivalent well 58 miles away would never be adequate for data collection for hydraulic fracturing operations. It shouldn't be adequate for injection wells. Secondly, the proposed well in this case was being permitted for 20,000 bbls/day (almost 14 bbls/min), while the offset well step rate test was limited to a range of 4 to 9 bbls/min. Consequently, this referenced test does not address whether the permitted rate limit for the new well is adequate. Also, the report on the test was that no fracturing was detected between 4 and 9 bbls/min. The intent of the step rate test should be to induce fracturing so that a measure of the fracturing stress can be made. If no evidence of fracturing was detected, then the test was

inconclusive and inadequate. Finally, a surface pressure of 2,000 psi for a fluid with a 9.6 ppg density implies as much as 0.79 psi/ft injection pressure (neglecting flow

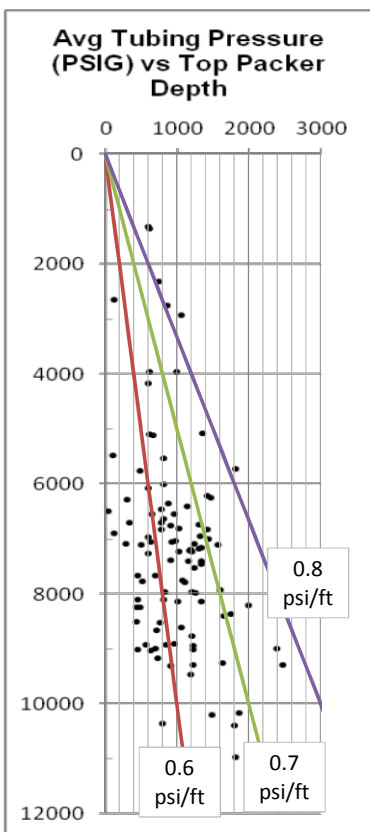


Figure 36. Injection well surface pressure vs. packer depth for the Ellenburger Fm. in the Fort Worth Basin. From Ficker (2012).

pressure loss down the pipe) at the top (7000 ft) of the proposed injection interval. The friction pressure loss for the proposed 3.5 inch injection tubing would be on the order of 500 psi, which would reduce the downhole injection pressure to 0.71 psi/ft, still within the range of fracturing pressure for the Barnett.

A summary of injection data (Figure 36) collected from Railroad Commission files by Ficker (2012), all stated to be Ellenburger wells in the Fort Worth Basin, shows recorded surface injection pressure values versus depth. I added an overlay showing the downhole pressure gradient implied assuming no friction pressure loss in the tubing. There are some shallow wells (2,000 to 3,000 ft depth) injecting at greater than 0.8 psi/ft, but most of the deeper wells are at less than 0.7 psi/ft. Nonetheless, without a good step rate test where fracturing pressure is determined, the safety of these injection pressures cannot be assessed.

Avoiding fracturing pressure in injection wells is intended to prevent the injected fluid from escaping to another zone, but it does not necessarily mitigate induced seismicity. Shear failure can occur on critically stress faults at pore pressures significantly less than fracturing pressure. As is evident in the Fort Worth Basin, there are felt earthquakes associated with injection wells even though wells are restricted to inject below fracturing pressure. To generate a felt earthquake (~M3.0), faults must slip over fairly large patches (Table 10). A M3.0 earthquake implies almost 1 meter of slip on a fault with a dimension of 80 meters, which doesn't pose any serious risk to a structure like Joe Pool

dam, but a M5.0 earthquake implies 8 meters of slip over an 800 meter patch, which could cause serious surface deformation even if it didn't breach the surface.

To assess seismic risk to Joe Pool Dam, earthquake magnitude and proximity are needed. Frohlich (2012) suggests that induced earthquakes should have magnitudes that are less than or equal to the largest natural earthquake in a region. The largest recorded earthquake anywhere in Texas was a M5.8 on the Richter scale, which occurred in 1931 in Valentine, Texas (Stover and Coffman, 1993) and is considered of natural occurrence. The largest induced earthquake in Texas was a M4.6 near Snyder, Texas in 1978 (Appendix B), attributed to waterflood operations in an oilfield. Given the sparse seismic record for North Texas and the historical precedent of the M4.6 quake in Snyder, it seems reasonably conservative to choose M4.5 to M5.0 as the range for the maximum possible earthquake induced by a Barnett injection well. Structural damage to the dam requires sufficient ground acceleration, which is proportional to earthquake magnitude and dies off with distance from the earthquake source.

Joyner and Boore (1981) provide a way to estimate the radiation of ground acceleration as a function of earthquake magnitude. The peak ground acceleration (PGA) for an earthquake of moment magnitude,  $M_w$ , as a function of distance is given by

$$\log (PGA) = -1.02 + 0.249M_w - \log R_{JB} - 0.00255R_{JB} \quad (30)$$

where

$$R_{JB} = (d^2 + 7.3^2)^{1/2} \quad (31)$$

and  $d$  is the distance from the surface projection of the fault. Using M4.5 to M5.0 as the induced earthquake size, and assuming a maximum allowable acceleration of 0.2g (personal communication, USACE), Fig. 37 shows that the earthquake source would need to be 2 to 4 km (6560 – 13,120 ft) distant from the dam to keep induced ground motions within acceptable limits. Given that an injection well can raise the pore



pressure over a broad area (a reasonable radius of influence would be 1 km), the epicenter of an induced quake wouldn't necessarily be centered at the well surface location. Combining all these factors and their uncertainty, a conservative exclusion zone for injection wells around Joe Pool Dam should be at least a 16,400 ft (5 km) radius. Extending the stand-off to 32,810 ft (10 km) would reduce likely ground acceleration to the 0.2g threshold for even a M5.8 (the magnitude of the Valentine quake).

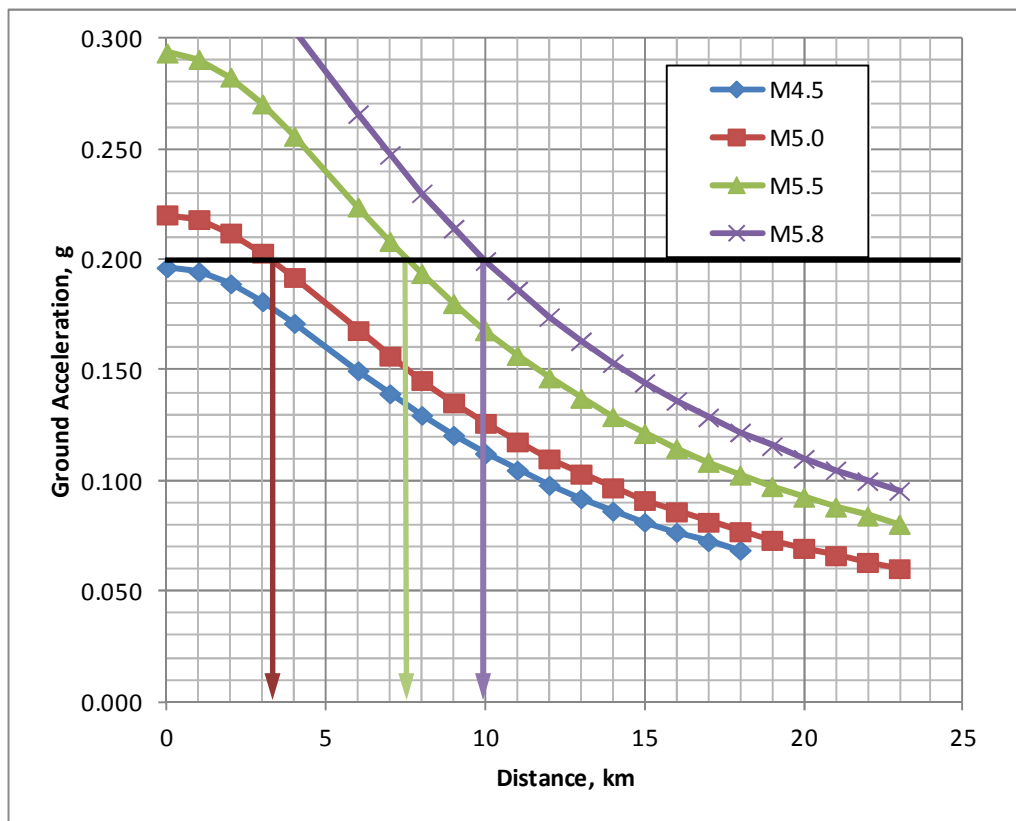


Figure 37. Peak ground acceleration values versus distance from epicenter for various magnitude earthquakes (M4.5 to M5.8). Computer using equations from Joyner and Boore (1981).

With regard to water protection, the assessment of the industry and much of the environmental community is that upward propagation of a hydraulic fracture proposes minimal risk if any (Fisher and Warpinski, 2012; Davies et al., 2012), while the main risk is poor well construction and surface spills (King, 2012). King (2012) put together a risk assessment diagram to evaluate the probability and severity of surface spills and subsurface contamination for the complete life cycle of exploration through

abandonment (Fig. 38). The x-axis on the plot is probability, and the y-axis is severity, with the least severity (1) being equivalent to a 5 gallon or less spill of a non-toxic household chemical to the worst (10) being equivalent to unmitigated acid mine drainage. His assessment for a mature shale gas play is the worst likely severity would be a 5 with a probability of 1 in a million. It is unclear how rigorous the statistics are, but it represents a comprehensive survey of the possibilities. Also interesting is his list of potential events, of which there are 21 (numbers key into events on Fig. 38), and I have included King's probabilities for these events:

1. Spill of a transport load (130 bbls) of water without chemicals (Probability,  $P \sim 20$  out of 1 million)
2. Spill of 500 gallons of concentrated liquid biocide or corrosion inhibitor ( $P \sim 1$  in 4.5 million)
3. Spill of 500 lb of dry additive, expecting <10% loss ( $P \sim 1$  in 4.5 million)
4. Spill of 300 gallons of diesel from a ruptured saddle tank on a truck in a roadway accident ( $P \sim 66$  to 195 in 1 million, depending on whether single or double wall tank)
5. Spill of 3500 gallons diesel from a roadway wreck (standard field location refueler load) ( $P \sim 0.5$  to 1 in a million, depending on whether tank is compartmentalized)
6. Spill of leak of 500 bbl well-site storage tank, either fresh or salt water ( $P \sim 1$  in 1000)
7. Spill of water treated with biocide ( $P \sim 1$  in 10,000)
8. Spill of diesel while refueling pump trucks ( $P \sim 1$  in 10,000 to 100,000, lower if using semi-permanent fuel lines on site instead of hoses)
9. Spill of 500 bbl of backflow water ( $P \sim 1$  in 1000)
10. Fracture pressure ruptures surface casing at the depth of a freshwater sand ( $P \sim 1$  in 100,000, impact mitigated by active annular monitoring in well during completions)
11. Fracture fluid cooling in wellbore compromises tubing/annulus seal ( $P \sim 1$  in 1,000)
12. Fracture opens a mud channel in the cement on a well less than 2000 ft deep, leaking 25 gallon/minute for an entire 4 hour fracture treatment (probably penetration into formation of 30 ft) ( $P \sim 1$  in 1,000)

- Figure 34 - Risk Evaluation of a frac in a known area after necessary technology application on earlier wells.**
- 
- Consequence (more severe)**
- Occurrence (more frequent)**
- Figure 38. Matrix of risk and consequence for various events that could be associated with shale gas fracturing. From King (2012).**

Figure 38. Matrix of risk and consequence for various events that could be associated with shale gas fracturing. From King (2012).

In King's discussion, several mitigation strategies that could be considered best practices were highlighted:

- cement around casing should be run high enough to cover all productive gas zones above the main pay zone (in the local Joe Pool wells, it looks like the cement is run to about 2,000 ft above the Barnett)
- if old wells are properly abandoned, even intersecting them with a fracture treatment should have no impact
- the use of "green" chemicals can reduce the impact of spills and leaks

Another aspect of King's conclusions is that in many gas basins, water wells are already "naturally contaminated" with methane. Thus, proper assessment of the impact of drilling and hydraulic fracturing operations requires pre-testing of existing water wells for methane or other contaminants.

Finally, the subsidence calculations in Section 6 indicate that there could be enough ground motion to affect dam performance, but there is a fair amount of uncertainty as to the appropriate input parameters for the calculations. This uncertainty recommends two courses of action. One is to make it a priority to collect a good number of core samples from the reservoir in order to assess its elastic compaction coefficient and creep potential. The log from the Joe Pool vicinity indicates a Young's modulus lower than much of what has been published, and the importance of nonelastic processes is not well documented for the Barnett. From what I found in the literature, there was only one 3 hour creep test reported for the Barnett Shale. The other problem with published values on the Barnett is that most of the work has been done in the core area of the East Newark Field, which is quite a distance away and substantially shallower than the Barnett in the vicinity of Joe Pool. The second course of action is to create a monitoring plan for subsidence. A long leveling line that starts well outside the predicted subsidence bowl (15 miles to the east of Joe Pool) and goes at least 5 miles to the west would be ideal. The survey should be repeated once per year for the first two years to get an idea of variability, and then every 5 years should be sufficient after that. The other type of monitoring that can be done is for seismic, but there is quite a bit of activity

with local universities installing extra instrumentation, so this is already being addressed. If it is not already being done, periodic water quality testing should be done, but given that shale gas operations started in the area in 2007, it is probably too late to get any baseline data with which to compare to. I wouldn't recommend any local ban on hydraulic fracturing fluid make-up beyond what might be happening regionally, but it is certainly worthwhile promoting greener completions fluids, and industry is already moving in that direction.

## **11. Recommended Best Practices: Drilling, Hydrofracturing and Extraction & Well Construction.**

In June of 2012, the International Energy Agency (IEA) recently came out with a "World Energy Outlook Special Report on Unconventional Gas" titled *Golden Rules for a Golden Age of Gas*. The main point of this report is that natural gas is a valuable energy resource for much of the world, but if development and public relations related to the development is not done right, the public resistance (from private citizens and governmental agencies) to industry efforts could seriously hamper results, particularly if widespread bans on drilling and completions are put in effect. With this as a background, the IEA report basically outlines best practices for all of unconventional gas development, of which shale gas is a large part. They note that unconventional gas has a larger environmental footprint than conventional gas, requiring more wells and stimulation techniques like hydraulic fracturing. More intense operations require more land and water usage and increase the potential for air pollution, land and water contamination. Production is also more energy intensive, so it emits more greenhouse gases than conventional operations.

The technology and know-how exists to produce unconventional gas in an environmentally sound manner, but companies need to work to get public acceptance – it is not guaranteed (according to the IEA). Industry needs to follow best practices technically AND socially, while governments need to pursue science-based regulations, hire sufficient compliance staff, and promote public access to information. The IEA

estimates that implementing the best practices in their report could increase production costs by 7%, which might sound difficult to absorb for a low margin business given the current price of natural gas, but prices are only depressed in the United States, they have the prospect to improve, and IEA concludes that without better public acceptance, future production is at risk.

The “Golden Rules” outline several different areas for improvement or increased acceptance of best practices:

- assess deep faults for earthquake and leak potential
- monitor hydraulic fractures to assure they don’t escape from the production zone
- consider setting a minimum safe depth above which fracturing will not be allowed
- be diligent in preventing surface spills, but have plans and contingencies for spill containment
- dispose of contaminated water responsibly (even when treatment facilities that cannot handle the contaminants are willing to accept the water)
- reduce freshwater usage by increased recycling
- find and promote more environmentally benign additives for drilling and completion fluids
- implement efforts to reduce fugitive gas
- develop robust regulatory regimes and well-trained compliance staff
- create emergency plans that match the scale of the risk

With regard to well construction, there are several best practices to follow:

- use multi-well pads to reduce the land usage footprint (this is already being widely used throughout the Barnett)
- inspect well site carefully
  - assess run-off potential for spills
  - estimate transportation/traffic impact
  - evaluate geologic risk (faults, depth)

- survey for old wellbores
- store mud in tanks or high quality pits
- to maximize casing integrity
  - drill wells to design without extra doglegs
  - use adequate centralization during cementing (oft cited as the biggest problem with cement jobs)
  - use good quality cement (design for good liquid properties while pumping, adequate set time, and strength and flexibility after setting)
  - verify cement seal (with returns to surface or logging)
  - monitor integrity regularly over the lifetime of the well
  - cement needs to withstand fracturing pressures as well as production loading (follow API standards)
- with regard to induced seismicity, the area should be surveyed for large faults and monitored during operations
- make financial provisions for plugging and abandoning (this is required in Texas)
- plan upfront for water usage and disposal
- possible ways to reduce water usage include using more viscous gels (instead of slickwater fracs), using foams or using hydrocarbon fluids (These methods have been tried in the Barnett, and although there is still debate on their efficacy. One of the successes of early development in the Barnett was refracturing wells with slickwater after they had initially been fractured with cross-linked gel and foam – Fig. 39.)

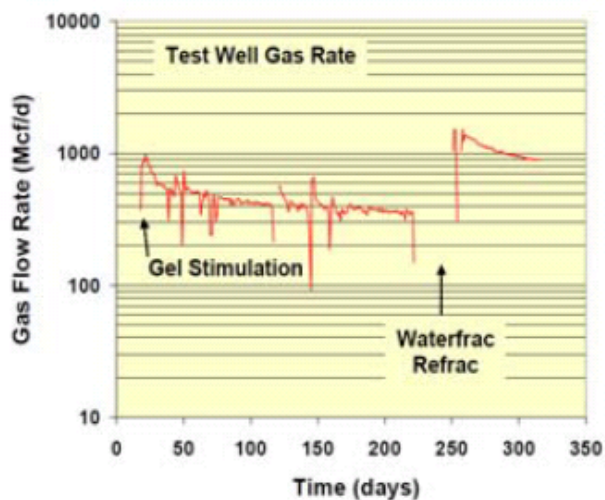


Figure 39. Improving gas rate by refracturing in the Barnett Shale for wells originally stimulated with gel instead of slickwater. From Cipolla (2005).

- use weather-proof containers for fluids to prevent spills and overflows
- geologic leakage is assessed to have garnered too much attention, and is stated by IEA to be “the least significant of the hazards”
- preventing improper discharge of contaminated/used fluids requires proper regulation
- the first priority is to prevent venting – flaring is preferred as CO<sub>2</sub> is less of a greenhouse gas than methane – but IEA recommends spending the extra money to have gas processing facilities operational during the drilling and completions stage
- establish baseline data for groundwater before development begins
- report water usage, chemicals employed (see [www.fracfocus.org](http://www.fracfocus.org)), and water disposed
- eliminate infield trucking of water with pipelines
- create closed loop water recycling facilities
- long term monitoring
  - collect a 3d seismic baseline
  - maintain longterm microseismic monitoring
- work to optimize drilling and the number of fractures per well
  - avoid drilling and completion in low productivity zones
  - less fracturing will use less resources and generate less waste

Additional best practices mentioned earlier from King (2012) include:

- cement around casing should be run high enough to cover all productive gas zones above the main pay zone (in the local Joe Pool wells, it looks like the cement is run to about 2,000 ft above the Barnett)
- if old wells are properly abandoned, even intersecting them with a fracture treatment should have no impact
- the use of “green” chemicals can reduce the impact of spills and leaks

With regard to mitigating geologic hazards from reservoir compaction and induced seismicity, in addition to surveying for large scale faults and other structures, the following would have been helpful for this study.



- site-specific static elastic property data (collect core from the reservoir interval in a regular fashion – there can be significant variability even in neighboring wells)
- determine the degree to which the reservoir rock will creep, being sure to assess with long term tests (months), and loading to full abandonment depletion conditions
- establish a baseline leveling line through the region – even though most shale resource plays are in “hard rock” country, the fact that development will occur basin wide at as close a well spacing as economics will permit means a significant fraction of the compaction experienced in the reservoir will most likely be transmitted to the surface as subsidence
- require step rate testing for all injection wells (this should be a low cost item)
- consider a transient testing program at the beginning of the injection program to detect boundaries within the injection zone (this could be a fault that might cause induced seismicity problems), and consider doing tests periodically to assess pore pressure increase.

More detail with regard to cementing best practice unconventional gas completions was published by Darbe and Ravi (2010). They suggest the following practices:

- Circulate the hole with completion fluid before cementing to clean hole of drilling fluid and leftover cuttings (possibly even running a wiper trip) to assure good contact between cement and formation. Otherwise problems may arise with mud and cuttings accumulating on the bottom side of the hole in the deviated/horizontal section, and this could create uncemented channels in the annulus behind pipe that give fracturing fluids and hydrocarbons access to other shallow zones.
- The use of foamed cement (typically by adding nitrogen) can result in less brittle, higher compressibility cement that can better handle fatigue loading (repeated hydraulic fracture cycles) without cracking. Foamed cement also has more energy for placement to aid in hole cleaning. Another advantage to foam is that it inhibits volume shrinkage during curing.
- Gas percolation through cement while it is curing can be a problem. A thixotropic slurry, by quickly gelling once emplaced, helps prevent gas migration. Also, as the cement cures and transitions to a solid, hydrostatic head is lost. At that point gas pressure can exceed that in the cement and percolate through the cement can occur, so a quick transition is also desirable.
- Centralization is particularly important in deviated and horizontal wells, but it is sometimes left out because of the difficulty of running casing through the bend

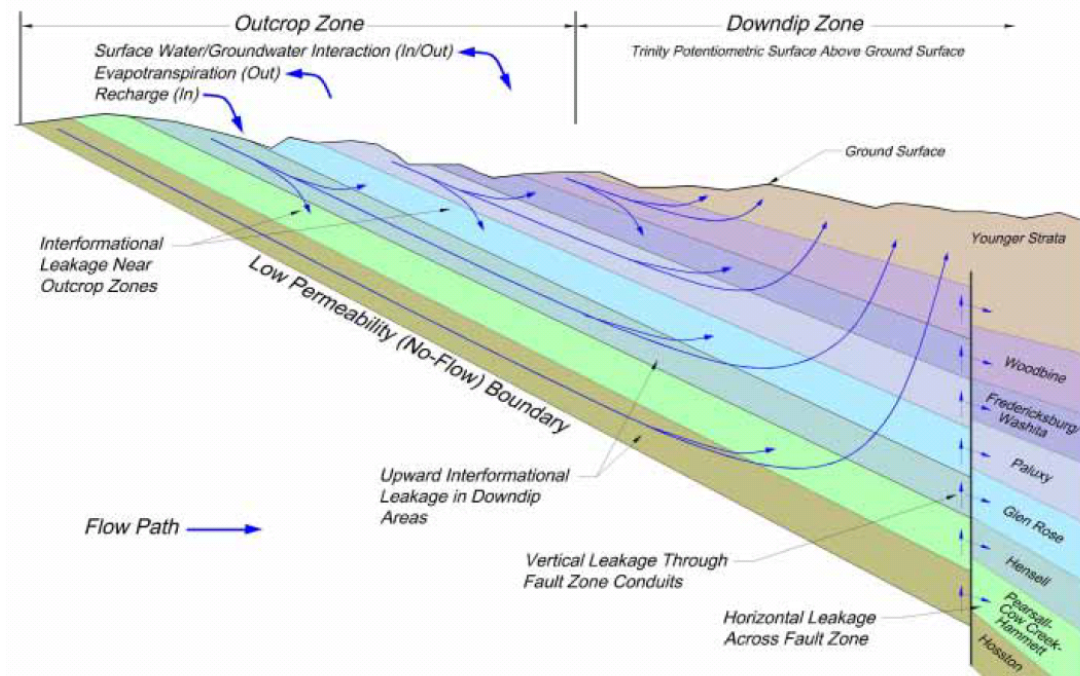
and along the horizontal section. Without centralization, however, there is a higher likelihood for poor annular flow and lack of uniform cement placement around the pipe. Rotation can also help with better flow performance in the annulus while cementing.

## **12. Other Potential Impacts.**

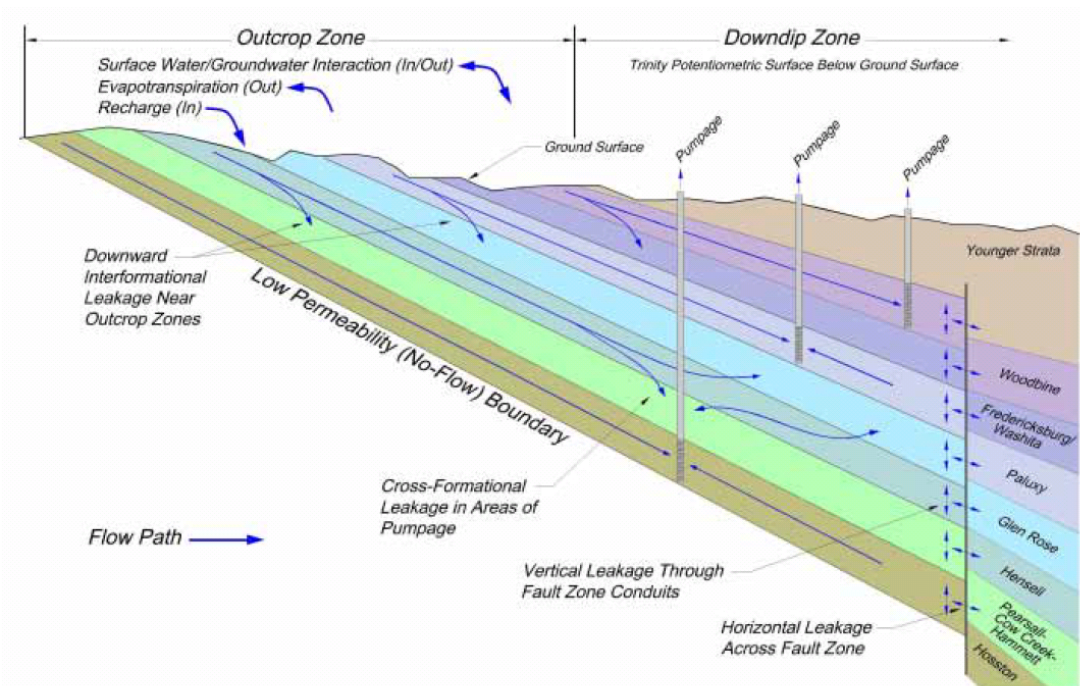
The topic of injection wells, which is the primary “potential impact” other than drilling, hydrofracturing and extraction, has been discussed extensively under the *Risk Reduction* topic. A discussion of the chemicals used in drilling and completions is in Appendix A. Another topic not discussed thus far, which is an indirect piece of information concerning migration of hydrocarbons and injected fluids upward from the Paleozoic section, is the Texas Water Development Board’s assessment of groundwater flow in Cretaceous aquifers. Harden and Associates (2004) published the *Northern Trinity / Woodbine Aquifer Groundwater Availability Model*, evaluating the flow pathways through the shallow subsurface as they impact groundwater pumping and natural groundwater movement. They concluded that there was vertical communication between the different Cretaceous units (Figure 40) but not along faults. With regard to faulting, the report states:

Extensive faulting throughout most of Texas offsets the Trinity/Woodbine sediments, and affects regional groundwater flow. Major fault zones, including the Balcones and the Luling-Mexia-Talco, can exhibit hundreds of feet of displacement effectively juxtaposing vertically distinct hydrostratigraphic units. However, the relatively insoluble character of the Woodbine, Paluxy, Hensell, and Hosston sediments results in the smearing of materials in the fault zone, and precludes significant dissolution of arenaceous fault-zone materials. For this reason, little if any vertical or horizontal interformational flow is thought to occur in fault planes or across faulted sediments (Yelderman, 2002). For this reason, the Luling-Mexia-Talco Fault Zone defines the downdip boundary of groundwater flow.

They also presumed as a part of their modeling that the rocks beneath the Paleozoic-Cretaceous unconformity were essentially impermeable (Figure 40).



a)



b)

Figure 40. Trinity - Woodbine aquifer system and inferred flow paths a) before development by domestic water wells and b) after well pumping.

### **13. Evaluation of Baldwin Hills Failure and Comparison to Joe Pool.**

The Baldwin Hills Dam failure is well documented in reports by James et al. (1988) and Hamilton and Meehan (1971), and some of the details of production from the nearby Inglewood Oil field are found in Oefelein and Walker (1964). On December 14, 1963, the Baldwin Hills Dam failed and emptied its entire 250 million gallons into the nearby community (Hamilton and Meehan, 1971). Failure was attributed to differential movements caused by either fault slip or differential compaction that promoted failure of the dam's liner and foundation. Post-failure inspection indicated sink-holes and other indications of erosive flow associated with fault trends. There was evidently significant pre-existing dissolution or fault offset related cavities in the near subsurface that could accommodate flow. The location of Baldwin Hills (Figure 41) is quite exceptional in that it was located along a 75 km, active fault trend in the Los Angeles Basin, described as slipping 0.6 mm/year and capable of a magnitude M7.0 earthquake ([http://en.wikipedia.org/wiki/Newport-Inglewood\\_Fault](http://en.wikipedia.org/wiki/Newport-Inglewood_Fault), accessed July 8, 2012). In addition, there appeared to be a direct fault connection between the nearby Inglewood Oilfield in the subsurface and the Baldwin Hills Dam and impoundment (Figure 42). At the time of failure, there were 3 active wells within 700 ft of the south rim of the Baldwin Hills reservoir.

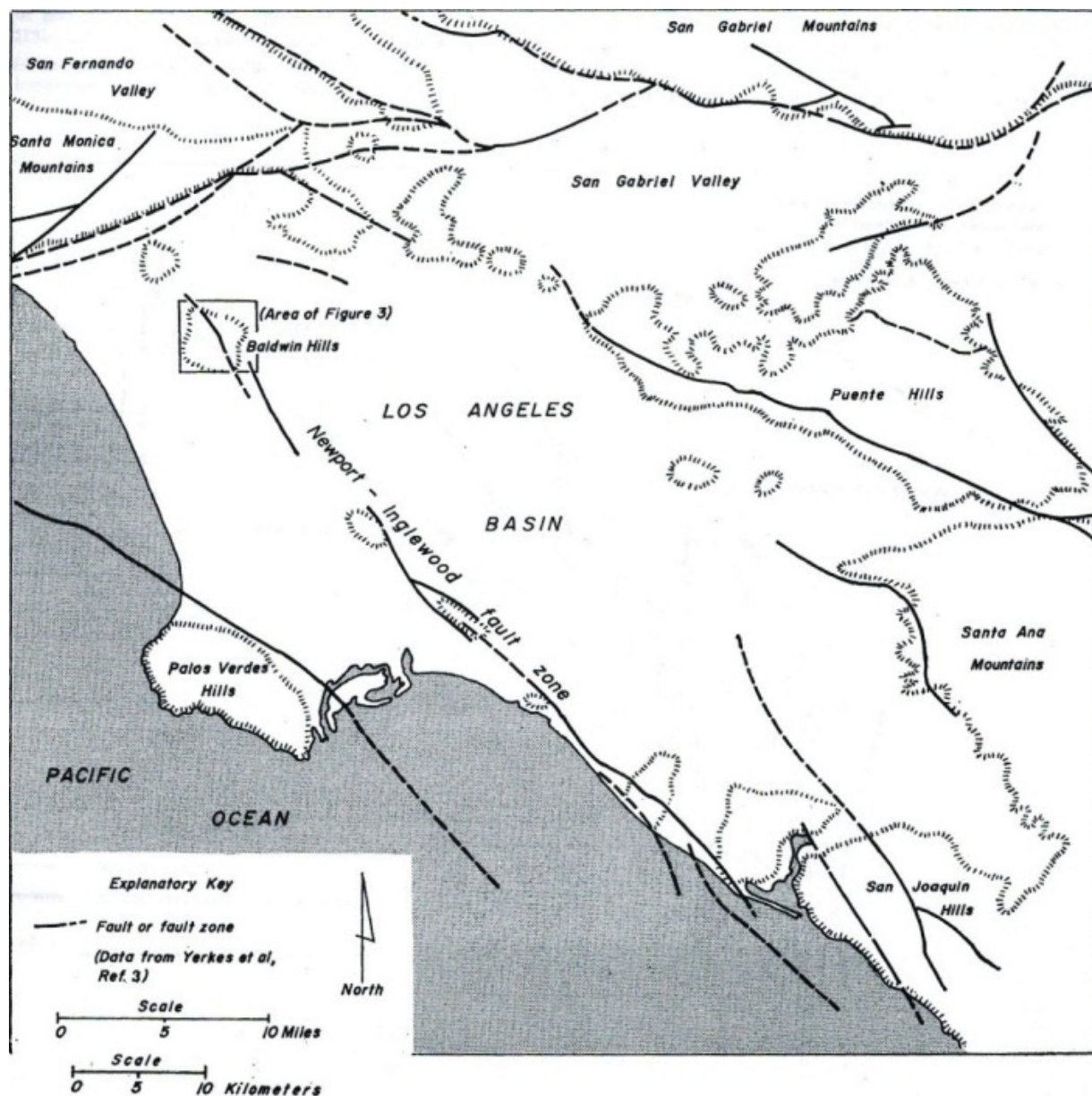


Figure 41. Regional map showing location of Newport-Inglewood fault zone and Baldwin Hills reservoir. From Hamilton and Meehan (1971).



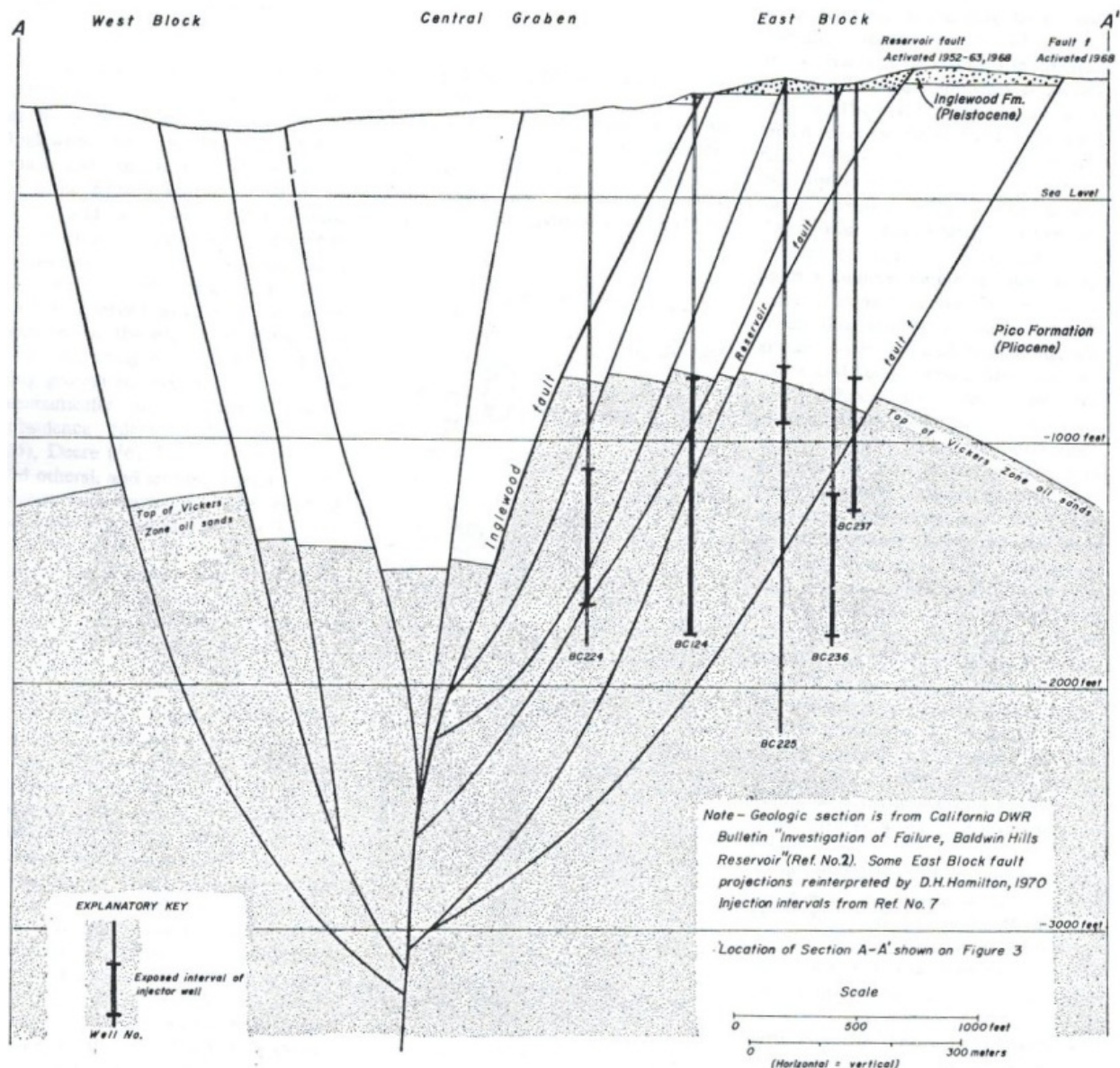


Figure 42. Cross section of Inglewood Field, showing classic “negative flower structure” where a through-going strike slip fault (coming out of the page) blossoms into multiple graben style normal faults that also have strike-slip components. Cross-section suggests that faults run from oil reservoir to the surface underneath the Baldwin Hills dam. From Hamilton and Meehan (1971).

The Inglewood field has been producing since 1924, has a 250 acre areal extent, and was assessed to have 73,500 acre-ft of oil sand. Oefelein and Walker (1964) state the reservoir consisted of 65 cp oil in a 1200 ft thick section of soft shale and unconsolidated sand, with 520 ft net sand (35% porosity and 752 md permeability) and 20 ft thick intervening shale zones. The depth range for the Vickers East pool is 1000 to

2200 ft (the second shallowest producing zone), and there are 8 zones, from 900 to 11,000 ft deep and from Pliocene to Upper Miocene in age (all very young). In the Vickers, the original pressure was 570 psi (hydrostatic), and declined to less than 100 psi after primary depletion. Operational problems were encountered with “running sand” conditions in producers (sand production), casing failure and sanding in injectors – all of these things suggesting a very weak, compressible formation. Hamilton and Meehan (1971) suggest that the casing failures around the injectors were a result of increased pore pressure inducing shear failure in the formation, possibly in places where the wells crossed faults. Because of all the sanding problems, they had to change from slotted liners to gravel packs in wells during waterflooding. Waterflooding initiated in 1954 and was fullscale by 1957, injecting 42,000 bwpd (bbls of water per day) by July 1963, with an oil production of 3400 bopd (bbls of oil per day) (Oefelein and Walker, 1964).

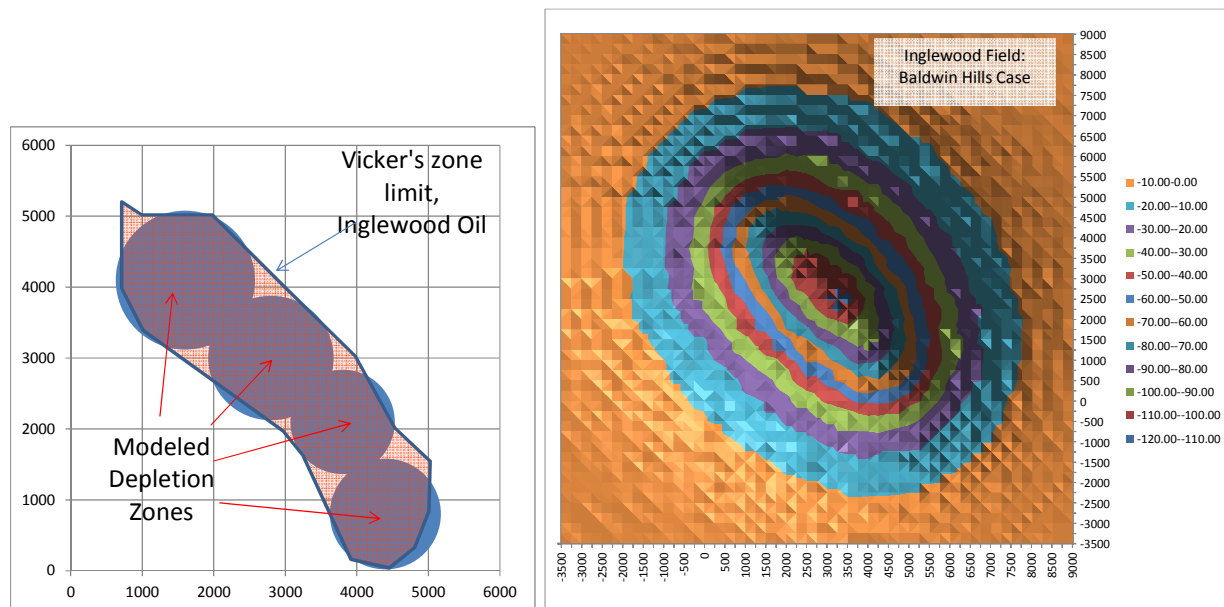


Figure 43. a) Reservoir discretization and b) subsidence bowl for the Baldwin Hills – Inglewood field case.

Based on the reservoir description from the literature, I modeled the ground surface subsidence after 500 psi of depletion (Figure 43). The depth to the NW reservoir disc was 1800 ft and the others were located at 1600 ft depth, with thicknesses of 1200 ft according to the published values. The one parameter that was not described was the compressibility of the sand, although it was clearly on the opposite end of the spectrum

from the Barnett. Based on published data for unconsolidated sands and experience in the laboratory measuring elastic modulus for sand at various confining stresses, Young's modulus could vary from as little as 10,000 psi to as high as 150,000 psi. I chose  $E = 30,000$  psi and  $\nu = 0.15$  to match the 10 ft maximum subsidence reported by Hamilton and Meehan (1971). The subsidence bowl shape is a reasonable reproduction of the map published by Hamilton and Meehan (1971).

Comparing this case to the Barnett shale, the rock type is totally different (uncemented sand vs. siliceous shale), and the Barnett has a Young's modulus on the order of 20 to 100 times higher. This results in a much lower compressibility for the Barnett, largely a function of the Barnett having been buried to greater depth (8600 vs. 1200 ft) for a longer time (300 million years vs. 10 million). Another factor making the Baldwin Hills case more extreme than the Barnett is the difference in reservoir thicknesses, 350 ft for the Barnett versus 1200 ft for the Vickers member (with an overall producing column thickness in the Inglewood field of 8000 ft). Yet another factor making the Inglewood field different than the Barnett is depth to the hydrocarbon bearing zone. In Inglewood, depth to the top of the reservoir is on the order of 1000 ft, while in the Barnett is about 8000 ft deep. The deeper the reservoir, the more muted the surface expression of any downhole compaction or inflation (technically the surface subsidence is a function of the ratio of reservoir diameter to depth – smaller reservoir diameter and greater depth both diminish surface effects).



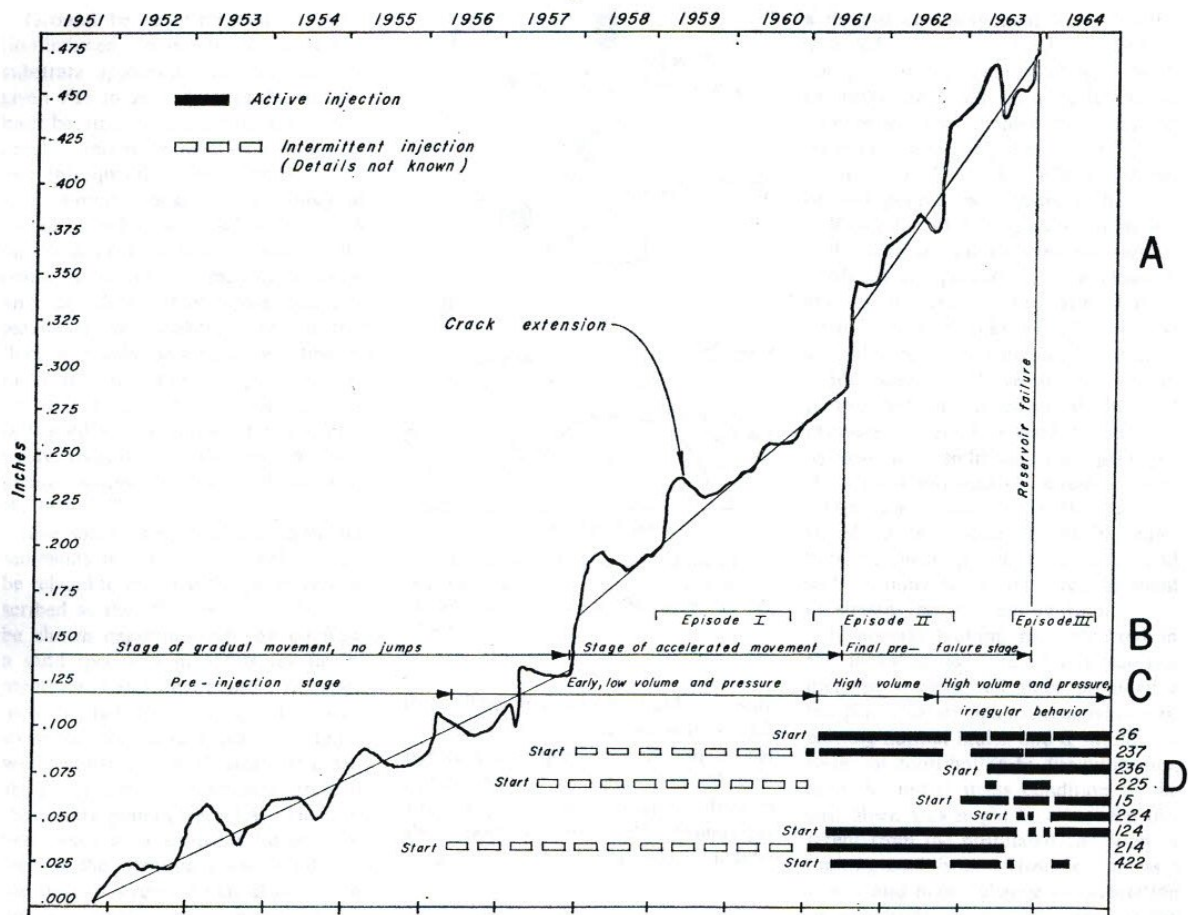


Figure 44. Diagram showing increasing subsidence with time where slope increases as water injection at the Inglewood Field increases. From Hamilton and Meehan (1971).

Finally, according to Hamilton and Meehan (1971), the waterflooding operation on the east flank of the Inglewood Field, very close to the southern rim of the Baldwin Hills reservoir, accelerated subsidence by causing slip on nearby faults (Figure 44). Oefelein and Walker (1964) report initial injection pressures of 0.95 psi/ft or less, but they speculate the pressure could be increased to 1 to 1.4 psi/ft. They stated that these high pressures were reasonable based upon a test of 11,000 bwpd at 1400 psi surface pressure (1.9 psi/ft gradient) which was achieved without evidence of parting or breakdown. There is no doubt that these high pressures would have significantly reduced frictional resistance of nearby faults, accelerating the ground motions that caused the dam to fail. The fact that injector wells were failing as they raised the pore pressure seems a pretty good confirmation of the process. The lack of associated seismic activity (at least none was reported) is probably due to the very ductile and

weak nature of the local rocks. The faults were probably creeping rather than propagating with high speed ruptures and earthquakes. In the Fort Worth Basin, there will be no 10 ft subsidence events - the conservative properties case from Section 6 predicts 7 inches of ultimate subsidence, almost 20 times less than the actual measurements in Baldwin Hills. The optimistic case of less than 2 inches of subsidence is 60 times less. As mentioned earlier, there are also no clear significant faults intersecting the surface that could cause the magnitude of near-surface slip experienced at Baldwin Hills.

#### **14. Recommendations.**

There are several additional studies that are suggested by the results from this work:

- Further research should be pursued to better determine the static mechanical properties of the Barnett Shale, assessing whether Young's modulus in the Joe Pool region is lower than in other areas as implied by the local log analyzed, and to determine the appropriate dynamic to static correction factor for the elastic moduli when dipole logs are available. Because of the very low permeability of the Barnett, low term testing may be required to properly assess drained modulus behavior in the rock. Better elastic property determination in the Joe Pool region would help better estimate expected compaction and subsidence from elastic models. There are numerous publications that discuss mechanical property results, but they do not always specifically state the well location, or the age of the work suggests that well location is probably more toward the core Barnett area NW of Joe Pool. The potential for stratigraphic heterogeneity (and structural heterogeneity) recommends for more site-specific information when examining processes affecting Joe Pool Dam and Lake.
- Further research should be pursued to determine the long term creep properties of Barnett shale in order to better constrain the enhancement of reservoir compaction and subsidence from non-elastic mechanisms. Only limited short-term creep testing was found in the literature, and no long term tests were found.
- If the worst case or conservative case compaction/subsidence calculations predict subsidence values that are of potential concern, more rigorous calculations should be pursued that can incorporate non-elastic effects, material anisotropy and material heterogeneity. Shales are expected to have high elastic anisotropies, and such properties could significantly alter the compaction behavior of the reservoir. Also, the effect of a stiffer underburden below the Barnett needs to be investigated to better evaluate subsidence potential.

- A leveling survey should be performed, and a follow-up program established, to empirically evaluate whether any surface subsidence is occurring in the Barnett Shale within the Joe Pool area.
- There is a remote chance that production from the Barnett could induce seismicity. In addition to the mechanical properties that would be pertinent to compaction/subsidence studies, rock strength testing should also be done for the Joe Pool area.
- Injection wells pose the greatest seismic risk. Injection wells should be located no closer than 5 km to Joe Pool Dam and related structures. To mitigate seismic risk and improve risk assessment, better data should be collected on the Ellenburger to assess fracture gradient, injectability and the presence of any boundaries to flow. It might be fruitful to run microseismic monitoring on an injection well also to assess the impacted volume of water injection.
- A stand-off of 3000 ft for production wells may be needed to mitigate risks due to underground and surface blowouts. This offset could be refined with better characterization of fault permeability and extent in the shallow subsurface (down to the basal Cretaceous unconformity).



Appendix A: The Barnett Shale:  
Geologic Setting, Oil and Gas Development Practices, and  
Environmental Considerations (May 2012)

**Appendix A:**

**The Barnett Shale:  
Geologic Setting, Oil and Gas Development  
Practices, and Environmental  
Considerations**

**May, 2012**

**Prepared by:**

**Kimberly Gordon, P.E.**

**Platt, Sparks & Associates, CPE Inc.**

**Consulting Petroleum Engineers**

**Texas Registered Engineering Firm F-1493**

**Austin, Texas**

**Prepared for:**

**Dr. Jon Olson**

## **The Barnett Shale: Geologic Setting, Oil and Gas Development Practices, and Environmental Considerations**

### **Introduction**

Gas production and exploration in the Barnett Shale play has been ongoing for more than thirty years. The play lies within the Fort Worth Basin and the productive part of the formation stretches from the city of Dallas west and south, covering 15,000 square miles and at least 23 counties. The discovery of the play in 1981 and the establishment of the Newark East Field in Wise County by Mitchell Energy Corp were followed by rapid expansion in the mid-1990s with advent of economic hydraulic fracture treatments. As of March 2012, the Texas Railroad Commission (TRRC) has 15,731 Barnett Shale gas wells on their records with an additional 3,112 permitted locations. The TRRC has also issued 193 permits for commercial disposal wells in the producing area. Since 1993 and through 2011, the Newark East Field has produced 10.8 trillion cubic feet of gas with annual rates of production still increasing despite declines in the number of new wells drilled.

This report describes the geology and important physical characteristics of the Barnett Shale and the overlying sediment and aquifers in the area of the play; the completion techniques in the Barnett Shale; and the features and practices that may have an environmental impact in the play area; and some of the best-practices that are protective of all of the resources in the area. The Barnett Shale is located in the Fort Worth Basin where continual subsidence and lateral shifting of delta positions and carbonate platform deposits through time resulted in the emplacement of sequences of deltaic deposits and channel sands overlain by impermeable shales or limestones resulting in ideal conditions for the generation of petroleum reservoirs. Delineation of the most productive portions of the Barnett Shale play is determined by stratigraphic constraints, organic content of the shale, and thermal maturity of the hydrocarbons. Separated by more than 5,000 ft from the Barnett Shale in the primary production areas, formations overlying the Fort Worth Basin sediments, the sands of the Trinity and Woodbine Groups are the primary groundwater aquifers in the play area. Other formations are also known to yield some ground water of varying quality in the area.

The Barnett Shale can be described as an unconventional, low permeability low porosity reservoir where well construction and completions practices have continually evolved over the expanded development of that began in the early 1990s. Improvements in horizontal drilling techniques and increased efficiencies in hydraulic fracturing (fracing) practices considerably increased the development of the play. Along with this increased development in the Barnett Shale alongside of many urban and suburban areas, concern regarding the environmental impact of this development has also increased. Although there is some small risk from hydraulic fracture treatments, the most significant environmental risks associated with development of the Barnett Shale are from poor drilling and well completion practices and surface spills. The risks are reduced when best practices and proper planning are implemented.

## **Location**

The Barnett Shale play area is located in North-Central Texas as shown on Figure 1. The total areal extent of the play is approximately 15,000 mi<sup>2</sup>. The producing area includes twenty-three counties: Archer, Bosque, Clay, Comanche, Cooke, Coryell, Dallas, Denton, Eastland, Ellis, Erath, Hill, Hood, Jack, Johnson, Montague, Palo Pinto, Parker, Shackelford, Somervell, Stephens, Tarrant, and Wise. Focused field development has occurred in Denton, Tarrant, Parker, Wise, Johnson, and Hood having the most wells. The Barnett Shale production area also encompasses several metropolitan areas in north-central Texas including most of the Dallas-Fort Worth Metroplex except the most eastern and north-eastern portions.

## **Geologic and Hydrogeologic Setting**

**Physiography and topography.** Ground surface elevations range from approximately 1,500 feet in the western portion of the study area to about 300 feet in the eastern portion of the study area near the Trinity River. The study area includes the Brazos River and Trinity River Basins. The physiography is generally controlled by the surface geology and outcrops that occur in a series of north-trending linear belts that alternate between prairies and rolling timbered hills. The topography is more varied and rugged in the far western parts of the region with some resistant formations standing as westward facing escarpments in some locations (Peckham et

al., 1963). The land surface transitions from gently rolling hills in the western portion of the study area to generally flat to undulating in the east. (Baker et al., 1990)

**Structure.** The Barnett Shale and overlying sediments are roughly contained within the Fort Worth Basin. The Fort Worth Basin is a foreland basin associated with the Ouachita structural front. The northern extents are defined by the Red River arch and the Muenster arch (faulted basement uplifts). The elongated, wedge-shaped basin trends roughly north-south and shallows southward. On the western side, the basin shallows near the Bend arch, Eastern shelf, and Concho platform. The Llano Uplift, a domal structure that exposes Precambrian and Paleozoic rocks, truncates the southern end of the basin. A schematic of the basin structural features is shown in Figure 2 from Thomas (2003). The basin fill reaches a maximum depth of about 12,000 ft in the northeastern reaches near the Muenster Arch. Deposits include 4,000-5,000 ft Ordovician-Mississippian carbonates and shales, 6,000-7,000 ft of Pennsylvanian clastics and carbonates, and a relatively thin veneer of Cretaceous sediments in parts of the basin. Stratigraphic analyses and interpretations of depositional history indicate significant portions of Pennsylvanian and Permian strata were eroded before the invasion of Early Cretaceous Seas.

Productive oil and gas intervals are generally found within the Pennsylvanian and older aged sediments, while the most of the water bearing units that contain water of usable quality are found in Cretaceous sediments. Maps showing the base of the Cretaceous formations and top of the underlying Barnett shale indicate that more than 5,000 ft separates these formations.

Other structural features in the basin include major and minor faulting, local folding, fractures, and karst collapse features. Major basement faults occur along the southern extents of the Red River-Muenster arch complex. Along the Muenster arch, a normal fault defining the approximate perimeter of the basin has an estimated displacement of 5,000 ft. The arches formed during the Pre-Cambrian, and were reactivated during the Ouachita Orogeny (Bruner and Smosna, 2011). The Mineral Wells Fault and the Lampasas arch are smaller scale basement structures. The Mineral Wells fault joins the Newark East fault system in the Newark East field. Researchers indicate that the Mineral Wells fault has influenced the depositional history and the thermal history and hydrocarbon migration within the Barnett Shale and the Bend Group (Thompson, 1982; Pollastro et al., 2003). Other faulting has been noted throughout the basin,



including thrust faulting with hundreds of feet of throw that results repeat sections of the Barnett Shale, the Atokan Group, and the Strawn. Slump faulting is commonly observed in outcrops of the Strawn Group (Grayson and Trite, 1988). Periods of basin subsidence are also believed to be associated with growth faults and Ellenburger karst solution-collapse features that intersect multiple strata; however, these features rarely penetrate the Strawn Group indicating that this structural movement occurred primarily during the Atoka time. Evidence of these karst collapse features in the Ordovician-aged Ellenburger is provided by three-dimensional seismic studies (Hardage et al., 1995). Mapping suggests a large karst feature in the northwestern portion of Johnson County.

Within the Barnett Shale there are small-scale natural fractures but they are usually sealed with calcite thought to have originated from mineralized water from the underlying Ellenburger Formation. The lack of open natural fractures is important for the formation of the reservoir. If open natural fractures existed, gas would have escaped to other units, decreasing pore pressure and precluding overpressured conditions (0.49 psi/ft to 0.52 psi/ft) observed today (Bowker, 2007). Healed fracture zones are thought to improve hydraulic fracturing by acting as preferential zones of weakness that deflect induced fractures resulting in a more diffuse fracture network. The highly faulted and fractured zones are also sealed, and similarly the nearby matrix porosity is filled. The understanding of the impact of larger scale faults and fractures on productivity in the Barnett Shale has evolved over time. Originally, operators targeted these zones thinking that faulted zones would have higher permeability and fracture porosity. However, better results are reported for wells outside of fault zones because within fault zones induced fractures can be propagated along fault planes and into the underlying water-bearing Ellenburger. Wells located on or in structural flexures tend to be poorer producers (Bowker, 2007).

**Depositional Environment and History.** As described by Cleaves and Erxleben (1985), the base of the Fort Worth Basin is defined by the erosional surface of the Ellenburger shelf-carbonate system that in the early to middle Paleozoic formed the Concho platform. The Middle to Upper Mississippian saw an alternating series of shallow marine carbonates and black, organic-rich shales, including the Barnett Shale. Loucks and Ruppel (2007) have postulated that deposition of the Barnett Shale occurred in a deep-water slope to basinal setting, where the long narrow

basin was poorly connected to the open ocean where dysaerobic to anaerobic conditions developed. Sedimentation resulted from suspension settling, turbidity currents, debris flows and contour currents, and although fossils are common in the Barnett strata, they were likely transported from adjacent shelves and upper slope settings. During the late Mississippian and early Pennsylvanian, rapid subsidence in the Fort Worth Basin caused an eastward-dipping monoclinial flexure along the eastern margin of the platform. In the late Desmoinesian, the eastern flank of the basin was sharply uplifted by the Ouachita orogeny resulting in a thrust-faulted fold belt. During this same time, epeirogenic uplift gradually tilted the Concho platform forming a westward dipping moncline forming the Bend arch (Figure 3, Cleaves and Erxleben, 1985). During its formation, the basin received sediments consisting of terrigenous, clastic deposits of sandstone and mudstone, and marine sediments including limestone and carbonaceous shales. Contemporaneous deposition varied regionally across the basin, more than 5,500 ft of Atoka clastics and 4,500 ft of Strawn sandstone and shale accumulated in the northern part of the basin at the same time the Caddo carbonates accreted on the Concho platform. Deposition occurred until the Llano Uplift and the Ouachita fold belt caused more regional tilting to the west. This shift to the west caused only a small portion of the area to receive Permian sediments, and a significant unconformity between Pennsylvanian and Cretaceous sediments indicates a long period of emergence and erosion. Pennsylvanian aged Canyon and Cisco Groups feature lobate-deltaic sediments that are prominent in the north-northeastern areas of the region, and carbonate banks in the western portion of the study area, trending roughly along the Bend arch. This depositional setting resulted in a complex sequence of interfingered deltaic and shallow marine depositional environments (Nordstrom, 1988).

The Cretaceous Period saw major invasions of the seas of the Comanche and Gulf series and the depositions of thick sequences of limestone and other fine-grained sediments on a relatively flat erosional surface (paleoplain). These sediments form a southeastern-thickening wedge from north-central and central Texas outcrop areas to the East Texas Basin (Nordstrom, 1982). During late Cretaceous times, general uplift in the west and withdrawal of the seas left only the eastern portion of the study area covered. Following the uplift and withdrawal of the seas, transgressions and regressions of the seas resulted in alternating deposits of marine and continental sediments. During the Tertiary, land was eroded and contoured by streams, and in the Quaternary, streams deposited alluvial sediments (Nordstrom, 1982).

### **Stratigraphy and Lithofacies**

Table 1 provides a generalized stratigraphic column for the sediments found in the Fort Worth Basin beginning at the base with the Ordovician Ellenburger through the youngest alluvial sediments. Physical properties of specific units are often not well characterized or reported; however where information is available and applicable, the table provides a brief physical description of the sediments and their physical properties. Similarly, lithofacies for individual units are often not well characterized. A more detailed description of each stratigraphic unit is provided below in the text. Where studies are available, a summary of the lithofacies is provided in the stratigraphic description.

**Basement Carbonates.** Depending on location within the basin, the Barnett Shale is underlain by the Lower Ordovician Ellenburger Group, Middle to Upper Ordovician Viola and Simpson Carbonates, or the Mississippian Chappel Limestone (see Figure 4 originally from Loucks and Ruppel, 2007). Throughout the basin, the Barnett section overlies a major unconformity that spans 100 m.y. and is overlain by the Pennsylvanian Marble Falls carbonates.

### **Paleozoic-Ordovician**

**Ellenburger Group.** The carbonate rocks of the Ellenburger Group that forms the basement of the Fort Worth Basin represent a broad epeiric carbonate platform that covered most of Texas during the Early Ordovician. The sequence is comprised of porous dolomite and limestone with abundant chert (Bruner and Smosna, 2011). A drop in sea level following the deposition of the Ellenburger Group resulted in prolonged exposure and extensive karsting in the upper portion of the carbonate sequence. Contours of this surface are shown in Figure 5 from Pollastro et al. (2007). The irregular unconformity of this generally water-bearing group was the depositional surface for the overlying Mississippian Barnett Shale. Karsting and vuggy porosity is commonly observed in the Ellenburger carbonates. Matrix porosity estimates range from 2% to 14%. Permeability ranges from less than 1 md to greater than 1,000 md in karsted portions of the formations. Within the Newark Field area, the Ellenburger is commonly used for salt-water injection (Loucks, 2007). Permits for salt-water disposal wells filed with the TRRC report maximum allowable injection rates as high as 25,000 barrels/day.

**Viola and Simpson Groups.** Carbonates of the Viola-Simpson Groups are found in the northeastern portion of the basin, and consist of dense crystalline limestone, and dolomitic limestone. The Viola also contains sandstone, anhydrite, and halite (Bruner and Smosna, 2011). These sediments dip eastward toward the Ouachita thrust-fold belt and thin to zero thickness along a northeast-southwest erosional line through Wise, Tarrant, and northeastern Johnson counties. West of this line, Mississippian sediments (i.e. the Barnett Shale) overly the water bearing Ellenburger Formation (Montgomery and others, 2005). Figure 6 shows a north-south structural cross-section depicting the limits of these formations.

### **Paleozoic-Mississippian**

**Chappel Limestone.** The Chappel-carbonate platform located in the northwestern part of the basin along the Bend arch, is comprised of crinoidal limestone and local pinnacle reefs up to 300 ft thick, and is productive of hydrocarbons (Montgomery et al, 2005). The Chappel Limestone was deposited on the Ellenburger unconformity. In this area the Barnett Shale thins and drapes over pinnacle reef and mounds forming seals for the Chappel Limestone reservoirs (Pollastro et al., 2007).

**Barnett Shale.** The Barnett Shale is comprised of siliceous shale, limestone, and minor dolomite. Specific lithofacies are described as organic shale, fossiliferous dark shale; dolomite rhomb shale, dolomitic shale; concretionary carbonate; spiculitic shale, spiculite, spiculitic chert; phosphorites, pelletal grainstone, phospholitic shale; spiculitic sandstone; and shelly glauconitic quartz sandstone. In the northeastern portion of the basin, the Barnett contains significant limestone and is separated into upper and lower formations by a low-porosity, non-productive unit informally known as the Forestburg Limestone. Near the Muenster Arch, this limestone averages 200 ft in thickness with maximum thicknesses of more than 1,000 ft. The Forestburg thins rapidly to the south and west and is extinguished completely in southern Denton and Wise counties. In the rest of the basin the Barnett is an undifferentiated single formation and thins to the northwest, south, and west. The regional extent is controlled by the same controls as the overall basin. On the western margin of the basin, overlying the Chappel shelf carbonates, the Barnett Shale thins to only a few tens of feet. Further to the west and along the Llano Uplift in the south, the shale increases in limestone content and has undergone erosion. To the north and northeast, along the Red River Arch and Muenster Arch the shale has been eroded. At

exposures near the Llano uplift the shale is 30 to 50-ft thick and petroliferous and the sediments thicken towards the Muenster Arch. An isopach map (Figure 7) from Pollastro et al. (2007) shows that in the area of the Newark East Field, the average thickness is about 400 ft. Along the Muenster Arch, thicknesses of greater than 1,000 ft are observed. In the Newark East Field area the depth to the top of the Barnett Shale is found between 6,900 and 7,500 ft. A structure map from Pollastro et al. (2007) showing the subsea contours of the top of the formation is shown Figure 8. The relative thicknesses of the Barnett section and the overlying Marble Falls Formation are shown in stratigraphic cross section in Figure 9 and Figure 10.

### **Paleozoic-Permian and Pennsylvanian**

**Atoka Series.** Between the overlying Caddo Limestone and the underlying Marble Falls Formation the Atoka Group, thins toward the northwest and thickens toward the southeast within the basin. Features associated with these deposits include channel incision and delta progradation, braided fluvial systems, braid-plain deposits, and river-dominated deltas (Maharaj and Wood, 2009).

**Bend Group.** The Marble Falls Limestone lies conformably on top of the Barnett Shale and consists of platform carbonate facies that include calcarenite bars, algal bank Limestone, and platform margin spiculite and is interbedded with gray-black shale (Kier et al., 1979 and Grayson and Trite, 1988). The Marble Falls Limestone is differentiated from the underlying Barnett by less organic matter, and lack of radioactive signals on logs. Faults and fractures that cut across both the Barnett Shale and the Marble Falls have been noted (Thomas, 2002). The Marble Falls undergoes a depositional pinch out along and east west line through northern Dallas and central Tarrant counties (Montgomery et al., 2005) with an average thickness of approximately 300 ft. Where it exists in the basin, the Marble Falls Limestone has relatively uniform thickness suggesting a stable platform setting during deposition.

As the Concho platform subsided, during westward migration of basin sediments the Smithwick shale was deposited on the Marble Falls carbonates. The Smithwick is about 250 ft thick and consists of dark-colored mudstone. The lower portion of the Smithwick is black spiculitic and fissile shale deposited under dysaerobic conditions. Upper portions of the Smithwick are lighter colored silty-shale containing ironstone concretions (Grayson and Trite, 1988).

The Bend conglomerates of Atokan series are defined as the interval between the top of the Marble Falls Limestone and the base of the Caddo Limestone. Within the Fort Worth Basin thicknesses of the Bend Conglomerates ranges from 1,000 ft to 1,200 ft and occurs at depths of 4,500 to 6,000 ft. The Bend conglomerates are likely derived from the Muenster-Red River Arch complex to the north of the basin rather than the Ouachita fold belt (Hardage et al., 1995). Prograding, high-constructive deltas or fluvial-dominated deltas produced a number of distinctive facies that include bar sequences, channel fill deposits, crevasse-splay deposits, backswamp-marsh deposits, and prodelta and delta front deposits (Lovick et al., 1982). The bird-foot form of the Mississippi River Delta is a modern example of a high-constructive delta. The sandstones and conglomerates of these formations are significant hydrocarbon reservoirs within the basin (Boonsville and Ranger Fields).

**Strawn Group.** The Strawn Group is separated from the overlying Canyon group and underlying Atokan sediments by shales (Nordstrom, 1988). Strawn and Canyon Groups are comprised of coal, shale, sandstone, and carbonates and were accumulated in fluvial, deltaic, embayment, open shelf, and carbonate bank depositional systems (Cleaves and Erxleben, 1985). Within study area, the primary water-bearing formations are pebble-sandstone conglomerates interbedded with thin mudstone stringers. Stramel (1951) describes these units as well-cemented where flow occurs mainly along bedding planes and joints. Slump faults are widely recognized in the Strawn Group from outcrop studies (Grayson and Trite, 1988). Usually, the slump structures are located along the projected trends of faults or horst blocks. The gravity slumps are comprised of deformed sequences of shale interbedded with sandstone

**Canyon and Cisco Groups.** Pennsylvanian aged Canyon and Cisco Groups are comprised of mostly shale, sandstone, mudstone, and limestone derived from deltaic and carbonate bank deposits. The primary water bearing formations within these groups are sandstone sequences. Within the study area, four thick limestones members interstratified with shales and sandstones identify the Canyon Group. The sandstone facies are part of a progradational low-gradient fluvial and deltaic system that include delta front (thin-bedded sheet sandstone and siltstone), channel fill (massive fine-to medium grained sands), and confined alluvial valley deposits (gravel and coarse sand at the base with gravel content decreasing upward) (Nordstrom, 1988).

Oil and/or gas have been discovered and produced in the Ellenburger, Chappel Limestone Barnett Shale, Marble Falls, Atoka, and Strawn sediments throughout the Fort Worth Basin. Oil and gas are found throughout the Paleozoic section, but the majority of hydrocarbon reservoirs are found in Pennsylvanian sediments. The first indications of hydrocarbons within the basin were shows of oil and gas wells drilled for groundwater in the mid-nineteenth century (Ball and Perry, 1996). The first commercial production of oil in the basin occurred in the early 1900s, and the basin reached a mature stage of production by the 1960s. Table 2 describes the plays identified in the Fort Worth Basin and Bend Arch province.

### **Cretaceous**

Cretaceous formations were deposited throughout the Comanchean and the early Gulfian Series, and are subdivided from oldest to youngest into the Trinity, Fredericksburg, Washita, and Woodbine Groups. Because of the depositional variability and resulting significant heterogeneity in formation lithology and extent, geologic nomenclature describing the Cretaceous sequences is complex and varies by author and region for studies of the area. Recently adopted nomenclature by the Texas Water Development Board groups formations below the Glen Rose into the Lower Trinity including (from lower to upper) the Hosston, Pearsall, and Hensell members of the Travis Peak Formation. The Upper Trinity is comprised of the Glen Rose and Paluxy Formations where defined. In the western portion of the study area where the Glen Rose is not present, the undifferentiated Trinity Group is known as the Antlers Formation. Cretaceous formations unconformably overly the westward dipping and well-indurated Pennsylvanian sediments and trend or strike north-northeast and dip east – southeastward. Geologic cross sections by Nordstrom (1982) in Figure 12 through Figure 14 show the general stratigraphic relationships and formation thicknesses of the sequence in the study area.

Although some usable quality groundwater is derived from Pennsylvanian sediments within the study area, the primary water bearing formations in the study area the Trinity and Woodbine Groups are Cretaceous in age, and most of the groundwater wells within the study area are completed within these groups (Figure 15). Faulting is not known to greatly influence the water bearing units of the Cretaceous units in Barnett Shale area, however, west of the Ouachita

structural front in central and northeastern Ellis county surface faults that are part of the Balcones system show some influence on groundwater flow. Some indication of connections to underlying Pennsylvanian sediments is given by the occurrence of thermogenic methane observed in some groundwater wells in the area. Fresh to slightly saline water occurs in primarily in four sand-rich units of the Cretaceous sediments. From oldest to youngest these units are the Hosston and Hensell Members of the Travis Peak Formation, the Paluxy Formation, and the Woodbine Formation. Four relatively impermeable units separate and confine the aquifer sands these units include Pearsall of the Travis Peak Formation, the Glen Rose of the upper Trinity Group, the Fredericksburg/Washita Groups, and the Eagle Ford Formation. Availability of groundwater as a useable source of drinking water depends on maximum contaminant levels and secondary constituent levels ("secondary standards") established in the Texas Administrative Code (30 TAC, Chapter 290, Subchapter F). Useable quality water for irrigation purposes depends on salinity and the overall amount of total dissolved solids. Recommendations for the screening levels of constituents for irrigation water are provided by the Texas Cooperative Extension (Fipps, 2003). The base of the useable quality groundwater varies across the basin, and with levels of increasing total dissolved solids but can be generally defined as the base of the Hosston/Trinity Group sediments.

**Trinity Group.** The topography of the erosional surface where Cretaceous Lower Trinity sediments were deposited following the early Mesozoic influenced the thickness and geometry of these sediments. A map showing the outcrop location of the Trinity Group within the study area is shown in Figure 15. Commonly known as the Lower Trinity sand or the Second Trinity, the Hosston is one of the most productive aquifers in the area. Underlain by pre-Cretaceous sediments and capped by the Pearsall Member of the Travis Peak Formation, the Hosston is unconfined in the outcrop areas of the formation and exhibits artesian pressures in confined down-dip areas. Within the study area, the Hosston sandstone has been described as medium- to coarse-grained, moderately well-sorted sand; gray, silty clay; and siliceous conglomerate composed of well-rounded pebbles (Hall, 1976). The sands are thin to massively bedded, and crossbedding is commonly associated with the conglomeritic parts of the unit. The Hensell Member is the upper aquifer of the Travis Peak Formation and is separated from the Paluxy Formation by the Glen Rose Formation. The Hensell consists of fine- to medium-grained, light



gray to buff well-sorted sandstone. The sandstone is crossbedded and contains pebbles similar to those in the Hosston.

**Glen Rose Formation.** The Glen Rose Formation typically does not produce water of sufficient quantity or quality for any use in the study area. The Glen Rose crops out in the west-central part of Johnson County and varies in thickness from zero feet to 925 ft in Hill County to the south. The lower contact is gradational with the Hensell Formation, while the upper contact forms a sharp boundary with the overlying Paluxy Formation. The Glen Rose is comprised of medium to thickly bedded limestone (shallowing-upward cycles grading from subtidal to intertidal and supratidal fossiliferous lime mudstone and wackestone to miliolid and peloidal grainstone and packstone) with some sandstone, sandy shale, shale, and anhydrite (Mancini and Scott, 2006). Because of the anhydrite component of the formation, any water that is produced is usually highly mineralized (Thompson, 1969).

**Paluxy Formation.** The Paluxy Formation of the Lower Cretaceous is comprised predominantly of fine- to coarse-grained, friable, homogeneous, white quartz sand interbedded with sandy, silty, calcareous, or waxy clay and shale. In general the Paluxy grades upward from coarse-grained sand in the lower part to fine-grained sand with variable amounts of shale and clay. The sands are usually well sorted, poorly cemented, and crossbedded. Pyrite and iron nodules are often associated with the sands and frequently contribute a red stain to the individual beds (Nordstrom, 1982). In some areas along the outcrop, high iron concentrations are present in ground-water analyses. In the northern portion of the Barnett Shale play area where the Glen Rose is absent, the Paluxy merges with Hosston and Hensell members of the Trinity Group. The Paluxy increases in total thickness from zero ft to more than 600 ft in the northern portion of the study area. The sands and silts of the Paluxy are described by Klemm et al. (1975) as fine-grained, friable, quartz grains that are generally well sorted, poorly cemented, and crossbedded. Based on pumping test data, the geometric mean of the transmissivity is approximately 600 ft<sup>2</sup>/day and mean hydraulic conductivity is 5 ft/day (Bene et al., 2007).

**Fredericksburg and Washita Groups.** The Fredericksburg and Washita Groups separate the Woodbine Formation from the Paluxy. The Fredericksburg Group is comprised of the Walnut Formation, Comanche Peak, and Edwards Formation in the study area. The Kiamichi Clay forms

the basal unit of the Washita Group and is easily recognizable on geophysical logs. The Fredericksburg and Washita Groups consist of a thick sequence of limestone, dolomite, marl, and shale facies, and have a combined thickness ranging from 450 to 900 ft (Bene et al., 2007).

**Woodbine Group.** The Woodbine crops out in Johnson, Tarrant, Denton, Cooke, and Grayson counties, and trends in a north-south direction that extends from the Red River to McClennan County. The thickness of the Woodbine ranges from about 230 ft near the southern margins of the outcrop to about 700 ft near the downdip limit of fresh to slightly saline groundwater. In the study area, the Woodbine Formation is comprised of friable, fine-grained sand and sandstone with interbedded shale, sandy shale, and laminated clay. Historically, the Woodbine aquifer has exhibited high sulfate levels associated with extensive lignite beds, especially in the southern outcrop areas of Tarrant and Johnson counties (Baker and others, 1990). Based on pumping test data, the mean transmissivity is approximately  $400 \text{ ft}^2/\text{day}$  and mean hydraulic conductivity is 6 ft/day (Bene et al., 2007).

**Other Gulf Series Groups.** The Navarro, Taylor, Austin, and Eagle Ford overly the Woodbine Formation and crop out in the eastern most portion of the study area in Tarrant and Dallas Counties (see Figure 14). The Taylor and Eagle Ford Groups are comprised of mostly shale, limestone, clay, and marl and yield only small amounts of water in localized areas. The Navarro and Austin groups consist of chalk, limestone, marl, clay and sand. The sandy units are known to yield small amounts of water locally.

### **Tertiary and Quaternary**

Tertiary formations include the Wilcox and the Midway Groups and are generally found to the east of the study area. Alluvial sediments of the Quaternary are locally important sources of groundwater particularly around the Brazos and Trinity Rivers. Thickness of this unit varies within the study area but can be up to 100 ft thick. Alluvial sediments consist of sand, silt, clay and gravel.

## **Barnett Shale Reservoir Delineation and Characteristics**

The Barnett Shale can be described as an unconventional, low permeability low porosity reservoir. Productive portions of the formation have average porosities of 5-6% and permeabilities of less than 0.01 md to nanodarcies. No free water exists in the reservoir. Average water saturations are approximately 25% but increase with carbonate content. Gas content occurs in the reservoir as free gas in mostly matrix porosity and sorbed to organic matter in the reservoir. Free gas in the matrix is thought to be related to the slightly overpressured conditions (0.49 psi/ft to 0.52 psi/ft) observed in the reservoir. Gas content or gas yield per mass of rock—studies on gas content indicate that at reservoir conditions (3,000-4,000 psi) sorbed gas content is approximately 105-115 scf/t (standard cubic feet per ton of rock/shale) with estimations of free gas content ranging from 45 to 55% of the average total gas content (Montgomery, et al., 2005).

The shale also exhibits a distinctive log response with high resistivity and radioactivity but is not useful for log analysis for reservoir characterization. Primary identification of productive intervals has relied mainly on core analyses. The Barnett shale also contains extensive natural fractures but most are sealed with calcite. The general orientation of natural fractures in the Barnett Shale is northwest to southeast and hydraulically induced fractures are usually northeast to southwest (Coulter et al., 2004). In the Newark East Field, fractures generally strike northwest (azimuth 100-120°) and dip 74° to the southwest, approximately parallel to the Meunster Arch (Montgomery et al., 2005).

The delineation of the most productive portions of the Barnett Shale play is determined by the stratigraphic constraints, organic content, and thermal maturity. Overall thickness of shale intervals also influences the economic quantities of gas and varies from basin to basin. Within the Fort Worth Basin, the minimum commercially productive thickness appears to be approximately 100 ft. An isopach map of the shale thickness (Figure 7) shows the thickest portions of the shale intervals occur in the northeastern portion of the basin along the Muenster Arch near the Newark East Field production area. Units underlying and overlying the Barnett Shale impact fracture development during hydraulic fracturing and subsequent water incursion

from the Ellenburger. The organic content and thermal maturity of the hydrocarbons determine the amount and quality of hydrocarbons.

**Stratigraphic Constraints.** The location and coincidence of the underlying Viola Limestone and the Forestburg Limestone that separates the Upper and Lower Barnett Shale play an important role in the development of the Barnett play and the relative commercial success of well locations. The Viola is a dense limestone that lies beneath the Barnett Shale and overlies the Ellenburger in the northeast portion of the basin. Generally, vertical wells completed to the west of the Viola erosional limit have been unsuccessful. The presence of the Viola prevents fracture propagation of induced fractures extending into the Ellenburger that result in excess water production. For horizontal wells, the presence of the Viola-Simpson is not as important. Estimated ultimate recoveries for horizontal wells drilled in Tarrant and Johnson Counties suggest that equivalent wells can be completed on either side of the Viola-Simpson erosional limit. Where present, the Forestburg limestone that divides the Upper and Lower Barnett Shale also limits the induced fracture growth. For most wells, the upper Barnett yields 20-25% of total production, while the lower Barnett typically delivers 75-80% (Montgomery, 2005). Where the Forestburg limestone is present, the upper Barnett typically has a higher fracture gradient (0.70 ft/psi) than the lower Barnett (0.50-0.60 ft/psi). The Depositional pinch-out of the Marble Falls Formation lies along an east west line through northern Dallas and central Tarrant Counties. Like the underlying Viola-Simpson, the overlying Marble Falls provides an upper barrier to fracture growth within the Upper Barnett Shale. Stimulation south of this line increases the risk of induced fractures penetrating overlying mixed-gas and water-bearing Pennsylvanian clastics.

**Organic Content and Thermal Maturity.** Organic carbon content within the Barnett ranges from less than 0.5 wt% to more than 6 wt%, averaging about 4.5 wt% with the most productive regions of the play. Intervals with higher organic carbon content usually exhibit higher gas in place, higher matrix porosity and lower clay content. Within the Barnett shale, the organic content is highest in siliceous intervals that are more abundant in the lower intervals below the Forestburg Limestone. Thermal maturity of a reservoir describes the degree of transformation with temperature of organic matter to oil-phase hydrocarbons to combined oil and gas phase hydrocarbons to gaseous hydrocarbons. During this conversion, vitrinite is also commonly formed. Vitrinite exhibits reflectivity under microscopic inspection and vitrinite reflectance

(recorded as the percentage  $R_o$ ) is the most commonly used index of thermal maturation. Table 3 shows the range of observed vitrinite reflectance and the corresponding hydrocarbon type in the Barnett Shale.

Table 3: Thermal maturation ranges for hydrocarbon types observed in the Barnett Shale

<b>Ro (percent)</b>	<b>Hydrocarbon Type</b>
0.20-0.60	none
0.60-1.00	oil
1.00-1.40	oil and gas
1.40+	dry gas

Adapted from Bruner and Smosna (2007).

Based on reflectance patterns shown in Figure 16, hydrocarbons within the Barnett reservoir vary across the basin. A westward change occurs from dry gas (more thermal maturation) to mixed oil and gas in the central basin to oil along the Bend Arch and carbonate platform.

## Completion Practices in the Barnett Shale

The discovery well in the Barnett Shale was drilled in 1981 in Wise County by Mitchell Energy Corp to test the productivity of the Viola Limestone. The Viola was unproductive, however shows of gas were observed in the Barnett Shale. Initial well stimulation used nitrogen, and initial production was 246 Mcfg/d in 1982. Early completion procedures (mid 1980s through the late 1990s) used 30 to 50 lb/1,000 gal of crosslinked gels with initially titanium and zirconium and later borate compounds in fracture stimulation fluids. The ensuing development of the play and Newark East field through the late 1990s involved mostly vertical wells with fracturing fluids shifting from gels to largely water. Water fracs increased in popularity because of perceived improvement in cleanup and lower cost, and used large-volume, high-rate slick water treatments.

Beginning in the early 2000s, improved drilling techniques and more favorable production results saw a shift from vertical to horizontal wells. Horizontal wells can be positioned well above the base of the Barnett and do not require the single massive hydraulic fracture that is required by a vertical well. Generally, within the Barnett Shale, horizontal wells have historically

produced approximately twice as much as vertical wells (Tian and Ayers, 2010). Horizontal wells increased wellbore exposure to the reservoir and reduced the footprint of surface locations in often urban and suburban locations.

Early horizontal wells were uncased and uncemented open-hole completions along the productive interval and used a single stage fracture treatment along the length of the horizontal portion of the well. These early completions for horizontal wells did not use mechanical diversion methods for fracture fluids and fracture propagation did not necessarily occur at perforation locations (Lohoefer et al., 2010). As an attempt to divert fracture fluids to desired intervals, operators began using cemented liners and higher pumping rates with additional fluid diversion through the use of ball sealers or rock salt although these attempts still saw mostly random fracture generation. As hydraulic fracturing processes improved and evolved, treatments were applied to multiple short stages along the productive zone. The smaller, multiple stage fracs decrease the risk of hydraulic fracture extending into water-bearing Ellenburger. Further improvements in the knowledge of the Barnett Shale and hydraulic fracturing noted that more directional control of the stimulated fractures was achieved when the well was cemented through the shale interval. Prior to 2004, wells were completed with cemented liners and multi-stage fracturing. Well construction involved cemented casing with mechanical isolation in the liner by setting bridge plugs. The well was then perforated and fractured with the cement providing a diversion of fracture fluids in the annulus, while the plugs diverted fluids in the liner. The plugs were subsequently drilled out and the next stage of completion would begin.

Beginning in 2004, the next and most recent evolution in the well completion practices in the Barnett Shale involves the use of uncased and uncemented, open-hole, multi-stage fracturing. External packers were developed to isolate sections of the wellbore. These packers seal against the wellbore and do not require removal for production. Wells completions also began to include sliding sleeve tools to create ports between the packers to produce the well without perforating the casing. Using these methods, fracture treatments are performed as part of a continuous pumping operation without the need to drill out plugs between completion stages (Lohoefer et al., 2010).

As wells were completed with longer laterals (as long as 5500 ft) and more stages, corresponding increases in proppant and water usage for each completion were needed. Various sizes of proppant grain size were tested and developed, and to better characterize fracturing techniques and efficiency, integrated completion and diagnostic practices were also developed. These techniques included microseismic mapping of induced fracture networks and the addition of tracers to fracture fluids. The tracers are used monitor fracture placement and up to 20 unique tracers can be used to distinguish frac stages. Current development strategies include installation of multi-well or multi-lateral well groups with simultaneous stimulations to create interwell (or inter-lateral) fracture communication (Leonard, 2008). Communication has been observed at distances of 1,000 ft or more. The current industry trend is toward longer cemented laterals uses several slick water frac stages typically pumped at 50-80 bpm (Leonard et al., 2007). Current practices usually involve horizontal lateral lengths of approximately 2,500 to 3,000 ft, with the wells drilled perpendicular to the expected direction of fracture propagation (Leonard, 2008 and Gale et al., 2007). Fluid volumes of 500,000 to 1,000,000 gal and proppant volumes of 250,000 to 700,000 lb per stage are not uncommon. Improved well performance is more closely related to the volume of sand/proppant used than to the volume of water. The most commonly used proppant sizes range from 100 mesh to 20/40 white sand. Larger volumes of smaller mesh proppant are typically used during the early time of the treatment because it is more easily transported along the longer distances in the wellbore by the low viscosity water (Leonard et al., 2007).

A recent description (Bozeman and Degner, 2009) of typical well completion construction practices uses a 5.5-in, 17 lb/ft, N-grade production casing, cemented through the horizontal section of the well. The production casing is typically installed and cemented before demobilization of the drilling rig. Depending observations during the cementing process, cement evaluation logs or other well integrity tests are also run before the demobilization of the drilling rig. Once the drilling operations are complete, a workover rig is moved into place and preparations for well conditioning, perforating and hydraulic fracturing begin. Current practices include hydraulic fracturing in multiple stages or segments along the horizontal length of the well. The stage length varies (usually between 150 to 550 ft) depending on the presence or absence of underlying or overlying formations and proximity to fault zones. Fracture stage injected volumes of fluid are typically comprised of about 500,000 lb proppant and 1,000,000 gal

fluid (mostly water). Total well fracturing volumes of injected fluids are about 2,500,000 lb proppant and 5,000,000 gal fluid (i.e. 5 stages). Well perforations vary by operator, but can be a single perforation cluster or six or more clusters typically spaced 50 or more feet apart. Key factors identified for successful completions include large fractured network length and area, large proppant volumes, large fracture fluid volumes, contained height fracture growth, fault/karst avoidance, effective cement zonal isolation (cemented laterals), fracture fluid recovery. Inefficient completions are usually affected by gaps in the fractured network area, inefficient fracture initiation, high horizontal stress anisotropy (resulting in poor fracture development), inefficient perforation placement, and improper centralization and cement slurry design (Leonard et al., 2007)

## **Environmental Considerations**

There are two primary pathways for subsurface contamination from anthropogenic activity. The first path is from spills or leaks at or near the ground surface. Contaminants migrate through the subsurface through the unsaturated zone until they reach the water table. With this pathway, unconfined aquifers are at a greater risk for potential contamination than confined aquifers because confining layers for aquifers are comprised of lower permeability materials that limit or prohibit the transmission of water or other fluids. In the area of the Barnett Shale play, the primary aquifers, the Trinity and Woodbine, are unconfined in the area where those geologic units crop out at the ground surface. These outcrop areas are also the areas of primary recharge for these aquifers. The Trinity aquifer crops out in Wise, Parker, and Hood Counties, an area of significant Barnett Shale drilling and development. The Woodbine aquifer crops out in Denton, Tarrant, and Johnson Counties.

The second primary pathway for the migration of anthropogenic contaminants is through artificial penetration (usually a well) that can penetrate and/or pass through confined or unconfined formations. This could involve direct injection into a well from the surface like brine disposal wells and industrial waste injection wells, or improper sealing or deterioration over time of well casing and cement that isolates upper fresher aquifers from deeper low quality aquifers or hydrocarbon bearing units (O'Rourke et al., 2011). During fluid injection in disposal



wells, high injection pressures could cause upward migration of injected fluids into overlying strata if there are hydraulic connections (such as natural fractures or other zones of connected permeability) between layers. Injection pressures must also be monitored to ensure that unintentional fracturing of the injection zone does not create migration pathways for injected fluids. In the area of Barnett Shale development, brine disposal wells are permitted for disposal into the Ellenburger group below the Barnett. Figure 17 shows the location of all of the disposal wells in the play area. There is no information currently available that indicates any contamination of shallow groundwater aquifers from these wells. Construction and regulation of these wells is permitted by the TRRC.

Oil and gas production and hydraulic fracturing are typically accompanied by large volumes of water (brine) characterized by high concentrations of total dissolved solids. Produced brine is a major contaminant of the state's aquifers (O'Rourke et al., 2011). During the early period of oil and gas production in the state of Texas and including the area of current gas production in the Barnett Shale, brine disposal was not regulated and was often discharged into unlined pits that could infiltrate to the subsurface or overflow into nearby surface water. Table 4 lists the typical constituents found and concentrations found in oil field brines. The TRRC implemented a statewide no-pit order beginning in January 1969. Since 1984, unpermitted new reserve, mud circulation, and fresh water make-up pits have been authorized by the TRRC (16 Texas Administrative Code 3.8). Rule 8 restricts fluid content in these pits and establishes time frames for removal based on chloride content. Reserve and mud circulation pits can contain drilling fluids, cuttings, rig wash, drill stem test fluids, and blowout preventer test fluids. Current rules require operators to take precautions to prevent pollution of surface and subsurface water, but do not include specific construction requirements for pits. The TRRC publishes a Surface Waste Management Manual that provides guidance for pit design and construction. Many operators use liners in areas where the soil is permeable and local governments can require the use of lined pits. Pits containing waste fluids or produced brines require a permit from the TRRC, and large pits typically used for large volumes of mixed-water for fracture operations require a proposal to store waste above ground level within dikes prepared under the seal of an engineer registered in Texas.

Table 4: Typical Constituents of Oil Field Brines

<b>Element</b>	<b>Concentration (ppm)</b>
Sodium	12,000 to 150,000
Potassium	30 to 4,000
Lithium	1 to 50
Rubidium	0.1 to 7
Cesium	0.01 to 3
Calcium	1,000 to 120,000
Magnesium	500 to 25,000
Strontium	5 to 5,000
Barium	5 to 5,000
Chloride	20,000 to 250,000
Bromine	50 to 5,000
Iodine	1 to 300

From O'Rourke et al., 2011

Groundwater contamination related to hydrocarbon production has been observed at various locations within study area including many instances prior to the development of the Barnett Shale (Preston, 1977, Nordstrom, 1982 and Baker et al., 1990). Reported contamination appears to be mainly associated with oil and gas wells that are not properly cemented through fresh water zones and improper disposal of brines at the ground surface. The chemical fingerprint of water typically reflects the sediment and rocks through which it has passed. As the groundwater moves through pore space, minerals from surrounding rocks are dissolved. Generally, concentrations of dissolved minerals increase with depth and temperature. Figure 18 from Nordstrom (1982) shows the chemical signature of groundwater from sampled water wells and a sample of oil-field brine from nearby location (center diagram). Based on these signatures, one of these samples appears to be contaminated with the same constituents from the brine. The most reliable sentinel compounds are total dissolved solids, chloride, and divalent cations like calcium, magnesium and iron (Coleman, 2011).

Highly corrosive brines can cause deterioration of steel well casings and fittings over time if the casing is not coated with plastic or other non-reactive material. Potential migration pathways created by improperly abandoned wells and improperly installed or deteriorated well casing

could allow fluid flow along the wellbore access to formations that would normally be protected. Vertical flow from deeper formations (usually) must overcome the entry pressure into the more shallow at the wellbore in order to penetrate the formation that can be confined or unconfined. In addition, surface casing is set and cemented in wells based on TRRC recommendations providing isolation of the water bearing zones even if well fluids migrate behind the production string. Cement bond logs or cement quality logs are typically not run on surface casing, however this relatively inexpensive test could provide a definitive demonstration of ground water protection. Operators should also be afforded flexibility to set additional surface casing based upon wireline logs, mud logs or cuttings from the surface hole that could more precisely identify the base of the Cretaceous than an estimate from nearby well control.

In addition to produced brines, oil and gas production involves the use of drilling and fracturing fluids with various chemical additives, acids and other chemicals used to treat wells, corrosion inhibitors that can include arsenic compounds, fuels and other substances. Fracture treatment fluids that are most commonly used in the Barnett Shale contain a friction reducer without gelling agents known as slick water fracturing. Most often, fresh water (< 500 ppm TDS) makes up about 98% to 99% of the total volume of fracture fluids, although recycled and produced water is increasingly used. In addition to water and proppants, slick water fracture treatments can include friction reducers, disinfectants or biocides, surfactants, gelation chemicals, scale inhibitors, hydrochloric acid, and corrosion inhibitor (King, 2012). Table 4 lists specific chemicals of the primary components that are commonly used for slick water fracturing.

Table 5: Common Additives to Slick Water Fracture Fluids

Additive	Primary Component	Function
Friction reducers	Polyacrylimide, potassium chloride	Reduces friction resulting in reduced pressure needed to pump fluids into the wellbore
Dilute acids	Hydrochloric acid, various	Used during initial treatment to clean out cement and debris around perforations
Biocide	Gluteraldehyde, bromine-based solutions, ozone, chlorine dioxide, UV	Prevents the growth of bacteria in the well
Surfactants	Various	Reduces surface or interfacial tension
Gelation Agents	Guar and cellulose	Thickens water to help transport proppant
Scale Inhibitors	Ethylene glycol, phosphonate and	Controls precipitation of certain carbonate and sulfate minerals

	polymers	
Corrosion Inhibitors	N,n-dimethyl formamide, ammoium bisulfite	Prevents degradation of steel well casing, used only when acids are used

While some of the components are considered hazardous or toxic, particularly corrosion inhibitors (King, 2011), and care must be taken by field workers when handling these fluids, groundwater contamination by specific components of fracture fluid is not well documented or has not been observed. Injection of the chemicals used in fracture stimulation in the Barnett Shale occurs thousands of feet below the base fresh water aquifers used in the play area for domestic and agricultural purposes (compare Figure 8 and Figure 11). Since the induced fractures are typically less than 500 ft in length, there is little potential for fluids containing these chemicals to be introduced into fresh water aquifers directly by the fracturing process. Surface spills could allow fracture fluids to infiltrate the subsurface and into ground water, but it is unclear whether or not components, when mixed in fracturing fluids, would be of sufficient concentration to cause concentrations in groundwater to rise above levels of concern. Spills of pure components stored on drilling sites would be a more likely cause of subsurface soil and ground water contamination.

Flow back water is water produced immediately following the hydraulic fracture treatment and typically includes fracture treatment fluids and formation brines. With Barnett Shale production, these formation brines could include fluids from adjacent (primarily Ellenburger Group) water bearing formations. The amount of fracture treatment fluids recovered varies, and ranges from 20% to 70% of injected fluids for the Barnett Shale. The bulk of the injected fluids are typically returned within the first two to three days following the fracture treatment. However, this time can extend up to the life of the well. Shorter return periods reflect more efficient completion techniques (Bruner and Smosna, 2011). Flow back waters from the injection of fracturing fluids may also contain naturally occurring radioactive material (NORM) or dissolved heavy metals because it passes through rocks that contain these materials. Subsurface formations can contain low levels of radioactive materials such as uranium and thorium and their daughter products, radium 226 and radium 228. The TRRC notes that the most commonly found NORM elements in produced water are the radionuclides, radium 226 and 228. Produced natural gas can also contain small amounts of radon gas, a radium daughter.

Levels of NORM in produced waters and natural gas from the Barnett Shale are typically less than background limits set by regulatory agencies. However, NORM in produced waters and gas can become concentrated through temperature and pressure changes that occur in the course of oil and gas production operations. As produced waters containing radium 226 and 228 pass through well casing and surface equipment, these elements may co-precipitate with barium sulfate forming scales. Radium 226 and 228 may also be concentrated in sludge that accumulates in oilfield pits and tanks generating radioactive waste. Radon in natural gas streams decays to lead-210, then to bismuth-210, polonium-210, and finally to stable lead-206. Radon decay elements can create a film on the inner surface lines and equipment principally associated with propylene, ethane, and propane processing streams. The highest risk of exposure to oil and gas NORM is to workers employed to cut and ream oilfield pipe, remove solids from tanks and pits, and refurbish gas-processing equipment (TRRC, 2012).

Risks posed by chemical spills at drilling sites can be reduced through the selection of less toxic and less concentrated components and additives to drilling and hydraulic fracturing fluids. Risks from chemical spills can be further reduced during transport and storage through the use of double wall containers, collision proof totes, and/or the use of dry additives. Using impermeable container mats underneath pipe connections, and impermeable containment berms around tanks can help to contain leaks (King, 2011). Tank fluid levels should be monitored regularly to account for leaks. Reducing the overall surface footprint by using multi-well pad sites also reduces their environmental impact and typically provides time and economic efficiencies. Similarly, multi-well pad sites allow focused monitoring efforts during drilling and post drilling activities. Groundwater monitor wells can be drilled around the perimeters of sites with site-specific monitoring plans developed for each pad site. Pre-development baseline sampling of groundwater could identify existing impacts from historic production activities or natural background levels. In the Barnett Shale development area, particular care should be observed when drilling pads are located over outcrops (recharge zones) of known groundwater producing formations. These areas include outcrops of the Trinity and Woodbine Groups as well as lower formations in some areas.

As previously discussed, spills and wells both are potential pathways for subsurface contamination during oil and gas production. Proper well construction and maintenance that

conforms to local geologic conditions insures fluid control at stimulation and production pressures. King (2012) provides a detailed discussion of ways to mitigate risk through proper well construction. The basic guidelines from that work are presented here. The primary goals for well design are to protect surrounding non-hydrocarbon zones and freshwater aquifers, prevent damage to the well from external sources (corrosion, scale), stabilize the well from external forces and movement (earthquakes, subsidence) (King, 2012). Wells are constructed by running coupled sections of casing into the drill hole. The casing is cemented to the wellbore by pumping cement down the pipe and up the annulus (the space between the wellbore and the casing). Surface casing strings that pass through aquifer zones are usually set and cemented several hundred feet below the bottom of these formations before drilling proceeds to the hydrocarbon zones effectively isolating them from any of the subsequent drilling activities. Effective seals are gauged through monitoring cement volumes and pressure tests. Secondary tests in the form of cement bond logs are run to evaluate the strength of the seal between the cement and the formation. Secondary casing strings are set before the production strings and may or may not be cemented across the entire interval. Within the Barnett Shale, wells are commonly set with a surface string and a long casing string run to the toe of the horizontal length of the well. These secondary casing strings may pass through non-targeted zones containing hydrocarbons and salt water. If these zones are not properly isolated, fluid pressures can build up in the annulus of the well that could potentially migrate into shallow zones not behind the surface string and upward in the formation into freshwater zones that are protected behind the surface string. Monitoring of annulus pressures can establish whether or not pressures are sufficient for entry into overlying formations. Surface-casing setting depth and cement quality become particularly important in this situation. Operators should research nearby historic or current non-Barnett Shale production and well information before designing a casing and cementing program.

While well design to properly isolate and protect zones is important, effective cement seals are also important. King (2012) observes that poor cement jobs suffer from three primary problems. The first involves the use of too little or too much cement. Failure to bring cement high enough in the annulus of the well (too little cement) will prevent isolation desired zones. Too much cement or cement that is too heavy may damage or fracture formations. Lighter cement and multiple stage cement jobs can prevent these issues. The second reason cement

jobs commonly fail is incomplete cleaning of drilling mud from the annulus prior to cementing the casing. Without proper safeguards, drilling mud can contaminate the cement and inhibit proper bonding with the formation. Problems with mud remaining in the annulus can occur when centralizers are not used in the cemented sections, drilling mud remains after the cement preflush, and insufficient amounts of cement are used. Finally, gas migration can occur through interconnected microchannels in the cement. During the drilling process, mud or fluids in the wellbore offset the formation pressure in the well keeping fluids in the formation. As cement displaces the mud in the annulus, imbalances in the pressure on the sidewalls of the wellbore could potentially allow small amounts of gas in the cement before it is completely gelled forming small microchannels in the cement. If these channels are interconnected, migration pathways for wellbore fluids and formation fluids are created.

Migration pathways for fluids could also be created by improperly abandoned wellbores. Strict regulation of abandoned wellbores by the TRRC has only been in place for the past 60 or so years, meaning increased potential for encountering improperly abandoned wellbores in Barnett Shale development areas because of historical oil and gas production in the area. Risk of contamination through abandoned wellbores or other wells is reduced through surveys of the surrounding areas prior to drilling. The risk for contamination increases with the proximity of abandoned wellbores to the proposed drilling locations. Jordan and Hare (2002) provide a detailed protocol for site preparation surveys and the location of potential migration pathways prior to drilling activities that include the following steps:

1. **Geologic Investigation.** An investigation performed by a qualified geologist that identifies porous and permeable zones, as well as any outcrops and confining units in the area. The investigation should also identify any faults and unconformities that could potentially be migration pathways. These details should be integrated with engineering knowledge of the hydrocarbon zone to determine the potential for unwanted fluid migration and direction of flow.
2. **Wide-Area Survey.** A survey to compile historical information from state and county records that would include locations of active and abandoned wells (both hydrocarbon and water wells). Prior monitoring efforts in the area should also be identified. The result of this survey should classify areas of high and low risk, and eliminate areas with no risk.

3. **Corrective Action and Monitoring.** Following the area survey, wells that have been identified as improperly plugged should be re-entered and plugged, or monitored for signs of migration. Monitor plans should also be developed to address potential migration in the subsurface and surface-based monitoring for fluids and atmospheric gases.

It should be noted that the situations described above, spills, leaks, well construction issues are very rare. Proper well construction practices and site specific work plans limit the risk from spills. Risk is further mitigated when plans are in place to recover spills before they occur.

## **Summary and Conclusions**

The Barnett Shale is an unconventional, low permeability low porosity reservoir that lies within the Fort Worth Basin within a complex stratigraphic and structural framework. Deposition of the sediments within the basin was controlled largely by the Ouachita orogeny to the west, the development of the Concho Platform to the east, and the incursion and retreat of shallow seas over the depositional history of the basin. The thermal maturity of the hydrocarbons within the basin varies across the basin, but the oil content generally increases south and west of the ancestral Muenster Arch and Ouachita front. The underlying Ellenburger Formation produces water and is the target of disposal well injection within the play area. Faulting and Ellenburger karst-related structural features are generally associated with increased water production. Where the Viola-Simpson Limestone is present, it provides a barrier to hydraulic fracture generation that could potentially penetrate the Ellenburger resulting in water incursion into producing wells. Well completion techniques in the Barnett Shale have evolved since the discovery of the Newark East Field in 1981. Initial completions were vertical wells with fracture stimulations using gel treatment, while current practices almost exclusively use horizontal wells with slick water fracture treatments. Small-scale natural fractures within the Barnett Shale are usually sealed with calcite cement and do not indicate increased porosity or permeability of the formation. The natural fractures do impact the induced fracture networks, generally resulting in more diffuse and complex fracture patterns.

The Trinity and Woodbine Groups are primary water-bearing formations in the Barnett Shale development area. In the most productive areas, the Barnett Shale is separated from the overlying aquifers by a thick sequence of more than 5,000 ft of interbedded and interfingering



basin and carbonate platform sediments that sometimes also produce hydrocarbons. The potential for subsurface contamination of groundwater and sediments from development activities with the Barnett Shale occurs primarily along two pathways: spills or leaks at the ground surface or migration of fluids in the subsurface from and through wellbores or other permeable pathways. For surface spills, particular areas of concern include areas where aquifers are unconfined and crop out at the ground surface. The Trinity aquifer crops out in Wise, Parker, and Hood Counties. The Woodbine aquifer crops out Denton, Tarrant, and Johnson Counties. Consolidation of drilling sites into multi-well pads reduces the environmental footprint of development activities in these areas.

Proper well construction and maintenance that conforms to local geologic conditions insures fluid control at stimulation and production pressures, particularly well cementation, also reduces the risk of contamination. Characterization of the potential pathways of migration prior to drilling activities can help identify high risk areas. Oil and gas production has been occurring within the Fort Worth Basin for more for almost a century. Continued attention to best development practices by operators in the Barnett Shale play will reduce risks related to hydrocarbon production.

## References

Baker, B., G. Duffin, R. Flores, and T. Lynch, 1990, Evaluation of Water Resources in Part of North-Central Texas. Texas Water Development Board Report 318, p. 1-67.

Ball, M. M., and Perry, W.J., Jr., 1996, Bend Arch-Fort Worth Basin Province (045), *in* Gautier, D. L., Dolton, G.L., Takahashi, K.I., and Varnes, K.L., ed., 1995 National assessment of United States oil and gas resources; results methodology, and supporting data: U.S. Geological Survey Digital Data Series DDS-30, Release 2.

Bowker, K.A., 2007, Barnett Shale as production, Fort Worth Basin: Issues and discussion: American Association of Petroleum Geologists Bulletin, v. 91, no. 4, pp. 523-533.

Bozeman, T., and D. Degner, 2009, Cemented, Ball-Activated Sliding Sleeves Improve Well Economics and Efficiency: SPE 124120, SPE Annual Technical Conference and Exhibition, New Orleans, Louisiana, U.S.A. 10 p.

Brown, L.F., A.W. Cleaves, and A.W. Erxleben, 1973, Pennsylvanian Depositional Systems in North Central Texas, A Guide for Interpreting Terrigenous Clastic Facies in a Cratonic Basin, Bureau of Economic Geology Guidebook Number 14, 122 pp.

Bruner, K. and R. Smosna , 2011: A Comparative Study of the Mississippian Barnett Shale, Fort Worth Basin, and Devonian Marcellus Shale, Appalachian Basin. U. S. Department of Energy, National Energy Technology Laboratory.

Cleaves, A.W. and A.W. Erxleben, 1985, Upper Strawn and Canyon Cratonic Deposition of the Bend Arch, North-Central Texas, Southwest Section AAPG 1985 Transactions.

Coleman, N.P., 2011, Produced Formation Water Sample Results from Shale Plays: EPA Frac Workshop, Washington, D.C. March 10-11, 2011.

Coulter, G.R., E.G. Benton, and C.L. Thomson, 2004, Water Fracs and Sand Quantity: A Barnett Shale Example, Paper SPE 90891 presented at the Annual Technical Conference and Exposition, September 2004.

Fipps, Guy, 2003, Irrigation Water Quality Standards and Salinity Management; Texas Cooperative Extension publication, Texas A&M University, p. 20.

Gale, J. F. W., Reed, R. M., and Holder, J., 2007, Natural fractures in the Barnett Shale and their importance for hydraulic fracture treatments: AAPG Bulletin, 91: 603-622.

Grayson, R.C. and E.L. Trite, 1988, Middle and Upper Pennsylvanian (Atokan-Missourian) strata in the Colorado River Valley of Central Texas, Geological Society of America Centennial Field Guide--South-Central Section.

Hall, W. D., 1976, Hydrologic significance of depositional systems and facies in Lower Cretaceous sandstones, North-Central Texas: The University of Texas at Austin, Bureau of Economic Geology Geological Circular 76-1, 29 p.

Hardage, B. A., Carr, D. L., Lancaster, D. E., Simmons, J. L., Jr., Elphick, R. Y., Pendleton, V. M., and Johns, R. A., 1996, 3-D seismic evidence of the effects of carbonate karst collapse on overlying clastic stratigraphy and reservoir compartmentalization: Geophysics, v. 61, p. 1336-1350.

Kier, R. S., Brown, L. F., Jr., and McBride, E. F., 1979, The Mississippian and Pennsylvanian (Carboniferous) Systems in the United States—Texas U.S. Geological Survey Professional Paper 1110-S, 45 p.

King, G.E., 2012, Hydraulic Fracturing 101: What Every Representative, Environmentalist, Regulator, Reporter, Investor, University Researcher, Neighbor and Engineer Should Know About Estimating Frac Risk and Improving Frac Performance in Unconventional Gas and Oil Wells. SPE 152596. SPE Hydraulic Fracturing Technology Conference, The Woodlands, Texas, USA, February 6-8 2012.

Klemt, W. B., Perkins, R. D., and Alvarez, H. J., 1975, Ground-Water Resources of Part of Central Texas with Emphasis on the Antlers and Travis Peak Formations: Austin, Texas, Texas Water Development Board, Report 195, v. 1, p. 7-61.

Leonard, R., R. Woodroof, K. Bullard, M. Middlebrook, and R. Wilson, 2007, Barnett Shale Completions: A Method for Assessing New Completion Strategies, Paper SPE 110809 presented at the SPE Annual Technical Conference and Exhibition, November, 2007.

Leonard, R., 2008, Barnett Shale Completion Evolution: Utilizing Completion Diagnostics to Optimize Close Offset Development and Refracs, SPE Northside Study Group Presentation.

Lohoefer, D., D.J. Snyder, R. Seale, D. Themig, 2010, Comparative Study of Cemented Versus Uncemented Multi-Stage Fractured Wells in the Barnett Shale: Paper SPE 135386 presented at the SPE Annual Technical Conference and Exhibition, September, 2010.

- Loucks, R. G. and S.C. Ruppel, 2007. Mississippian Barnett Shale; lithofacies and depositional setting of a deep-water shale-gas succession in the Fort Worth Basin, Texas (*in* Special issue; Barnett Shale) *AAPG Bulletin* (April 2007), 91(4):579-601
- Loucks, R.G., 2007. Review of the Lower Ordovician Ellenburger Group of the Permian Basin, West Texas. Bureau of Economic Geology, Austin, Texas. 97 pp.
- Lovick, G.P., C.G. Mazzine, D. A. Kotila, 1982, (Atokan Clastics – Depositional Environments in a Foreland Basin, , Dallas Geological Society, Volume , Pages 193 - 211 (1982).
- Maharaj, V. T., and L. J. Wood, 2009, A quantitative paleogeomorphic study of the fluvio-deltaic reservoirs in the Atoka interval, Fort Worth Basin, Texas, U.S.A.: Gulf Coast Association of Geological Societies Transactions, v. 59, p. 495-509.
- Mancini, E. A., and R. W. Scott, 2006, Sequence stratigraphy of Comanchean Cretaceous outcrop strata of northeast and south-central Texas: Implications for enhanced petroleum exploration: Gulf Coast Association of Geological Societies Transactions, v. 56, p. 539-550.
- Montgomery, S.L., D.M. Jarvie, K.A. Bowker, and R.M. Pollastro, 2005, Mississippian Barnett Shale, Fort Worth basin, north-central Texas: Gas-shale play with multi-trillion cubic foot potential: American Association of Petroleum Geologists Bulletin, v. 89, no. 2, pp.155-175.
- Nordstrom, P. L., 1982, Occurrence, Availability, and Chemical Quality of Ground Water in the Cretaceous Aquifers of North-Central Texas: Texas Department of Water Resources, Report 269, v. 1, p. 15-54.
- Nordstrom, P. L., 1982, Occurrence, Availability, and Chemical Quality of Ground Water in the Cretaceous Aquifers of North-Central Texas: Texas Department of Water Resources, Report 269, v. 2, test data, p. 1-386.
- O'Rourke, D., B. Cross, and L. Symank, 2011, Anthropogenic Groundwater Contamination in Texas Aquifers, Volume 1, Prepared for the Texas Water Development Board, Austin, Texas, 119 pp.
- Richard C. Peckham, R.C, V. L. Souders, J. W. Dillard, and B. B. Baker, 1963, Texas Water Commission, Bulletin 6309 – Reconnaissance Investigation of the Ground-Water Resources of the Trinity River Basin, Texas, 115 pp.
- Pollastro, R. M., R. J. Hill, D. M. Jarvie, and M. E. Henry, 2003. Assessing Undiscovered Resources of the Barnett-Paleozoic Total Petroleum System, Bend Arch–Fort Worth Basin Province, Texas, AAPG Southwest Section Meeting, Fort Worth, TX, March, 2003, 17 pp.
- Pollastro, R. M., D. M. Jarvie, J. H. Ronald, and C. W. Adams, 2007, Geologic framework of the Mississippian Barnett Shale, Barnett-Paleozoic total petroleum system, Bend Arch–Fort Worth Basin, Texas: AAPG Bulletin, v. 91, no. 4, p. 405–436, doi:10.1306/103006060008.

Thomas, J.D., 2003, Integrating Synsedimentary Tectonics with Sequence Stratigraphy to Understand the Development of the Fort Worth Basin, AAPG Search and Discovery Article #90023, 2002 AAPG Southwest Section Meeting, Ruidoso, New Mexico, June 6-8, 2002 (2003).

Thompson, G.L., 1969, Ground-Water Resources of Johnson County, Texas: Austin, Texas, Texas Water Development Board, Report 94, p. 1-84.

Thompson, D. M., 1982, Lower Atoka Group (lower Middle Pennsylvanian), northern Fort Worth Basin, Texas; depositional systems, facies, and hydrocarbon distribution: American Association of Petroleum Geologists Bulletin, v. 66, p. 247.

Tian, Y., and W.B. Ayers, 2010, Barnett Shale (Mississippian), Fort Worth Basin, Texas: Regional Variations in Gas and Oil Production and Reservoir Properties, Paper CSUG/SPE 137766 presented at the Canadian Unconventional Resources & International Petroleum Conference, Calgary, Alberta, Canada.

Table 1: Stratigraphic Column for Fort Worth Basin Sediments

Era	System	Series	Group or Stratigraphic Unit					
Cenozoic	Quaternary	Recent	Alluvium					
		Pleistocene	Fluviatile terrace deposits					
	Tertiary	Eocene	Wilcox					
		Paleocene	Midway					
Mesozoic	Cretaceous	Gulf	Navarro					
			Taylor					
			Austin					
			Eagle Ford					
			Woodbine					
		Comanche	Washita					
			Fredericksburg					
			Trinity	Antlers	Paluxy			
				Glen Rose				
				Twin Peaks				Hensell
					Pearsall			
					Hosston			
MAJOR UNCONFORMITY								
Paleozoic	Permian	Ochoan-Guadalupian						
		Leonardian						
		Wolfcampian	Cisco					
	Pennsylvanian	Virgilian						
		Missourian	Canyon					
		Desmoinesian	Strawn					
		Atokan	Bend					
			Smithwick					
		Morrowan	Marble Falls Limestone					
		Mississippian	Chesterian-Meramerican	Barnett Shale				
	Osagean		Chappel Limestone					
	MAJOR UNCONFORMITY							
	Ordovician		Viola Limestone					
			Simpson					
			Ellenburger					

Table 2: Conventional Oil and Gas Plays within the Fort Worth Basin

Age	Group or Formation		Overall Thickness (ft)	Reservoir Thickness (ft)	Porosity (%)	Permeability (mD)	Drilling Depths (ft bls)	Reservoir Structure	Discovery	Associated Fields
Desmoinesian	Strawn	Strawn Sands	1,000 to > 5,000	65 - 400	14 - 23	> 100	1,000 - 7,000	combined structural/stratigrphic traps	1931	KMA
		Caddo Limestone	up to 800	80 - 174	7 - 14	3 - 15			1919	Breckeridge
Lower Pennsylvanian	Bend Group	Bend Sandstone and Conglomerate	0 to > 5,000	20 - 25	up to 20	up to 100	2,000 - 10,000	variable	1917, 1950	Ranger, Boonsville
		Marble Falls Limestone								
Mississipian	Chappel Limestone		up to 350	up to 350	< 10	0.1 - 100	3,000 -9,000	pinnacle reefs	1954	Shackelford, Lee Ray
Cambrian/Ordovician	Ellenburger Group		500-5,000	10-100	10	< 5	2,000 -9,000	anticlines combined structural/stratigrphic traps	1942	Hildreth

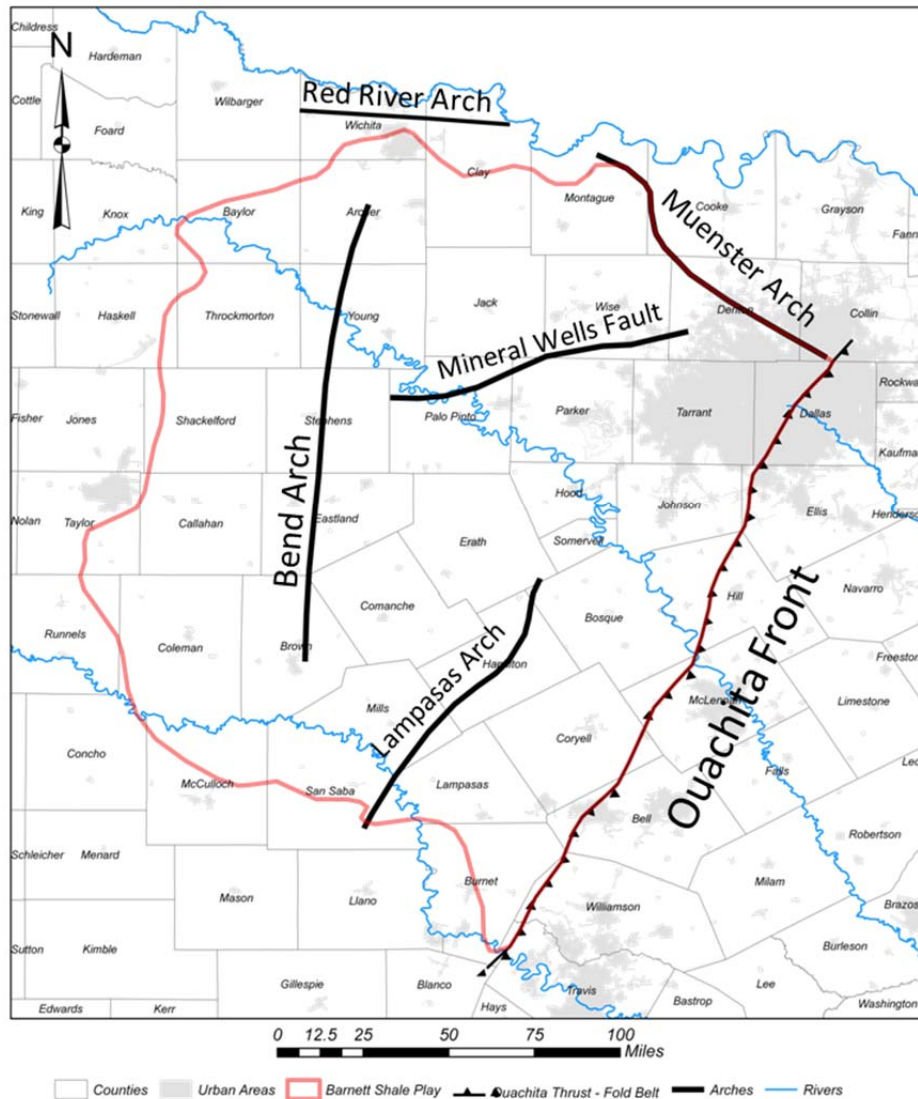


Figure 1: Location of the Barnett Shale play in north-central Texas.



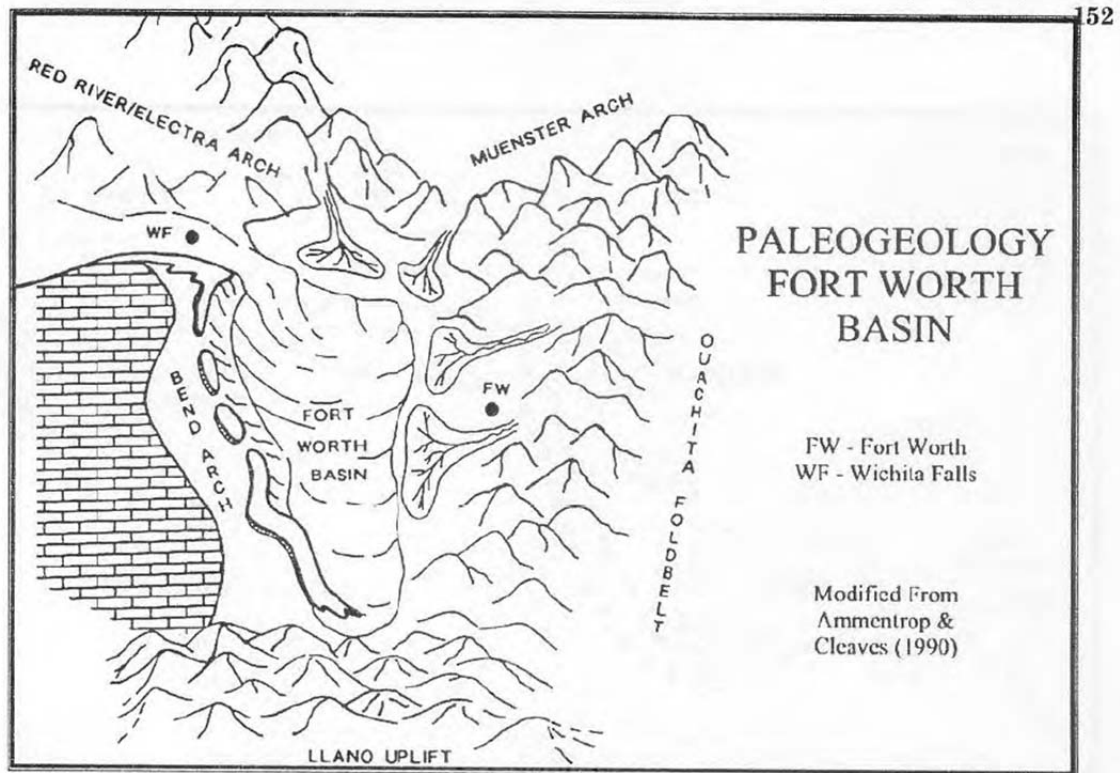


Figure 2: Basic structural features of the Fort Worth Basin from Thomas (2003) and Ammentrop and Cleaves (1990).

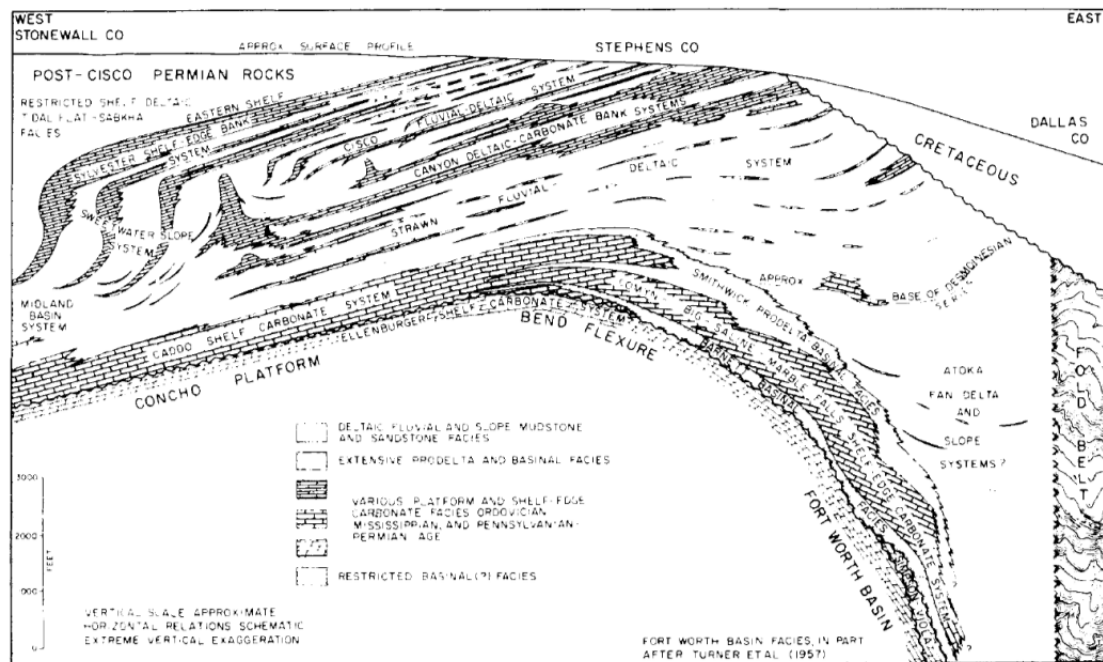


Figure 3: Generalization of depositional systems of the Fort Worth Basin from Cleaves and Erxleben (1985).

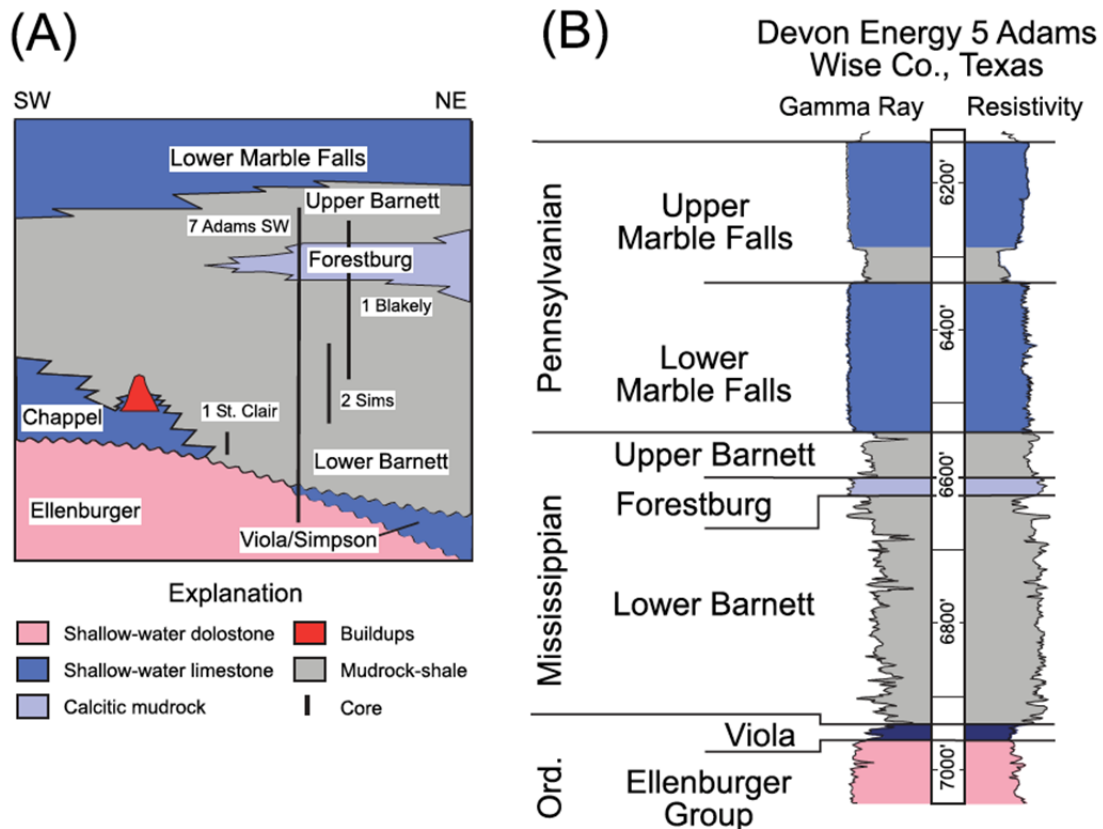


Figure 4: From Loucks and Ruppel (2007). General stratigraphy of the Ordovician to Pennsylvanian section in the Fort Worth Basin. (A) Diagrammatic cross section of the stratigraphy of the Fort Worth Basin after Montgomery et al. (2005). Approximate stratigraphic location of cores used in the study is shown. (B) Wire-line log with major stratigraphic units.

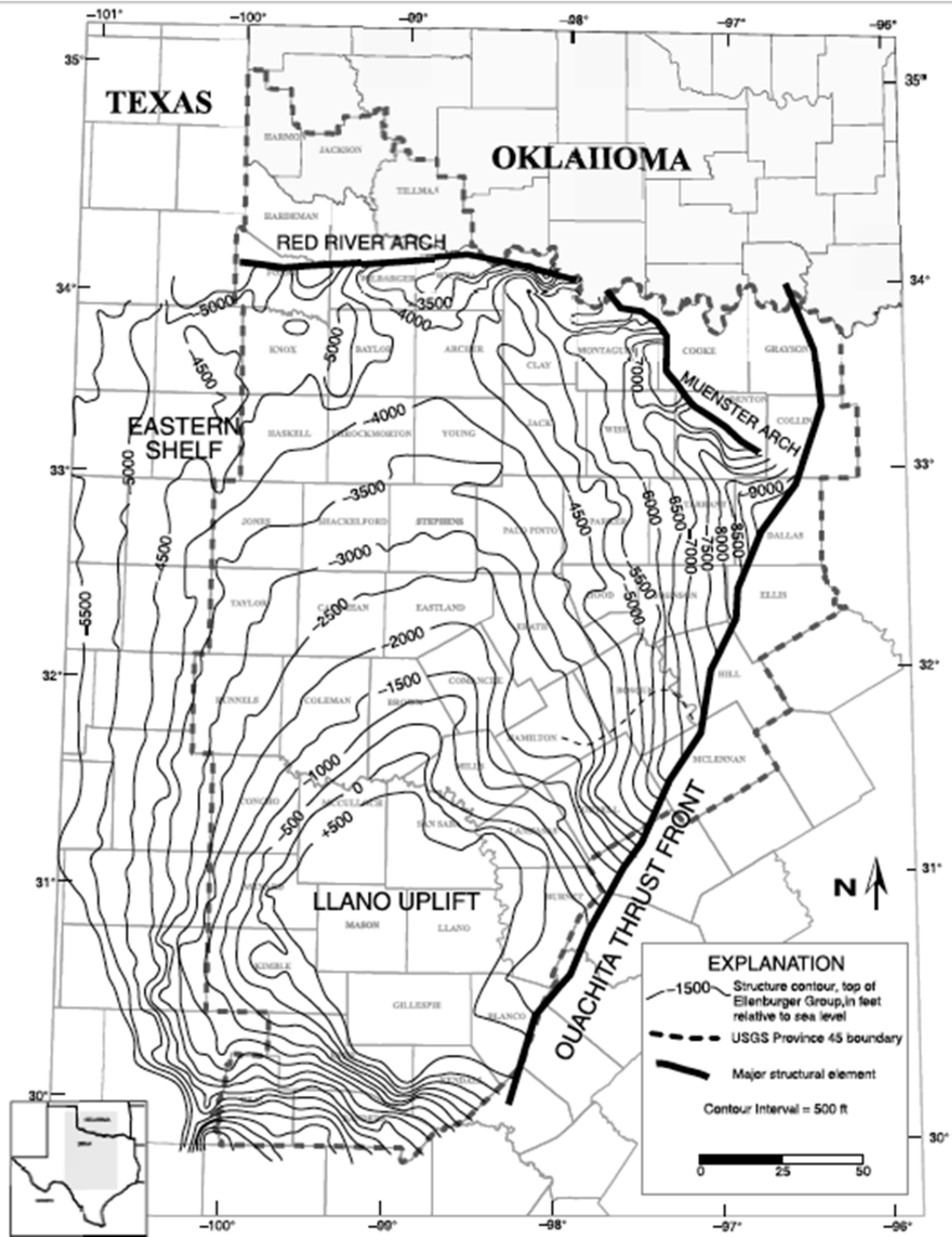


Figure 5: Structure of the base of the Ellenburger Group in the Fort Worth Basin from Pollastro et al. (2007).

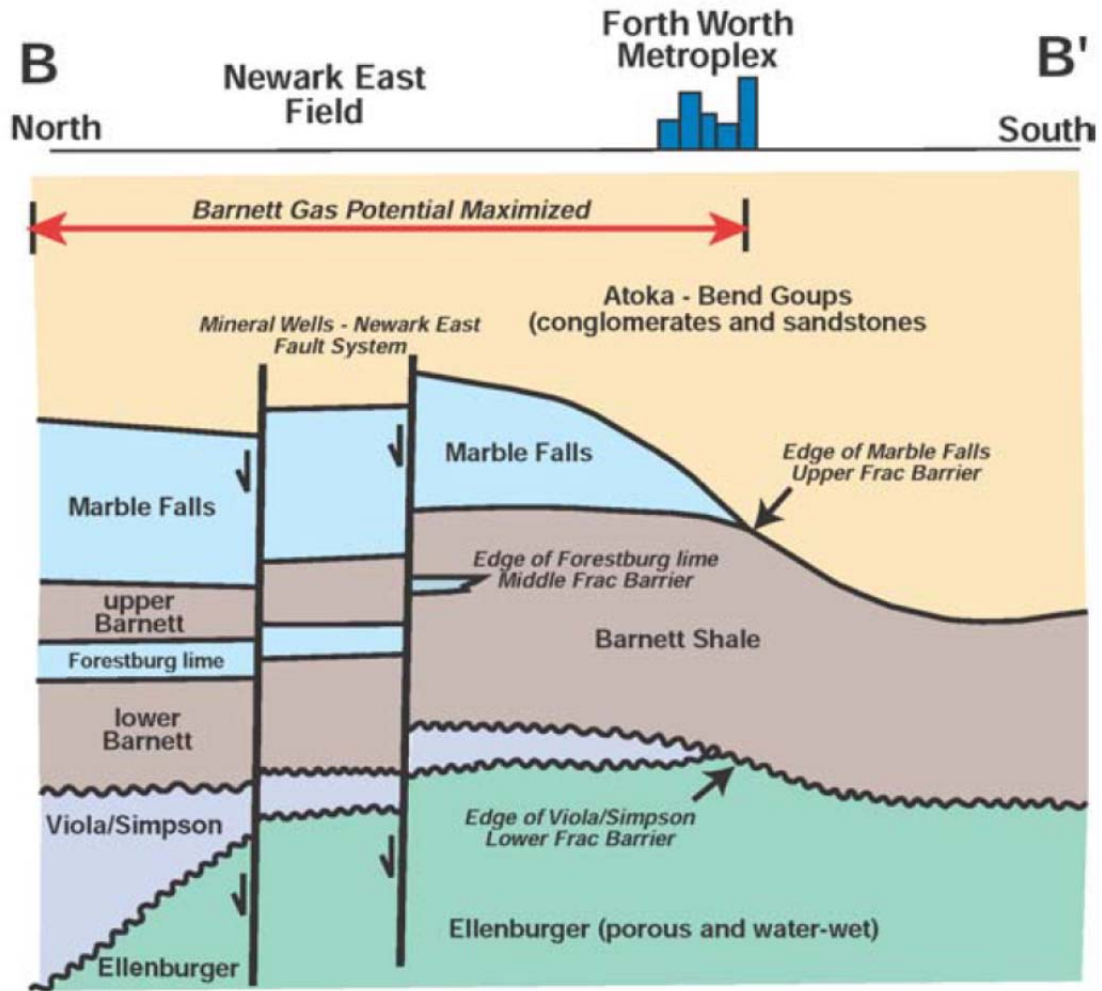


Figure 6: From Montgomery et al. (2005), a schematic cross section showing the limits of the carbonate units associated with the Barnett Shale in the Fort Worth Basin.

A-40

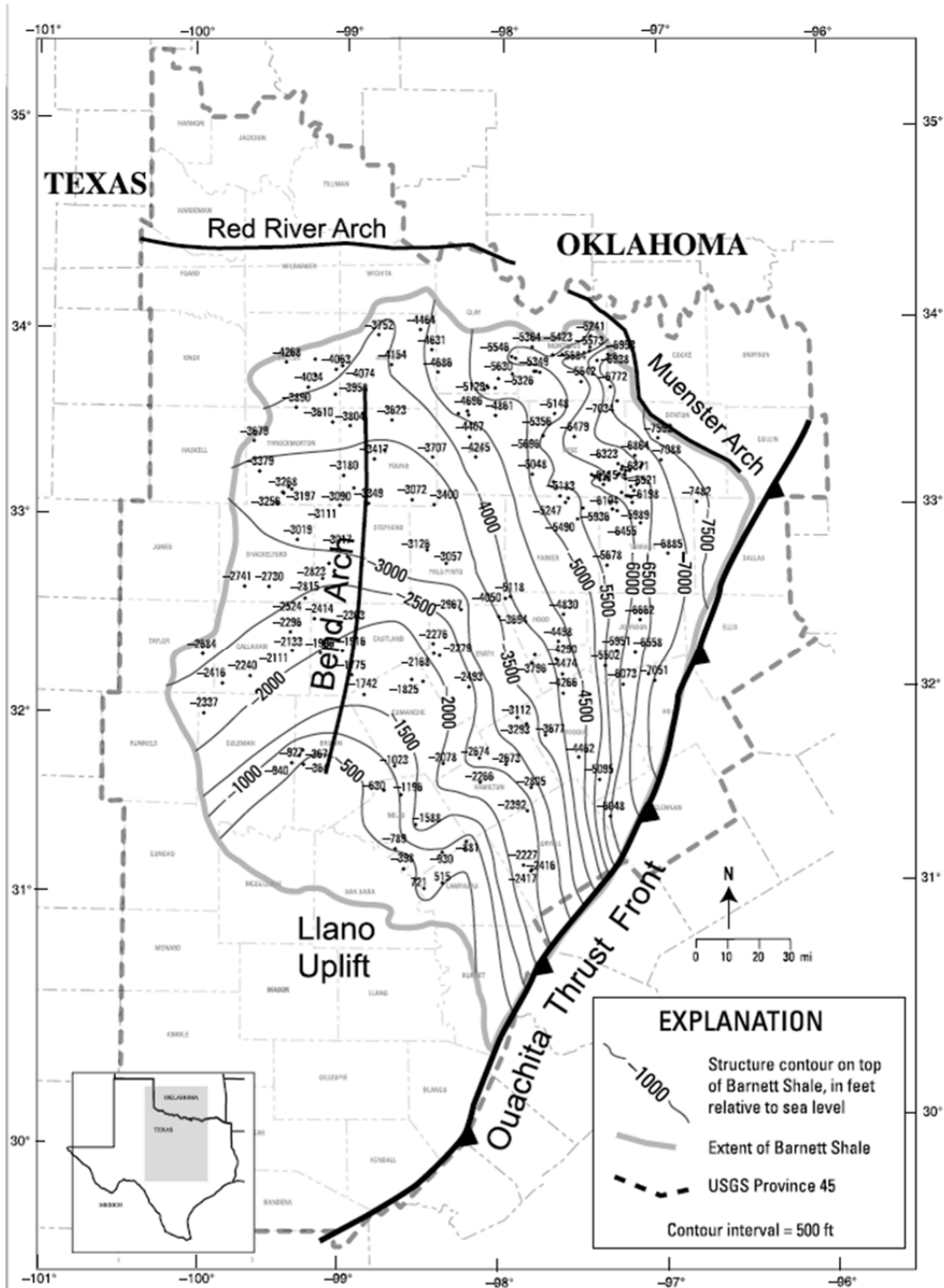


Figure 8: Structure contour map on top of the Barnett Shale from Pollastro et al. (2007).

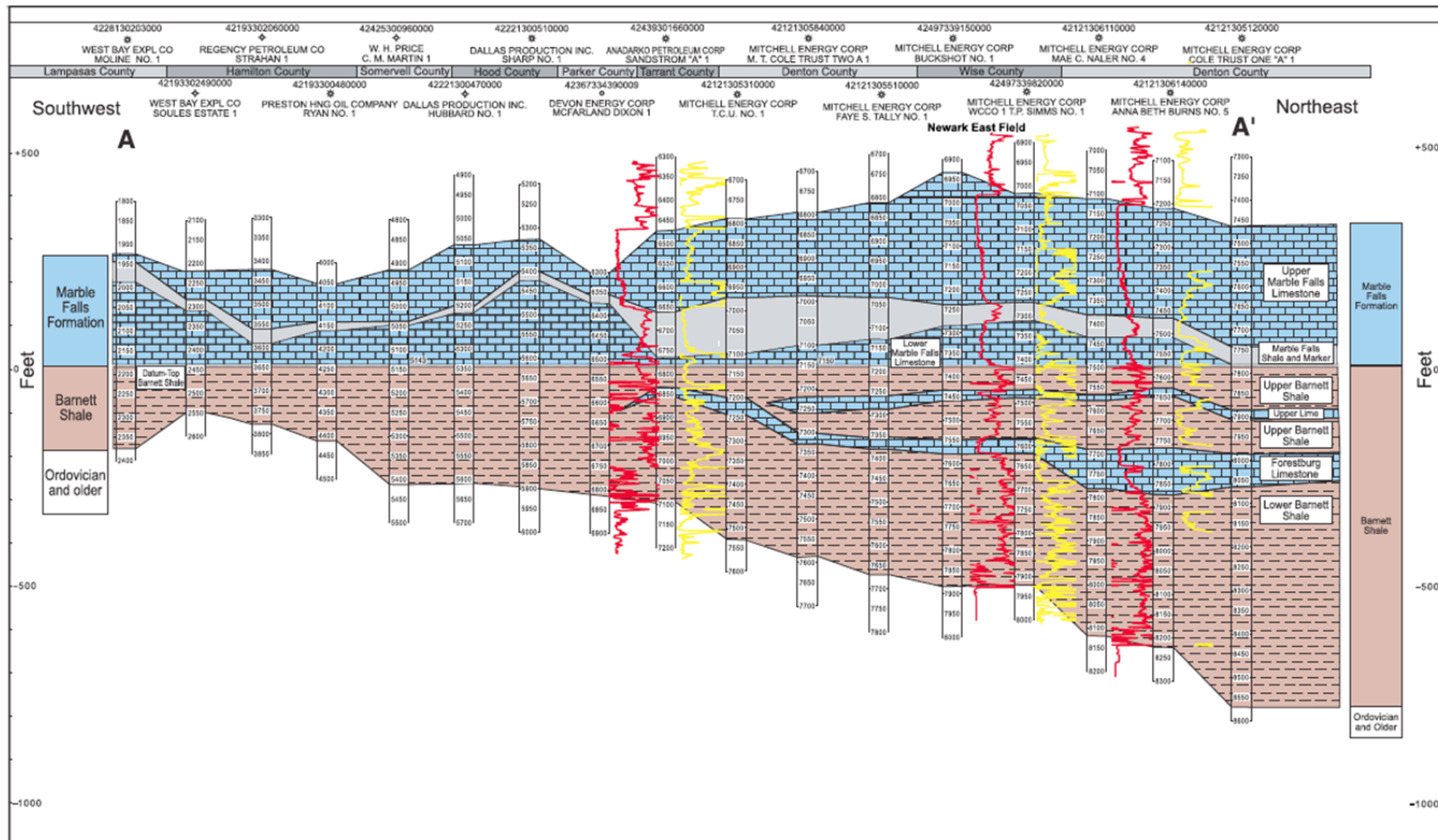


Figure 9: North to south stratigraphic cross sections based on well-log correlations from Pollastro et al. (2007). Gamma-log profiles (red) and resistivity log profiles are shown for reference on selected wells. Lines of section are shown on Figure 6.



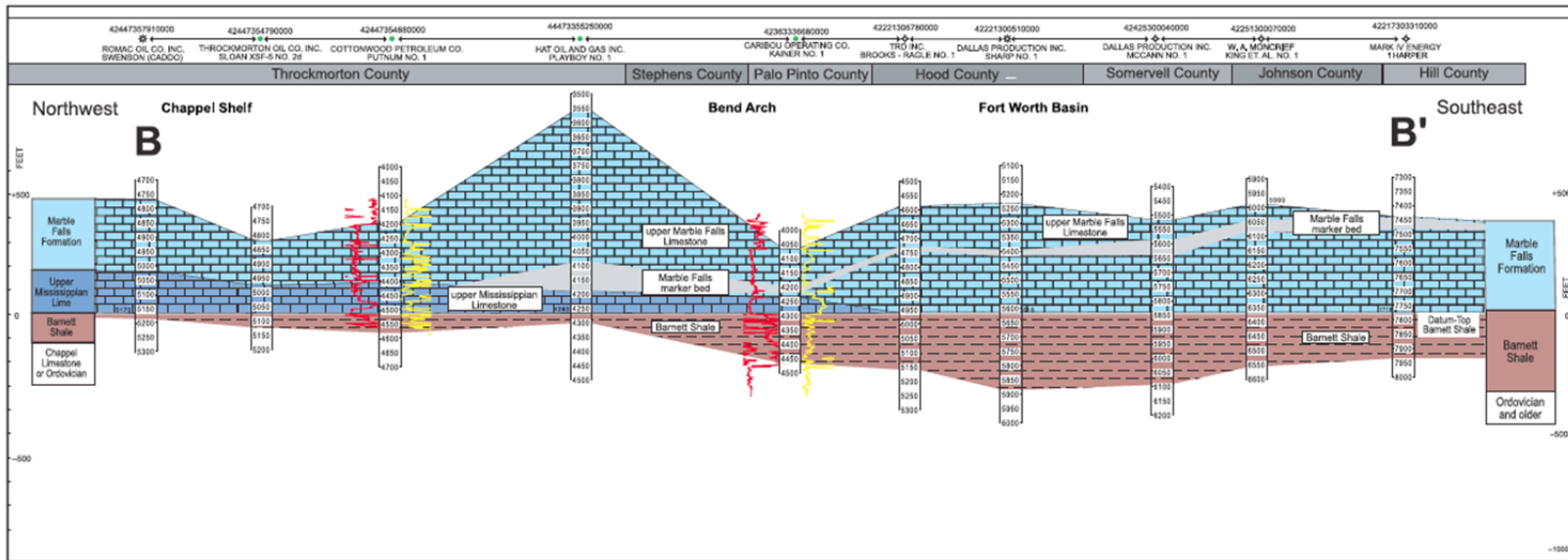


Figure 10: West to east stratigraphic cross sections based on well-log correlations from Pollastro et al. (2007). Gamma-log profiles (red) and resistivity log profiles are shown for reference on selected wells. Lines of section are shown on Figure 6.

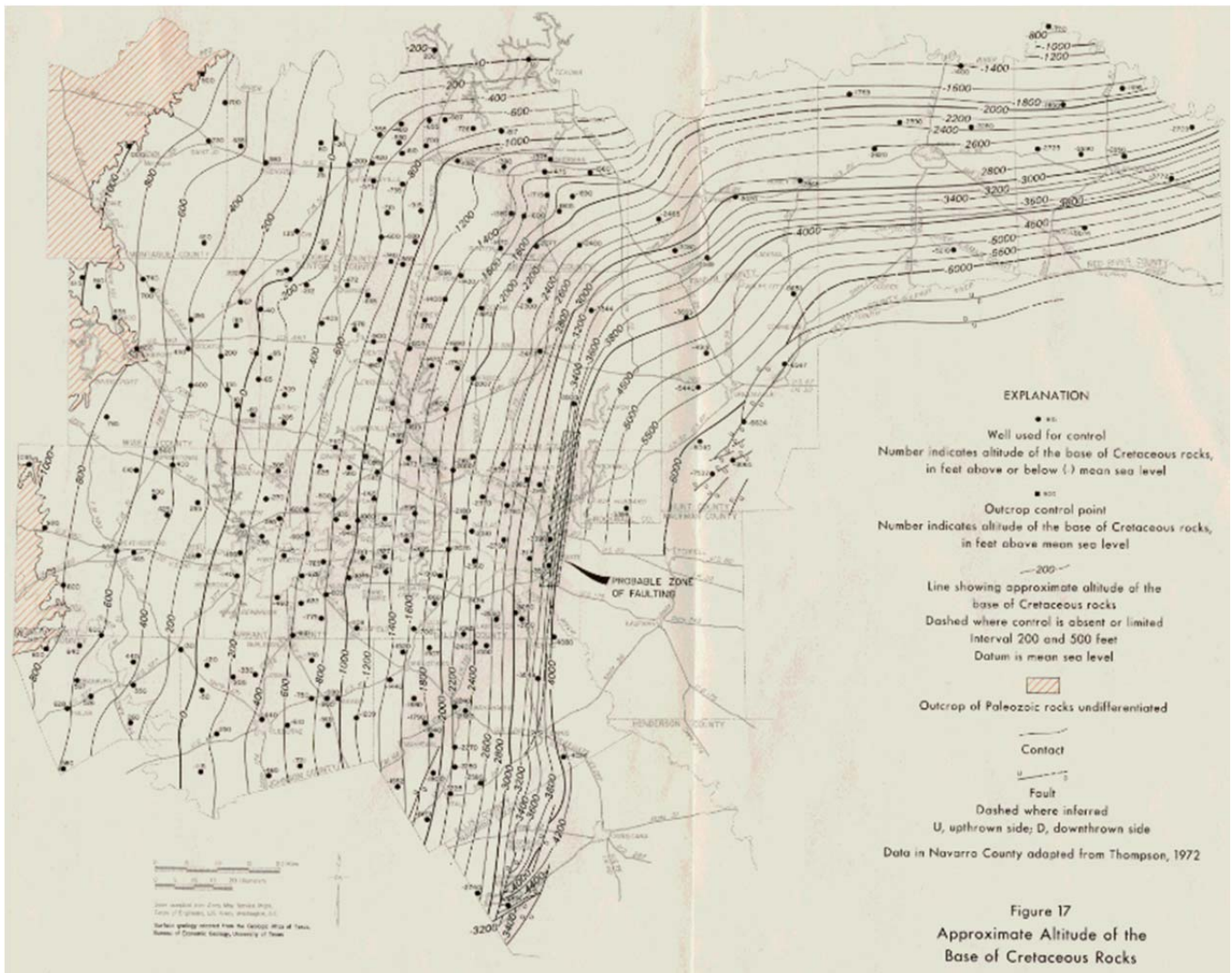


Figure 11: Map of the base of the Cretaceous formations in north-central Texas from Nordstrom (1982).

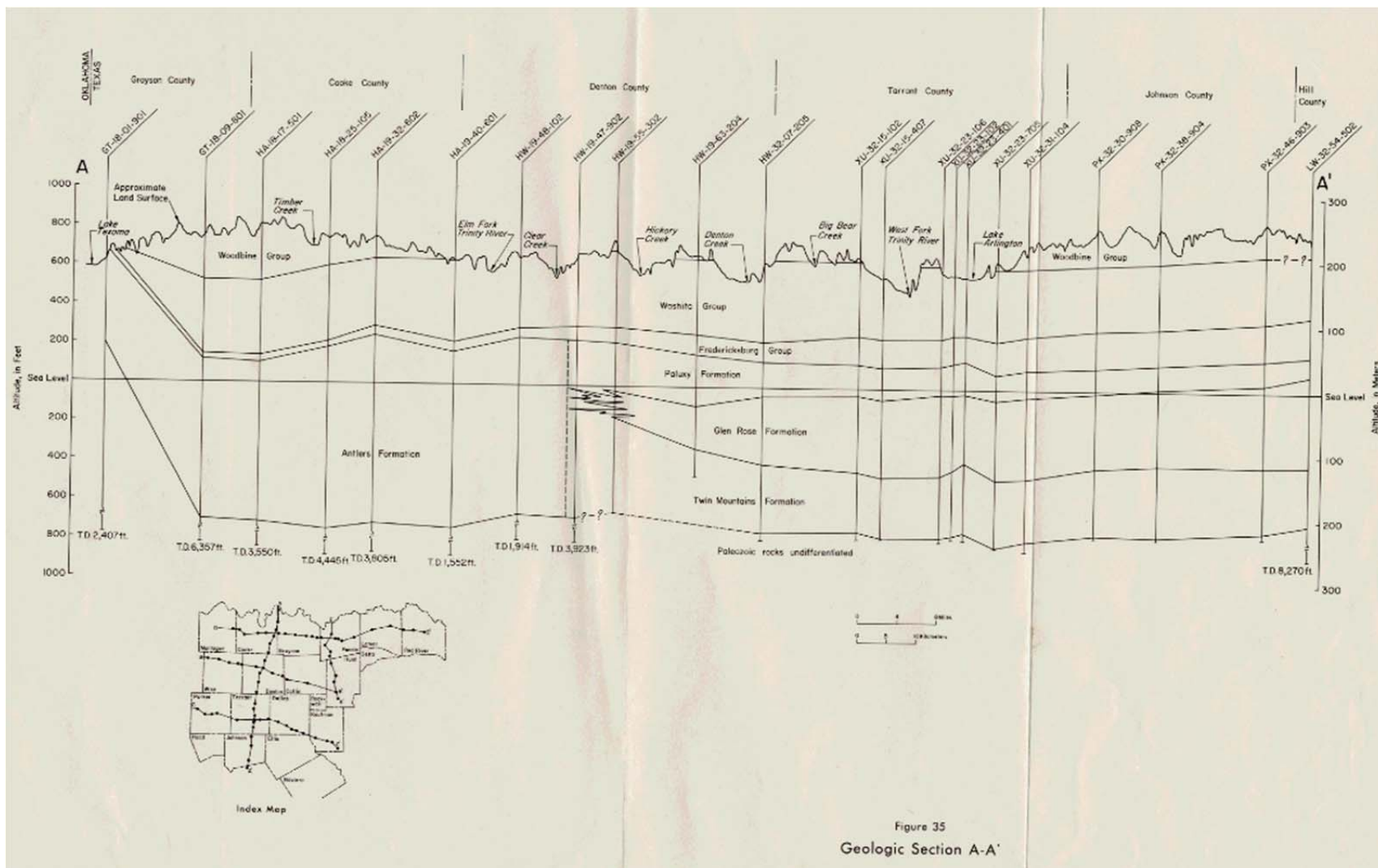


Figure 12: North-South cross-section showing Cretaceous formations from Nordstrom (1982).

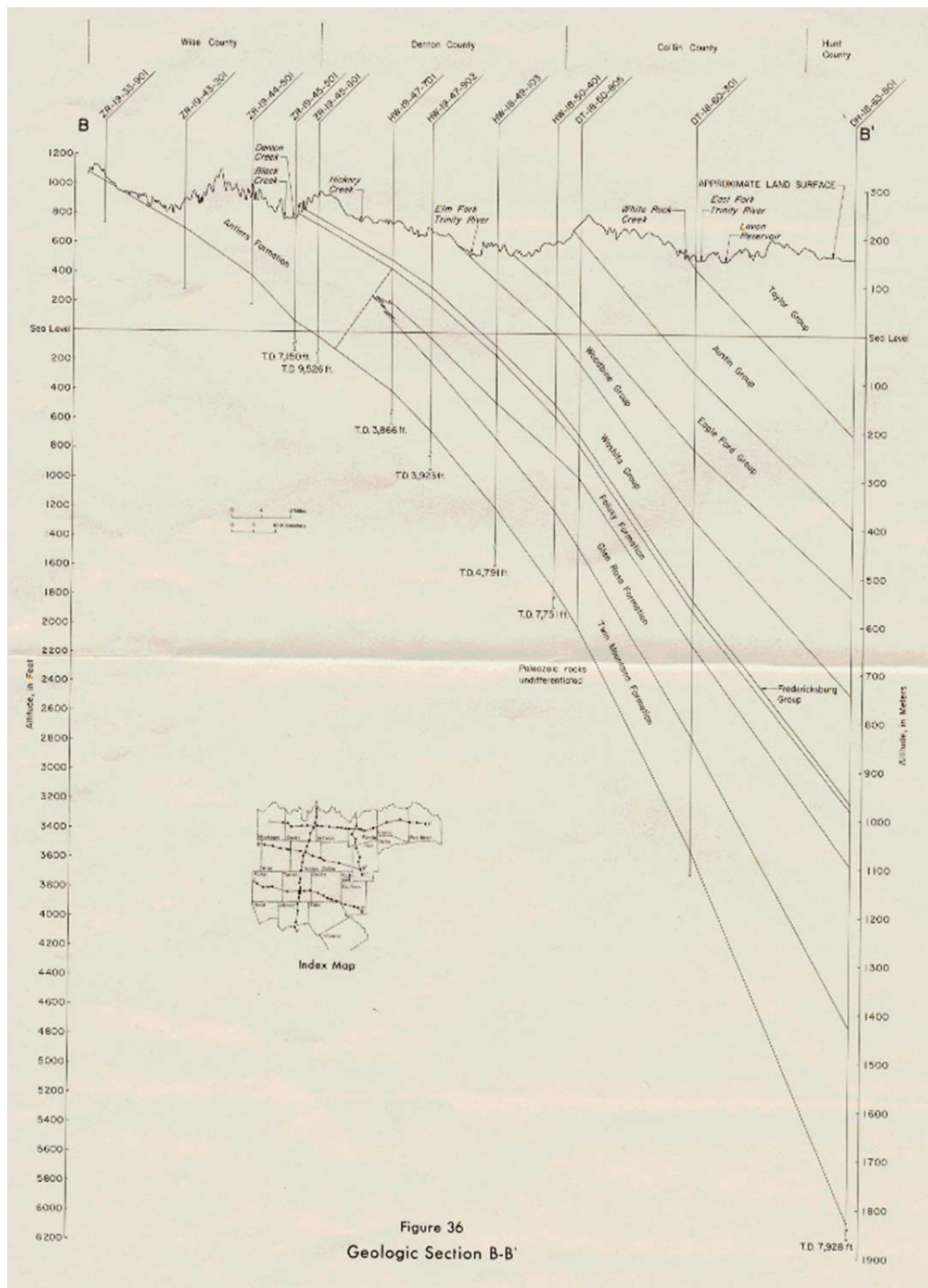


Figure 13: West to East cross section showing Cretaceous formations from Nordstrom (1982).



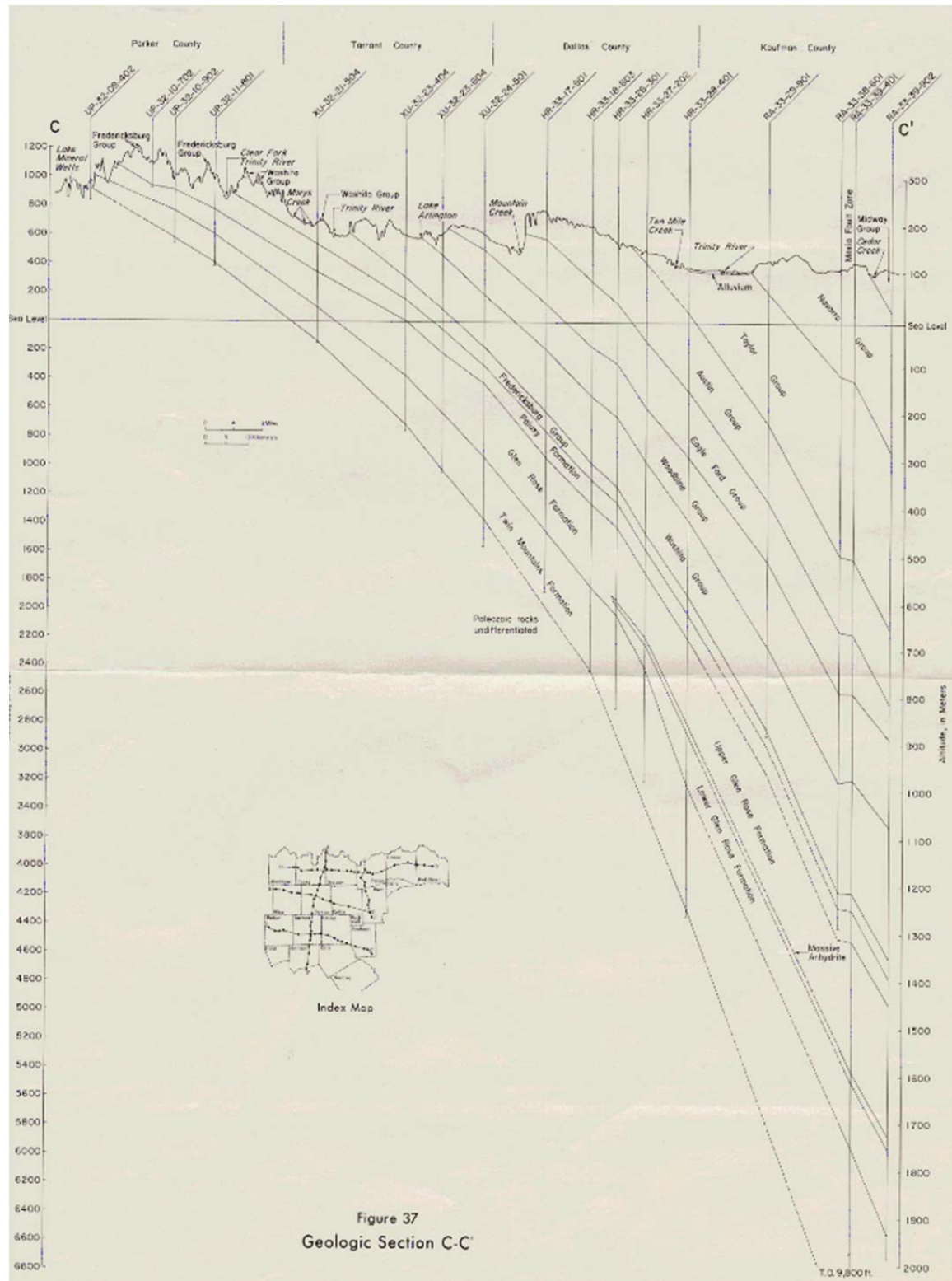


Figure 14: West to East cross section showing Cretaceous formations from Nordstrom (1982).

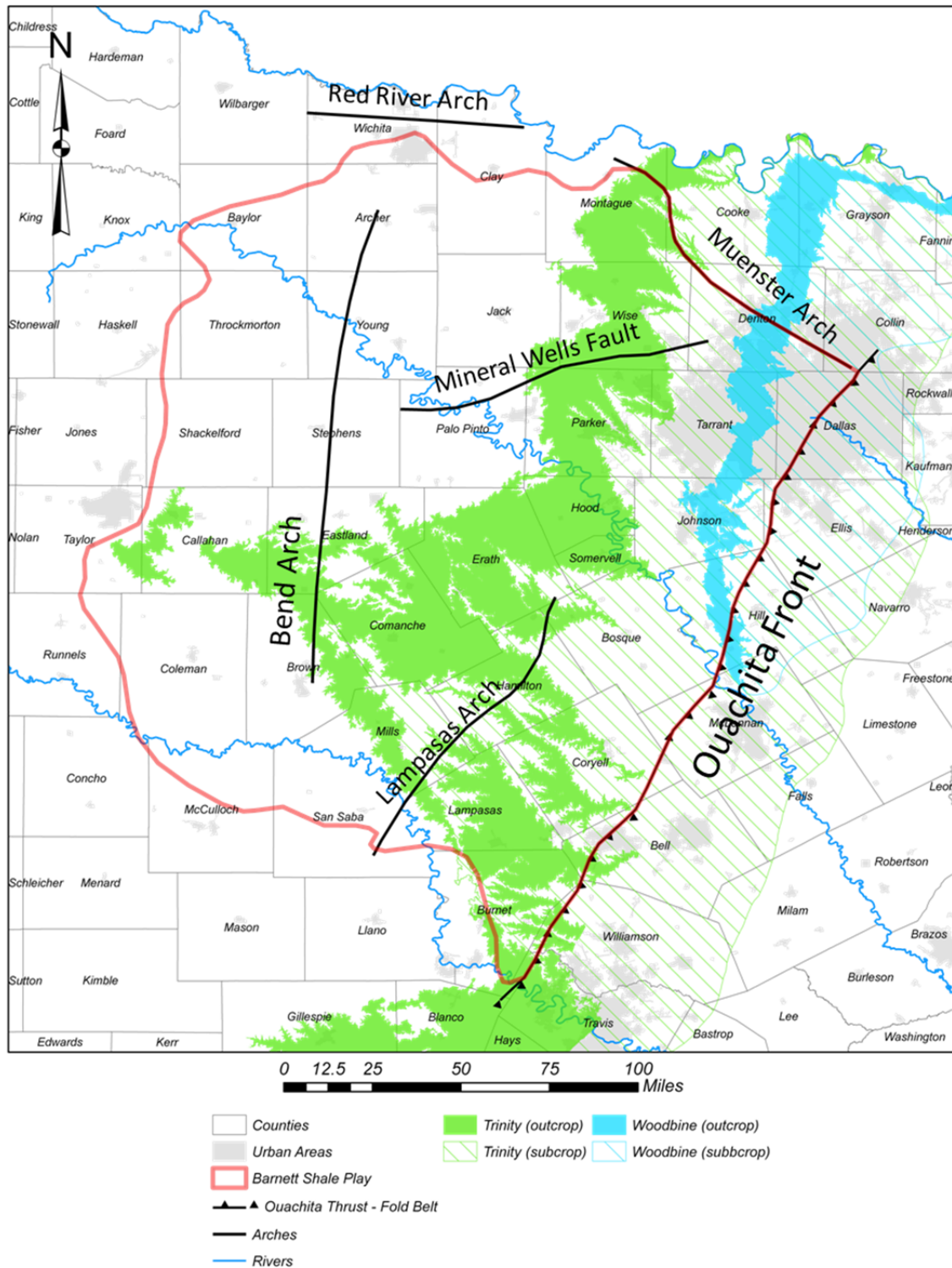


Figure 15: Outcrop and subsurface locations of the Trinity and Woodbine Groups within the study area.

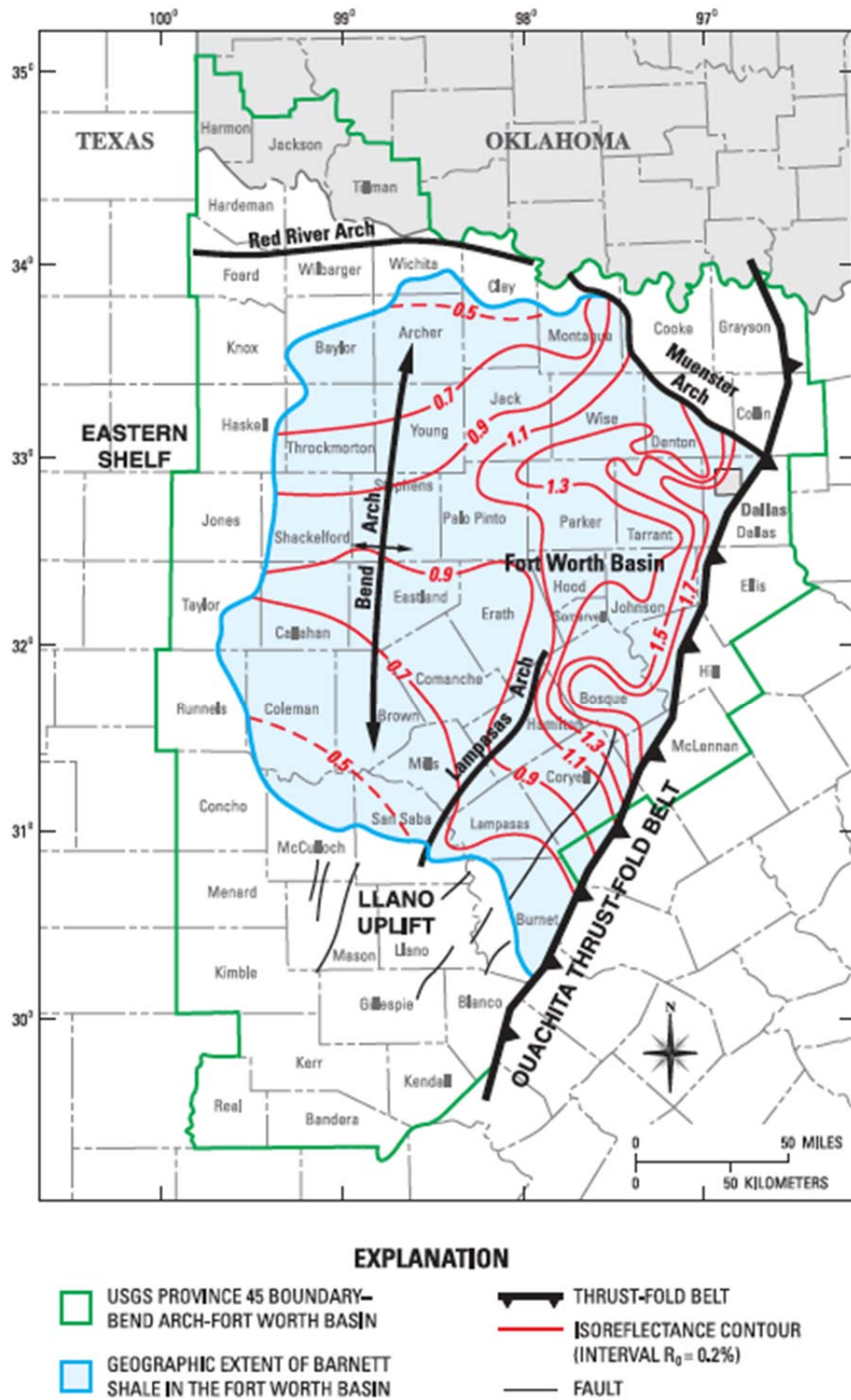


Figure 16: Isoreflectance map, Fort Worth Basin and Bend Arch. Modified from Montgomery et al. (2005) and Bruner and Smosna (2011).



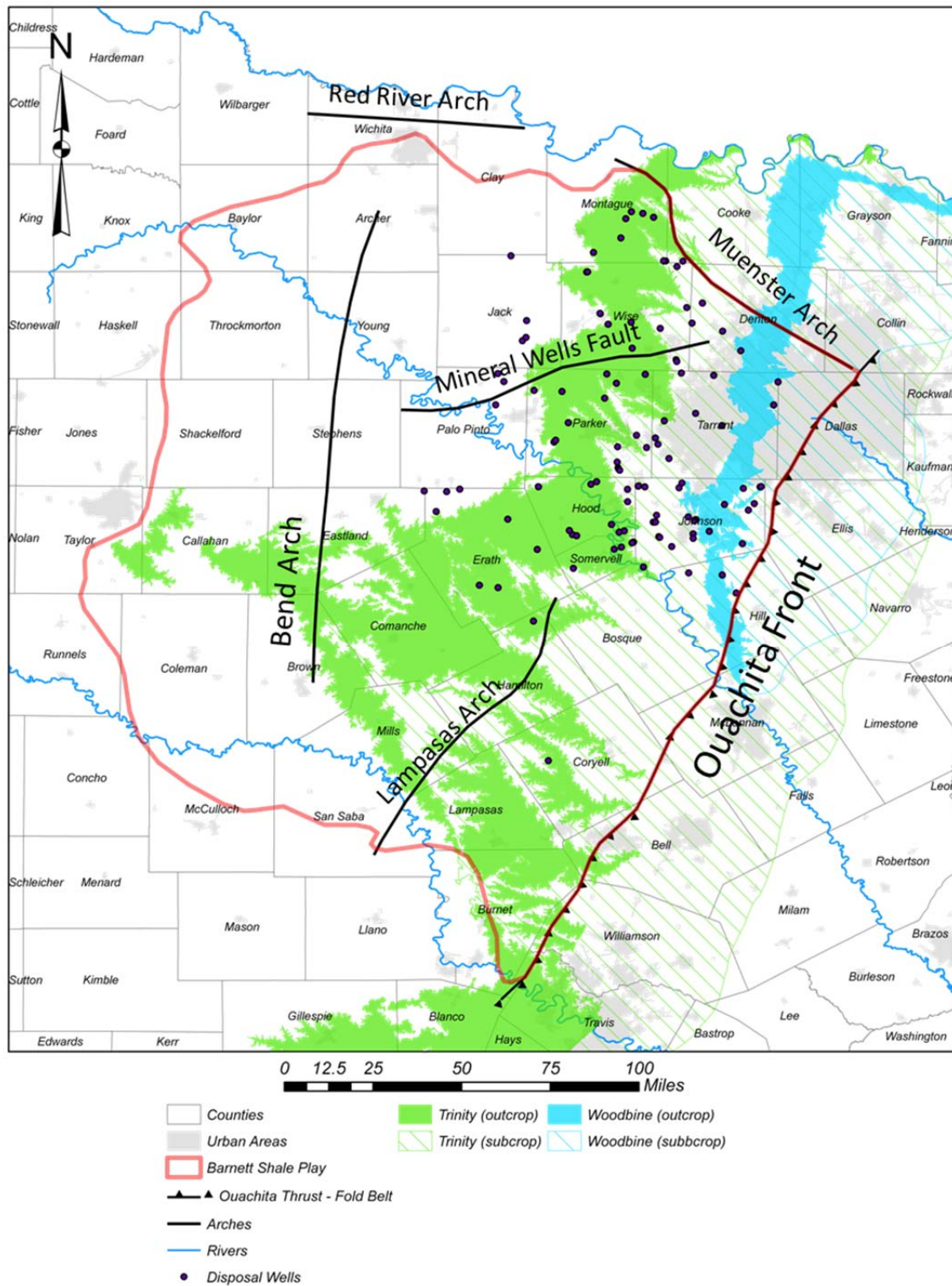


Figure 17: Location of disposal wells within the Barnett Shale play.



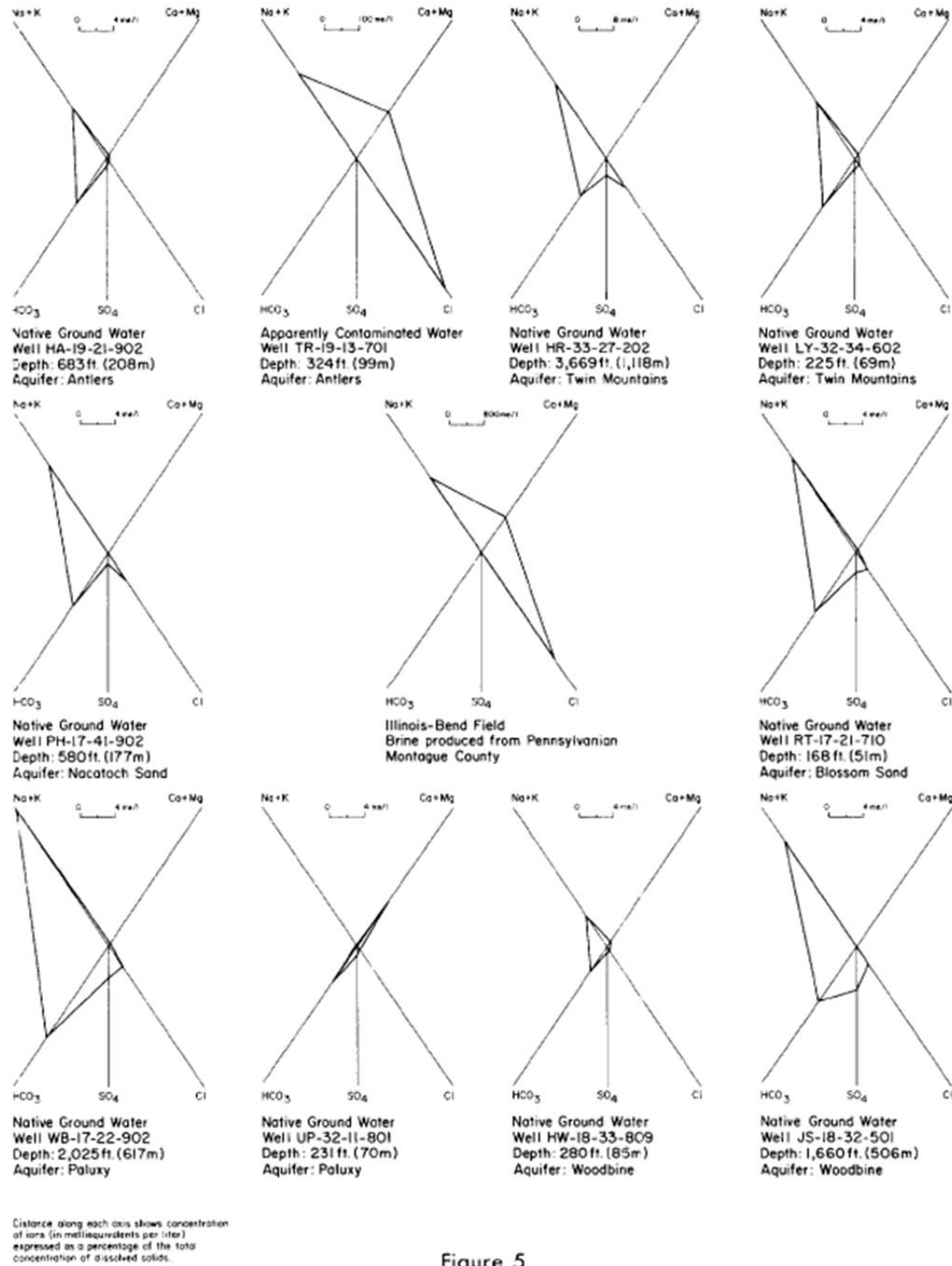


Figure 18: Chemical signatures of selected groundwater samples and a typical oil field brine from Nordstrom (1982).

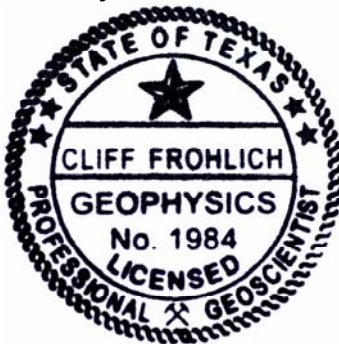
## Appendix B: Review of Earthquakes Triggered by Human Activities, Focusing on Texas and the Barnett Shale

# **Appendix B:**

## **Review of Earthquakes Triggered by Human Activities, Focusing on Texas and the Barnett Shale**

prepared by Cliff Frohlich  
Texas P.G. #1984; e-mail: cliff@ig.utexas.edu

Institute for Geophysics; Jackson School of Geosciences  
University of Texas at Austin



18 February 2012

**ABSTRACT:** This report reviews examples of earthquakes apparently induced/triggered by human activity, focusing particularly on events in Texas, and especially within the Barnett Shale of north-central Texas. There are empirical and physical reasons to categorize such earthquakes by considering the nature of the activity that appears to trigger them (fluid extraction for oil or gas production, hydrofracturing, multi-well injection for secondary petroleum recovery, multiple-well injection for geothermal energy production, or single-well injection for waste disposal) and also the magnitude level of regional historically-reported natural seismicity near triggered earthquake locations. For the Barnett Shale and central Texas, the historical record indicates extraction-triggered earthquakes are less of a concern than injection-triggered earthquakes. No injection-triggered earthquakes with magnitudes exceeding M3.5 have occurred in the Barnett Shale. My compilation shows that with two exceptions, globally-occurring injection-triggered earthquakes having magnitudes exceeding M4.0 all are in environments where natural earthquakes with larger magnitudes occur within 100 km of the well. One exception (Snyder, TX; M4.6 1978) was in a field undergoing decades-long waterflooding at more than 100 wells spaced on a ½-km grid. The compilation found no examples where injection-triggered earthquakes having magnitudes exceeding M3.5 occurred near injection wells used for waste disposal in environments where the largest known natural earthquakes within 100 km had magnitudes of 3.5 or less. Thus for disposal-well operators seeking to avoid inducing earthquakes, one possible strategy is to confine injection operations to environments where nearby historically-reported natural earthquakes are absent or have some other acceptably low value.

## I. INTRODUCTION

It has been known that human activities can induce or trigger seismic activity since a series of earthquakes occurred in the 1930's following the construction of the Hoover Dam and the filling of Lake Meade (Carder, 1945). Subsequently it was established that earthquakes sometimes accompany mining or cavity collapse, the removal of fluids from the subsurface, and fluid injection into the subsurface. In the literature a situation where earthquakes accompany human activity is termed induced seismicity, even though usually it is impossible to prove categorically that the human activity caused the seismic activity. Thus triggered seismicity is probably a more accurate term, since regional tectonic stresses appear to be responsible for most 'induced' seismicity, and human activities simply encourage or accelerate the release of regional stress along preexisting faults. This report will not discuss earthquakes triggered by reservoir impoundment (for reviews, see Gupta, 1992; 2002) or mining/cavity collapse (for reviews, see Gibowicz, 1991; 2001; 2009).

Recently several widely publicized earthquakes have occurred that coincide with the development of unconventional gas resources in the Barnett Shale of Texas (Figure 1). These include two sequences of small earthquakes near Dallas-Fort Worth (DFW), TX, in October-November 2008 and May 2009 (Frohlich et al., 2010; 2011), and several small earthquakes near Cleburne, TX (Howe et al., 2010). The recent development of natural gas resources was stimulated by technological advances in horizontal drilling technology and improved hydrofracturing methods ("fracking"). Developing a producing well involves four steps: drilling the well; hydrofracturing various sections of the well; producing gas from the well, accompanied by the return to the surface of some of the hydrofracture fluid; and the disposal of this recovered fluid. In the Barnett this disposal is usually accomplished by injecting it into the Ellenburger formation, a highly permeable strata that lies just beneath the Barnett.

This report will review situations where oil and gas production, hydrofracturing, and fluid injection appear to have triggered earthquakes; I am unaware of any instance where drilling *per se* has triggered an earthquake (Figure 2). Wherever possible this report will use examples from Texas and/or very recent examples that have received attention in the media but are too recent to be discussed in standard reviews. Such reviews include Segall (1989), Nicholson and Wesson (1990) and Suckale (2009; 2010). The report will focus mostly on injection, since both the DFW and Cleburne earthquake sequences occurred near injection disposal wells.

Injection may be used to accomplish several objectives, including waste disposal, the production of geothermal energy, and waterflooding to enhance recovery of petroleum. There are examples where all three activities (and hydrofracturing, which involves injection) have triggered earthquakes. In addition to reviewing reported incidents of triggered seismicity, this report will also categorize such incidents with respect to the magnitude level of regional historical seismicity near well locations, and with respect to the nature and purpose of the injection program

(hydrofracturing; single-well injection for waste disposal; multiple-well injection for geothermal; multi-well injection for secondary petroleum recovery).

This report compiles empirical data concerning the magnitude of different varieties of triggered earthquakes, and compares these to the largest known natural earthquakes occurring nearby (within 100 km). These data indicate that earthquakes triggered by hydrofracture and by injection for waste disposal have magnitudes no larger than the largest nearby natural earthquakes. In contrast, in environments where earthquakes accompany injection at numerous closely spaced wells (waterflooding or secondary recovery), or where earthquakes accompany fluid extraction (production of oil and gas), some triggered earthquakes are larger than nearby natural earthquakes.

## **II. EXAMPLES OF EARTHQUAKES ASSOCIATED WITH FLUID EXTRACTION (OIL/GAS PRODUCTION)**

Historically, no earthquakes have occurred within the Barnett Shale that appear to have been triggered by fluid extraction. However, there are four other oil/gas fields in east/central Texas where such events have occurred (Figure 1).

*Wortham-Mexia, Texas:* On 9 April 1932 an M4.0 earthquake produced severe shaking near the towns of Wortham and Mexia, TX (Figure 3). Sellards (1931) thoroughly surveyed the felt area one month later and reported that that a small area near Wortham experienced Modified Mercalli Intensity<sup>1</sup> (MMI) VI, while at distances of 30-40 km the earthquake was barely perceptible or went unfelt. The high intensities in a very localized area suggest that the focal depth was unusually shallow, probably at most a few km.

The region of maximum intensity coincided with the boundaries of the Wortham oil field, and the MMI V-VI regions included the Mexia field. When this earthquake occurred, more than 110 million barrels of oil had been extracted from the Mexia and Wortham oil fields, which had been produced since 1920. This fact and the inference that the focal depth was shallower than for most natural earthquakes both suggest that the Wortham-Mexia earthquake may have been triggered by production.

---

<sup>1</sup> The Modified Mercalli Intensity is a Roman numeral between 'I' and 'XII' assigned to assess the strength of earthquake-induced shaking at a particular location; it is most useful when instrumental information is unavailable. This report mentions intensities between MMI III and MMI VI: III corresponds to shaking felt only indoors—hanging objects swing, vibrations like passing of light trucks occur, and the event may not be recognized as an earthquake; IV corresponds to windows, dishes, and doors rattling, vibration like passing of heavy trucks or a jolt like a heavy object striking the walls; V is felt outdoors, sleepers are awakened, and small unstable objects are displaced or upset; VI is felt by all, many people are frightened and may run outdoors, dishes are broken and objects fall off shelves, furniture is moved or overturned, and weak plaster and unreinforced masonry suffers cracks.

*Gladewater, Texas:* On 19 March 1957 at least four earthquakes (largest M4.7) occurred near the towns of Gladewater, Longview, and Marshall in northeastern Texas. The area experiencing the maximum intensity, MMI V, had a diameter of about 80 km. The center of this region coincides with the northern part of the East Texas oil field. At the time of this field's discovery in 1930 it was the largest field in the western hemisphere, and when the earthquakes occurred it had produced more than 3.5 billion barrels of oil. Various investigators have suggested that the Gladewater quakes may have been triggered by fluid extraction (e.g., see Frohlich and Davis, 2002).

*Alice, Texas:* On 24 March 1997 and again on 25 April 2010, two earthquakes (M3.8 and M3.9) occurred southeast of Alice, Texas, a small community situated about 75 km west of Corpus Christi (Figure 4). The earthquakes were nearly identical in all respects: they had similar magnitudes and felt areas, and at stations measuring both events, nearly identical seismograms (Frohlich et al., 2012). Analysis of seismograms from the 2010 event indicated it had a focal depth of 3 km or less; thus its location places it along the mapped trace of the Vicksburg fault zone and at the depth of the Frio formation, the principal productive member in the Stratton field, which has produced at least 2.7 trillion cubic feet of gas and about 100 million barrels of oil since production commenced in 1938. Although both earthquakes occurred long after the peak years of production in the Stratton field (Figure 5), their unusually shallow focal depth and location at the boundary of the Statton field suggest that production in the field contributed to their occurrence.

*Fashioning, Texas:* On 20 October 2011 an M4.8 earthquake occurred near Fashioning, TX, about 80 km SE of San Antonio. The epicenter lies within the Eagle Ford Shale, which is being developed extensively and subject to numerous hydrofracture operations. However, published investigations of the regional seismicity near Fashioning indicate that numerous earthquakes have been reported since 1974, including an M4.3 in 1993 (Pennington et al., 1986; Davis et al., 1995). These studies concluded the 1974-1993 seismicity was probably triggered by stress adjustments caused by fluid extraction, i.e., production from various regional fault-bounded fields. Unless future investigations establish a definitive correlation with fluid injection, I conclude that the 2011 earthquake is not injection-triggered, but production-triggered like past events.

### **III. EXAMPLES OF EARTHQUAKES ASSOCIATED WITH HYDROFRACTURING**

Since fracturing intact rock is essential to hydrofracturing, in a strict sense hydrofracturing causes earthquakes; however, these fractures are small, and when they are measured by downhole seismic arrays they typically have magnitudes in the range of -3 to +1—too small to be felt at the surface by humans, and too small to be recorded by regional seismograph networks. Also, various kinds of evidence suggest that the fractures produced by hydrofracturing are physically unlike the fault ruptures that cause natural earthquakes; e.g., the size distribution of

hydrofracture events, as measured by arrays of downhole seismometers, is unlike the size distribution of natural earthquakes (e.g., Shapiro and Dinski, 2009). Considering that tens of thousands of wells are hydrofractured each year, it is significant that almost none have caused sensible earthquakes. And in the three cases reported in the literature (see below) where hydrofracturing induces felt earthquakes, their magnitudes have been M3.5 and less, too small to pose a hazard.

However, the three examples that follow do demonstrate that it is possible for hydrofracturing to trigger earthquakes, although it occurs only rarely. I am unaware of any reported example in Texas where hydrofracturing has triggered earthquakes.

*Orcutt, California:* Kanamori and Hauksson (1992) describe a M3.5 earthquake that occurred on 31 January 1991 few hours after a hydrofracturing operation finished. Hydrofracturing at a pressure of 80 bars was being done at depths of 100-300 meters; because liners in several wells were deformed at these depths they concluded that the earthquake was caused by failure of sediments at shallow depth. This is remarkably shallow for an earthquake—much shallower than the depths of most earthquakes of tectonic origin—and Kanamori and Hauksson's (1992) paper focuses more attention on the peculiar seismograms generated by the earthquake than on its relationship to hydrofracturing.

*Garvin, Oklahoma:* Holland (2011) describes a series of small earthquakes (largest M2.8) that occurred 17-23 January 2011 near Garvin, OK, with epicenters 1-4 km from an ongoing hydrofracturing operation. The earthquakes began about 7 hours after hydrofracturing commenced, and mostly stopped occurring within 24 hours after hydrofracturing ceased. The U.S. Geological Survey's National Earthquake Information Center (NEIC) reports earthquakes with M4.2 and 4.5 occurring in 1994 and 1997 at distances of 30 km and 90 km.

*Fylde Coast (Blackpool), United Kingdom:* News reports and de Pater and Baisch (2011) describe two small earthquakes (M1.5 and M2.3) occurring in April and May, 2011, occurring within 2 km of an experimental hydrofracture operation on the Fylde Coast near Blackpool, United Kingdom. Injection operations began in March, 2011; following the May 2011 earthquake, the operator terminated the project, allegedly "Britain's only shale gas project". The NEIC reports several previous M3-M4 earthquakes within 100 km of this location; M5.4 and M5.0 earthquakes at distances of 130-160 km occurred in 1984 and 2002.

#### **IV. RECENT EXAMPLES OF EARTHQUAKES ASSOCIATED WITH FLUID INJECTION**

*Dallas-Fort Worth, Texas:* Beginning on 31 October 2008, a series of small earthquakes (largest magnitude M3.0) occurred and were widely felt near in Dallas-Fort Worth (DFW). The NEIC locations were scattered over an area 10-20 km in extent; however analysis of data collected between November 2010 and January 2010 by a temporary network deployed by scientists at Southern Methodist

University (SMU) indicated all the activity originated at a depth of about 4.5 km from a SW-NE-trending linear region on the Dallas-Fort Worth airport property having a dimension of about a km (Frohlich et al., 2010; 2011; see Figure 6). This trend of activity approximately coincides with a fault mapped by Ewing (1990). In the DFW area there was no previous historical seismicity known prior to these events.

The DFW activity was situated less than a km from a 4.2 km-deep SWD well operated to dispose of hydrofrac fluids produced at nearby production wells. Injection volumes at the well were about 10,000 barrels/day (BWPD), and injection had begun only in September 2008, six weeks before the seismic activity commenced.

A second series of felt earthquakes occurred in May 2009 (largest magnitude M3.3). Although injection was discontinued at the SWD well in August, 2009, by this time the operator had installed a seismic monitoring system. They have since reported occasional small unfelt earthquakes continued into 2010 along the trend of the 2008 activity (Keller, 2010).

*Cleburne, Texas:* In June 2009 several small locally felt earthquakes (largest magnitude M2.8) occurred near Cleburne, Texas, 65 km south of the DFW activity. This activity has continued, with felt events being occasionally reported in 2010 and 2011. Here also SMU scientists installed a temporary network; preliminary locations indicated that the Cleburne activity occurred along a N-S trending linear region with length about 2 km; preliminary focal depths were mostly between about 3-4 km (Howe et al., 2010). There was no previous historical seismicity known near Cleburne prior to these events.

There were two active injection wells within about a km of the Cleburne earthquakes. At one, injection with rates of ~10,000-20,000 BWPD had been ongoing since September 2005; injection ceased in September 2009. Injection at the other well began in August 2008 and has continued, but rates have mostly been less than 3000 BWPD.

*Braxton County, West Virginia:* Since April 2010, news reports indicate that a series of small earthquakes (largest M3.4) occurred near Frametown, Braxton County, West Virginia; seven of these were large enough to be located by the NEIC. The West Virginia Department of Environmental Protection permitted a well near Frametown to dispose of hydrofrac fluids produced by wells in the Marcellus Shale. The news reports indicate that the operator has disposed of about 240,000 barrels of drilling fluid at the well since 2009.

I am unaware of any previous historical earthquakes near Frametown. However, a M3.5 natural earthquake occurred at a distance of about 100 km in 1991, and the August 2011 Mineral, VA M5.8 earthquake was about 250 km distant.



*Guy-Greenbrier, Arkansas:* Between October 2010 and March 2011 about 200 earthquakes locatable by a local network occurred at depths of 3-7 km along a 15-km long SW-NE linear trend between Guy and Greenbrier, AK (Horton, 2012). Several of these had magnitudes of M3.7-M4.0; then on 27 February 2011 an M4.6 earthquake occurred.

The trend of this activity lay within about three km of a 3.34 km-deep well where injection had been ongoing since August 2010. There are also several other injection wells in the area, including at least two that may have caused small triggered earthquakes as early as 2009. Following the February 2011 earthquake the Arkansas Oil and Gas Commission ordered a moratorium on injection at these wells.

There is a well-established record of natural seismicity in this region. Two intense swarms of earthquakes, each including M4.6 events, occurred in 1982 and 2002 near Enola, AK, 15 km southeast of the Guy-Greenbrier activity. Maps available from the Arkansas Geological Survey indicate several faults within 10 km of the recent earthquakes, including three prominent enough to be named, the Morrilton Fault, the Enders Fault, and the Heber Springs Fault.

*Snyder, Texas:* On 11 September 2011 an M4.4 earthquake occurred north of Snyder, TX. This was the second-largest in a series of earthquakes near Snyder associated with the Cogdell Oil Field, which has been undergoing salt water injection for secondary recovery since 1956 (Davis and Pennington, 1989). Earthquakes large enough to be located by the USGS and other organizations have been occurring near Snyder since 1974; the largest event had magnitude M4.6 and occurred on 16 June 1978. Analysis of surface waves indicated this earthquake had a depth of about 3 km (Voss and Herman, 1981).

The Cogdell Field has undergone waterflooding for decades. The field has dimensions of ~5 km X 20 km, with injection wells spaced at intervals of ~0.5 km. Davis and Pennington (1989) present data showing that between 1963 and 1983 injection at rates of  $2\text{--}8 \times 10^6 \text{ m}^3/\text{yr}$  proceeded in the field, with injection at wells near the field's boundaries progressively moving inward to drive oil towards the center. Since no earthquakes were known near Snyder prior to 1974, because of the massive scale of the waterflooding operation there, and because of modeling indicating that the earthquakes occurred in locations where fluid pressure gradients were high, Davis and Pennington (1989) concluded that the Snyder earthquakes were triggered by the waterflood operations.

I am unaware of any detailed analysis of Snyder earthquakes since 1989. However, the Cogdell Field is still active and it is likely that more recent events including the 2011 earthquake are triggered by injection or production activities.

*Sparks, Oklahoma:* On 6 November 2011 an M5.6 earthquake occurred near Sparks, OK, a small town in Lincoln County. Reports indicate there are more than 100 active injection wells in Lincoln County; however, on 9 April 1952 there was a highly

similar natural earthquake with magnitudes various reported between M5.5 and M5.9 and with an epicenter 95 km west of 2011 epicenter (Miller, 1956; Frohlich and Davis, 2002). Until further analysis is published, either a natural or triggered origin is possible.

*Youngstown, Ohio:* Between March and December 2011, a series of small felt earthquakes occurred near Youngstown, OH, (largest: M4.0 31 December 2011) with epicenters about one km from a well where injection had been ongoing since 2010. The timing and location of activity suggest injection triggering. Larger, natural earthquakes have occurred in northeastern Ohio within 100 km of the Youngstown activity; these include an M4.5-4.7 earthquake that occurred about 65 km to the west on 9 March 1943 (Nicholson et al., 1988). There was also an M5.0 earthquake that occurred on 31 January 1986; however, this epicenter lay about 12 km from high-volume waste-disposal injection wells. Nicholson and Wesson (1988) note that the 1986 earthquake may be triggered, but also state that it may be natural since the region has experienced moderately frequent natural earthquakes at least since 1823.

## V. COMPILATION

My compilation of reports of possibly injection-triggered earthquakes (Table 1 and Figure 7) includes recently-occurring examples described in the previous two sections, recently-reported examples related to geothermal projects, and all examples I could find in the literature where the possibly-injection-triggered earthquake had a reported magnitude of 4.0 or greater. Nicholson and Wesson (1990) and Suckale (2009) list other examples.

Other than the M4.6 1978 Snyder, TX, earthquake, all of the possibly-injection-triggered earthquakes in Table 1 having magnitudes of 4.0 or greater occur in environments where similarly large or larger natural earthquakes also occur within 100 km:

- M5.6 – 2011 Sparks, OK: The M5.5-5.9 April 1952 El Reno earthquake occurred about 90 km from the 2011 epicenter.
- M5.3 – 1967 Denver Rocky Mountain Arsenal, CO: Regional natural earthquakes occur nearby and an earthquake with estimated magnitude M6.6 occurred in 1882 at about 100 km distance;
- M4.7 – 2011 Guy-Greenbriar, AK: NEIC reports natural earthquakes within 20 km with M4.7 in 1982 and 2002;
- M4.6 – 1982 Geysers, CA: M7 and larger earthquakes occur regularly on nearby San Andreas Fault. NEIC reports several M4.5-M5.0 earthquakes within 100 km.
- M4.4 – 2003 Berlin, El Salvador: This project is near a volcano in a subduction-zone environment in a small country with a history of damaging earthquakes (e.g., M7.5 in 1986).
- M4.3 – Paradise Valley, CO: Here natural earthquakes occurred within 20 km of the site prior to the initiation of injection; in 1994 an M4.6 occurred at a distance of 80 km. Several earthquakes larger than M5.0 have occurred within 100-150 km (Ake et al., 2005).

- M4.0 – Permian Basin, TX: The 1992 M5.0 Rattlesnake Canyon natural earthquake (Sanford et al., 1993) occurred within the Permian Basin.
- M4.0 – 2011 Youngstown, OH: A 1943 M4.5-4.7 earthquake occurred at about 65 km distance (Nicholson et al., 1988).

A second way to categorize injection projects concerns the number of injector wells and project's objective. Most waste-disposal operations utilize a single well and usually strive to avoid injecting too close to mapped faults since wastes reaching a fault might travel upward and contaminate groundwater. Many waste-disposal wells are used only sporadically or are in operation for only a few years. In contrast, geothermal operations often utilize several wells situated a few km apart, injecting fluids into some and extracting hot water or steam from others. Successful geothermal operations may operate indefinitely; the Geysers geothermal field in California has been in operation for about 50 years. And secondary recovery operations may involve numerous wells on a grid spacing of a km or less, injecting enormous amounts of fluid during a several-year period when a field is being produced.

For example, the 1978 M4.6 and 2011 M4.4 Snyder, TX, earthquakes are perfect examples. At the Cogdell Field where they occurred, there was injection into more than 100 wells, spaced at half-km intervals and extending over an area with dimensions ~5 km X 20 km, lasting for decades, with volumes of several million barrels of water per month, pumped with the express intent of creating significant overpressures for extended periods over extensive regions. Although the Snyder earthquakes apparently are triggered by fluid injection and do occur in a region that had been previously virtually aseismic, the physical changes induced in the subsurface by these massive waterflooding operations dwarf those caused by ordinary waste disposal operations.

Although geothermal operations usually involve multiple injecting wells and may be active for decades, none have yet triggered an earthquake with magnitude exceeding M4.6 (Figure 7). Both examples where the triggered earthquake had a magnitude exceeding M4.0 (Geysers, CA; and Berlin, El Salvador) occurred near plate boundaries in environments where large natural earthquakes are common.

In contrast, several reportedly triggered earthquakes occur near single-well injectors in a tectonic environment where regional seismicity is absent or of small magnitude:

- Triggered M3.3 - Dallas-Fort Worth, TX: largest natural earthquake within 100-130 km have M3.3 or 3.4;
- Triggered M2.8 – Cleburne, TX: largest nearby natural earthquake is M3.4 at 140 km distance;
- Triggered M3.4 – Braxton County, WV: largest natural earthquake within 100 km is M3.5.

Note that all of these examples have magnitudes of M3.5 and smaller.

## VI. DISCUSSION

An important conclusion of this study is that there are several different categories of induced or triggered seismicity. The research available at present research suggests that each category has distinct properties.

*Extraction-triggered earthquakes:* One category is earthquakes apparently triggered by fluid extraction. Events assigned to this category include most of the largest-magnitude earthquakes in central and east Texas, such as the M4.7 Gladewater earthquake of 1957 and the M4.8 Fashing earthquake of 2011. It is noteworthy that fluid extraction-triggered earthquakes generally occur in fields where field development has been ongoing for a decade or more before seismicity is reported, and production has occurred on massive scales. For example, for the Stratton Field where earthquakes occurred in 1997 and 2010, Frohlich et al. (2012) calculated that the oil and gas extracted over the history of production was equivalent to a layer of oil 16 cm thick and a layer of liquefied natural gas 1 m thick, covering the entire area of the field.

No known extraction-triggered earthquakes have occurred historically within the Barnett Shale. And the way that unconventional gas development affects the subsurface is highly unlike what occurs in conventional oil and gas field. Waste disposal operations tend to be localized at isolated, geographically well-distributed wells. While is conceivable that long-term and large-scale effects could eventually afflict waste disposal operations there is no evidence for this at present.

*Hydrofracturing-triggered earthquakes:* Currently there is no evidence that hydrofracturing causes earthquakes large enough to pose a hazard. The seismic signals typically generated by hydrofracturing typically have magnitudes of -3.5 to 1.0; the majority of larger triggered earthquakes of concern for hazard analysis are clearly not 'frack jobs that got out of hand'. Indeed, I could find only three instances in the literature (see Section III) where earthquakes caused by hydrofracture had magnitudes exceeding M2, and none of these had magnitudes exceeding M3.5. There have been unconfirmed media reports of earthquakes associated with hydrofracturing elsewhere, such as in the Horn River Basin, British Columbia, Canada. But the reports do not establish whether the activity is associated with hydrofracturing or fluid injection, and they indicate that the earthquakes are M3.5 and smaller. Considering the enormous number of hydrofracturing operations undertaken in recent years, true hydrofrac-caused earthquakes are extraordinarily rare. None have been reported within the Barnett Shale, although thousands of wells have undergone hydrofracturing there (e.g., see Figure 8).

*Fluid-injection triggered earthquakes:* Fluid injection into the subsurface for different purposes takes place on different scales, and the empirical evidence suggests that these affect subsurface stress dynamics differently. For example, the 1978 Snyder, TX, M4.6 earthquake was associated with a massive waterflooding project involving injection for more than 20 years at more than 100 injection wells,

a situation highly unlike the injection related to the disposal of hydrofracture fluids in SWD wells. And geothermal operations may continue for decades and typically involve pumping and extracting fluids from several wells.

Earthquakes triggered by waste-disposal operations are of most concern in the Barnett Shale. At least two earthquake sequences near waste disposal wells, in Dallas-Fort Worth (Frohlich et al., 2010; 2011) and Cleburne (Howe et al., 2011), have occurred which received considerable media attention. And my preliminary analysis of publically available data indicates that small earthquakes (M2-M3), not reported by the NEIC, have occurred near at least a half-dozen other injection wells (e.g., Figure 9). However, it is worth noting that all the injection-triggered earthquakes within the Barnett Shale have been small (M3.3 or less), and that there is no seismic activity detected near the vast majority of injection wells (Figures 8 and 9).

*Current research, and possible mitigation strategies:* Why triggered earthquakes occur in some environments and not others is poorly understood, and scientific progress on this question is undergoing rapid change (e.g., see Frohlich and Potter, 2012). Earthquake researchers only established that fluid injection could induce earthquakes in the 1960's. For obvious reasons, much of the published research describes analysis of post-earthquake data following those exceptional events large enough to be noticed by the public. With a few exceptions (e.g. Paradise Valley, CO; Ake et al., 2005), most of the literature describes situations where local monitoring networks were only set up after the earthquake occurred. The current literature hasn't adequately addressed the question of how large a yet-to-occur triggered earthquake might be.

Nevertheless, three relevant trends are evident from the compilation (Figure 7 and Table 1):

- The largest apparently injection-triggered earthquake from any cause in any tectonic environment had magnitude M5.3 (Denver, CO, 1967). The M5.6 2011 Oklahoma earthquake is slightly larger, but at this writing there is insufficient information to characterize it as either natural or triggered.
- With the exception of M<3 triggered earthquakes in environments where no natural nearby seismicity occurs, all but two of the possibly injection-triggered earthquakes are no larger than the largest natural earthquake occurring within 100 km. The remaining exceptions, such as the 1978 Snyder, TX, M4.6 earthquake and (possibly) the 2011 Fanning, TX, M4.8 earthquake, occurred in environments highly dissimilar to waste disposal operations.
- In environments where no natural earthquakes have M>3.5 and where injection is to dispose of wastes, the largest triggered earthquakes have M<3.5.

The observation that injection-triggered earthquakes tend to be no larger than nearby regional natural earthquakes is mechanically plausible. Surveys of crustal

stress and observations from deep boreholes at several locations worldwide indicate:

- (1) stress in continental interiors is fairly uniform within regional provinces having dimensions of hundreds of km (Zoback and Zoback, 1980);
- (2) the brittle crust is in a state of failure equilibrium (Zoback and Townend, 2001); with
- (3) the stress levels being controlled by networks of pervasive naturally-occurring faults, where failure, enhanced by fluid flow, occurs according to Coulomb frictional failure theory along optimally oriented, critically stressed faults (Barton et al., 1995).

Thus any change to the stress field—e.g., induced naturally by erosion, deposition or lithospheric cooling, or alternatively by manmade activities such as reservoir impoundment or fluid extraction—can potentially increase the stress locally and induce failure along favorably oriented faults. Moreover, if there is fluid injection ongoing, this may also act to induce failure if the fluid reaches a favorably oriented fault and reduces the normal stress, decreasing fault strength. But the maximum size of natural and triggered earthquakes is controlled by regional stress level and the properties (sizes, orientations) of regionally occurring faults, not by particular properties of the injection process.

There is some evidence emerging for the hypothesis that nearby suitably-oriented subsurface faults are responsible for injection-triggered earthquakes. For example, the 2008-2009 Dallas-Fort Worth earthquakes occurred within one kilometer or less of a SW-NE trending fault, and this trend direction favors normal fault motion in response to the known regional stress pattern (Frohlich et al., 2010; 2011). Similarly, the literature describes the presence of faults near epicenters of the 2011 Guy-Greenbriar, AK, earthquakes (Horton, 2012), the 2011 Fylde Coast (Blackpool), UK, earthquakes (de Pater and Baisch, 2011), and the Garvin, OK, earthquakes (Holland, 2011). Thus it is plausible that the absence of nearby faults, or the absence of suitably-oriented nearby faults, may explain why earthquakes occur near some injection wells in Figures 8 and 9, and not near others.

For injection well operators, the compiled data (Table 1 and Figure 7) suggest that a viable strategy for avoiding inducing earthquakes is to limit disposal operations to wells in regions where the historical record indicates nearby natural earthquakes are acceptably small. Moreover, if the arguments in the previous two paragraphs are correct, injection wells are unlikely to induce earthquakes if wells are situated far enough from subsurface faults so that injected fluids cannot reach the faults.

## REFERENCES

- Ake, J., K. Mahrer, D. O'Connell, and L. Block, 2005, Deep-injection and closely monitored induced seismicity at Paradox Valley, Colorado: *Bulletin of the Seismological Society of America*, **95**, 664-683, doi:10.1785/0120040072.
- Barton, C. A., M. D. Zoback, and D. Moos, 1995, Fluid flow along potentially active faults in crystalline rock: *Geology*, **23**, 683-686
- Carder, D.S., 1945, Seismic investigations in the Boulder Dam area, 1940–1944, and the influence of reservoir loading on earthquake activity: *Bulletin of the Seismological Society of America*, **35**, 175–192.
- Davis, S. D., and W. D. Pennington, 1989, Induced seismic deformation in the Cogdell oil field of West Texas: *Bulletin of the Seismological Society of America*, **79**, 1477-1495.
- Davis, S. D., P. Nyffenegger and C. Frohlich, 1995, The 9 April 1993 earthquake in south-central Texas: Was it induced by fluid withdrawal?: *Bulletin of the Seismological Society of America*, **85**, 1888-1895.
- de Pater, C. J and S. Baisch, 2011, *Geomechanical Study of Bowland Shale, Synthesis Report*: Cuadrilla Resources, LTD..
- Doser, D. I., M. R. Baker, M. Luo, P. Marroquin, L. Ballesteros, J. Kingwell, H. L. Diaz, and G. Kalp, 1992, The not so simple relationship between seismicity and oil production in the Permian Basin, West Texas: *Pure and Applied Geophysics*, **139**, 481-506.
- Ewing, T., 1990, *Tectonic Map of Texas*: University of Texas Bureau of Economic Geology.
- Frohlich, C. and S. D. Davis, 2002, *Texas Earthquakes*: University of Texas Press, Austin, Texas, 275 pp.
- Frohlich, C., E. Potter, C. Hayward, and B. Stump, 2010, Dallas-Fort Worth earthquakes coincident with activity associated with natural gas production: *The Leading Edge*, **29**, 270-275, doi:10.1190/1.3353720.
- Frohlich, C., C. Hayward, B. Stump, and E. Potter, 2011, The Dallas-Fort Worth earthquake sequence: October 2008 through May 2009: *Bulletin of the Seismological Society of America*, **101**, doi:10.1785/0120100131.
- Frohlich, C., 2012 (submitted), Categories of induced earthquakes and relationship to natural regional seismicity: *Geophysics*.
- Frohlich, C., J. Glidewell, and M. Brunt, 2012 (in press), Location and felt reports for the 25 April 2010 mbLG3.9 earthquake near Alice, Texas: Was it induced by petroleum production?: *Bulletin of the Seismological Society of America*, **102**, doi:10.1785/0120110179.
- Frohlich, C. and E. Potter, 2012 (in press), What further research could teach us about 'close encounters of the third kind': Intraplate earthquakes associated with fluid injection: *Hedberg Conference Memoir Volume, Critical Assessment*

- of Shale Resource Plays*, AAPG/SEG/SPE/SPWLA Hedberg Conference, , Dec. 5-10, 2010, Austin, TX.
- Galloway, W. E., T. E. Ewing, C. M. Garrett, N. Tyler and D. G. Bebout, 1983, *Atlas of Major Texas Oil Reservoirs*: University of Texas Bureau of Economic Geology, Austin, TX.
- Gibowicz, S. J., 1991, Seismicity induced by mining: *Advances in Geophysics*, **32**, 1-74.
- Gibowicz, S. J., 2001, Seismicity induced by mining: Ten years later: *Advances in Geophysics*, **44**, 39-181.
- Gibowicz, S. J., 2009, Seismicity induced by mining: Recent research: *Advances in Geophysics*, **51**, 1-53.
- Gupta, H. K., 1992, *Reservoir-Induced Earthquakes*: Elsevier.
- Gupta, H. K., 2002, A review of recent studies of triggered earthquakes by artificial water reservoirs with special emphasis on earthquakes in Koyna, India: *Earth Science Reviews*, **58**, 279-310.
- Holland, A., 2011, *Examination of Possibly-induced Seismicity from Hydraulic Fracturing in the Eola Field, Garvin County, Oklahoma*: Open File Rept. OF1-2011, Oklahoma Geol. Survey, 28 pp.
- Horton, S., 2012, Disposal of hydrofracking waste fluid by injection into subsurface aquifers triggers earthquake swarm in central Arkansas with potential for damaging earthquake: *Seismological Research Letters*, **83** (in press).
- Howe, A. M., C. T. Hayward, B. W. Stump, and C. Frohlich, 2010, Analysis of recent earthquakes in Cleburne, Texas: *Seismological Research Letters*, **81**, 379.
- Hsieh, P. A., and J. S. Bredehoeft, 1981, A reservoir analysis of the Denver earthquakes—A case study of induced seismicity: *Journal of Geophysical Research*, **86**, 903-920.
- Kanamori, H. and E. Hauksson, 1992, A slow earthquake in the Santa Maria Basin, California: *Bulletin of the Seismological Society of America*, **82**, 2087-2096, 1992.
- Keller, W. K., 2010, Operator evaluation of the impact of fluid injection into shale reservoirs: *Abstracts: AAPG/SEG/SPE/SPWLA Hedberg Conference, Critical Assessment of Shale Resource Plays*, Dec. 5-10, 2010, Austin, TX.
- Kosters, E. C., D. G. Bebout, S. J. Seni, C. M. Garrett, L. F. Brown, H. S. Hamlin, S. P. Dutton, S. C. Ruppel, R. J. Finley, and N. Tyler, 1989, *Atlas of Major Texas Gas Reservoirs*: University of Texas Bureau of Economic Geology, Austin, TX.
- Levey, R. A., R. J. Finley and M. A. Sippel, 1994, Quantifying secondary gas resources in fluvial/deltaic reservoirs: A case history from Stratton Field, South Texas: *Report of Investigations No. 221*, Bureau of Economic Geology, Univ. Texas. Austin, 38 pp.



- Majer, E. L., R. Baria, M. Stark, S. Oates, J. Bommer, B. Smith, and H. Asanuma, 2007, Induced seismicity associated with Enhanced Geothermal Systems: *Geothermics*, **36**, 185-222, doi:10.1016/j.geothermics.2007.03.003.
- Miller, H., 1956, The Oklahoma earthquake of 9 April 1952: *Bulletin of the Seismological Society of America*, **46**, 269-279.
- Nicholson, C., E. Roeloffs and R. L. Wesson, 1988, The northeastern Ohio earthquake of 31 January 1986: Was it induced?: *Bulletin of the Seismological Society of America*, **78**, 188-217.
- Nicholson, C. and R. L. Wesson, 1990, *Earthquake hazard associated with deep well injection: A report to the U.S. Environmental Protection Agency*: U.S. Geological Survey Bulletin 1951, 74 pp.
- Pennington, W. D., S. D. Davis, S. M. Carlson, J. DuPree, and T. E. Ewing, 1986, The evolution of seismic barriers and asperities caused by the depressuring of fault planes in oil and gas fields of south Texas: *Bulletin of the Seismological Society of America*, **76**, 939-948.
- Pollastro, R. M., D. M. Jarvie, R. J. Hill and C. W. Adams, 2007, Geologic framework of the Mississippian Barnett Shale, Barnett-Paleozoic total petroleum system, Bend arch-Fort Worth Basin, Texas: *AAPG Bulletin*, **91**, 405-436, doi:10.1306/103000606008.
- Sanford, A., R. Balch, L. Jaksha, and S. Delap, 1993, *Location and fault mechanism of the 2 January 1992 Rattlesnake Canyon earthquake in southeastern New Mexico*: Open-file Rept. 70, Geophysical Research Center and Geoscience Dept., New Mexico Institute of Mining and Technology, 10 pp.
- Segall, P., 1989, Earthquakes triggered by fluid extraction: *Geology*, **17**, 942-946.
- Sellards, 1933, The Wortham-Mexia, Texas earthquake: *Contributions to Geology, University of Texas Bulletin 3201*, 105-112.
- Shapiro, S. A. and C. Dinski, 2009, Scaling of seismicity induced by nonlinear fluid-rock interaction: *Journal of Geophysical Research*, **114**, B09307, doi:10.1029/2008JB006145.
- Suckale, J., 2009, Induced seismicity in hydrocarbon fields, *Advances in Geophysics*, **51**, 55-106, doi:10.1016/S0065-2687(09)05107-3.
- Suckale, J., 2010, Moderate-to-large seismicity induced by hydrocarbon production: *The Leading Edge*, **29**, 310-319.
- Voss, J. A. and R. B. Hermann, 1981, A surface wave study of the June 16, 1978 Texas earthquake, *Earthquake Notes*, **51**, 3-14.
- Zoback, M. D. and J. Townend, 2001, Implications of hydrostatic pore pressure and high crustal strength for the deformation of intraplate lithosphere: *Tectonophysics*, **336**, 19-30.

Table 1. Recent and higher-magnitude reports of possibly injection-triggered seismicity. The table strives to be inclusive for locations reported since 2007 and for locations where largest-magnitude triggered earthquake was M4.0 or greater. Nicholson and Wesson (1990), Suckale (2009) and Figure 7 (this report) show additional locations where largest-magnitude triggered earthquakes were smaller than M4.0. Table is arranged in order of increasing size of reportedly triggered earthquakes.

<i>location and reference</i>	<i>category</i>	<i>injection properties duration, depth</i>	<i>earthquakes</i>	<i>regional natural earthquakes properties</i>	<i>notes</i>
Fylde Coast, Great Britain (de Pater and Baisch, 2011)	hydrofracturing	5 stages Mar-May 2011; depth 2.5-2.9 km	M2.3 in April 2011, 2 km from well	NEIC reports several M3-M4 quakes within 100 km; 1984 M5.4 and 2002 M5.0 quakes at 130-160 km	"Britain's only shale-gas project"
Cleburne, TX (Howe et al., 2010)	single-well injection; waste disposal	Sep 2005; some injection ongoing; depth 3.5 km	Quakes first felt June 2009, largest M2.8 within 2 km of well	local natural earthquakes rare or unknown	1997 M3.4 Commerce TX quake at 140 km distance
Garvin, OK (Holland, 2011)	hydrofracturing	17-23 Jan 2011; depth 2.2-3.3 km	About 40 quakes located 1-4 km from well; largest M2.8	NEIC reports 1997 M4.5 at 90 km; 1994 M4.2 at 30 km	
Soultz-sous-Forêts, France (Majer et al., 2007)	multi-well injection; ~9 wells; geothermal	late 1990's; depth 5 km	largest M2.9, June 2003	NEIC reports seven >M4.5 quakes within 120 km, including M5.9 in 1978	
Dallas-Fort Worth, TX (Frohlich et al., 2010; 2011)	single-well injection; waste disposal	Sep 2008- Aug 2009; 4.2 km well	quakes began Oct 2008; largest M3.3, within 1 km of well; continue into 2010 after injection stops	local natural earthquakes rare or unknown	NEIC reports 1985 M3.3 quake at 75 km distance; M4.0-4.5 OK quakes at 200-250 km distance
Braxton County, West Virginia (news reports; NEIC)	single-well injection; waste disposal	began Spring 2009	M3.4 in April 2010	largest NEIC-reported earthquake within 100 km was M3.5 in 1991	~250 km from M5.8 August 2011 Mineral, VA quake
Basel, Switzerland (Majer et al., 2007)	single-well injection?; geothermal	began 2 Dec 2006; depth 5 km	largest M3.4, 8 Dec 2006; near injection well	NEIC reports 2004 M4.8 within 100 km; numerous quakes with M>4	M6.5 damaged Basel in 1356; 2006 quake shut down geothermal project
Cooper Basin, Australia (Majer et al., 2007)	single-well injection; geothermal	began 2003; 4.4 km depth	largest M3.7 Dec 2003; most seismicity within 1 km of well	NEIC reports M3.6 at ~50 km distance in 1989	

<i>location and reference</i>	<i>injection properties</i>		<i>regional natural earthquakes</i>		
	<i>category</i>	<i>duration, depth</i>	<i>earthquakes</i>	<i>properties</i>	<i>notes</i>
Permian Basin, TX and NM (Doser et al., 1992; Nicholson and Wesson, 1990)	secondary recovery; multi-well; many different fields	began 1959 and subsequently; depths 0.74-3.66 km	quakes began March 2011; largest ~M4.0	largest natural quake in Permian Basin is M5.0 1992 Rattlesnake Canyon event	
Youngstown , OH (news reports)	single-well injection: waste disposal	began early 2011	largest M4.0 31 Dec 2011, ~1 km from well	natural M4.6 at 65 km in 1943	
Paradise Valley, western CO (Ake et al., 2005)	single-well injection; waste disposal	1996 – 2005...; 4.3-4.8 km well	thousands of quakes recorded by local network; largest M4.3 May 2000 about 3 km from injector	natural quakes within 20 km of well recorded by local network prior to injection; 1994 M4.6 at 80 km distance	four quakes with M>5 have occurred since 1970 within 150-300 km of well
Berlin, El Salvador (Majer et al., 2007)	multi-well injection; geothermal	1990's – present?; 8 wells 2003	M4.4 2003, 3 km from injection well	high-seismicity region; M7.7 2001 El Salvador earthquake	volcano nearby
Snyder, TX , Cogdell field (Davis and Pennington, 1989)	secondary recovery; injection at more than 100 wells on half-km spacing	began 1956- active to 1983; depth 2.1 km	largest M4.6 1978; quakes 1974-1982	local natural earthquakes rare or unknown	Nearest M5 natural quakes are 1992 Rattlesnake Canyon, and 1925, 1936 in Texas Panhandle
Geysers, CA (Majer et al., 2007)	multi-well injection; geothermal	~1960 –present; injection now at 9 wells separated by only a few km; Aug 2010 – Mar 2011; depth 3.5 km at well #5.	largest M4.6 1982; 2 or 3 M4.0 or greater each decade	NEIC reports several M4.5-M5.0 within 100 km of field	about 150 km from San Francisco; closer to San Andreas Fault
Guy-Greenbriar, AK (Horton, 2012)	single-well injection; waste disposal; several wells in 10-km area	Aug 2010 – Mar 2011; depth 3.5 km at well #5.	largest M4.7 Feb 2011; numerous smaller events	natural quakes within 20 km of well recorded by local network prior to injection	NEIC reports natural M4.7 quakes in 1982 and 2001 within 25 km of well
Denver, Rocky Mountain Arsenal, CO (Hsieh and Bredehoeft, 1981)	single-well injection; waste disposal	Mar 1962- Feb 1966; 3.67 km well	quakes began Apr 1962; several with M~5; largest M5.3 Aug 1967, several km from injector	natural M6.6 in Nov 1882 about 100 km N of Denver	quakes with M>5 have occurred since 1970 about 300 km from Denver to S, W, and N
Sparks, OK (news reports)	single-well injection; waste disposal	Many disposal wells in county where quake occurred	Largest M5.6 on 6 Nov 2011	natural M5.5-5.9 in 1952 about 90 km W of epicenter	very recent quake; limited information available

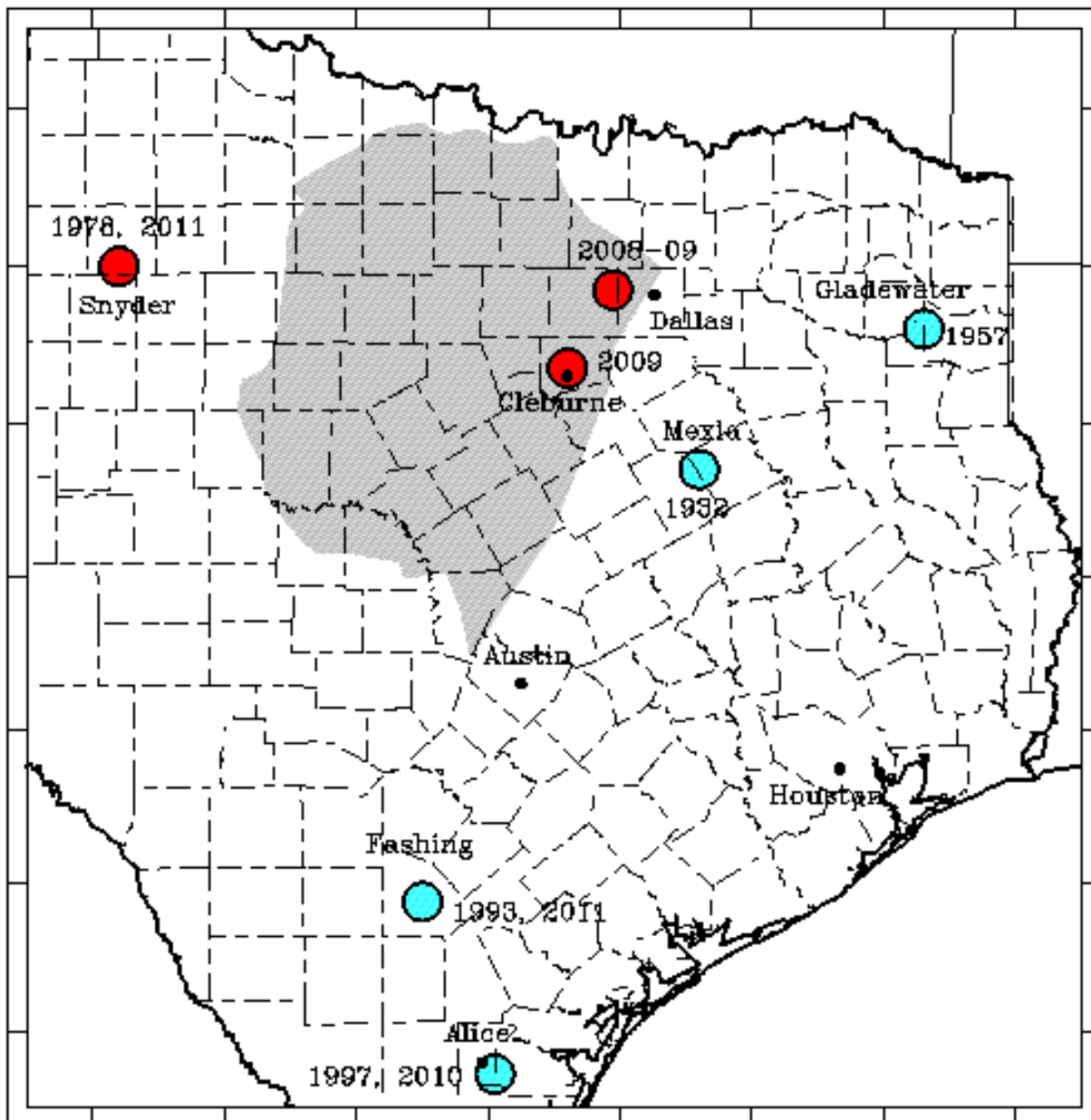


Figure 1. Map of eastern Texas showing earthquakes discussed this report. Red circles indicate earthquakes induced/triggered by injection; blue circles are earthquakes occurring in or near oil and gas fields and apparently triggered by production/extraction. Shaded area is the subsurface extent of the Barnett shale, the focus of increased natural gas production since about 2000. Barnett shale is as mapped by Pollastro et al. (2007).

<i>PROCESS</i>	<i>TRIGGERS EARTHQUAKES?</i>		
	<i>Never</i>	<i><u>very</u> rarely</i>	<i>sometimes</i>
• <u>drilling</u> wells	XXX		
• <u>fracking</u> wells		XXX	
• <u>extraction</u> of gas & fluids		XXX	
• <u>injection</u> for fluid disposal			XXX

Figure 2. Some human activities do trigger earthquakes, but some activities trigger earthquakes more often than others. Drilling wells never triggers earthquakes, and there are no earthquakes associated with the vast majority of oil and gas fields, injection wells, and hydrofracturing jobs. However, hydrofracturing and injection sometimes trigger earthquakes. Although extraction of gas and oil sometimes trigger earthquakes, at present there are no confirmed examples where this has been associated with unconventional gas development.

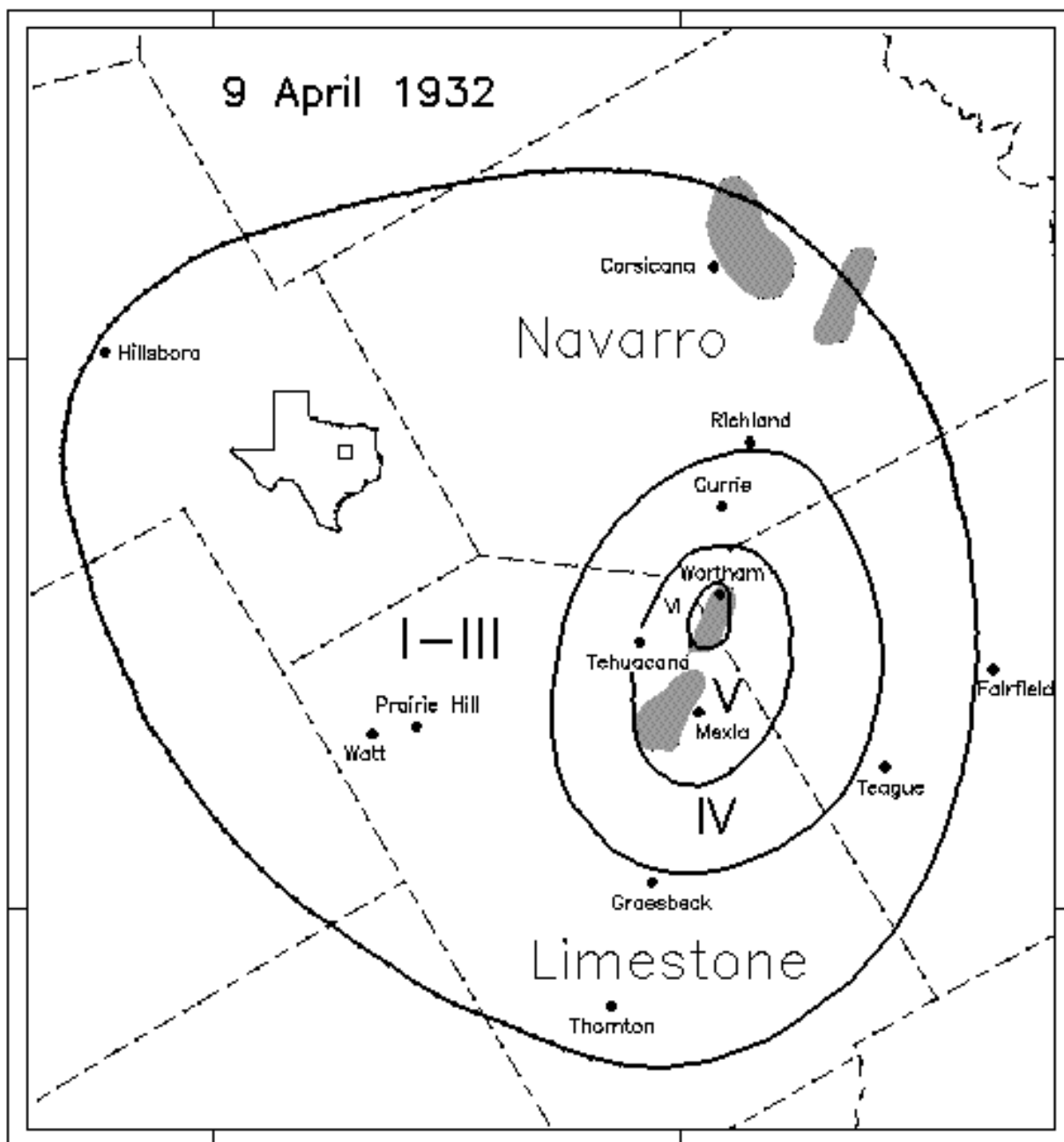


Figure 3. Felt area map for the 9 April 1932 Wortham-Mexia earthquake. Roman numerals denote Modified Mercalli Intensities; dashed lines indicate county boundaries. Shaded regions indicate major oil fields mapped by Galloway and others (1983) that were established prior to 1932. [Figure reproduced from Frohlich and Davis (2006).]

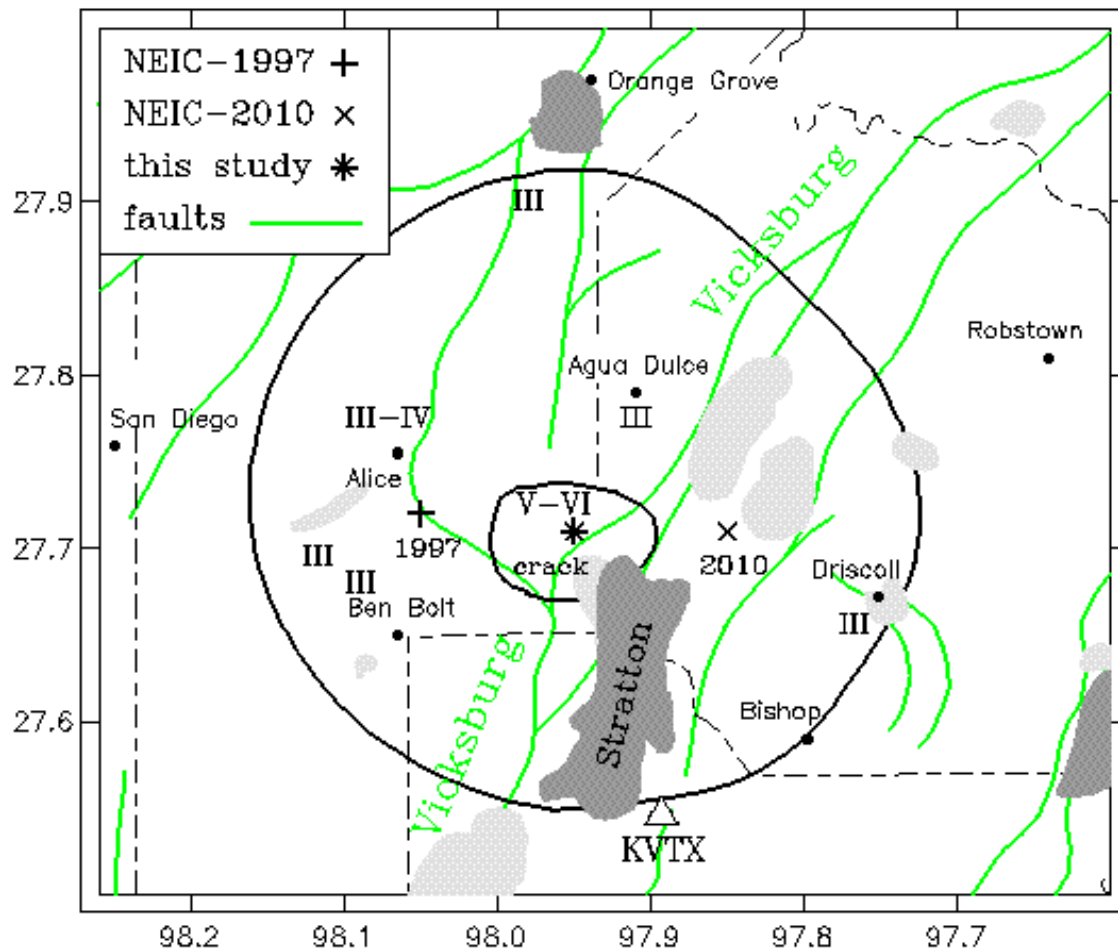


Figure 4. Felt reports for the 25 April 2010 Alice earthquake. Labels of MMI levels “III” and “III-IV” indicate locations where individuals provided felt information. Three individuals within MMI V-VI isoseismal region reported experiencing MMI V or VI during the 2010 earthquake. Location labeled “crack” indicates reported location of mile-long NE-SW crack following 1997 earthquake. The Symbols “+”, “X” and “\*” indicate respectively the epicenters reported by NEIC for the 1997 and 2010 earthquakes, and the location determined by Frohlich et al. (2012). Green lines are mapped faults are from Ewing (1990). [Figure reproduced from Frohlich et al. (2012).]

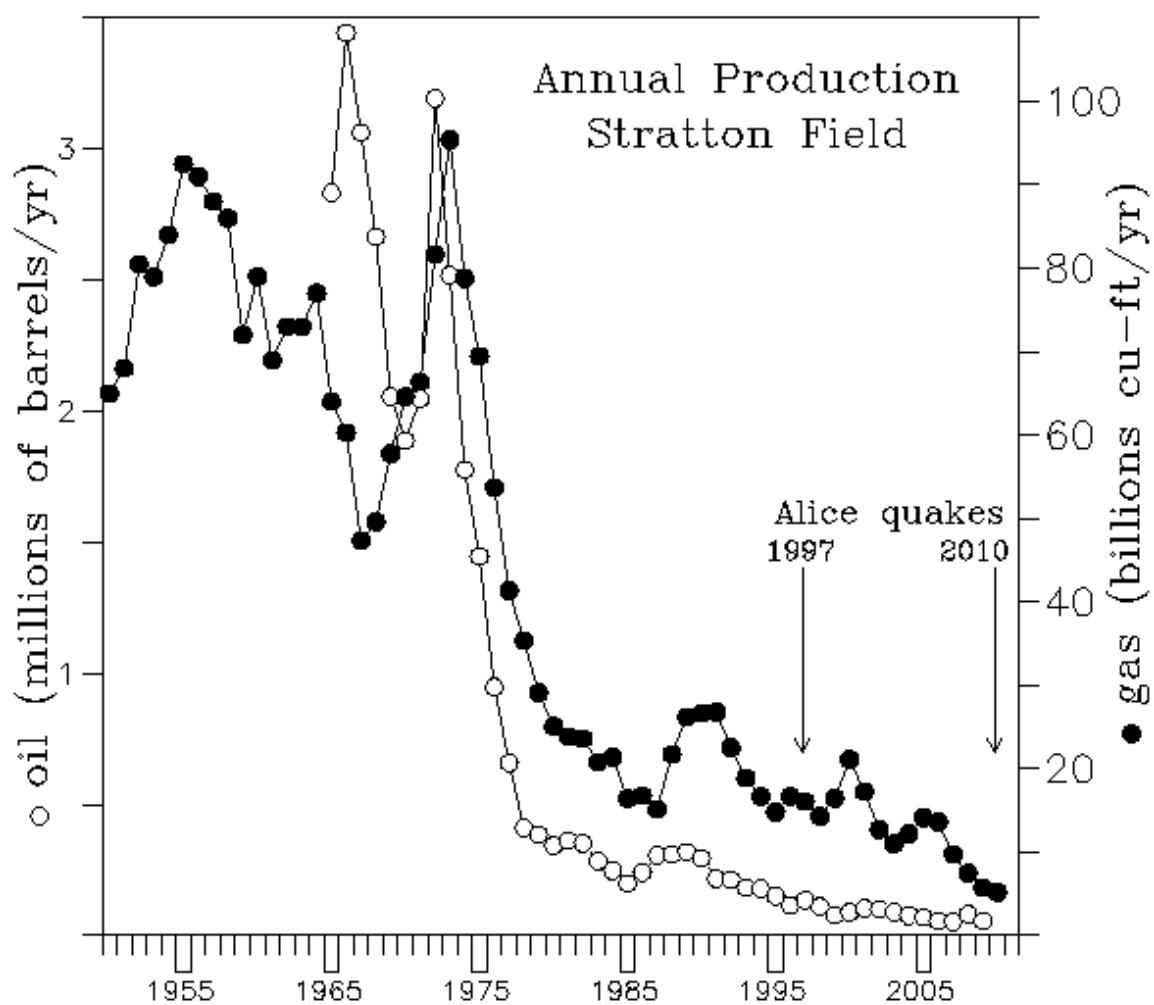


Figure 5. Annual gas and oil production in the Stratton field. Note that both the 1997 and 2010 Alice earthquakes occurred well after the highest production levels were reached in the 1965-1975 period. Data are from Levey et al. (1994) updated with information from the Texas Railroad Commission. [Figure reproduced from Frohlich et al. (2012).]



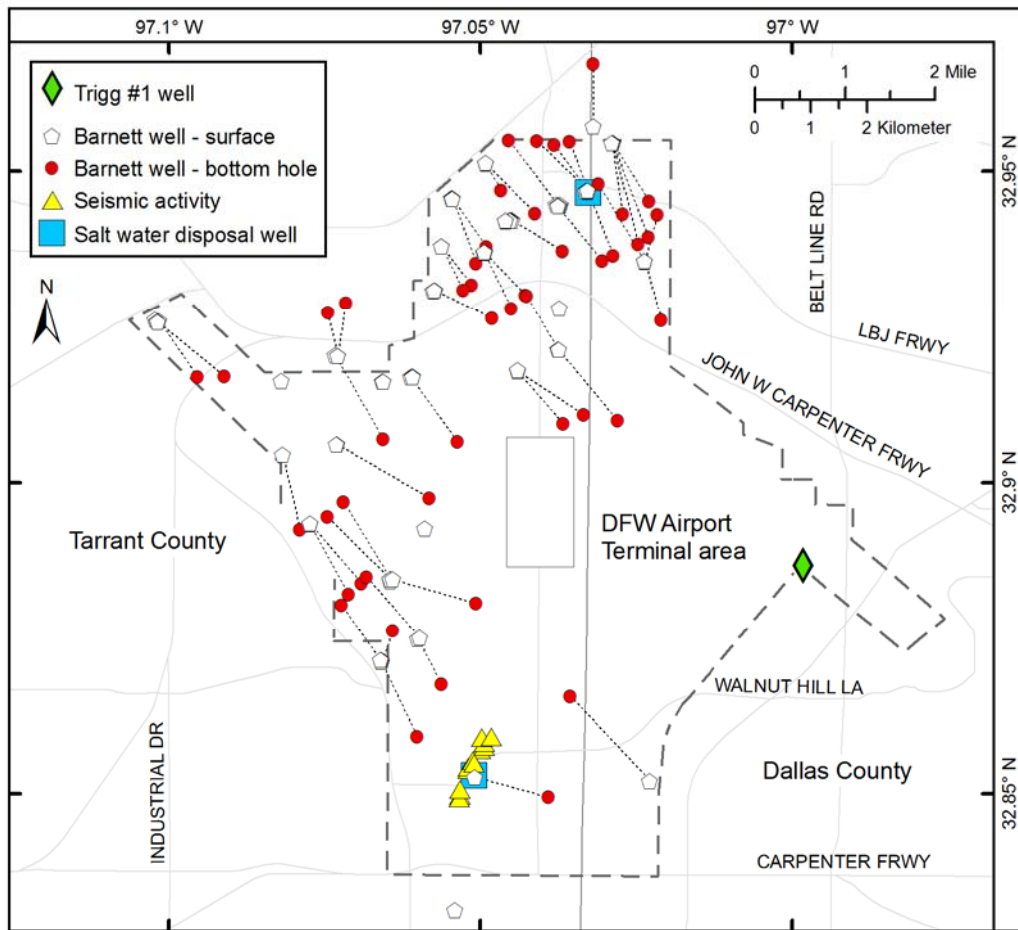


Figure 6. Map of region surrounding DFW airport, showing locations of earthquakes (triangles), producing gas wells (circles and pentagons), and salt water disposal (injection) wells (squares). Dashed line outlines DFW airport property; principal highways are labeled. [Figure reproduced from Frohlich et al. (2011).]

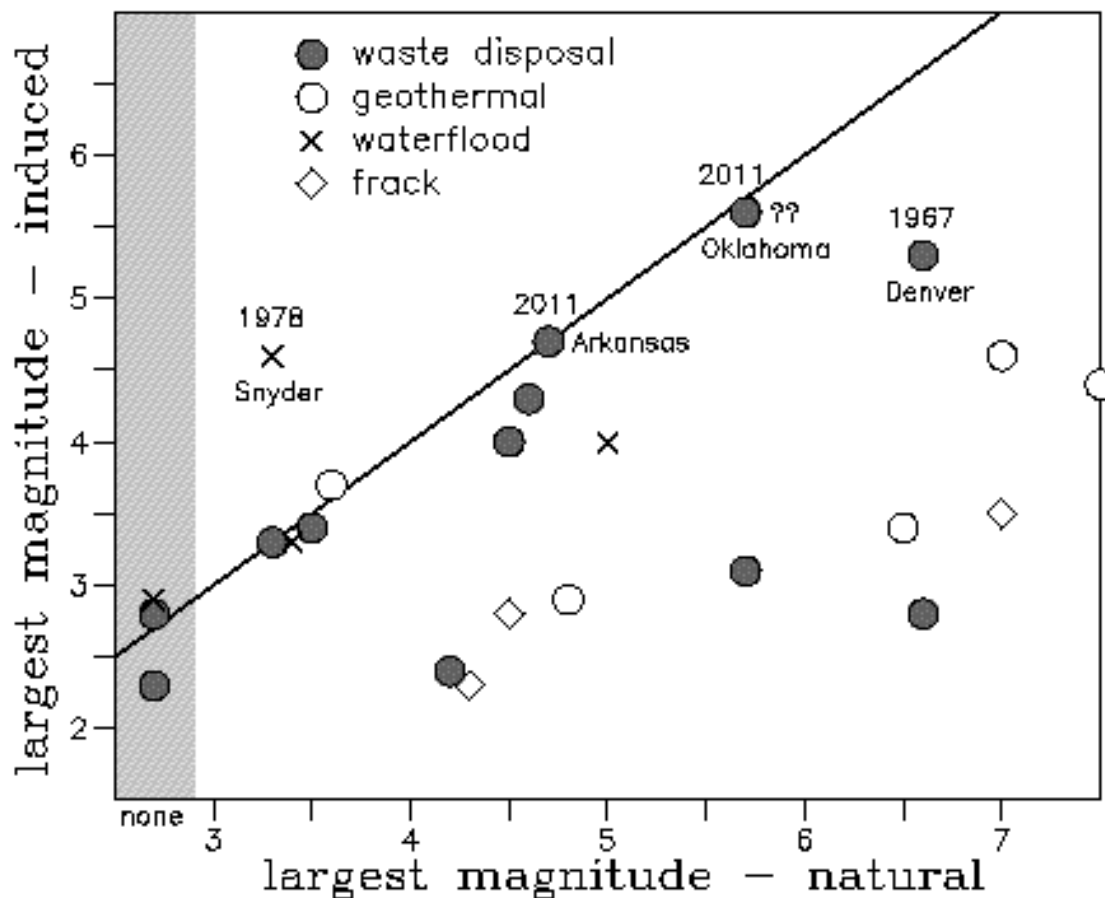


Figure 7. Comparison of largest magnitudes for possibly injection-triggered earthquakes and natural earthquakes occurring within 100 km of injection site; line indicates equal magnitudes for natural and triggered events. Magnitudes for triggered earthquakes are as reported in the literature; magnitudes for natural earthquakes are as reported by NEIC or, when known large events have occurred prior to 1973, from historical sources. Figure includes recently reported examples of possibly injection-triggered earthquakes, as well as all examples categorized as caused by injection reported by Suckale (2009), and all that Nicholson and Wesson (1990) categorized as caused by injection, excluding those categorized only as 'less well documented or possible'. Symbols indicate examples where purpose of injection was for waste disposal (usually at a single well), at a geothermal project (usually at multiple wells), for secondary recovery (always involving numerous wells), or hydrofracturing. Examples plotted on grey bar at left are triggered earthquakes where no historical earthquakes within 100 km were found. [Figure reproduced from Frohlich (2012).]

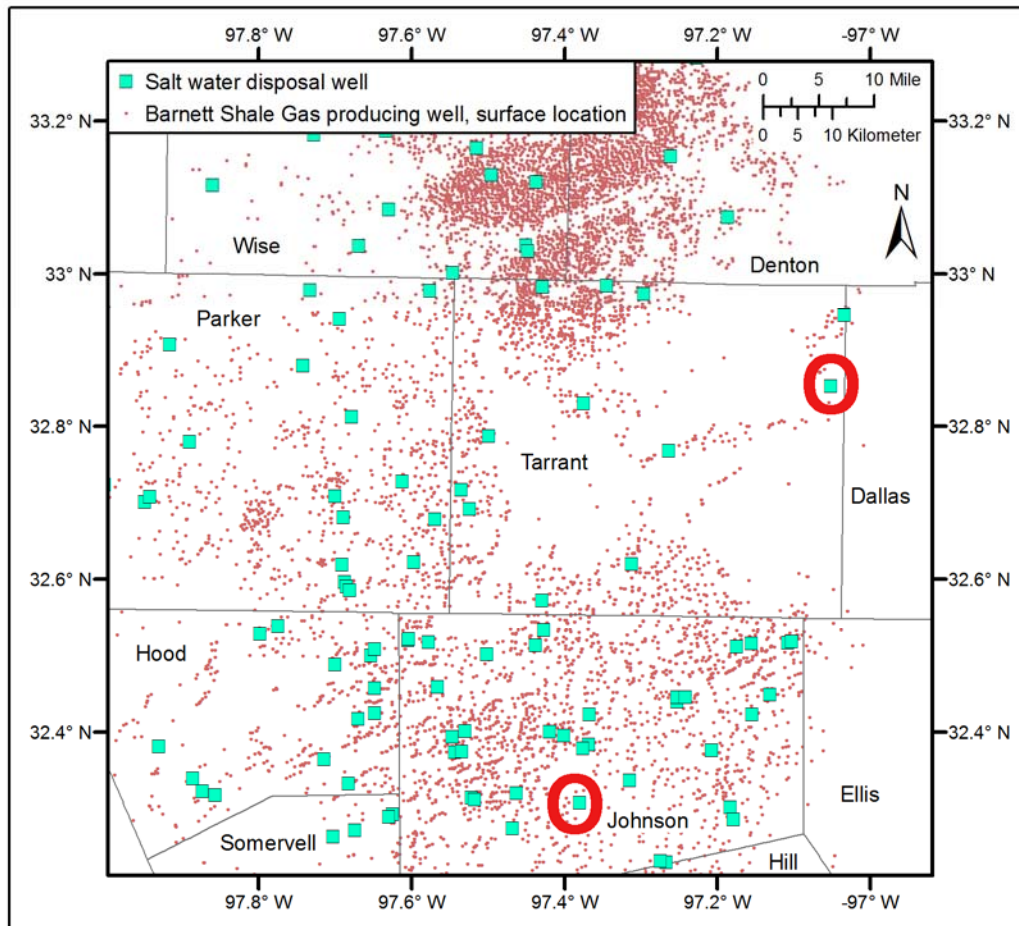


Figure 8. Map of producing natural gas wells and salt water disposal (injection) wells in Tarrant and surrounding counties as of 2009. Prior to June 2009, the NEIC had reported earthquakes near none of the producing wells and only the two salt water disposal wells indicated by red circles, one in Tarrant County at the Dallas-Fort Worth airport and one in Johnson County near Cleburne, TX. [Figure revised from Frohlich and Potter (2012).]

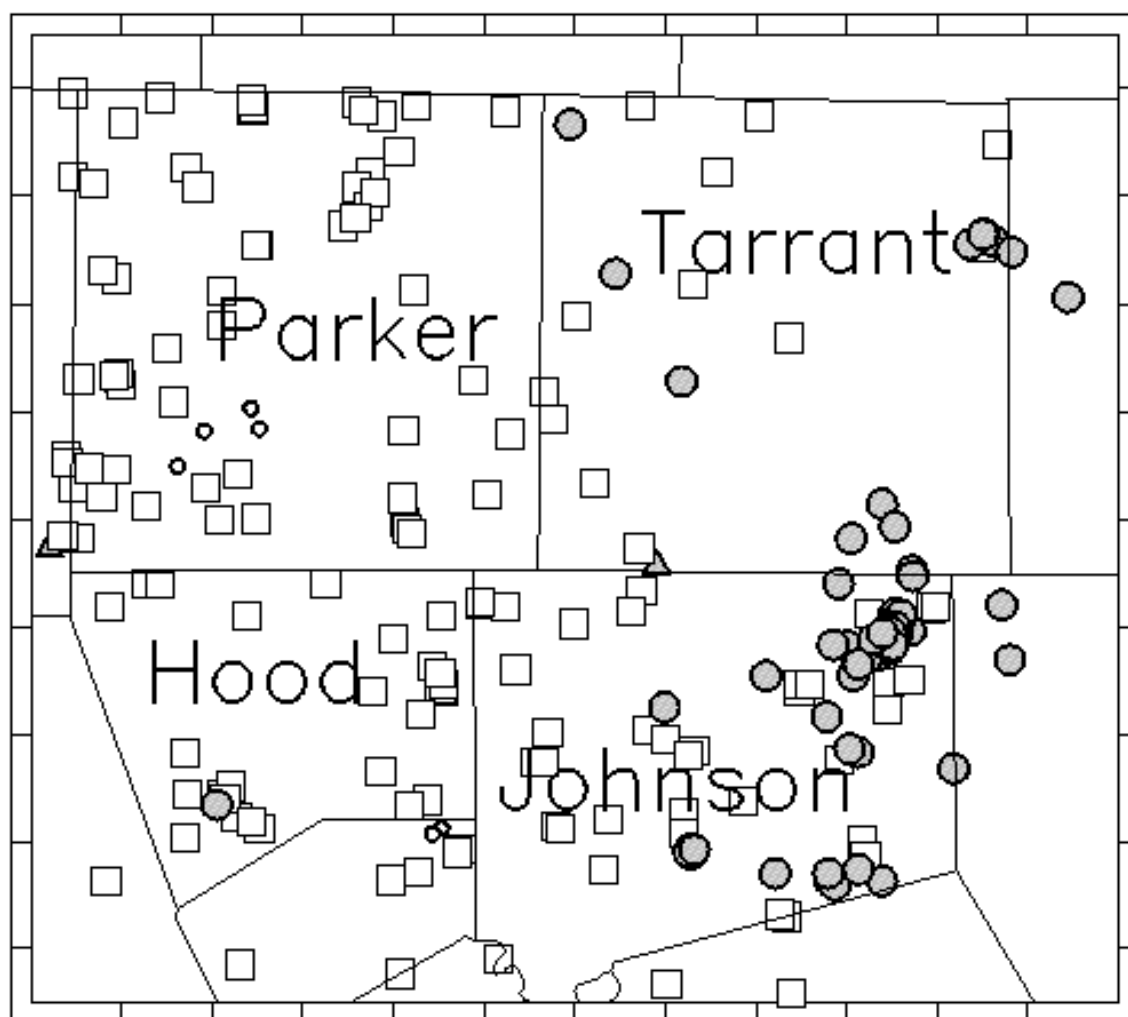


Figure 9. For four Texas counties within the Barnett Shale, preliminary results of a search for small earthquakes using data recorded 2009-2011 by temporary USArray seismic stations. The figure shows earthquakes (large grey circles), salt water disposal injection wells (squares), quarry blasts (small white circles) and USArray seismic stations (triangles). Note that most earthquakes in Johnson, Hood, and Tarrant Counties occur near waste disposal wells. However, at present it is unclear why some injection wells in Johnson County cause numerous earthquakes, while there is no seismicity associated with wells in other areas such as Parker County. [Figure summarizes unpublished research by this report's author (Frohlich).]

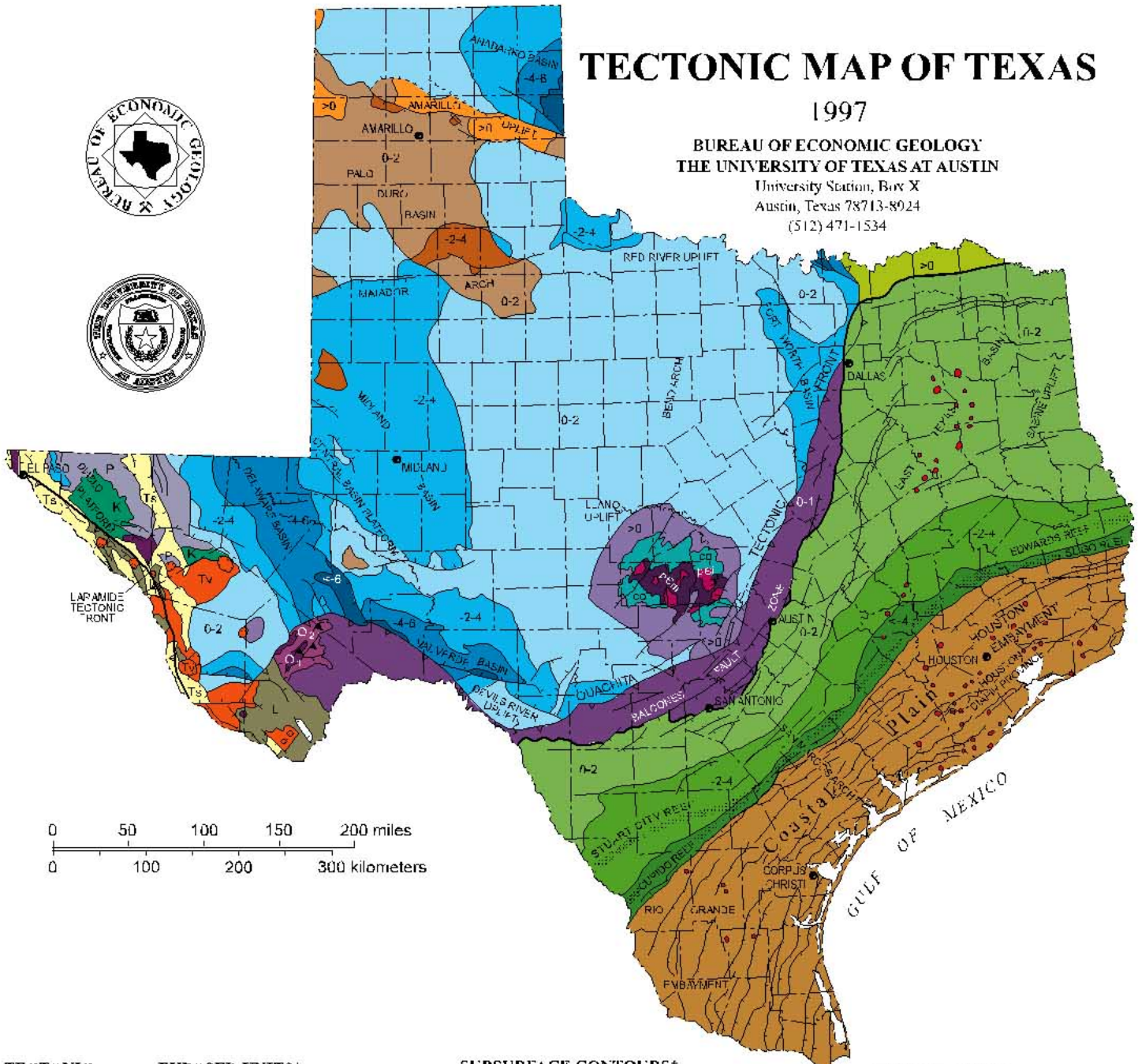
## Appendix C: Texas Tectonic Map

# TECTONIC MAP OF TEXAS

1997

BUREAU OF ECONOMIC GEOLOGY  
THE UNIVERSITY OF TEXAS AT AUSTIN

University Station, Box X  
Austin, Texas 78713-8924  
(512) 471-1534



## TECTONIC EPISODE

### Tertiary

- Ts Late Tertiary extensional basin
- Tv Trans-Pecos igneous

### Laramide

- L Deformed Cretaceous strata

### Gulf Coast

- K Cretaceous strata

### Ouachita

- P Foreland: Upper Paleozoic
- CO Lower Paleozoic

- Marathon: Upper Paleozoic (Hysch)
- D<sub>1</sub> Lower Paleozoic

### Llano

- pEi Precambrian igneous
- pEm Precambrian metamorphic

## SUBSURFACE CONTOURS\*

(elevation in kilometers\*\*)

Top of pre-Tertiary

<-4

Base of Austin Chalk or  
Top of Edwards Group  
Cretaceous

>0 0 to -2 -2 to -4 <-4

Top of Ellenburger  
Paleozoic

>0 0 to -2 -2 to -4 -4 to -6 <-6

Top of Precambrian

>0 0 to -2 -2 to -4

Buried Ouachita facies  
Paleozoic

0 to -1

\* Note changes in mapped horizon.

\*\* >0, elevation greater than sea level;

<-6, depths greater than 6 km below sea level

## OTHER FEATURES



Caldera



Salt diapirs



Lower Cretaceous reef trend



Normal fault, indicating downthrown side



Thrust fault, teeth on upper plate

## TECTONIC FRONTS



Laramide tectonic front



Ouachita tectonic front



Gulf Basin margin



# Tectonic Map of Texas

Proper appreciation of regional and global deformation comes only from seeing our planet as a fluid overlain by a thin, brittle crust. Although Earth's rocky face seems solid and stationary, it is made of plates that move over millennia because of flow of rocks far below Earth's surface. *Tectonics* is the study of regional and global deformation history and the plate tectonic processes that control such movement. Our understanding of past movements is summarized on *tectonic maps*, such as this *Tectonic Map of Texas*.

The plates that compose Earth's surface move horizontally and vertically relative to each other, at a rate of as much as a few centimeters per year. Motion of Earth's surface can be abrupt, as those who live in earthquake-prone areas can testify, but it is usually gradual and imperceptible. Yet over long periods of time—millions of years—parts of Earth's surface can move tens of thousands of miles relative to other parts. Texans who have handled rock samples recovered from the state's deep petroleum and geothermal wells know that such rocks can be nearly too hot to touch. At greater depth, temperatures are higher still. Because rock strength decreases exponentially with increasing temperature, Earth's interior is weak and able to flow plastically. It is this deep-seated flow that causes mountain ranges to be thrust up and plateaus torn apart to form ocean basins.

Tectonic maps document movement history by highlighting structural relationships among segments of Earth's crust that may extend across hundreds of miles. Such maps show crustal architectural patterns that indicate the sequence of tectonic events. To better understand the uses of these maps, compare this *Tectonic Map of Texas* with the Bureau of Economic Geology's page-size *Geology of Texas* map.

Geologic maps show where rock strata (layers) occur at Earth's surface or under a thin veneer of soil and vegetation. These maps have elaborate color patterns because their purpose is to depict many distinctive rock formations.

In contrast to the complicated color pattern of the geologic map, the *Tectonic Map of Texas* has a simple color pattern that depicts basic map elements, called tectonostratigraphic units. These units are sequences of sedimentary rock strata or groups of metamorphic and igneous rocks that share a common history of deformation. Combining individual geologic formations removes distracting detail that obscures the shared deformation histories of large blocks of crust. On the *Tectonic Map of Texas*, for example, the various Paleozoic formations between Midland, Dallas, and Amarillo have been combined. Not shown is the thin veneer of younger Cretaceous, Tertiary, and Quaternary deposits that lie at the surface over much of the area.

Structural information taken from records of deep wells is illustrated on the tectonic map by color coding that shows depth to a particular formation chosen as a reference horizon. Different rock formations have been used in various parts of Texas as reference horizons; these once were nearly horizontal layers at Earth's surface. As a result of deformation, parts of these formations have been raised or lowered, and color coding on the map shows how deeply buried these horizons are now. For example, in West Texas darker shades of blue mark the deep West Texas and Anadarko Basins. The reference horizon used there is the Paleozoic Ellenburger Formation, a petroleum reservoir rock widely penetrated by oil and gas drilling.

Tectonic maps show major structural features, including tectonic fronts that mark edges of major basins and former mountain ranges (orogenic belts). Crosscutting relations show the relative ages of features. For example, the blue patterns of Paleozoic basins and uplifts in West Texas are crosscut by the light green of the younger Gulf Coast Basin east of San Antonio, Austin, and Dallas.

Several tectonic cycles have affected Texas. These are informally listed on this map as "tectonic episodes," but they are actually local subdivisions of global plate movements that did not begin or end everywhere at the same time, and which—to a certain extent—are arbitrary milestones in a continuous history of movement. Each cycle produced tectonostratigraphic units that record initially the generation of rifts and divergent continental margins, followed by destruction of an ocean basin and mountain building (orogeny). The *Tectonic Map of Texas* distinguishes three principal tectonic cycles:

(1) Precambrian cycles are recorded in the ancient rocks of the Llano region and near Van Horn and El Paso. Of these the best known is the Llano cycle of between 1,200 and 1,080 million years ago (mya). At the close of this cycle, parts of present-day Texas were attached to rocks that now are located in Antarctica and southwest Australia.

(2) The Paleozoic Ouachitan cycle began with continental rifting about 550 mya, followed by inundation of much of Texas by shallow seas. This cycle closed with the collision of South and North America, which caused the Ouachita mountain-building event, ending about 245 mya. At this time much of Texas was in the shadow of vast mountain ranges that crossed the southern and east-central part of Texas.

On the tectonic map, two major features record this Ouachitan history. The most prominent is the foreland area of West Texas, shown in shades of blue. Here the legacy of ocean opening and the rise and fall of sea level created the stratigraphic and

structural features that would later trap vast quantities of oil and gas. The term foreland signifies that the paleophysiography and structure of this area were shaped by a nearby mountain belt. The ancient and almost entirely eroded mountain belt is the other Ouachitan feature shown on the map. The Ouachitan mountain belt lay south and east of the Ouachita tectonic front. Its mostly buried roots extend from the Marathon area of West Texas, where deeply eroded relics of the mountain belt are exposed, through a great northward-curving arc to near Dallas, thence into Oklahoma. This zone of profound crustal contraction continues in the Appalachian Mountains of eastern North America and beyond.

(3) The current tectonic cycle in Texas is the Gulf Coast, which began in Texas with continental rifting in the Late Triassic about 220 mya and eventually led to creation of oceanic crust in the Gulf of Mexico. Well after this ocean began to open in South and East Texas, between 85 and 50 mya (Late Cretaceous to Paleocene), a mountain-building event called the Laramide Orogeny occurred in West Texas. This event is part of widespread deformation in the western United States, Canada, and Mexico that created the Rocky Mountains.

The *Tectonic Map* indicates where the Gulf Coast and Laramide events had their strongest impact on Texas geology. Rocks shown in green and brown (Gulf Coast Cretaceous and Tertiary strata), mainly east of Dallas, Austin, and San Antonio, were deposited during the creation of the Gulf of Mexico and Atlantic Ocean. Byproducts of basin formation depicted on the map include normal faults and intrusions of mobile salt (salt diapirs). Between Del Rio and Dallas, the edge of the Gulf Coast Basin follows the older Ouachitan tectonic front, testifying to the tendency for deformation to be localized through time along preexisting fault zones. Green and tan patterns and fault traces extending southeast of El Paso mark the edge of the Laramide orogenic belt and the frontal edge of the Rocky Mountains.

Formation of both the Gulf of Mexico and the Rocky Mountains is part of continuing global deformation. The Atlantic Ocean is widening as Europe and North America separate, while the Pacific Ocean basin is closing as the North American plate and Asia converge. The earliest phases of this modern pattern of movement can be read in the Gulf Coast and Laramide tectonic history of Texas.

Tectonic maps help illustrate Earth's restless history by highlighting the major episodes of plate tectonic motion, including mountain building and ocean formation. With this map as a guide, map users can retrace the experience of Texas in Earth's history of regional and global movement.

—Text by Stephen E. Laubach

## Bureau of Economic Geology

The **Bureau of Economic Geology**, established in 1909 as the successor to the Texas Geological Survey and the Texas Mineral Survey, is a research entity of The University of Texas at Austin. It also functions as the State Geological Survey, a quasi-State agency, and the Bureau Director serves as the State Geologist. Advisory, technical, and informational services relating to the resources and geology of Texas are provided by the Bureau to governmental agencies, private industry, and the general public. The Bureau conducts basic and applied research projects in energy and mineral resources, coastal and environmental studies, land resources, geologic mapping, and other research programs in areas such as hydrogeology, basin analysis, and geochemistry. Reports and maps published by the Bureau are available for a nominal price. A list of publications is available on request.

## Appendix D: Texas Oil and Gas Map



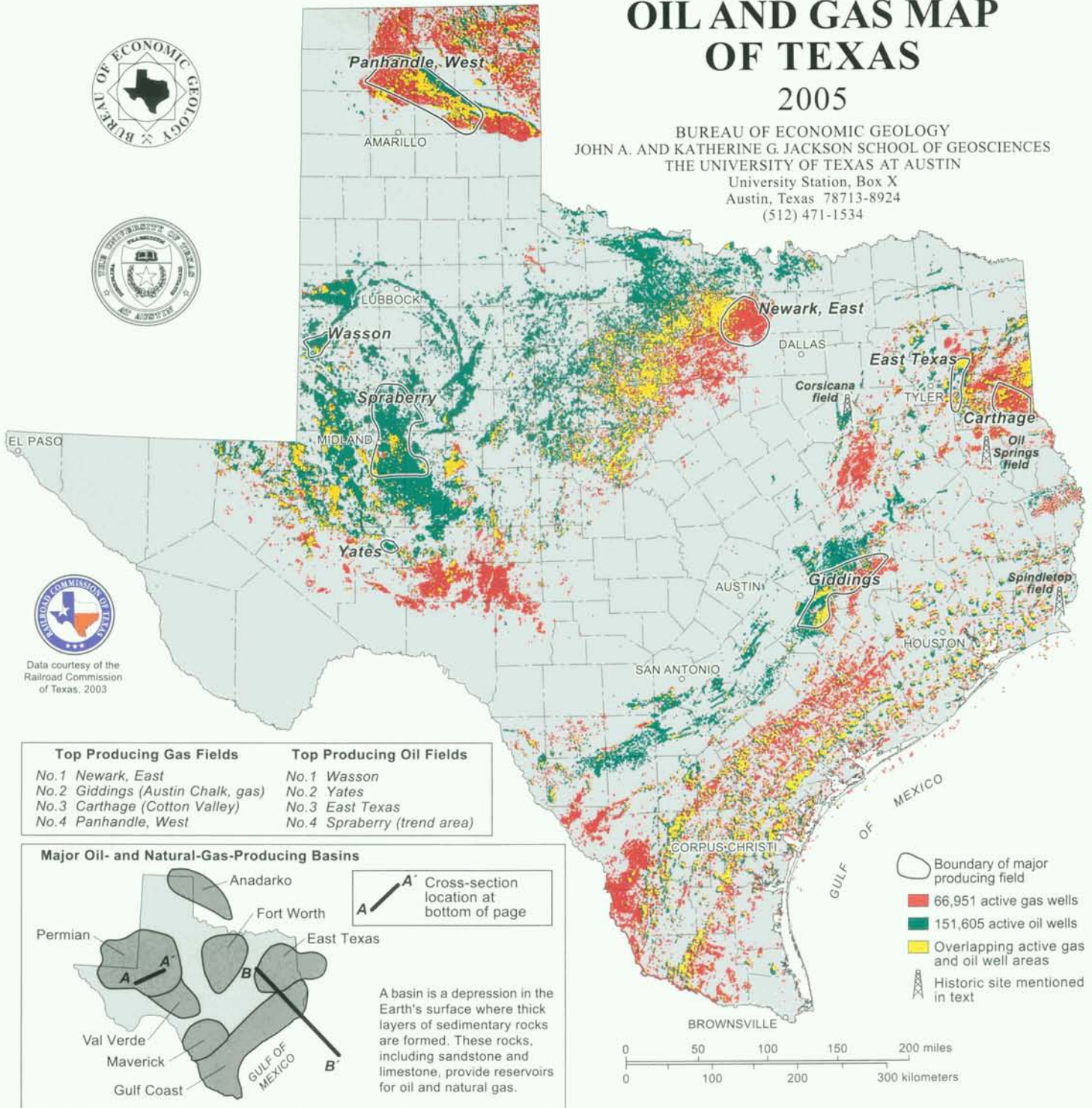
# OIL AND GAS MAP OF TEXAS

2005

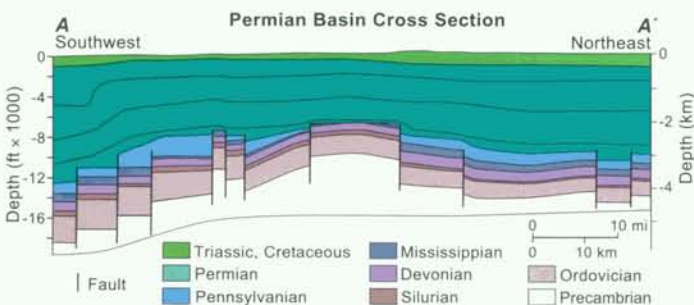
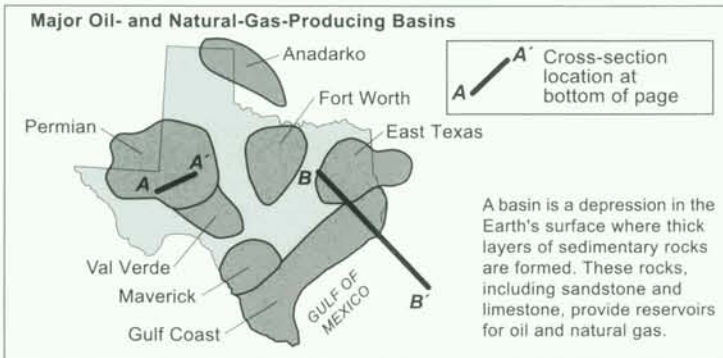
BUREAU OF ECONOMIC GEOLOGY  
JOHN A. AND KATHERINE G. JACKSON SCHOOL OF GEOSCIENCES  
THE UNIVERSITY OF TEXAS AT AUSTIN  
University Station, Box X  
Austin, Texas 78713-8924  
(512) 471-1534



Data courtesy of the  
Railroad Commission  
of Texas, 2003

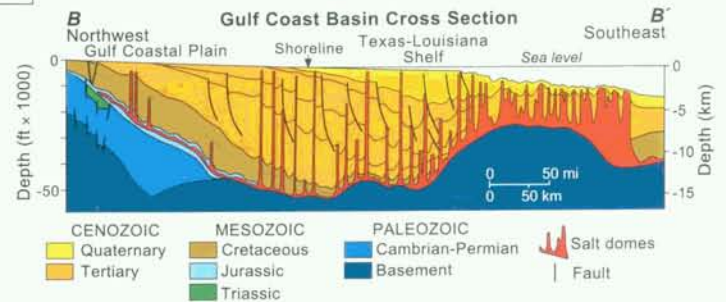


Top Producing Gas Fields	Top Producing Oil Fields
No.1 Newark, East	No.1 Wasson
No.2 Giddings (Austin Chalk, gas)	No.2 Yates
No.3 Carthage (Cotton Valley)	No.3 East Texas
No.4 Panhandle, West	No.4 Spraberry (trend area)



Modified from Bebout, D. G., and Meador, K. J., 1985, Regional cross sections—Central Basin Platform, West Texas: The University of Texas at Austin, Bureau of Economic Geology, 4 p., 11 pls.

More than half of the oil and gas production from Texas comes from the Permian Basin of West Texas. Nearly three-quarters of this production comes from carbonate rocks of Permian age.



Modified from Worral, D. M., and Snelson, S., 1989, Evolution of the northern Gulf of Mexico with an emphasis on Cenozoic growth faulting and the role of salt tectonics, in Bally, A. W., and Palmer, A. R., eds., The geology of North America—an overview: Geology of North America, v. A, p. 97-138.

Most oil and gas production in the Texas Gulf Coast comes from Tertiary-aged sandstones. Many reservoirs are associated with faults and salt domes.

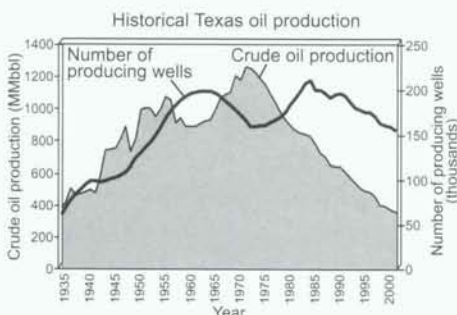


# Oil and Gas Production in Texas

Texas has produced more oil and natural gas than any other state and to date remains the largest daily producer. Oil and natural gas are found in most parts of the state. No state or any other region worldwide has been as heavily explored or drilled for oil and natural gas as Texas. Currently (August 2003), 151,605 active oil wells and 66,951 active gas wells produce oil and natural gas in the state.

## TEXAS OIL PRODUCTION

Although Texas wasn't the first state to produce oil, Texans weren't far behind. Drilling for oil in Texas occurred at Oil Springs, near Nacogdoches in East Texas, in 1866, less than a decade after Colonel Edwin Drake's 1859 Titusville, Pennsylvania, well brought the U.S. into the age of oil. Oil had been found before in Texas, but it had been either through natural surface seeps or drilling for water. Then, in 1894, the Texas age of oil began with the first major discovery, Corsicana field, in East Texas. The first boom came in 1901 with Spindletop field in the Gulf Coast Basin. Thousands of other discoveries have followed. East Texas oil field, the largest oil field in Texas or in any of the U.S. Lower 48 states, was discovered in 1930. Annual Texas oil production peaked in 1972 at 1,263 MMbbl (million barrels), and thereafter production rapidly dwindled. Although oil production in Texas is in decline, significant opportunities for incremental recovery exist in advanced exploration and production technologies. On average, only 35 percent of original oil in place in Texas reservoirs has been recovered. Technology plays a pivotal role in increasing recovery rate, improving economics, and assisting in exploration of complex oil reservoirs. If technology can be applied to an increasingly complex and mature resource base, oil production decline in Texas can be slowed.



tion and production technologies. On average, only 35 percent of original oil in place in Texas reservoirs has been recovered. Technology plays a pivotal role in increasing recovery rate, improving economics, and assisting in exploration of complex oil reservoirs. If technology can be applied to an increasingly complex and mature resource base, oil production decline in Texas can be slowed.

## TEXAS NATURAL GAS PRODUCTION

Historically, natural gas in Texas was discovered as a byproduct of oil. This form of natural gas, which is in contact with crude oil in the reservoir, is termed *associated gas*, and in earlier years it was wastefully flared and vented off without being produced. With increased oil exploration and discoveries in Texas, annual natural gas production steadily rose and peaked also in 1972 at 9.6 Tcf (trillion cubic feet). However, unlike oil production, since the early 1980's, Texas gas production has maintained a steady production level. This was achieved through several large field discoveries,

such as Newark, East, field in North-Central Texas, as well as a multitude of smaller sized fields that required application of advanced exploration and development technologies. Texas natural gas production levels were maintained by increasing numbers of producing wells, which are now at an all-time high. Today many of the new exploration and production activities involve natural gas rather than oil.

## U.S. AND WORLD RANKING

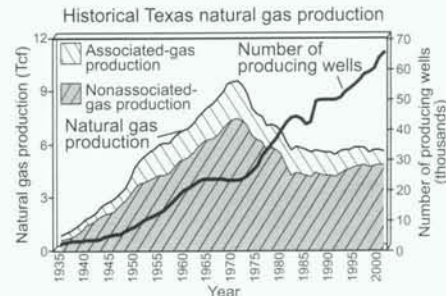
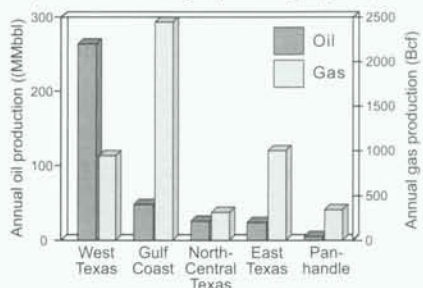
Through the application of advanced technologies, incremental oil recovery from mature oil fields continues to make Texas the state that leads in oil production. In terms of year 2002 oil and natural gas production, Texas produced 17 percent (366 MMbbl) and 30 percent (5.7 Tcf), respectively, of the U.S. total. Indeed, if Texas were a nation, it would rank as one of the top 10 producers in the world. In terms of proved oil and natural gas reserves, Texas has 22 percent (5,015 MMbbl) and 23 percent (44.3 Tcf), respectively, of the U.S. total. Reserves are the estimated quantities that analysis of geological and engineering data demonstrates with reasonable certainty in future years to be recoverable from known reservoirs, under existing economic and operating conditions.

## MAJOR PRODUCING REGIONS

Oil and natural gas production in Texas can be divided into seven major producing basins. The Permian Basin dominates oil production in the state, and the Gulf Coast Basin dominates natural gas production. Major oil fields in Texas include Wasson, Yates, and Spraberry in West Texas, as well as the largest Texas oil field, East Texas field in the East Texas Basin. The Permian Basin has been the most prolific oil-producing province in U.S. history. East Texas field has produced more oil than any other field in the lower 48 states. Major natural gas fields in Texas, in terms of today's production rate, include Newark, East, field in the Fort Worth Basin; Carthage field in East Texas; Panhandle, West, field in the Anadarko Basin; and Giddings field in the Gulf Coast Basin. Excluding Panhandle, West, field, all major natural gas fields in Texas are a product of application of advanced technologies, such as hydraulic fracturing and horizontal drilling, which have resulted in increased production from these low-permeability and complex fields.

Although oil and natural gas production in Texas has declined from its peak, advanced exploration and production technologies will enable

Major Texas oil- and gas-producing regions, 2002



ration and development technologies will enable Texas to remain the major oil and natural gas producer in the U.S. Because easy-to-find oil and natural gas resources have been fully exploited in Texas, the future mix of oil and gas resources will be increasingly complex and technologically challenging.

## ECONOMIC IMPACT

Oil and natural gas production in Texas, although not as great as in the past, remains an important source of economic benefit, in terms of value, jobs created, and taxes. According to the Texas Comptroller's input-output model of Texas' economy, the total economic value of oil and gas is 2.91 times the value of production. Additionally, 19.1 jobs are created per million dollars of oil and gas production. Assuming oil and natural gas prices of \$25/bbl and \$5/Mcf, and year 2002 annual production of 366 MMbbl and 5.7 Tcf, wellhead value exceeds \$37 billion. Annual natural gas value is currently 3.1 times that of the oil wellhead value to Texas. In terms of economic value trickled down through the Texas economy and jobs created, this figure equates to nearly \$110 billion and 719,115 jobs. Severance, ad valorem, and indirect taxes provide additional economic benefits of more than \$6 billion to Texas. The leasing of mineral rights to State- and University-owned lands statewide, moreover, provides royalty and leasing revenue that replenishes the Permanent University and School Funds, important sources of revenue for public education in Texas.

## RAILROAD COMMISSION OF TEXAS

The Railroad Commission of Texas, established in 1891, is the oldest regulatory agency in the state and one of the oldest of its kind in the nation. The Railroad Commission has regulatory divisions that oversee Texas' oil and natural gas industry, gas utilities, pipeline and rail safety, safety in the liquefied petroleum gas industry, and surface mining of coal and uranium. As the regulatory agency for the oil and gas industry, it provides extensive drilling and production statistics. The Railroad Commission continues to serve Texas in its stewardship of natural resources and the environment, its concern for the individual and communal safety of citizens, and its support of enhancing development and economic vitality for the betterment of Texas as a whole.

—Text contributed by  
Eugene M. Kim and  
Stephen C. Ruppel

## Bureau of Economic Geology

The **Bureau of Economic Geology**, established in 1909, is a research entity of The University of Texas at Austin that also functions as the State Geological Survey. The Bureau, part of the Jackson School of Geosciences, conducts basic and applied research projects in energy and mineral resources, coastal and environmental studies, land resources, and geologic mapping. Reports and maps published by the Bureau are available for a nominal price. A list of publications is available on request.

## Appendix E: References Cited

## Appendix E: References Cited

- Akrad, O., Miskimins, J., and Prasad, M., 2011, "The effects of fracturing fluids on shale mechanical properties and proppant embedment", SPE Annual Technical Conference and Exhibition, Paper #146658, October 30-November 2, Denver, CO.
- Anderson, R.A., Ingram, D.S., and Zanier, A.M., 1973, "Determining fracture pressure gradients from well logs", *Journal of Petroleum Technology* (November), 1259-1268.
- Baree, R.D., Gilbert, J.V., and Conway, M.W., 2009, "Stress and rock property profiling for unconventional reservoir stimulation", SPE Hydraulic Fracturing Technical Conference, Paper #118703, The Woodlands, TX, January 19-21.
- Blanton, T. L. and Olson, J. E., 1999, "Stress Magnitudes from Logs: Effects of Tectonic Strains and Temperature," *SPE Reservoir Evaluation and Engineering*, 62-68.
- Bowker, K.A., 2007, "Barnett Shale gas production, Fort Worth Basin: Issues and discussion", *AAPG Bulletin*, 91(4), 523-533.
- Chan, A.W., and Zoback, M.D., 2007, "The role of hydrocarbon production on land subsidence and fault reactivation in the Louisiana coastal zone", *Journal of Coastal Research*, **23**(3), 771-786.
- Corbett, K, Friedman, M. and Spang, J., 1987, "Fracture development and mechanical stratigraphy of the Austin Chalk, Texas", *AAPG Bulletin*, 71: 17-28.
- Darbe, R. and Ravi, K., 2010, "Cement considerations for tight gas completions", SPE Deep Gas Conference and Exhibition, Paper #132086, Bahrain, January 24-26.
- Davies, R.J., Mathias, S.A., Moss, J., Hustoft, S. and Newport, L., 2012, "Hydraulic Fractures: How far can they go?", *Marine and Petroleum Geology* (in press).
- Du, J., and Olson, J.E., 2001, "A poroelastic reservoir model for predicting subsidence and mapping subsurface pressure fronts", *Journal of Petroleum Science & Engineering*, v. 30, p. 181-197.
- Earlougher, R.C., 1977, Advances in Well Test Analysis, SPE Monograph Series, Vol. 5, 264 pp.
- Ficker, E., 2012, "Five Years of Deep Fluid Disposal into the Ellenburger of the Fort Worth Basin", *Search and Discovery Article #80227*.
- Fisher, M.K., Wright, C.A., Davidson, B.M., Goodwin, A.K., Fielder, E.O., Buckler, W.S., and Steinsberger, N.P., 2005, "Integrating fracture mapping technologies to improve stimulations in the Barnett Shale", *SPE Production and Facilities* (May), 85-93.
- Fisher, K., and Warpinski, N., 2012, "Hydraulic fracture height growth: Real data", *SPE Production and Operations* (February), 8-19.
- Friedman, M., Kwon, O., and French, V.L., 1994, "Containment of natural fractures in brittle beds of the Austin Chalk", in Rock Mechanics, Nelson, P. and Laubach, S., editors, 833-840.

- Geertsma, J., 1973, "Land subsidence above compacting oil and gas reservoirs", *Journal of Petroleum Technology* (June), 734–744.
- Geertsma, J., 1989, "Two dimensional fracture propagation models", in *Recent Advances in Hydraulic Fracturing*, edited by J.L. Gidley et al., 295-302.
- Guegen, Y., and Bouteau, M., 2004, Mechanics of fluid saturated rocks, Elsevier, 450 pp.
- Hagin, P.N. and Zoback, M.D., 2004, "Viscous deformation of unconsolidated reservoir sands (Part 2): Linear viscoelastic models", *Geophysics*, **69**, 742–751.
- Hamilton, D.H., and Meehan, R.L., 1971, "Ground rupture in the Baldwin Hills", *Science*, 172 (3981), 333-344.
- Hanks, T.C., and Kanamori, H., 1979, "A moment magnitude scale", *Journal of Geophysical Research*, 84(B5), 2348-2350.
- Hardin, R.W., and Associates, 2004, "Northern Trinity / Woodbine Aquifer Groundwater Availability Model", Prepared for The Texas Water Development Board, 391 pp.
- Healy, J.H., Rubey, W.W., Griggs, D.T., and Raleigh, C.B., 1968, "The Denver earthquakes", *Science*, 161(3848), 1301-1310.
- International Energy Agency, 2012, *Golden Rules for a Golden Age of Gas: World Energy Outlook Special Report on Unconventional Gas*.
- James, L. B.; Kiersch, G. A.; Jansen, R. B.; Leps, T. M. (1988). "Lessons from notable events." in *Jansen, RB ed. "Advanced dam engineering for design, construction, and rehabilitation"*. NY.: Van Nostrand Reinhold
- Joyner, W.B. and Boore, D.M., 1981, "Peak horizontal acceleration and velocity from strong-motion records including record from the 1979 Imperial Valley, California, earthquake", *Bull. Seism. Soc. Am.*, v. 71, 2011-2038.
- Kim, Y. and Sanderson, D.J., 2005, "The relationship between displacement and length of faults: a review", *Journal of Structural Geology*, 68, 317-334.
- King, G.E., 2012, "Hydraulic fracturing 101", SPE Hydraulic Fracturing Technical Conference, Paper #152596, The Woodlands, TX, February 6-8.
- Lewis, A.M., and Hughes, R.G., 2008, "Production data analysis of shale gas reservoirs", SPE Annual Technical Conference and Exhibition, Paper #116688, September 21-24, Denver, CO.
- Lohoefer, D., Athans, J., Seale, R., 2006, "New Barnett Shale completion lowers costs and improves efficient", SPE Annual Technical Conference and Exhibition, Paper #103046, September 24-27, San Antonio, TX.
- Montgomery, S.L., Jarvie, D.M., Bowker, K.A., Pollastro, R.M., 2005, "Mississippian Barnett Shale, Fort Worth basin, north-central Texas: Gas-shale play with multi-trillion cubic foot potential", *AAPG Bulletin*, 89(2), 155-175.
- Narr, W. and Currie, J.B., 1982, "Origin of fracture porosity: Example from the Altamount Field, Utah", *AAPG Bulletin*, 66(9), 1231-1247.



- Nolte, K.G. and Smith, M.B., 1981, "Interpretation of fracturing pressures", JPT (Sept.), 1767-1775.
- Oefelein, F.H., and Walker, J.W., 1964, "California flood yields profitable recovery of heavy oil from multilayered reservoir", Journal of Petroleum Technology (May), 509-514.
- Olson, J.E., 2008, "Multi-fracture propagation modeling: Applications to hydraulic fracturing in shales and tight gas sands", 42nd U.S. Symposium on Rock Mechanics, San Francisco, CA, June 29-July 2.
- Pollard, D.D., and Segall, P., 1987, "Theoretical displacements and stresses near fractures in rock: with applications to faults, joints, veins, dikes and solution surfaces", in Fracture Mechanics of Rock, edited by B.K. Atkinson, Academic Press, London, 277-350.
- Pollastro, R.M. Jarvie, D.M., Hill, R.J. and Adams, C.W., 2007, "Geologic framework of the Mississippian Barnett Shale, Barnett-Paleozoic total petroleum system, Bend arch-FortWorth Basin, Texas", AAPG Bulletin, 91(4), 405-436.
- Prats, M., 1981, "Effect of burial history on the subsurface horizontal stresses of formations having different material properties", SPE Journal (December), 658-662.
- Pyrak-Nolte, L.J., 1996, "The seismic response of fracture and the interrelations among fracture properties", International Journal of Rock Mechanics, Mining Science and Geomechanics Abstracts, 33(8), 787-802.
- Raleigh, C.B.; Healy, J.H., and Bredehoeft, J.D., 1976, "An experiment in earthquake control at Rangely, Colorado", Science, **191**, 1230-1237.
- Segall, P. and Pollard, D.D., 1983, "Joint formation in granitic rock of the Sierra Nevada", GSA Bulletin, 94, 563-575.
- Segall, P. and Fitzgerald, S.D., 1998, "A note on induced stress changes in hydrocarbon and geothermal reservoir", Tectonophysics, 289, 117-128.
- Sone, H. and Zoback, M.D., 2011, "Visco-plastic properties of shale gas reservoir rocks", 45th US Rock Mechanics / Geomechanics Symposium held in San Francisco, CA, June 26-29.
- Texas Railroad Commission, 2007, The Application of EOG Resources, Inc. to dispose of oil and gas waste by injection in to a reservoir not productive of oil or gas, Dishop SWD Lease Well No. 1, Newark, East (Barnett Shale) Field, Erath County, Texas, Oil and Gas Docket No. 09-0249380.
- Tutuncu, A.N. and Mese, A.I., 2011, "Relationship between Permeability, Acoustic, Mechanical and Strength Anisotropies in Unconventional Reservoirs and Seal Shales", 45th US Rock Mechanics / Geomechanics Symposium held in San Francisco, CA, June 26-29.
- Valko, P. and Economides, M.J., 1995, Hydraulic Fracture Mechanics, Wiley, 298 pp.
- Walsh, J.B., 1965, "The effect of cracks on the uniaxial elastic compression of rocks", Journal of Geophysical Research, 70, 399-411.
- Warpinski, N.R., 1989, "Elastic and viscoelastic calculations of stress in sedimentary basins", SPE Formation Evaluation (December), 522-530.

- Warpinski, N.R., Du, J. and Zimmer, U., 2012, "Measurement of hydraulic fracture induced seismicity in gas shales", SPE Hydraulic Fracturing Technical Conference, Paper #151597, The Woodlands, TX, February 6-8.
- Wells, D.L. and Coppersmith, K.J., 1994, "New empirical relationships among magnitude, rupture length, rupture width, rupture area and surface displacement", Bull. of the Seismological Society of America, 84, 974-1002.
- Zoback, M.D., 2007, Reservoir Geomechanics, Cambridge University Press.
- Zoback, M.D., and Gorelick, S.M., 2012, "Earthquake triggering and large-scale geologic storage of carbon dioxide", Proceedings of the National Academy of Sciences, 109(26), 10164-10168.
- Zoback, M.D. and Healy, J.H., 1987, "Friction, faulting and in situ stress", Annales Geophysicae, 2(6), 689-698.